ENERGY DISSIPATION OPTIMIZATION FOR CIRCULAR CULVERTS

FINAL REPORT

David M. Admiraal (PI) and Chi Zhang

Department of Civil and Environmental Engineering

University of Nebraska – Lincoln
Lincoln, NE 68588-0531

TECHNICAL REPORT DOCUMENTATION PAGE

1. Report No. FY21(009)	2. Government Accession No.	3. Recipient's Catalog No.	
4. Title and Subtitle Energy Dissipation Optimization for Circular Culverts		**5. Report Date** 9/5/2023	
		6. Performing Organization Code	
7. Author(s) David M. Admiraal Chi Zhang		**8. Performing Organization Report No.**	
9. Performing Organization Name and Address Department of Civil and Environmental Engineering University of Nebraska – Lincoln Lincoln, NE 68588-0531		**10. Work Unit No.**	
		11. Contract FY21(009)	
12. Sponsoring Agency Name and Address Nebraska Department of Transportation Research Section 1400 Nebraska Parkway Lincoln, NE 68502		**13. Type of Report and Period Covered** Final Report 7/1/2020 – 9/5/2023	
		14. Sponsoring Agency Code	

15. Supplementary Notes

16. Abstract

Two types of energy dissipation devices at circular culvert outlets were investigated: full-length weirs and staggered weirs. Related literature was reviewed; a model broken-back circular culvert and dissipation basin was built; instrumentation was installed to measure discharge, piezometric head, and velocities; and four sizes of full-length and staggered weirs were tested over a range of discharges and tailwaters. Weir heights ranged from D/8 to 4D/8, in which D was the culvert diameter. The two weir types were subjected to two styles of tests: (1) tests unaffected by tailwater and (2) tailwater-influenced tests. For tall full-length weirs (3D/8 and 4D/8), basin outlet depths could be reasonably predicted with a simple weir equation, general assumptions about the upstream flow, and the energy equation with no head losses. For shorter weirs (D/8 and 2D/8), the flow skimmed the weir and the weir equation was invalid, especially for high discharges. In these cases, the weirs were not effective energy dissipators. For the tallest weirs, the ratio of outlet energy and the critical depth was roughly constant. The outlet specific energy was about 3.2 and 2.9 times the critical depth for weir heights of 4D/8 and 3D/8, respectively. Similar results were found for the staggered weir, but specific energy was found to be 2.7 and 2.9 times the critical depth for weir heights of 4D/8 and 3D/8, respectively. Results can be used to determine dissipation basin outlet velocities for incoming runout Froude numbers in the range of 3.8 to 4.6 for full-length and staggered weirs with heights ranging from D/8 to 4D/8.

17. Key Words Energy dissipation, Culvert outlet, Broken-back culvert, Scour prevention, Weirs, Staggered Weirs, Baffles	**18. Distribution Statement** No restrictions. This document is available through the National Technical Information Service. 5285 Port Royal Road Springfield, VA 22161		
19. Security Classification (of this report) Unclassified	**20. Security Classification (of this page)** Unclassified	**21. No. of Pages** 182	**22. Price**

Form DOT F 1700.7 (8-72)   Reproduction of completed page authorized

DISCLAIMER

The contents of this report reflect the views of the authors, who are responsible for the facts and the accuracy of the information presented herein. The contents do not necessarily reflect the official views or policies neither of the Nebraska Department of Transportations nor the University of Nebraska-Lincoln. This report does not constitute a standard, specification, or regulation. Trade or manufacturers' names, which may appear in this report, are cited only because they are considered essential to the objectives of the report.

ABSTRACT

The principal goal of the current research is to develop and improve weir-based energy dissipator designs for circular culverts. In particular, design information is needed for energy dissipation devices at the outlets of circular culverts; in the present case we are interested in full-length weirs and staggered weirs. A great deal of research on weir energy dissipators for rectangular culverts has already been conducted (e.g., Hotchkiss and Larson, 2005). However, there is far less design information for weir-style energy dissipators for circular culverts. The flow behavior for this type of conveyance is significantly different than in rectangular culverts.

The tests reported in this document were intended to facilitate the development of a design procedure for weir energy dissipators downstream of circular culverts. With that in mind, a review of related literature was completed and reported; a test facility was carefully designed and constructed to collect flow information in a basin downstream of a model broken-back circular culvert; instrumentation was installed to measure discharge, piezometric head, and velocities; and four sizes of full-length and staggered weirs were tested over a range of discharges and tailwaters. The tested weir heights ranged from D/8 to 4D/8, in which D is the culvert diameter. The two weir styles were subjected to two types of tests: (1) tests in which the weirs were unaffected by tailwater and (2) tailwater-influenced tests. Data were processed to assess energy dissipation and hydraulic jump position associated with each dissipator configuration.

Dissipation basin outlet depths predicted with a simple weir equation, some general assumptions about the flow upstream of the weir, and the energy equation with no head losses were reasonably close to measured outlet depths for the tallest full-length weirs (weirs with heights of 3D/8 and 4D/8). For the shorter weirs (weirs with heights of D/8 and 2D/8), the flow appeared to skim the weir and the weir equation was invalid, especially for high discharges. In these cases, the weirs were not effective energy dissipators. For the two tallest full-length weirs, the ratio of the outlet energy and the critical depth was roughly constant over the range of discharges tested. The outlet specific energy for the tallest weir (4D/8) was found to be 3.2 times the critical depth. For the second tallest weir (3D/8) it was found to be 2.9 times the critical depth. Similar results were found for the staggered weir, but the optimal weir was the tallest weir (4D/8), for which the specific energy was found to be 2.7 times the critical depth. The specific energy for the second tallest weir (3D/8) was found to be 2.9 times the critical depth.

We attribute these differences to the fact that for the full-length weir, once optimal dissipation is achieved, increasing the height of the weir will only reduce total energy dissipation of the weir/expansion/culvert system; the same is not necessarily true for the staggered weir, for which some flow does not pass over the weir. This leads us to believe that that the geometry of the staggered weir can be altered to optimize its design – perhaps something similar to a baffle system. Both weir types reduce the outlet energy significantly, but there is room for

improvement. Optimal energy dissipation will result in an outlet energy that is as low as 1.5 times the critical depth when there is no tailwater. It would also be beneficial to re-examine these results over a wider range of Froude numbers than can be provided by the current test setup without modification.

When installing weirs for dissipation in rectangular channels, it is generally recommended that the length of the jump upstream of the weir is long enough to ensure that the jump is fully formed – roughly five times the upper sequent depth of a classical jump. The present configuration is complicated by the circular culvert cross section and expansion. Forcing the toe of the jump to approach the culvert break for all tested discharges required the outlet of the culvert to be submerged to about 1.1D by the tailwater. This result was independent of the weirs that were tested because at this submergence the weirs had little influence on energy dissipation. The result was not independent of discharge, and higher discharges than those tested may require greater submergence. However, raising the weir to achieve full submergence is not advisable based on the present observations since taller weirs will lead to higher basin outlet velocities. This is because jumps within the culvert do not appear to dissipate as much energy as is dissipated when the high velocity flow impacts the weir. In other words, forcing a jump to form within the runout section does not appear to be optimal for energy dissipation purposes. Testing taller weirs would help corroborate this observation.

Table of Contents

1. Introduction

1.1 Introduction to Energy Dissipation in Culverts

Culverts provide management and conveyance of storm water runoff for roadway systems. However, short culverts on steep slopes may result in downstream erosion if high-energy discharge is present at the culvert outlet. Erosion of the stream bed has many adverse impacts: Lowering of stream water level and groundwater level; damage to infrastructure such as bridges, culverts, and roadway embankments; and downstream siltation that damages aquatic habitat and affects water quality. The purpose of an energy dissipator is to dissipate as much flow energy as possible prior to releasing the flow to downstream areas and to mitigate the adverse impacts of bed erosion.

Energy dissipation structures are costly, especially when they require a lot of space. Thus, efforts have been made to reduce the width and length of dissipation basins and to eliminate as much land use as possible when installing the basins. The overarching aspiration of the present research is to do just that, to fit maximum energy dissipation in minimum space without increasing susceptibility of the structure to scour and undermining. The way in which to do this is to develop more efficient energy dissipators, and that is the reason to investigated weirs and staggered weirs.

1.2 Brief Summary of Previous Work

Previously, many types of energy dissipators have been used. Peterka (1978) proposed several stilling basins (USBR Basins Type II – VI) for different structures. HEC-14 (2006) also identified the Saint Anthony Falls (SAF) Basin. Among the stilling basin types Peterka proposed, the impact wall stilling basin (USBR Basin Type VI) is of most interest for the scope of this research because it is an impact-type, box-like energy dissipator for cylindrical pipe outlets. Sills also can be used to control hydraulic jumps. Forster and Skrinde (1950) used two types of sills - the sharp-crested weir and the abrupt rise to force a hydraulic jump to dissipate energy. Larson (2004) used a drop structure followed by a sill. These devices are similar to the devices described in the present work and are discussed in more detail in the literature review section. The present research is different from most of these in that the conveyance structure is cylindrical. This difference in geometry will impact the behavior of associated hydraulic jumps and expected energy dissipation.

1.3 Goals and Objectives of Current Research

The goal of the current research is to develop and improve weir-based energy dissipator designs for circular culverts. Research on weir energy dissipators for rectangular culverts has already been conducted (e.g., Hotchkiss and Larson, 2005) and the design procedure for such dissipators is included in HEC-14 (2006). However, there is still no formal design procedure for a weir

1

energy dissipator for circular culverts. Circular culverts differ from rectangular culverts in the sense that there is additional energy loss associated with the transition from the circular pipe to a rectangular box, and the transition involves changing from a flow with a circular boundary to a flow with a rectangular boundary.

The laboratory testing in this project focuses on two structures currently used by NDOT: the weir and the staggered weir. The data from tests reported in this document facilitate the development of a design procedure for weir energy dissipators downstream of circular culverts. Most importantly, proper selection of weir height and position will help to optimize energy dissipation. With that purpose in mind, the following tasks were performed:

1. A test facility was carefully designed and constructed to collect energy dissipation information in a basin downstream of a broken-back culvert.
2. Instrumentation was installed to measure discharge, piezometric head, and velocities within the facility.
3. Two types of energy dissipation weirs were tested in the facility: a full-length weir, and a staggered weir. These weirs were tested using two types of tests – (1) unrestricted outlet flow tests and (2) tailwater-influenced outlet tests.
4. Data were processed to assess energy dissipation associated with each dissipator configuration.

The unrestricted flow tests included a wide range of discharges for which the tailwater was set as low as possible so that it did not affect the outlet depth of the dissipation structure. Such tests are important because the energy dissipation associated with the dissipation structure configuration alone can be directly measured using piezometers, velocity and discharge measurements. The unrestricted flow tests utilized Prandtl measurements at the outlet to provide more accurate assessment of results because it was recognized that piezometer measurements were not extremely accurate for the high flow velocities at the dissipation structure outlet. The tailwater influenced outlet tests were done to observe how the hydraulic jump would behave for different downstream flow conditions.

The limiting case of the outlet depth of the dissipation basin is critical depth; this is because tailwater depths cannot be guaranteed for all culvert installations. Thus, designs of dissipation basins should strive to achieve critical depth at the basin outlet when there are no downstream controls – lower depths will result in higher outlet energy and higher depths cannot be enforced. In this work, we strive to provide designs that maximize outlet depth by investigating staggered and full-length weirs. The results of this investigation are presented in this report. Yet there is still much improvement that can be gained by optimizing weir geometry in future work.

1.4 Report Layout

This report is arranged into five chapters. Chapter 2 is a detailed literature review on energy dissipation in culverts. The characteristics of the simplest form of energy dissipation, free hydraulic jumps, are discussed. Different elements of dissipation geometries are presented.

Stilling basins, which combine multiple dissipation elements are examined at the end of the chapter. Chapter 3 provides a description of the experimental design, including both a description of the facility itself and the instruments used to collect the data. Chapter 3 also provides details about the experiments done in the test facility. Chapter 4 presents results of the experiments. In Chapter 5, conclusions of the study and information about how the results can be incorporated into culvert design are provided. There are also some suggestions concerning future testing options and procedures.

2. Literature Review – Energy Dissipation in Culverts

2.1 Introduction to Energy Dissipation

In order to prevent damage to streams and structures downstream of culverts, energy dissipation devices are required. Such devices have been studied for many years in the context of roadway culverts, storm sewers, dam spillways, and other conveyance systems. Many types of structures have been developed to date. Some of these can be categorized as shown in Figure 2.1. Categories include free hydraulic jumps over aprons, impact baffles, sills and weirs, drops, plunge basins, counterflow, flip buckets and design basins.
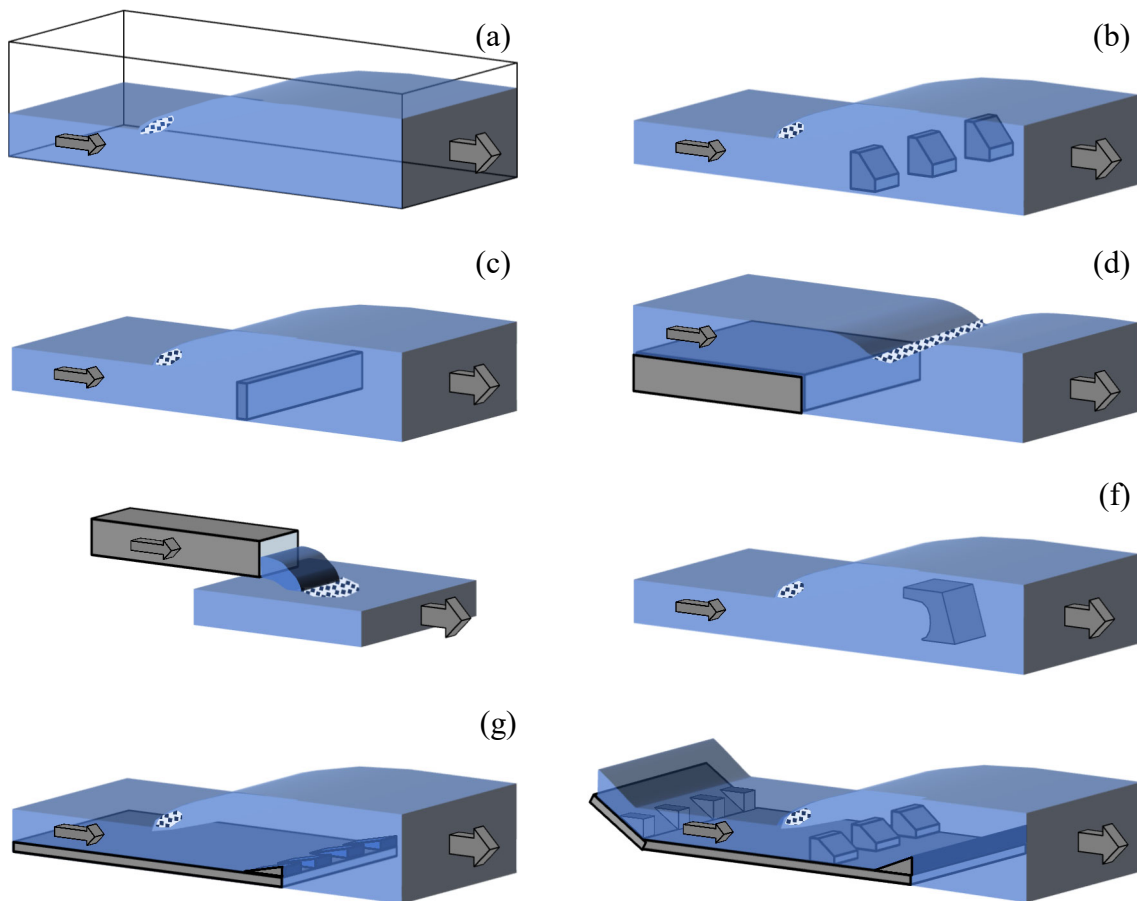
Figure 2.1 Examples of energy dissipation structures, including: (a) free hydraulic jump, (b) baffles, (c) sills, (d) drops, (e) plunge basins, (f) counterflow mechanisms, (g) flip buckets, and (h) design basins.

Free jumps are the simplest way to dissipate energy. An apron is usually required to prevent erosion of the bed beneath a jump. When an apron is required to prevent erosion, it is important

to keep the jump situated above the apron. With free jumps there is a lack of control of when and where the jump forms because the formation of the jump is dependent on downstream conditions. Most energy dissipation methods make use of hydraulic jumps to dissipate energy but utilize additional devices to stabilize the position of the jump and to guarantee its formation.

Baffles are one of the most commonly found energy dissipation methods. When high energy flow impacts baffles, the baffles have three effects. First, they directly dissipate flow energy by creating friction. Second, they redirect the flow into other flow streams to create shear, thereby dissipating additional energy. Finally, they reduce the overall velocity of the flow, which can induce the immediate formation of a hydraulic jump.

Sills function similar to baffles. Unlike baffles, however, the flow cannot go around a sill. Thus, sills require the flow to travel up and over the sill. One primary function of a sill is to induce hydraulic jump formation by absorbing some of the initial energy and driving the water surface upward towards a sequent depth. In stormwater systems, sills generally require weep holes to allow water to drain when there is little or no flow in the structure. This reduces ice damage in the winter and stagnant pools in the summer.

Drops dissipate energy primarily by impact and flow recirculation. Entrained air may also help to indirectly dissipate energy. Plunge basins function in a similar manner. The primary difference is that drops usually have a non-erodible bed, whereas plunge basins use deep pools so that shear stresses between the plunging jet and the water pool dissipate the energy. Plunge basins can be undesirable for ephemeral flows because the pool is stagnant when it is not in use.

Counterflow devices are designed to change the flow direction so that turbulence and shear in the flow dissipates most of the energy. Passive counterflow devices are similar to baffles, but are shaped to deflect the flow instead of to impact the flow. Active counterflow methods include the use of water jets (as opposed to concrete structures) that are directed against the incoming flow to dissipate energy.

Flip buckets direct part of the flow upwards, helping with the formation of a hydraulic jump. The bed downstream of a flip bucket must be non-erodible or armored. Design basins make use of multiple mechanisms to dissipate energy. Most design basins are intended for two-dimensional open-channel flows.

Energy dissipation structures reduce flow energy in four ways: (1) direct impact and the shear that results from impingement on a solid surface, (2) inducing shear within a flow by causing part of the flow to travel in a different direction than another part of the flow, (3) entraining air (in combination with turbulent motion, two-phase gas liquid mixtures can absorb energy), and (4) inducing the formation of hydraulic jumps. Note that entraining air, in and of itself, does not

dissipate much energy (Vischer, 1995). However, the presence of the air in a highly turbulent flow can enhance energy absorption.

For the present research, one goal is to provide effective energy dissipation for circular culverts while minimizing the footprint of the energy dissipation structure. This goal makes it difficult to use any of the structures that require downstream pools such as plunge basins and flip buckets, which can require significant space. Furthermore, an uncontrolled jump is not very useful since downstream tailwater conditions cannot be controlled. The primary mechanisms that are likely the most useful for the present goal include baffles and impact structures, sills, and possibly some forms of passive counterflow structures. Drops could also prove useful, but only in conjunction with other methods since downstream tailwater conditions cannot be controlled.

In this literature review, a general description of the hydraulics of energy dissipation will precede a section by section introduction to dissipation structures deemed relevant to the present research. Specific dissipation structures that will be discussed include sills, weirs, drops, expansions, various types of baffle blocks and stilling basins.

2.2 Hydraulic Jumps – Rectangular Channels

Hydraulic jumps are one of the main flow mechanisms that contribute to energy dissipation. Due to their importance, hydraulic jumps are briefly discussed in this section. A hydraulic jump occurs when the free-surface of a supercritical open-channel flow (Froude No. > 1) rises abruptly to a subcritical (Froude No. < 1) depth. This occurs when the amount of kinetic energy dissipated by the supercritical flow cannot be sustained as the flow travels downstream. A hydraulic jump in a prismatic channel (a channel with uniform channel cross-section and slope) is defined as a classical hydraulic jump. Figure 2.2 shows a diagram of a classical hydraulic jump. The upstream and downstream flows have depths of d_1 and d_2, respectively. The point where flow depth starts to rise rapidly is called the jump toe. The reversed flow occurring in the developed zone is called a roller, and is a primary contributor to energy dissipation (Jesudhas et al., 2018). For stronger jumps, air entrainment by the roller helps dissipate energy.
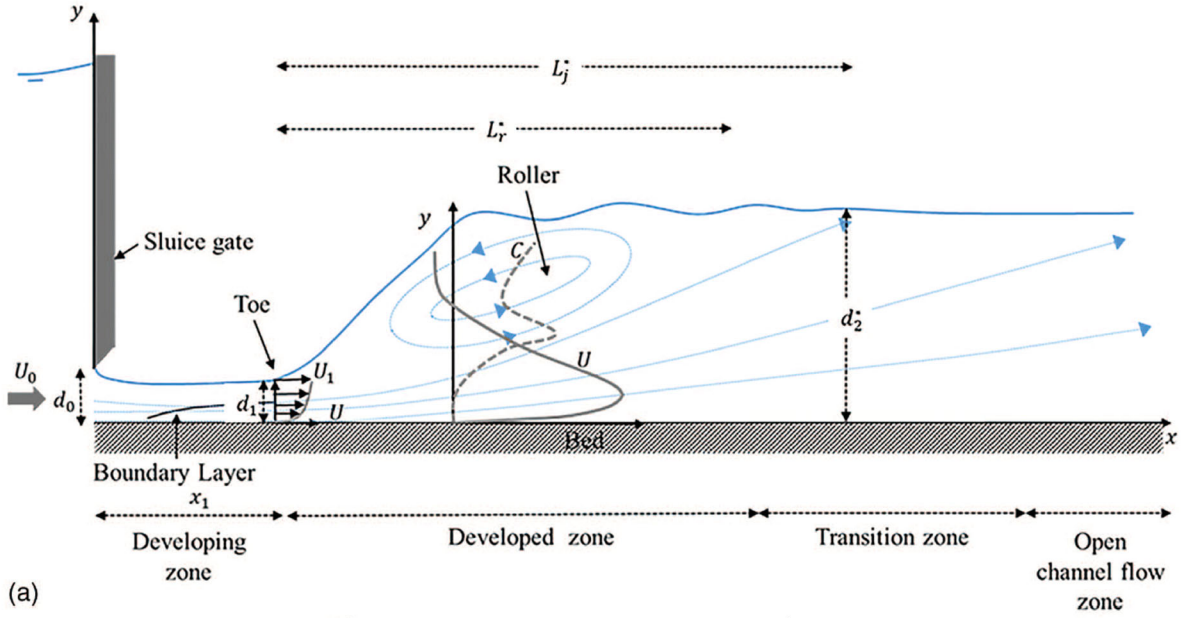
Figure 2.2 A classical hydraulic jump (after Jesudhas et al.,2018)

2.2.1 Sequent depths

The upstream and downstream flow depths (d_1 and d_2) of the hydraulic jump are called sequent depths or sometimes conjugate depths. For a horizontal, prismatic rectangular channel with negligible friction, the relation between sequent depths can be derived using conservation of specific force between the upstream and downstream sections:

$$\frac{Q^2}{gA_1} + \bar{z}_1 A_1 = \frac{Q^2}{gA_2} + \bar{z}_2 A_2 \tag{2.1}$$

Where $\bar{z}_1$ and $\bar{z}_2$ are centroids of the flow cross-sections at 1 and 2, A_1 and A_2 are cross sectional areas of the flow, Q is the discharge, and g is gravitational acceleration. The incoming velocity, V_1, can be computed as Q/A_1. For a prismatic rectangular channel, $\bar{z} = \frac{d}{2}$ and $A = by$.

Substituting $\bar{z}_1 = \frac{d_1}{2}$, $\bar{z}_2 = \frac{d_2}{2}$, $A_1 = b_1 d_1$, $A_2 = b_2 d_2$, and $Q = V_1 b d_1$ we get:

$$\frac{V_1^2 b^2 d_1^2}{gbd_1} + \frac{d_1^2 b}{2} = \frac{V_1^2 b^2 d_1^2}{gbd_2} + \frac{d_2^2 b}{2}$$

After simplifying,

$$\frac{V_1^2 d_1}{g} + d_1^2 = \frac{V_1^2 d_1^2}{gd_2} + \frac{d_2^2}{2}$$

7

This equation can be simplified using $Fr_1^2 = \frac{V_1^2}{gd_1}$, where Fr_1 is the incoming Froude Number, to get the equation:

$$\left(\frac{d_2}{d_1}\right)^3 - (2Fr_1^2 + 1) \cdot \frac{d_2}{d_1} + 2Fr_1^2 = 0$$

One of the roots of this cubic equation is the relationship between the sequent depths.

$$\frac{d_2}{d_1} = \frac{1}{2}(\sqrt{1 + 8Fr_1^2} - 1) \tag{2.2}$$

Equation 2.2 is called the Belanger equation. Using this equation, the downstream sequent depth can be calculated if the upstream depth (d_1), channel width (b), and discharge (Q) are known. A similar equation can be used to find the upstream sequent depth if downstream conditions are known.

2.2.2 <u>Length of the hydraulic jump roller</u>
The length of the roller (L_r) is defined as the distance from the jump toe to the end of the roller. Hager et al. (1990) developed equations for estimating the length of the roller in a classical hydraulic jump. The equations are as follows:

$$\lambda_r = -12 + 160 \tanh\left(\frac{Fr_1}{20}\right), \qquad \omega < 0.10 \tag{2.3a}$$

$$\lambda_r = -12 + 100 \tanh\left(\frac{Fr_1}{12.5}\right), \qquad 0.10 < \omega < 0.7 \tag{2.3b}$$

Where the relative length of the roller (λ_r) is given by $\lambda_r = \frac{L_r}{d_1}$ and the aspect ratio (ω) is found using $\omega = \frac{d_1}{b}$, in which b is the width of the channel. This set of equations can help with estimation of necessary apron lengths.

2.2.3 <u>Length of jump</u>
Peterka (1978) used 6 flumes identified as A through F to obtain a relationship between upstream Froude number (F_1) and the ratio of length of jump to the downstream depth ($\frac{L}{d_2}$). In his experiments, the length of the jump was measured from the front of the jump to a downstream point where either the high-velocity jet begins to leave the floor or to the point on the surface immediately downstream from the roller. His experimental results are shown by the data in Fig. 2.3. The widths of flumes A through F are 4.92 ft, 2.00 ft, 1.50 ft, 3.97 ft, 3.97 ft and 1.00 ft, respectively. Note that in the figure labels, D refers to the depth (d). The curve established by test data is labeled as "recommended" in the Figure. Peterka also shows the curves obtained by

8

three other groups. The curve obtained by Bakhmeteff and Matzke is labeled as curve one in the figure. It can be observed that up to $Fr_1 = 2.5$, the curve developed by Bakhmeteff and Matzke is consistent with Peterka's data. As Fr_1 increases further, the curve developed by Bakhmeteff and Matzke provides jump lengths that are much shorter than indicated by Peterka's data. In order to experimentally increase the upstream Froude number, the gate used to produce the supercritical flow must be lowered, reducing discharge and upstream depth. Peterka conjectured that in small flumes frictional resistance can become significant, resulting in jumps that are shorter than their equivalents in large flumes. Curve 4 obtained by Zurich laboratory and Curve 3 obtained by the Technical University of Berlin show the same trends as Peterka's curve but the predicted jump lengths are not in agreement with the data – especially the jump lengths predicted by Curve 3. Different criterion for measuring the length of the jump is the most likely reason for the discrepancies.
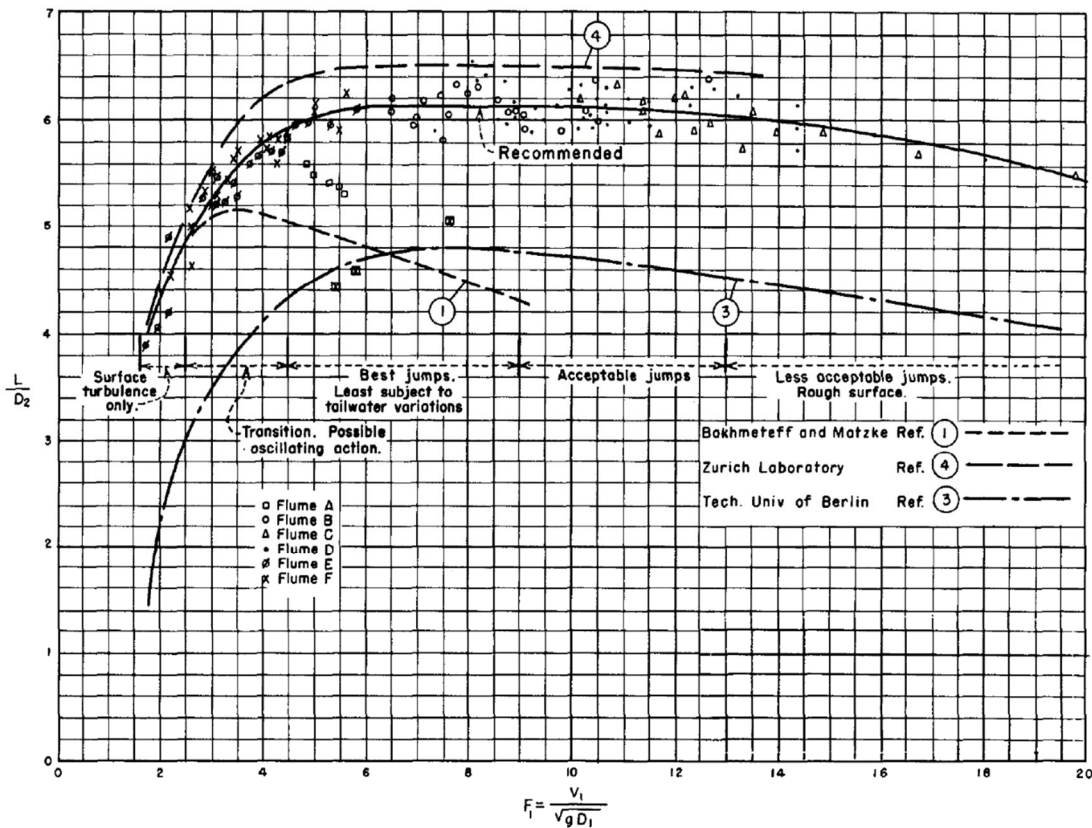
Figure 2.3 Relative jump length as a function of inlet Froude No. (Bradley and Peterka, 1957a)

A curve fit of the data collected by Bradley and Peterka (1957a) yields the relation between $\frac{L}{d_1}$ and Fr_1 as reported by Hagar (1992):

$$\frac{L}{d_1} = 220 \tanh\left(\frac{Fr_1 - 1}{22}\right) \tag{2.4}$$

9

Applying this to Equation 2.2 yields:

$$\frac{L}{d_2} = \frac{440 \tanh \left(\frac{Fr_1 - 1}{22} \right)}{-1 + \sqrt{1 + 8Fr_1^2}}$$ (2.5)

Equation 2.5 represents the recommended curve shown in Fig. 2.3.

2.2.4 <u>Energy loss and efficiency of a jump</u>
Chow (1959) used the difference of the specific energies (E) to derive an equation for energy loss of the jump:

$$\Delta E = E_1 - E_2 = \frac{(d_2 - d_1)^3}{4 d_1 d_2}$$ (2.6)

The efficiency of the jump is defined as the ratio of specific energy downstream of the jump to the specific energy upstream of the jump:

$$\frac{E_2}{E_1} = \frac{(8F_1^2 + 1)^{\frac{3}{2}} - 4F_1^2 + 1}{8F_1^2 (2 + F_1^2)}$$ (2.7)

This formula can be used to assess the ability of a jump to dissipate incoming energy. Similar formulas can be developed for dissipation structures to assess their efficiency.

2.2.5 <u>Hydraulic jump types</u>
Peterka (1978) classified hydraulic jumps into four distinct forms based on the inlet Froude number. As indicated in Figure 2.4A, for inlet Froude numbers ranging from 1.7 to 2.5, jumps are classified as pre-jumps. A pre-jump is also referred to as a weak jump by Chow (1959). A pre-jump has a smooth water surface and fairly uniform velocity distribution. The energy loss associated with pre-jumps is less than 20%. Jumps with inlet Froude numbers ranging from 2.5 to 4.5, as shown in Figure 2.4B, are referred to as transitional jumps. In a transitional jump, the incoming jet oscillates from the bottom to the surface over an irregular period. For this reason, a transitional jump is sometimes referred to as an oscillating jump (E.g., Chow, 1959; Chaudhry, 2007). The oscillation feature of the jet is indicated in the figure. This type of jump should be avoided to prevent damage to earth banks and riprap. Figure 2.4C depicts jumps resulting from inlet Froude numbers of 4.5 to 9.0. These jumps are referred to as good jumps (Peterka, 1978) or steady jumps (Chaudhry, 2007; Chow, 1959). Good jumps are least affected by tailwater variations. Peterka observed that the downstream extremity of the surface roller practically coincides with the point at which the high-velocity jet tends to leave the floor. The energy dissipation associated with good jumps ranges from 45%-70%. Finally, Figure 2.4D shows a strong jump condition where the inlet Froude number exceeds 9.0. The difference between sequent depths for this case is very large and the water surface is very rough. Slugs of water roll down the front face of the jump and fall into the high-velocity jet to generate additional waves downstream. The energy dissipation associated with strong jumps can be as high as 85%.
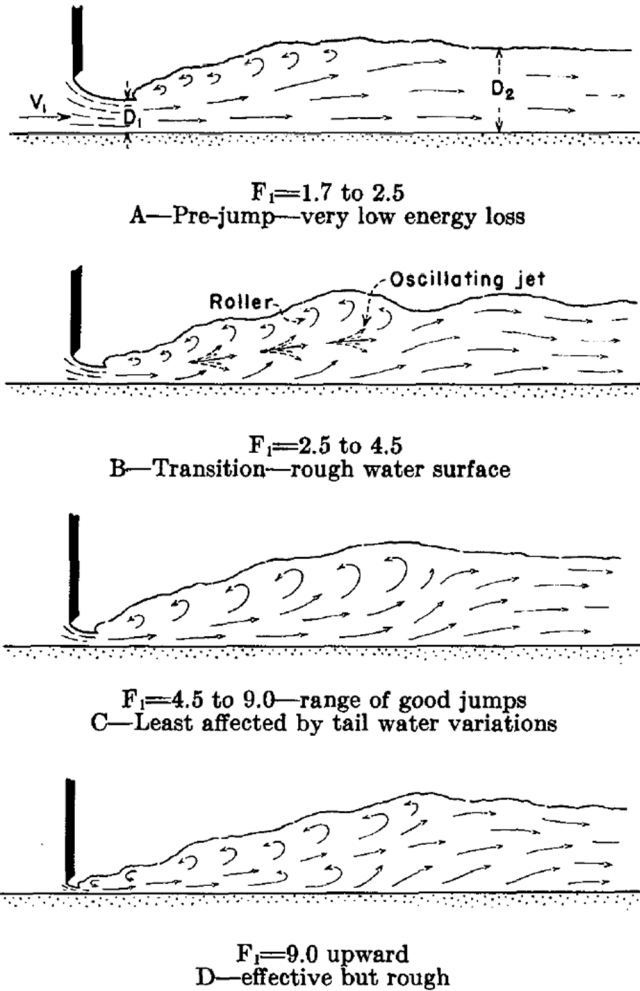
Figure 2.4 Jump types (after Peterka 1978)

2.3 Hydraulic Jumps – Circular Channels

Past research has mostly been applied to rectangular channels, but in the present research, circular channels are also of interest.

2.3.1 Critical Flow in Circular Channels

The Froude Number equals one when the velocity of the flow is equal to the velocity of a gravity wave in the flow. This condition defines the point at which a dynamic change to the flow can or cannot be felt upstream of where the change occurs. Since important changes in an open channel flow are transmitted upstream and downstream in the form of gravity waves, if the velocity of the flow is greater than the velocity of a gravity wave, flow changes cannot be transmitted upstream. Such a flow is referred to as a supercritical flow and has a Froude Number that is greater than one.

To better understand critical flow, we introduce flow energy relative to the bed of the channel:

11

$$E = d + \alpha \frac{V^2}{2g} \tag{2.8}$$

In which E is the specific energy of the flow, d is flow depth, V is the bulk average velocity of the cross section (Q/A), g is gravitational acceleration, and α is the Coriolis coefficient. Q is the discharge in the channel and A is the cross section of the flow area. The Coriolis coefficient is needed because velocity is not evenly distributed across the cross-section, and parts of the flow with high velocity carry more energy than parts with low velocity in a nonlinear fashion. This coefficient is often assumed to be one, but is always greater than one (thought it may be only slightly higher than one in some cases).

Eq. 2.8 is only valid for open channel flow, and if the flow becomes closed channel, we must also consider the pressure head to determine the flow energy. In such a case, the flow energy becomes:

$$E = \frac{p}{\gamma} + \frac{D}{2} + \alpha \frac{V^2}{2g} \tag{2.9}$$

Where p is the average pressure in the cross section and D/2 is the elevation of the center of the channel above the bed (which for circular channels is half the diameter). For open channel flows, Eq. 2.8 can be rewritten in terms of the cross-sectional area of the flow:

$$E = d + \alpha \frac{Q^2}{2gA^2} \tag{2.10}$$

The change in energy with respect to a change in depth is then given by:

$$\frac{\mathrm{d}E}{\mathrm{d}d} = 1 + \frac{Q^2}{2gA^2}\frac{\mathrm{d}\alpha}{\mathrm{d}d} - \alpha\frac{Q^2}{gA^3}\frac{\mathrm{d}A}{\mathrm{d}d} \tag{2.11}$$

The Coriolis Coefficient, α, is often assumed to be a constant value of 1.0, and $\mathrm{d}\alpha/\mathrm{d}d$ is considered to be negligible. Then, as shown by Hagar (2010), Eq. 2.11 becomes:

$$\frac{\mathrm{d}E}{\mathrm{d}d} = 1 - \frac{Q^2}{gA^3}\frac{\mathrm{d}A}{\mathrm{d}d} \tag{2.12}$$

The minimum specific energy can be found by setting the derivative in Eq. 2.12 equal to 0. For this condition, the sum of the potential and kinetic energy is minimized. For depths that are less than this condition, kinetic energy is dominant, and for depths above this condition, potential energy is dominant. It can be shown that the condition coincides with a Froude Number equal to one. Since $1 - \mathrm{d}E/\mathrm{d}d$ is the square of the Froude Number (Hagar, 2010), a relation that provides A as a function of d will allow us to calculate the Froude Number quite readily. For rectangular channels, $A = Td$, where T is the top width of the channel. Therefore, for a rectangular channel, the Froude number is:

$$\sqrt{\frac{Q^2}{gA^3}\frac{dA}{dd}} = \sqrt{\frac{Q^2}{gT^3d^3}}\,T = \sqrt{\frac{Q^2}{gA^2d}} = \frac{Q/A}{\sqrt{gd}} \tag{2.13}$$

For a circular channel, the relation between A and d is much more complex; so much so, that Hagar (2010) suggests using an approximation for the cross-sectional area:

$$A = \frac{4}{3}\left(\frac{d}{D}\right)^{3/2}\left[1 - \frac{1}{4}\frac{d}{D} - \frac{4}{25}\left(\frac{d}{D}\right)^2\right]D^2 \tag{2.14}$$

Or

$$A = \left[\frac{4}{3}\left(\frac{d}{D}\right)^{3/2} - \frac{1}{3}\left(\frac{d}{D}\right)^{5/2} - \frac{16}{75}\left(\frac{d}{D}\right)^{7/2}\right]D^2 \tag{2.15}$$

Then

$$\frac{dA}{dd} = \left[\frac{2}{D}\left(\frac{d}{D}\right)^{1/2} - \frac{5}{6D}\left(\frac{d}{D}\right)^{3/2} - \frac{56}{75D}\left(\frac{d}{D}\right)^{5/2}\right]D^2 \tag{2.16}$$

Using the equation for the Froude number:

$$F = \sqrt{\frac{Q^2}{gA^3}\frac{dA}{dd}} = \sqrt{\frac{Q^2\left[2\left(\frac{d}{D}\right)^{1/2} - \frac{5}{6}\left(\frac{d}{D}\right)^{3/2} - \frac{56}{75}\left(\frac{d}{D}\right)^{5/2}\right]D}{g\left[\left[\frac{4}{3}\left(\frac{d}{D}\right)^{3/2} - \frac{1}{3}\left(\frac{d}{D}\right)^{5/2} - \frac{16}{75}\left(\frac{d}{D}\right)^{7/2}\right]D^2\right]^3}} \tag{2.17}$$

Which can be simplified to:

$$F = \frac{Q}{\sqrt{gD^5}}\sqrt{\frac{\left[2\left(\frac{d}{D}\right)^{1/2} - \frac{5}{6}\left(\frac{d}{D}\right)^{3/2} - \frac{56}{75}\left(\frac{d}{D}\right)^{5/2}\right]}{\left[\frac{4}{3}\left(\frac{d}{D}\right)^{3/2} - \frac{1}{3}\left(\frac{d}{D}\right)^{5/2} - \frac{16}{75}\left(\frac{d}{D}\right)^{7/2}\right]^3}} \tag{2.18}$$

Or, as shown by Hagar:

$$\left.F\middle/\frac{Q}{\sqrt{gD^5}}\right. = \frac{\frac{3}{4}\left(\frac{3}{2}\right)^{1/2}}{\left(\frac{d}{D}\right)^2}\sqrt{\frac{\left[1 - \frac{5}{12}\frac{d}{D} - \frac{28}{75}\left(\frac{d}{D}\right)^2\right]}{\left[1 - \frac{1}{4}\frac{d}{D} - \frac{4}{25}\left(\frac{d}{D}\right)^2\right]^3}} \tag{2.19}$$

As pointed out by Hagar (2010), Eq. 2.19 can be used to show that $\left.F\middle/\frac{Q}{\sqrt{gD^5}}\right. * \left(\frac{d}{D}\right)^2$ is close to unity for most values of d/D in a circular pipe cross section, such that Eq. 2.19 can be used to show that the Froude number in a circular cross section can be closely approximated as:

$$F \approx \frac{Q}{\sqrt{gD^5}}\left(\frac{D}{d}\right)^2 \approx \frac{Q}{\sqrt{gDd^4}} \tag{2.20}$$

According to Hagar (2010) Eq. 2.20 is within about 3.4% for most of the useful range of the pipe cross-section. This also assumes that α is 1 and that the area approximation given by Eq. 2.14 is exact. Nevertheless, Eq. 2.20 is a reasonable approximation. If α is nonzero and does not vary quickly with depth, Eq. 2.20 can be modified to be:

$$F \approx \frac{Q}{\sqrt{\frac{g}{\alpha}Dd^4}} \tag{2.21}$$

In the present research, Eq. 2.21 was not used to calculate Froude number. The more widely used equation: $F = \frac{V}{\sqrt{gD_h/\alpha}}$ was used, in which the characteristic length scale is D_h, the hydraulic depth in the culvert. While Eq. 2.21 may be more correct, calculated runout Froude numbers were similar to those calculated with Eq. 2.21 for the range of conditions tested (within about 10 to 20%).

2.3.2 Sequent Depths in Circular Channels

Based on the momentum equation, Stahl and Hagar (1999) found the sequent depth ratio to be

$$\frac{d_2}{d_1} = 1.16F_1^{0.85} \tag{2.22}$$

Where d_2 is the outlet depth of the jump, d_1 is the incoming supercritical flow depth, and F_1 is the inlet Froude number based on Eq. 2.20. There are a number of approximations that are required to arrive at Eq. 2.22, and some of them have significant error. Nonetheless, Eq. 2.22 provides a basis of comparison with experimental data. Stahl and Hagar collected 18 data points for a range of inlet Froude numbers and only for flows that were not choked (free surface flow at both the upstream and downstream sequent depths). When plotted, the data demonstrated that Eq. 2.22 slightly overpredicted the sequent depth ratio and that a more accurate equation was:

$$\frac{d_2}{d_1} = 1.00F_1^{0.9} \tag{2.23}$$

A nice characteristic of Eq. 2.23 is that for an incoming Froude number of one, the sequent depths are equal, as expected. As pointed out above, Eq. 2.23 works for free surface flows alone. Flows that have a free surface at the inlet and are choked at the outlet are more complex.

Lowe et al. (2011) also discuss sequent depths in circular channels as well as in other closed conduits of different shapes that are typical of culverts and sewers, including rectangular, circular, elliptical, and pipe arch. The results of Lowe et al. can be used to predict sequent depths associated with incoming Froude numbers or to assess when an incomplete jump might form because of the closed nature of the conduit.

2.4 Sills and Drops

Sills are walls across a channel that force the flow upwards. Forster and Skrinde (1950) discuss two types of sills: the sharp-crested weir and the abrupt rise. The sharp-crested weir is also described by HEC-14. The sharp-crested weir and the abrupt rise are described in more detail in the next two sections. Drops are sudden reductions in the bed elevation in the direction of flow and are described in section 2.4.3.

2.4.1 The sharp-crested weir

A sharp-crested weir (See Fig. 2.5) is a thin plate mounted perpendicular to the flow direction with a sharp, beveled edge at the top of the plate to make the nappe spring clear from the plate. (Chaudhry, 2007)
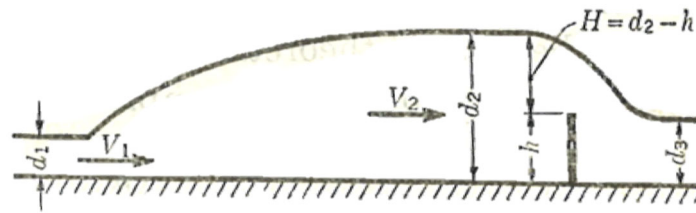
Figure 2.5 Geometry of a sharp-crested weir that forces an upstream jump (after Forster and Skrinde, 1950)

The height of a sharp-crested weir, h, which will cause formation of a hydraulic jump depends on V_1, d_1, g, d_3 and X, where V_1 and d_1 are the incoming velocity and depth of the upstream flow, g is the gravitational acceleration, d_3 is the depth downstream of the weir, and X is the distance from the jump toe to the weir. Thus:

$$h = f(V_1, d_1, g, d_3, X) \tag{2.24}$$

Based on these variables, dimensional analysis shows that $\frac{h}{d_1}$ is a function of $Fr_1, \frac{d_3}{d_1}$ and $\frac{X}{d_1}$. Theoretically, $\frac{X}{d_1}$ is considered a constant so it is eliminated in the equation. Tailwater does not affect the flow pattern as long as $d_3 < (d_2 - \frac{3}{4}h)$, in which case the term $\frac{d_3}{d_1}$ can also be eliminated. Thus, in the simplest form, $\frac{h}{d_1}$ is a function of Fr_1 alone:

$$\frac{h}{d_1} = f_1(Fr_1) \tag{2.25}$$

A theoretical relation between $\frac{h}{d_1}$ and Fr_1 (See *(a)* in Fig. 2.6) can be developed using the discharge equation for a weir:

$$q = C_1 C_2 C_3 \left(\frac{2}{3}\sqrt{2g}H^{2/3}\right) \tag{2.26}$$

15

In which q is the discharge per unit width of channel and C_1, C_2, and C_3 are correction coefficients. Using Fig. 2.6, it can be determined how high the weir must be in order to force a jump.
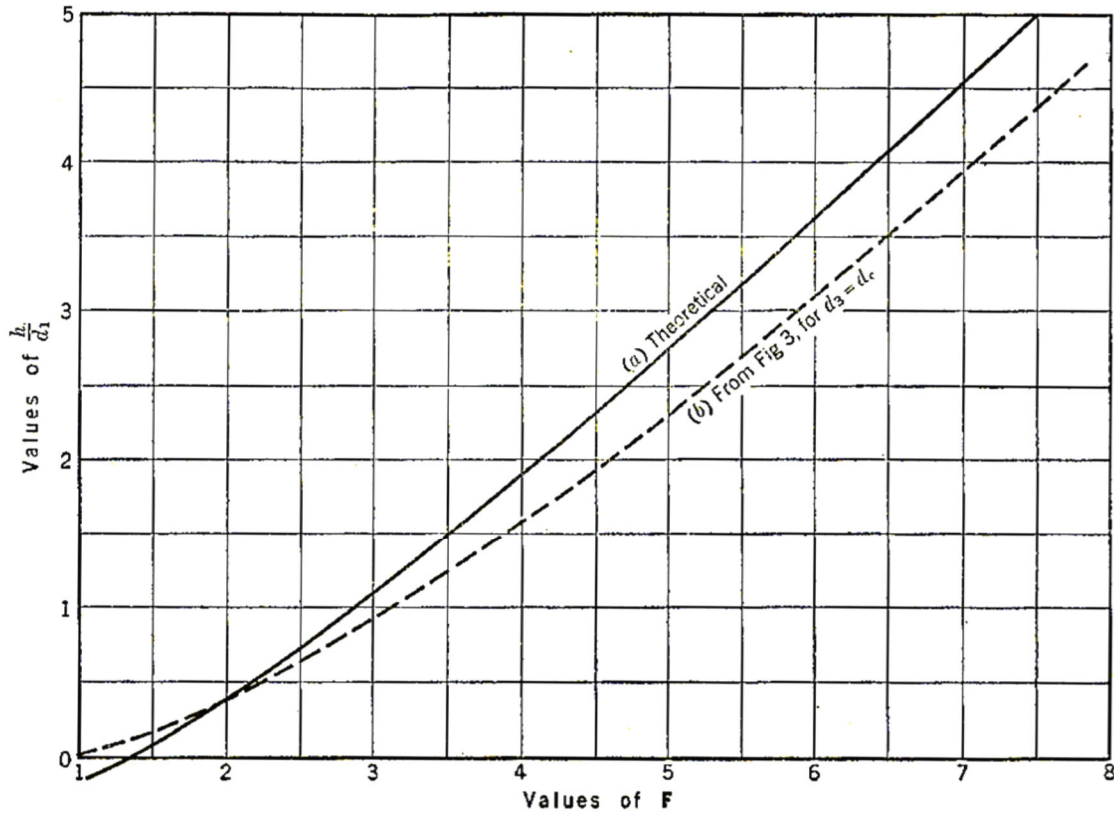
Figure 2.6 Variation of relative weir height with Fr (after Forster and Skrinde, 1950)

The experimental apparatus of Forster and Skrinde was designed such that incoming d_1 and V_1 could be controlled by adjusting an upstream sluice gate and regulating the flow rate. The downstream depth (d_3) was changed using a steel tailgate. Weir height h was adjusted by switching between brass plates of different sizes. Four values of h/d_1 were tested for several values of Fr_1. Water surface profiles were recorded. It was observed that for a constant h/d_1 setup, as the Froude number increased, the toe of the jump moved closer towards the weir. By interpolation, the Fr_1 values for X/d_2 of 3,5, and 10 were obtained for each h/d_1 setup and are shown in Fig. 2.7.
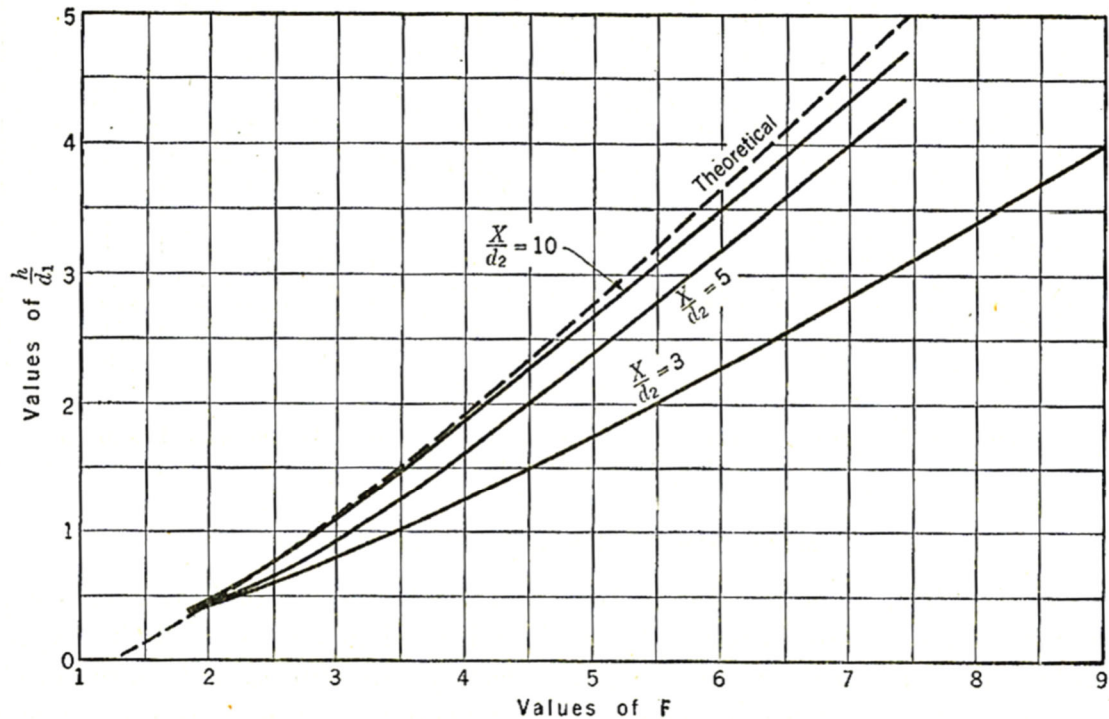
Figure 2.7 Experimental variation of relative weir height with Fr₁ (after Forster and Skrinde, 1950)

The discrepancy between the theoretical curve and the three experimental curves is due to the nonuniformity of the velocity distribution just upstream of the weir. As X/d_2 increases, and hence X increases, the velocity approaches closer to uniformity and the theoretical assumption is more accurate.

Fig. 2.7 is useful for evaluating the effectiveness of existing sharp-crested weirs as well as for design purposes. For an existing weir, the current operating point can be determined on the graph after calculating *Fr₁* and *h/d₁*. If the point lies above the curves, the value of h/d_1 is too high so the weir is too high. In this case, the hydraulic jump is forced upstream and will possibly lead to a drowned jump. For design purposes, it is suggested that the experimental curve $X/d_2 = 5$ be used under maximum discharge conditions.

2.4.2 The abrupt rise

An abrupt rise is a sudden rise in the elevation of the bed (see Fig. 2.8). The rise of the bed can force a hydraulic jump.
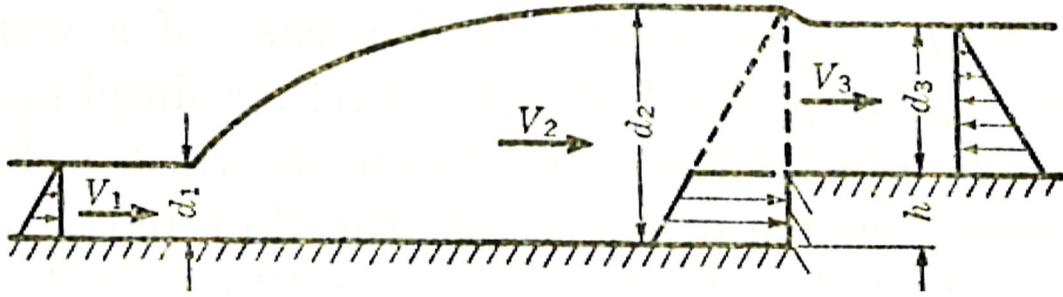
Figure 2.8 Geometry of an abrupt rise (after Forster and Skrinde, 1950)

As shown in the dimensional analysis in the sharp-crested weir case, $\frac{h}{d_1}$ is a function of Fr_1, $\frac{d_3}{d_1}$ and $\frac{X}{d_1}$. Unlike the sharp-crested weir case where the tailwater depth does not affect the flow pattern for an unsubmerged weir, the flow pattern is affected by tailwater for all conditions in an abrupt rise. Thus, the term $\frac{d_3}{d_1}$ cannot be eliminated:

$$\frac{h}{d_1} = f_2(Fr_1, \frac{d_3}{d_1}) \tag{2.27}$$

The theoretical equation for the function can be derived using the momentum equation and the continuity equation. The momentum equation at d_2 and d_3 is:

$$\Sigma F = P_1 - P_2 - F_{rise} = \rho q(V_3 - V_2) \tag{2.28}$$

$$\frac{\gamma d_2^2}{2} - \frac{\gamma d_3^2}{2} - \frac{\gamma h}{2}(2d_2 - h) = \rho q(V_3 - V_2) \tag{2.29}$$

Where P_1 and P_2 are unit pressure forces acting on the faces of the control volume between 2 and 3, and F_{rise} is the force per unit width exerted by the abrupt rise to the control volume.

Combining with the continuity equation $V_1 d_1 = V_2 d_2 = V_3 d_3$ and eliminating $d_2, V_2,$ and V_3 gives:

$$\left(\frac{d_3}{d_1}\right)^2 = 1 + 2Fr_1^2\left(1 - \frac{1}{\frac{d_3}{d_1}}\right) + \frac{h}{d_1}\left(\frac{h}{d_1} - \sqrt{1 + 8Fr_1^2} + 1\right) \tag{2.30}$$

A curve can be determined for each value of $\frac{h}{d_1}$ as shown in Fig. 2.9.

18
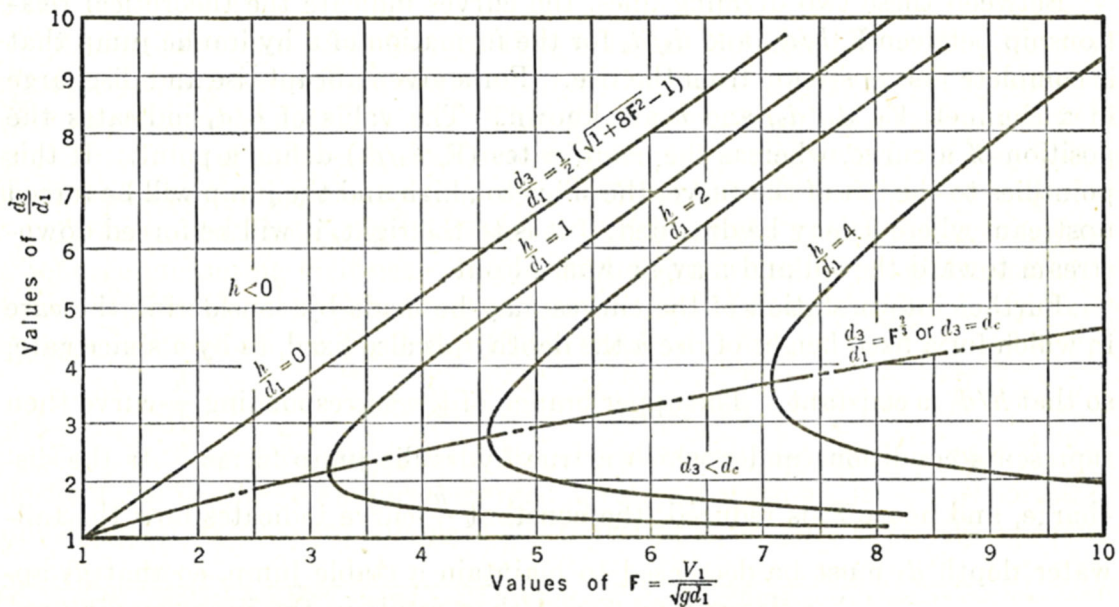
Figure 2.9 Theoretical variation of relative tailwater depth with Fr₁ (after Forster and Skrinde, 1950)

For the experiment, the distance from the jump toe to the rise was maintained to provide sufficient distance for the jump to complete before the rise. For each run, h/d_1 and Fr_1 were fixed. The tailgate was then adjusted to achieve $X = 5(h + d_3)$. The resulting experimental data plots are shown in Fig. 2.10.
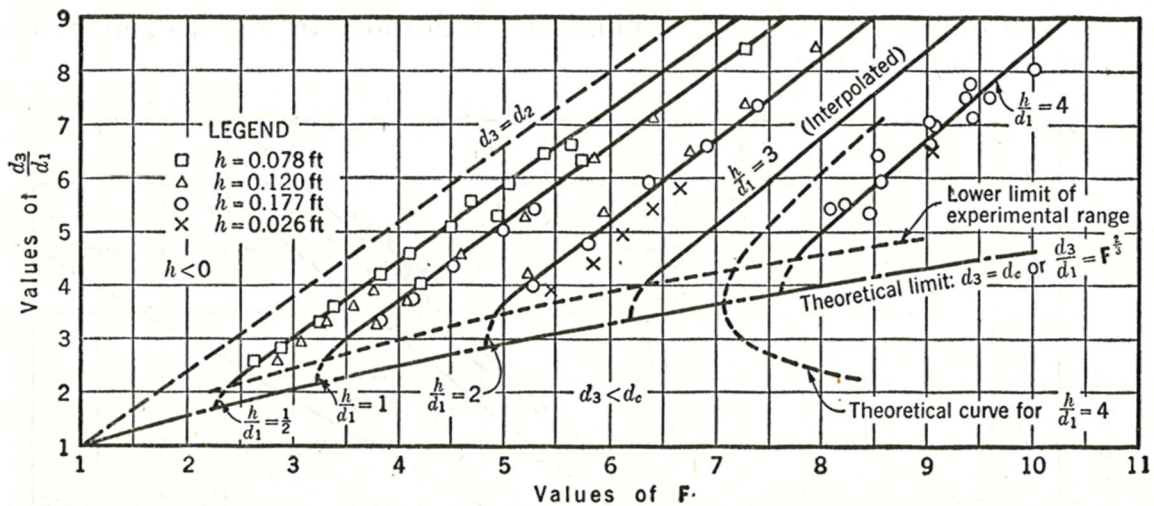
Figure 2.10 Experimental variation of relative tailwater depth with Fr₁ (after Forster and Skrinde, 1950)

19

All of the experimental curves are shifted to the right of the corresponding theoretical curve. It is observed that as h/d₁ increases, the discrepancy between experimental and theoretical curves increases. The discrepancy is due to the nonuniformity of the velocity at the rise. If the experiment is performed in a way such that c>5 where $X = c(h + d_3)$, the discrepancy decreases because longer jump lengths (X) allow the velocity distribution to become more uniform.

Like the experimental curves for the weir shown in Fig. 2.7, Fig. 2.10 is useful for both evaluation of existing structures and for design. For evaluation purposes, if a point lies above the line $d_3 = d_2$, then even a drop can maintain a hydraulic jump without the need for a rise, and a rise only encourages drowning of the jump. If a point lies between the line $d_3 = d_2$, and $d_3 = d_c$, then the Froude number and d₃/d₁ values can be plotted on the graph to determine the rise height necessary to cause a jump without drowning. For this case, if the rise height h is known and a point lies above the h/d_1 curve, then the rise is higher than it needs to be to force a jump. Likewise, for a given rise height, if a point lies below the h/d_1 curve, then the rise is too low to force a jump. If a point plotted in Figure 2.10 lies below $d_3 = d_c$, the downstream flow remains supercritical and no hydraulic jump will form.

2.4.3 Drop structures
Drop structures are used in locations where the downstream depth is higher than the sequent depth for a normal drop (Chow, 1959). In this case, the drop structure absorbs additional energy that a hydraulic jump cannot absorb.

A straight drop structure consists of an abrupt vertical drop. Fig 2.11 shows the geometry of a straight drop structure. When the upstream flow reaches the drop, a free-falling nappe is formed. After the jet hits the bed, the flow becomes supercritical. A hydraulic jump forms downstream. Here, q is the discharge per unit width for the flow, y_1 is the depth upstream of the jump, y_2 is the tailwater depth downstream of the jump, y_p is the depth of the water pool behind the jet, h is the height of the drop, and L_d is the distance from the drop to the beginning of the jump.
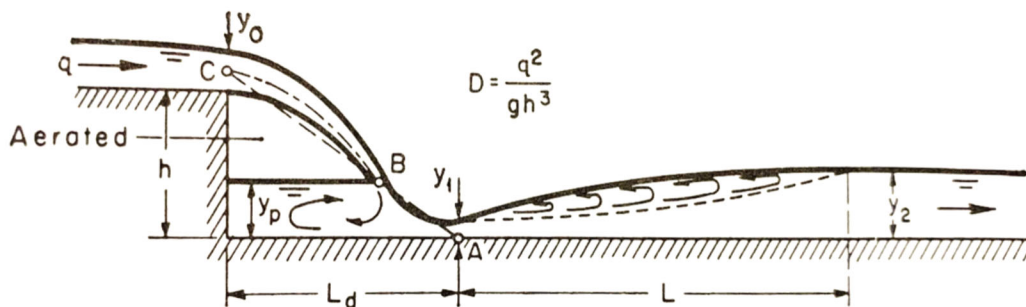
Figure 2.11 Geometry of a straight drop structure (after Chow 1959)

The straight drop flow geometries, namely h, L_d, y_1 and y_2, are functions of the drop number (D):

$$D = \frac{q^2}{gh^3} \qquad (2.31)$$

Where g is the acceleration of gravity. The following geometric relations are also applicable:

$$\frac{L_d}{h} = 4.30D^{0.27} \qquad (2.32a)$$

$$\frac{y_p}{h} = 1.00D^{0.22} \qquad (2.32b)$$

$$\frac{L_1}{h} = 0.54D^{0.425} \qquad (2.32c)$$

$$\frac{y_2}{h} = 1.66D^{0.27} \qquad (2.32d)$$

2.4.4 Vertical drop followed by a rectangular weir

Larson (2004) proposed a vertical drop structure followed by a rectangular weir for dissipating flow energy (Fig. 2.12). Here, the drop depth is h_d, the distance from the drop to the weir is L_d, the weir height is h_w. y_1 is the approach flow depth, y_2 is the flow depth just upstream of the weir and y_3 is the downstream flow depth.
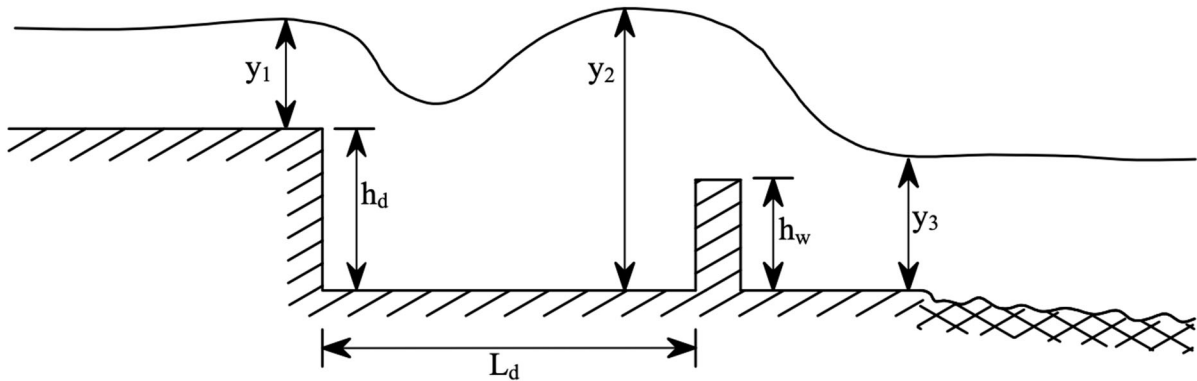
Figure 2.12 Vertical drop followed by rectangular weir (after Larson, 2004)

Larson plotted outlet flow depth against the outlet Froude number and found a relation between them. The plot is shown in Figure 2.13. A weir height, h_w, can be determined from Fig. 2.13 using measured outlet conditions.
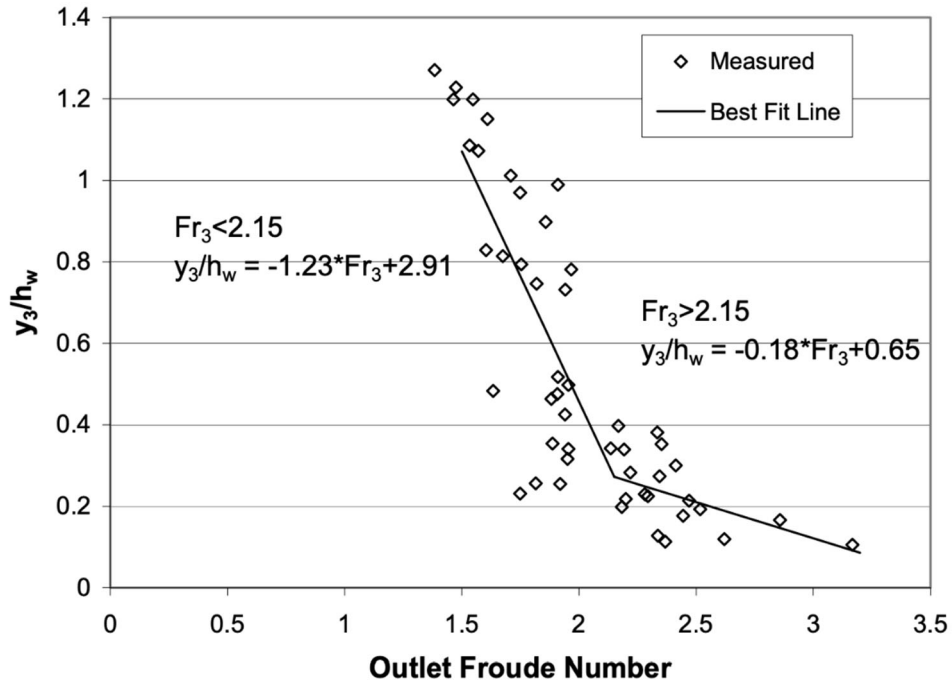
Figure 2.13 Relationship of outlet depth to outlet flow conditions for a drop/weir combination

The distance from the drop to the weir, L_d, is determined using the equation $L_d = 6(y_c + h_w)$. A drop height, h_d, can be found from the fitted curve shown in Fig. 2.14.
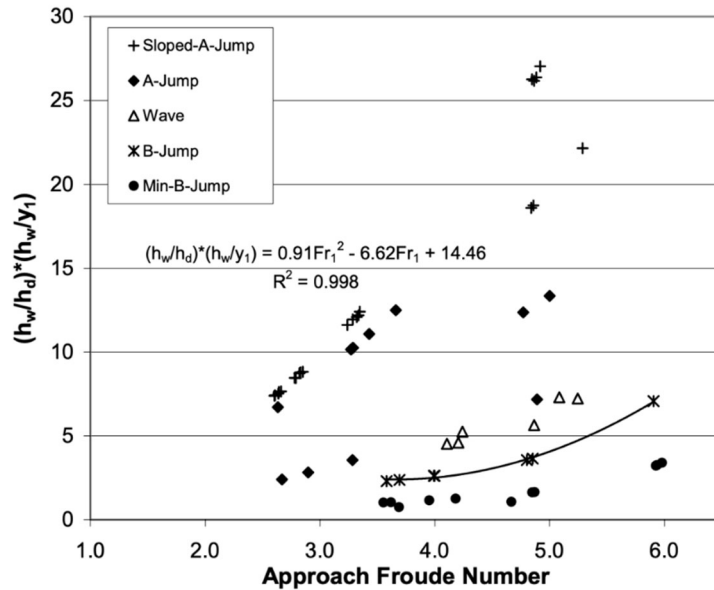
Figure 2.14 Hydraulic jump geometry (after Larson 2004)

2.5 Baffle Blocks

Baffle blocks are identical crenellated elements arranged in rows that are perpendicular to the direction of flow. They are often placed near the toe of a jump, serving as impact elements to shorten the length of a stilling basin and to reduce tailwater depth (Hager 1992). HEC-14 has incorporated baffle blocks in many basin designs, for example Basin II and III designs include baffle blocks. These designs are further discussed in section 2.7.

Baffle blocks are similar to sills except that flow is forced around as well as over the blocks. According to Hagar (1992), while they are considered to be better than sills, they are more expensive to construct. Figure 2.15 shows a typical sill arrangement.
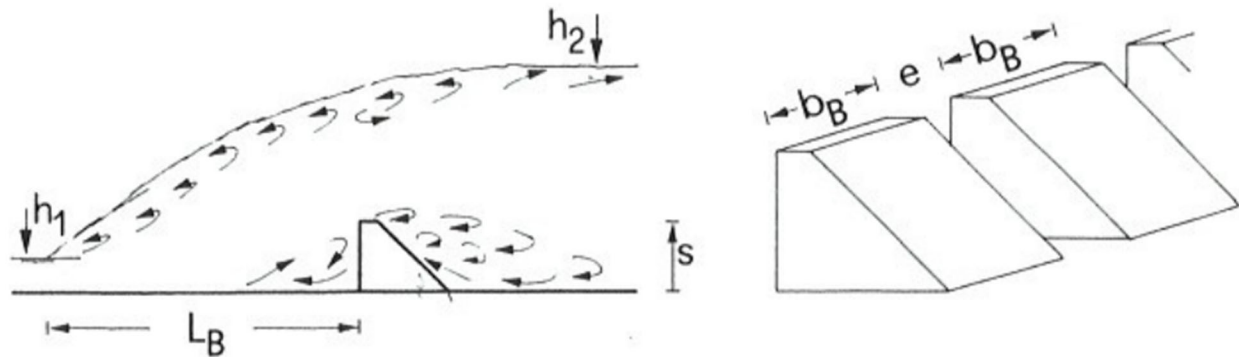
Figure 2.15 Flow over and around sills (Hagar, 1992)

Rand (1996, 1970) conducted experiments with one row of baffle blocks (see Fig. 2.16). In the experiment, baffle block geometry was defined based on the height of the block (s), width of the block perpendicular to the flow (W), and spacing between blocks (E). The blocks were spaced in a way such that the width of the block was equal to the spacing ($W = E$). The blockage (E_b) was defined as follows, and a blockage value of 0.5 is used:

$$E_b = \frac{W}{E + W} \tag{2.33}$$

In Fig. 2.16, D_1 is the depth of the supercritical flow entering at section A, D is the depth of tail water, L_t is the total transition length, and L_S is the distance from the entrance section at A to the baffle blocks.
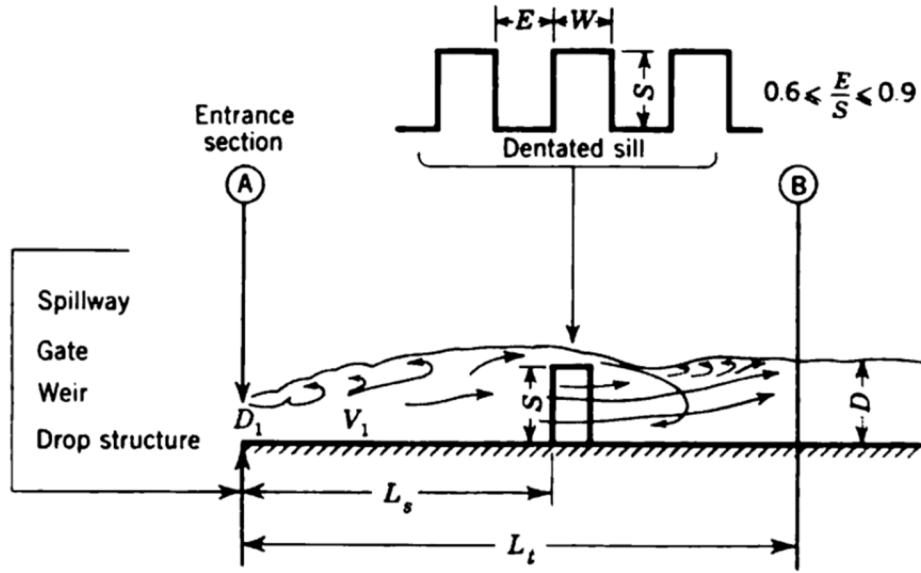
Figure 2.16. Flow over one row of baffle blocks (dentated sill) (after Rand 1966)

Tailwater reduction(ΔY_B) is a parameter corresponding to the effect of baffle blocks on tailwater reduction:

$$Y = Y^* - \Delta Y_B \tag{2.34}$$

Where $Y = D/D_1$ is the sequent depths ratio with the baffle blocks and $Y^* = D_2/D_1$ is the sequent depths ratio of a classical hydraulic jump, with D_2 being the subcritical classical hydraulic jump conjugate depth.

Rand (1966) found that the reduction of tailwater is a function of the relative height of blocks $S = s/D_1$:

$$\begin{aligned}\Delta Y_B &= 0.67S^{0.62} \quad , k = 0; \\ \Delta Y_B &= 0.09S \quad , 0.1 < k < 1;\end{aligned} \tag{2.35}$$

Where k, the position parameter, is defined as $k = \dfrac{L_B - L_{min}}{L_{max} - L_{min}}$ with L_B being the hydraulic jump toe position and L_{min}, L_{max} being the minimum and maximum positions of the hydraulic jump toe.

For shortening the length of the basin, Rand (1966) found that the total transition length with baffle blocks is shorter than the length of a classical hydraulic jump only at very low k values (when the toe of the jump is close to the baffle block). In Figure 2.17, the dotted line represents a classical hydraulic jump. It is observed from the figure that only when k<0.2 do the baffle blocks have basin shortening effect.

24
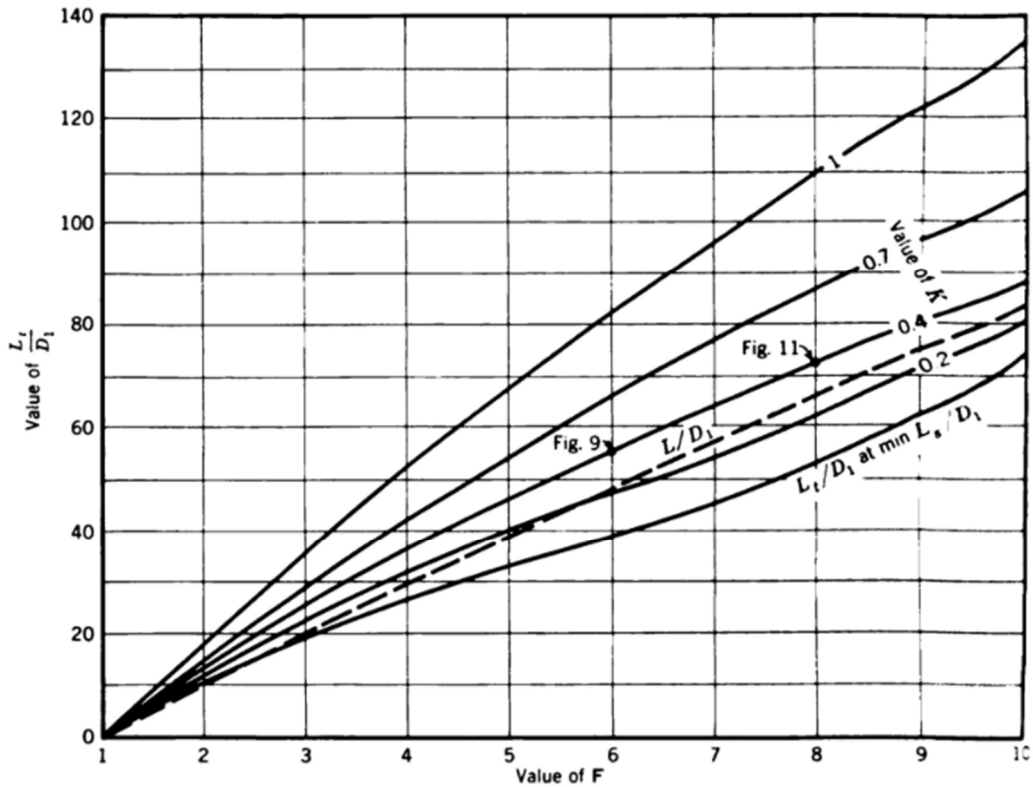
Figure 2.17. Length of Baffle block stilling basin (after Rand 1966)

Geometrically, Bradley and Paterka (1957b) and Hagar (1992) suggest that a vertical front face is best and that a sloped backside is better than vertical for downstream flow development. Sharp corners on the fronts of baffle blocks help dissipate energy. In the present research, these are considerations for design of the staggered weir, which is in some ways similar to two rows of baffle blocks. Bradley and Paterka (1957b) tested numerous baffle block shapes. The most effective baffle block shape that could be easily constructed consisted of a flat vertical front face with a sloping back face. They also tested a curved front face with sharp side corners that was quite effective for a variety of inflows, but it was more difficult to construct. The optimal block height has been found to be about 1.5 times the inflow depth. Rajaratnam (1964) found that about 50% flow blockage allows the baffle blocks to perform optimally (a sill has 100% flow blockage). When multiple rows of baffle blocks are installed, it is the first row that does the most energy dissipation.

In general, baffle blocks are not recommended for water velocities of higher than about 20 m/s without special design consideration of the blocks. Otherwise, cavitation can lead to their destruction.

2.6 Channel Expansions

In general, diverging channels result in energy loss. Energy dissipation is enhanced by channel expansions; that is, transitions from smaller to larger cross sections. An abrupt expansion and a tapered expansion are shown in Figure 2.18. In subcritical channels, Sturm (2010) gives the head loss (h_L) due to an expansion as:

$$h_L = K_L \left| \frac{1}{A_2^2} - \frac{1}{A_1^2} \right| \frac{Q^2}{2g}$$

(2.36)

In which A_1 and A_2 are the cross-sectional areas upstream and downstream of the expansion, respectively, Q is the discharge, and K_L is a head loss coefficient. Sturm says that an abrupt expansion dissipates the most energy. This occurs because of flow separation that occurs downstream of the expansion, as depicted in Figure 2.18a. Viscous dissipation within the separation zone reduces flow energy significantly.
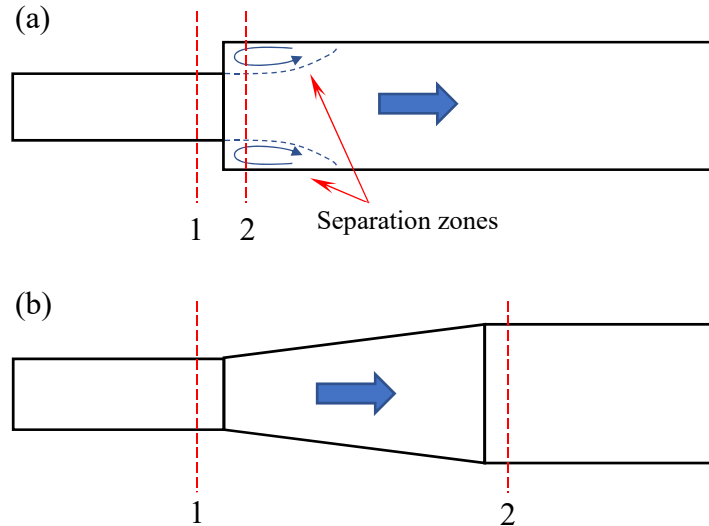
Figure 2.18 Plan views of channel expansions: (a) abrupt expansion and (b) tapered expansion.

For an abrupt expansion in a rectangular channel with a fixed bed elevation and an inlet Froude number less than 0.5, the loss coefficient increases as the ratio of the downstream area to the upstream area (A_2/A_1) increases, with a maximum value of one for an infinitely wide outlet. If the outlet is tapered, as shown in Figure 2.18b, the loss coefficient may be significantly lower than for an abrupt expansion, depending on the angle of expansion.

In an expansion, when a sub- or supercritical flow enters the tailwater channel, the flow will expand until it occupies the full width of the channel. Bremen (1990) and Bremen and Hager (1993) discuss three types of jumps in a sudden expanding channel based on the location of the jump toe: R-jump, S-jump and T-jump.

Fig. 2.19a shows an R-jump (or repelled hydraulic jump). An R-jump is a hydraulic jump for which the toe of the jump is located downstream of the expansion at point P. The point of impingement (P) is shown in Fig. 2.19a. The front of the jump is linear at the center portion and oblique at the sides. As the tailwater rises and the outer two fronts approach point P, the R- jump breaks down and a cyclic phenomenon appears.

Fig. 2.19(b) shows an S-jump (or spatial hydraulic jump). As mentioned above, a cyclic phenomenon may appear after the tailwater rises beyond the limits of an R-jump. This cyclic behavior includes oscillation of the water current from side to side within the expansion. The flow in an S-jump is highly non-uniform. Poor mixing is observed since the incoming flow does not expand very much in the tailwater channel. Bremen described the pattern as a surface jet rather than a jump.

Fig. 2.19(c) shows a T- jump (or transitional hydraulic jump). When the tailwater rises beyond that required for an S-jump, the toe of the jump moves upstream into the approaching channel. A T- jump is a hydraulic for which the toe of the jump is located at the approaching channel. As the toe moves upstream, backward flow and jump asymmetry decreases to show more resemblance to a classical hydraulic jump.
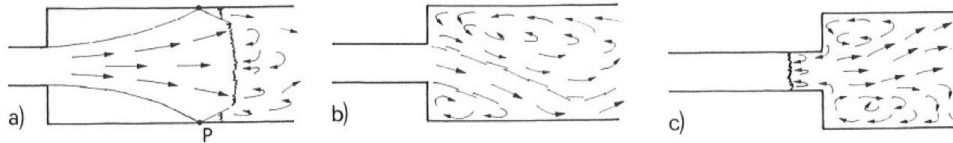
Figure 2.19 types of jump in a sudden expansion channel (after Hagar 1992)

The parameter Ψ is defined in Breman's work:

$$\Psi = \frac{Y^* - Y}{Y^* - 1} \tag{2.37}$$

where Y* is the sequent depth ratio for a classical jump and Y is the sequent depth ratio for the expansion.

Ψ depends on the expansion ratio and the toe position parameter:

$$\Psi = \Psi(B, X_1) = \left(1 - \frac{1}{\sqrt{B}}\right) * [1 - \tanh(1.9X_1)] \tag{2.38}$$

Here, the expansion ratio (B) is defined as the ratio of the width of tailwater channel and the approaching channel. The toe position parameter is $X_1 = \frac{x_1}{L_r^*}$, where x_1 is the distance from the jump toe to the expansion section and L_r^* is the length of roller of the classical jump. From Eq.

2.38 it can be observed that as the tailwater increases, the toe of the jump moves upstream from the expansion section.

2.7 Design Stilling Basins

2.7.1 Introduction to stilling basins

In this section, five stilling basins are discussed: Types II, III, IV, and VI proposed by Peterka (1978) and the Saint Anthony Falls basin (SAF) described in HEC-14 (2006). In general, stilling basins are complex combinations of baffles, sills, flip buckets and other energy dissipation elements. The stilling basins described here have been tested extensively and have been widely used in the field. Most of them have been designed with large flows in mind and require significant space, but they give a broader idea of the different combinations of elements that can lead to effective energy dissipation.

2.7.1.1 Type II basin

In Section 2 of Hydraulic Design of Stilling Basins and Energy Dissipators, Peterka (1978) recommends stilling basins for high dams, earth dam spillways and large canal structures. Peterka suggests a basin which is effective for incoming flow Froude numbers of 4 and greater called a Type II basin. (see Fig. 2.20) This type of basin consists of chute blocks and a dentated sill for dissipating energy. The chute blocks are placed at the end of the chute for the purpose of disrupting the jet to form energy dissipating eddies and thus decrease the length of the hydraulic jump. For choosing the size of the chute blocks, it is recommended that the height, width and spacing should equal the depth of incoming flow, D_1. A dentated sill is recommended at the end of the apron. For choosing the size of the dentated sill, it is recommended that the height of the sill be equal to $0.2D_2$ and the spacing and width of the blocks equal to $0.15D_2$, where D_2 is the sequent tailwater depth. Although intermediate baffle piers are used in some existing basins, Peterka does not recommend their use.
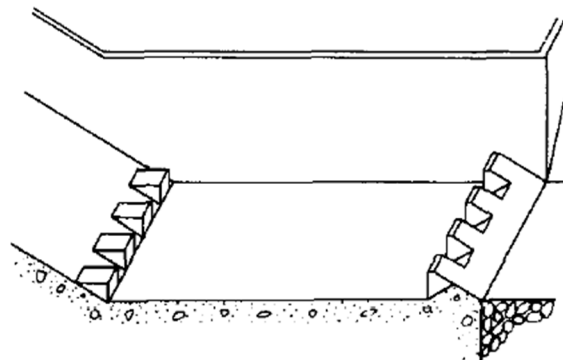
Figure 2.20 Type II Basin (after Peterka 1978)

28

2.7.1.2 Type III basin

In Section 3 of Hydraulic Design of Stilling Basins and Energy Dissipators, Peterka (1978) presents short stilling basins for canal structures, small outlet works, and small spillways Peterka suggests a Type III basin for moderate or low upstream velocities (Fig. 2.21) The maximum velocity of the incoming flow for this type of basin should be 50-60 ft/sec with a discharge per unit width of less than 200 ft^2/sec. A Type III basin consists of chute blocks at the end of the chute to stabilize the jump, baffle piers in the middle of the apron for primary energy dissipation and an end sill at the end of the apron for scour control.
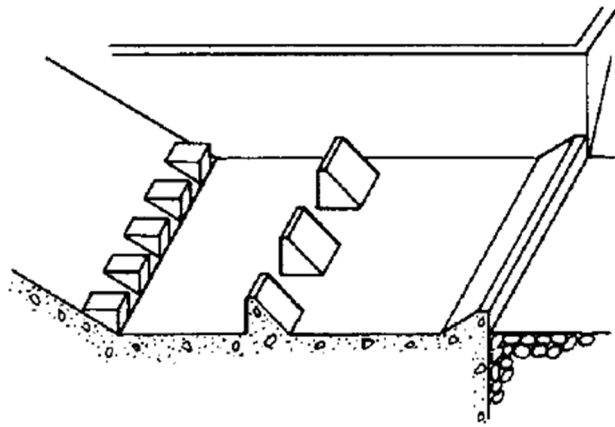
Figure 2.21 Type III Basin (after Peterka 1978)

2.7.1.3 Type IV basin

In Section 4 of Hydraulic Design of Stilling Basins and Energy Dissipators, Peterka (1978) presents a stilling basin for canal structures, outlet works and diversion dams. Peterka suggests using a Type IV basin for Froude numbers between 2.5 and 4.5. As discussed earlier in 2.2.5, the jumps in this Froude number range are transitional and have oscillating jets. The oscillating jets create destructive waves that damage downstream structures. Thus, the main purpose of this type of stilling basin for transitional jumps is to suppress the waves. Peterka designed the Type IV basin in a way such that the waves were suppressed at the source. Deflector blocks placed on the chute direct the jets into the roller and strengthen them. (see Fig. 2.22). The deflector blocks have a recommended width of $0.75D_1$, spacing of $1.875D_1$, and horizontal top length of at least $2D_1$, where D_1 is the upstream flow depth. The slope of the upper surface of the block should be 5 degrees in the downstream direction.
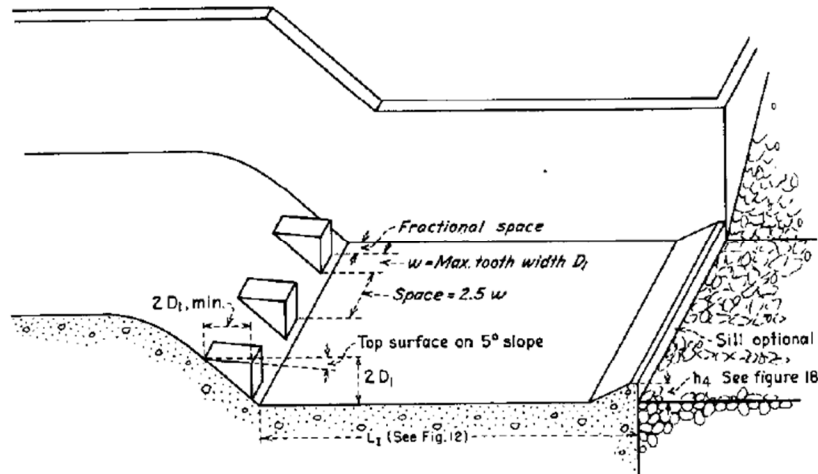
Figure 2.22 Type IV Basin (after Peterka 1978)

2.7.1.4 Type VI basin

In Section 6 of Hydraulic Design of Stilling Basins and Energy Dissipators, Peterka (1978) presents a stilling basin for pipe or open channel outlets. The Type VI basin is designed for low inlet velocities of up to 30 ft/sec and discharges of up to 339 ft^3/sec (see Fig. 2.23). This impact-type energy dissipator consists of an inlet pipe, a stilling basin with a vertical hanging baffle, an alternate end sill, and 45-degree side walls at the outlet.

The advantages of the Type VI basin are as follows. First, the vertical hanging baffle provides greater energy dissipation than a hydraulic jump does by creating vertical eddies as the flow strikes the baffle. Second, although there is an upper limit of the design discharge for Type VI basins, multiple units can be constructed in parallel to accommodate the need for discharges exceeding the upper limit. Third, the vertical hanging baffle simplifies the analysis and design process. Independent of upstream flow conditions (different depths and velocities in the supply pipe, different pipe sizes, or even the use of an open channel instead of a pipe), the flow exiting the structure will have nearly the same behavior, dependent only on the flow rate. Fourth, notches added to the baffle for self-cleaning purposes reduce sediment clogging in the basin as the sediment will be removed by concentrated jets created by the notches.

30
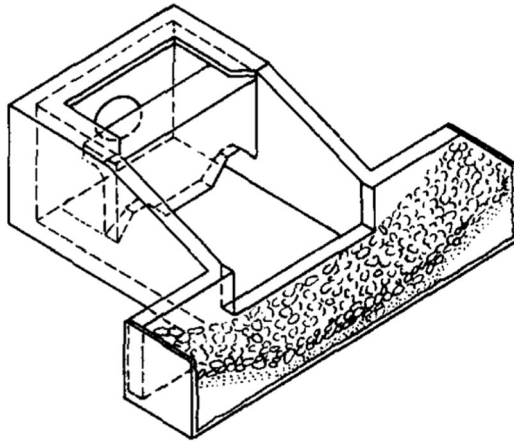
Figure 2.23 Type VI Basin (after Peterka 1978)

2.7.1.5 Saint Anthony Falls basin (SAF)

The Saint Anthony Falls basin (SAF) was developed at the St. Anthony Falls Hydraulic Laboratory. It consists of chute blocks, baffle blocks and an end sill (Fig. 2.24). This type of basin is used for small structures such as spillways, outlet works, and canals. The design of the basin is closely prescribed (HEC-14, 2006) as follows:

The basin width, W_B is equal to the culvert width for box culverts. For circular culverts, W_B is taken as the larger of the culvert diameter or

$$W_B = 1.7 D_0 \left(\frac{Q}{g^{0.5} D_0^{2.5}} \right) \tag{2.39}$$

where D_0 is the diameter of the culvert. The conjugate depth, C is a function of Froude number:

$$\begin{aligned}
C &= 1.1 - \frac{Fr_1^2}{120} \quad \text{when } 1.7 < Fr_1 < 5.5 \\
C &= 0.85 \quad\quad\quad \text{when } 5.5 < Fr_1 < 11 \\
C &= 1.0 - \frac{Fr_1^2}{800} \quad \text{when } 11 < Fr_1 < 17
\end{aligned} \tag{2.40}$$

The length of the basin L_B is

$$L_B = \frac{4.5 y_2}{C Fr_1^{0.76}} \tag{2.41}$$

For chute blocks, the height of chute blocks (h_1) is equal to y_1; The number of chute blocks (N_C) is $N_C = \frac{W_B}{1.5 y_1}$; The width of chute blocks (W_1) and spacing of chute blocks (W_2) are $W_1 = W_2 = \frac{W_B}{2 N_C}$. The height of baffle blocks (h_3) is equal to y_1; The number of baffle blocks (N_B) is

$N_B = \frac{W_{B2}}{1.5y_1}$; The width of baffle blocks (W_3)and spacing of baffle blocks (W_4) are $W_3 = W_4 = \frac{W_{B2}}{2N_B}$. Here, W_{B2} is the basin width at the baffle row. The baffle blocks should be placed such that the distance from the downstream face of the chute blocks to the upstream face of the baffle blocks is $\frac{L_B}{3}$, and the minimum distance between the outermost baffle blocks and the side wall must be greater than $\frac{3y_1}{8}$. For the end sill, the height (h_4) should be $h_4 = \frac{0.07y_2}{C}$.
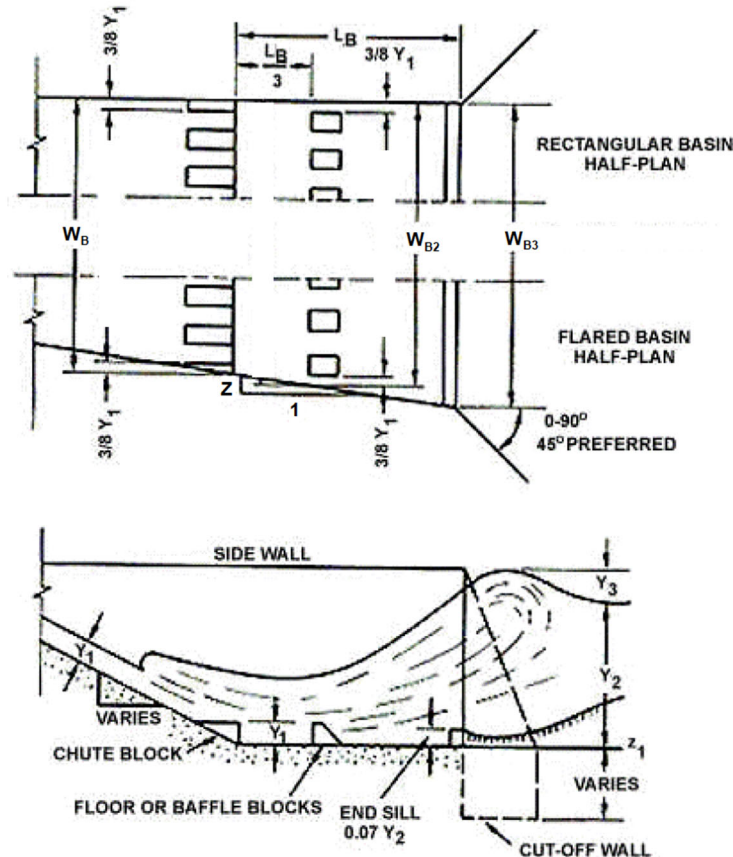
Figure 2.24 SAF basin (after HEC-14)

2.7.2 <u>Stilling basin selection based on Froude number</u>
As discussed in Section 2.2.5, hydraulic jumps behave differently based on Froude number ranges. Consequently, selecting a suitable basin type is important for maximizing energy dissipation efficiency.

The US Bureau of Reclamation (1987) discusses basin selection for different Froude numbers. For Froude numbers between 1.7 and 2.5, the jump type is pre-jump. Baffles or sills are not required for this case. For Froude numbers between 2.5 and 4.5, the jump type is transitional. Stilling basins are ineffective for transitional jumps. However, the Type IV basin should be used

if a stilling basin is needed. If used for a transitional jump, an auxiliary wave suppressor is needed because the waves cannot be fully dampened solely by a type IV basin. It is suggested that basin geometry can be manipulated to prevent the Froude number from falling into this range. By widening the basin, the depth of the upstream flow will be reduced, causing an increase in Froude number so that the jump type changes from a transitional to a good jump. For Froude numbers between 4.5 and 9.0, a true hydraulic jump will form. For an incoming velocity of less than 60 ft/s, it is suggested that a Type III basin should be used. The velocity limit accounts for the susceptibility of chute blocks and baffle piers to damage from impingement and cavitation. For an incoming velocity exceeding 60 ft/s, a Type II basin is recommended.

HEC-14 also discusses basin selection for different Froude numbers. For Froude numbers between 2.5 and 4.5, the recommendation is the same as the US Bureau of Reclamation recommendation that a Type IV basin should be used. For Froude numbers between 4.5 and 17, a Type III basin is applicable. And for Froude numbers between 1.7 and 17, an SAF basin is also applicable.

2.8 Erosion Downstream of Culvert Outlets

Emami and Schleiss (2010) researched the development of localized scour holes on natural mobile beds at culvert outlets. They built a hydraulic model test facility to evaluate natural bed erosion without any protection measures. The model consisted of a horizontal 10cm diameter pipe connected to a pump, an alluvial bed, a tailwater flip gate for tailwater level control, and a basin with a sharp-crest weir for discharge measurement. A total of 7 tests were performed with different experimental characteristics like discharge, outlet jet velocity and tailwater depth. Dimensional analysis showed that any geometric dimension (width, length, or depth) of the scour hole (Y) was a function of both densimetric Froude number (F_0) and the ratio of tailwater depth to pipe diameter ($\frac{h_{tw}}{D}$). Scour profile characteristics were observed and compared for both high and low tailwater depth. For high tailwater depth ($1.0 < \frac{h_{tw}}{D} < 1.1$), the location of maximum erosion depth occurred at about 40% of the maximum scour length distance and the scour depth at the pipe outlet was about 25% of the maximum scour depth. For low tailwater depth ($0.1 < \frac{h_{tw}}{D} < 0.2$), the maximum erosion depth was located at about 30% of the maximum scour length distance and the scour depth at the pipe outlet was about 75% of the maximum scour depth. The analysis of the experimental data shows that there is a logarithmic regression relationship between scour hole geometry and densimetric Froude number.

Abt et al. (1996) worked to enhance of the culvert outlet scour estimation equations of HEC-14. In the 1983 version of HEC-14, the general equation for estimating the scour geometry is:

$$\text{scour geometry} = \alpha \left(\frac{Q}{g^{\frac{1}{2}} D^{\frac{5}{2}}} \right) \left(\frac{t}{t_0} \right)^{\theta} \tag{2.42}$$

Depending on the material type, nominal grain size and desired scour hole dimension, the appropriate coefficients and exponents for the equation are selected from relevant tables. Abt et al. provide an improved, simplified general equation for estimating scour geometry and also take culvert slope and drop height into consideration with the addition of two coefficients (C_s and C_h, respectively). Three coefficients and exponents (α, β, θ) are used for estimating four different scour hole dimensions. The dimensions of scour attributed to varying pipe slopes and drop heights are normalized to 0% slope condition and 0 drop height condition, respectively, and coefficients (C_h, C_s) are incorporated into the general equation. The new equation is:

$$\text{scour geometry} = C_h C_s \frac{\alpha}{\sigma^{1/3}} \left(\frac{Q}{g^{\frac{1}{2}} R_h^{5/2}} \right) \left(\frac{t}{t_0} \right)^{\theta} \tag{2.43}$$

Here, σ is the bed material gradation and R_h is the hydraulic radius of the flow. The constant t_o is 316.

2.9 Conclusions
Based on the results of Rand (1966, 1970), it may be best to put the sill close to the outlet of the culvert to have the biggest impact on shortening the length of any jumps that form in the dissipation basin. However, there is a significant difference between the work of Rand and the present work in that the present work involves a rapid expansion from a partially filled culvert to a rectangular dissipation basin.

Based on observations by Hager (1992) and Bradley and Paterka (1957b), sharp corners on the weirs and staggered weirs will be better for dissipating energy. Fillets and rounding of the front face is not recommended.

Sharp corners are also recommended for baffle blocks. Literature suggests that the optimal block height is about 1.5 times the inflow depth for baffle blocks. This may also be true for staggered weirs which have a layout that is in some ways similar to baffle blocks. Similarly, for design basins, the height, width and spacing of chute blocks is recommended to be equal to the incoming flow depth. Optimal opening percentage for rows of baffle blocks is about 50%.

It appears that the Type VI basin is the most relevant type of design basin when considering the current application. This type of basin is the most similar in geometry to designs necessary for circular outlets. It may be of interest to explore a similarly styled design in future research.

3. Experimental Design and Methods

3.1 Introduction

The objective of the present research is to provide design guidance for energy dissipation structures at the outlets of circular culverts. The experimental design for testing different dissipation methods relies on Froude Similarity, which is briefly described in this chapter.   The experimental setup is based on typical design conditions. These design conditions are described in the prototype considerations section of this chapter. After the design conditions are explained, the chapter contains a discussion of the actual model geometries selected for the research. Then, the instrumentation used to collect measurements is discussed. The structures added to the dissipation basin to increase energy dissipation are also detailed. Finally, a dimensional analysis of the system is presented to identify important defining parameters.

3.2 Froude Similarity Conditions

In Froude-based similitude, only the Froude number and the Euler number are constrained to be the same in the model and the prototype. This type of similitude prevails if viscous forces, surface tension forces, and compressibility forces are negligible compared to gravitational forces. In such a case, Reynolds Number, Mach Number, and Weber Number effects are ignored. For the present research, any concerns that viscous forces are relevant can be more thoroughly addressed by estimating Reynolds Numbers. However, the roughness of concrete structures is significant, the velocities tested in the facility are high, the viscosity of water is low, and the distances over which energy is dissipated are short; all of these factors support the implementation of a Froude model with negligible viscous effects.

Froude based models result in fixed ratios of corresponding model and prototype variables. By making model and prototype Froude numbers equal, the ratios in Table 3.1 can be derived as a function of model scale, L_m/L_p, in which L_m and L_p are equivalent lengths in the model and prototype, respectively. For example, if the model pipe diameter is 12 inches and the prototype pipe diameter is 48 inches, the scale is $12/48 = 1/4$.

The subscripts m and p in Table 3.1 refer to model and prototype. Thus, if a 1/4 scale Froude model is used, the velocity in the model will be one half of the velocity in the prototype. Fixed scale ratios of parameters for scales of 1/4, 1/5, and 1/6 are shown in Table 3.1 for comparison. It is anticipated that the scale of the current model will approximately fall within this range of scales (1/4 – 1/6), depending on the size of the prototype culvert. It is allowable for the model scale to be smaller (e.g., 1/10 or even 1/25), but larger differences between the model and prototype sizes reduce the accuracy of the model. For a thorough discussion of physical models, see ASCE-97 (2000).

Table 3.1 Parameter Ratios based on Froude Similitude

Parameter	Description	Calculated Ratio	Fixed Scale Ratios		
			1/4 Scale	1/5 Scale	1/6 Scale
$\dfrac{V_m}{V_p}$	Velocity Ratio	$\sqrt{\dfrac{L_m}{L_p}}$	0.50	0.45	0.41
$\dfrac{Q_m}{Q_p}$	Discharge Ratio	$\left(\dfrac{L_m}{L_p}\right)^{5/2}$	0.0313	0.0179	0.0113
$\dfrac{n_m}{n_p}$	Manning Roughness Ratio	$\left(\dfrac{L_m}{L_p}\right)^{1/6}$	0.79	0.76	0.74
$\dfrac{\Delta p_m}{\Delta p_p}$	Pressure Ratio	$\dfrac{L_m}{L_p}$	0.25	0.20	0.17
$\dfrac{F_m}{F_p}$	Force Ratio	$\left(\dfrac{L_m}{L_p}\right)^{3}$	0.0156	0.0080	0.0046

3.3 Prototype Considerations

The intent of the current research is to simulate conditions that are representative of typical culvert designs. In light of this intent, typical culvert conditions have been provided by NDOT to aid with decisions about an appropriate scale and appropriate model geometries. In this section, these conditions are discussed. We begin with a discussion of the types of pipe material and pipe installations utilized by NDOT.

First, NDOT primarily utilizes two types of pipes: Reinforced Concrete Pipe (RCP) and Corrugated Metal Pipe (CMP). It would be useful to simulate both of these types of pipes because they have different roughness behavior. However, flow in CMP can be quite complex – especially when full, because the roughness elements are organized and can cause flow rotation (Silberman, 1970). Flow rotation influences the effective pipe roughness. In discussions with NDOT (Appendix A), it was apparent that testing RCP was more important to NDOT than testing CMP, primarily because RCP has lower wall roughness and will result in the highest outlet velocities. Thus, the first priority of the present research was to test pipes with uniform roughness that simulate RCP. Perhaps CMP can be tested in a future model, but this will require some fairly sophisticated model pipe design considerations, something that was not feasible for the present study.

Second, NDOT is interested in two types of pipe installations: broken back installations and straight pipe installations. Again, the broken back installations have priority over straight pipe installations, so broken back installations were tested, but the results are relevant to both types of installations as long as pipe outlet conditions are similar.

An example broken back culvert installation is shown in Figure 3.1. This is a 48-inch diameter broken back culvert with a total drop of 14 feet between the inlet an outlet. The runout section is 24 feet long and is horizontal. NDOT provided details of fifteen such sample culverts to aid in selection of baseline conditions. The culvert design details provided by NDOT include the culverts described in Table 3.2.

Based on the information in Table 3.2, it was decided in consultation with NDOT that representative conditions of a prototype culvert include a 48-inch diameter Reinforced Concrete Pipe (RCP) culvert with a maximum discharge of about 100 ft^3/s and a horizontal runout section that is about 24 to 32 feet (six to eight diameters) in length. Nevertheless, model results can be scaled to represent prototypes of different sizes.

3.4 Experimental Layout Overview

The experimental layout, shown in Figure 3.2, includes the testing section, the design of which is described in the next section, and all of the support equipment, including the supply pump and the v-notch weir for flow rate measurement. The overall layout is described in this section.

The experimental layout consists of a storage tank, a constant-head tank, a head box, a broken-back culvert, a tail box, and a V-notch weir box. The storage tank stores and recycles the water flowing through the entire system. Water in the storage tank is pumped into the constant-head tank by a pump with a maximum flow rate of about 85 L/s (3 ft^3/s). The constant-head tank uses weirs to ensure that the water going into the head box has a constant head. Flow into the head box is controlled using a butterfly valve. Four weirs are installed in the constant-head tank so that excess water recirculates to the storage tank without passing through the testing section. The water that is directed to the head box travels through the simulated broken-back culvert to the tail box. The dissipation basin in which the dissipation structures are installed is located within the tail box. Four drains at the bottom of the tail box convey water from the tail box to the v-notch weir. The tailwater depth can be adjusted by an adjustable gate upstream of the tail box floor drains. Water is conveyed into the V-notch weir by two pipes connecting the tail box and the V-notch weir. After the water travels over the V-notch weir, it flows back into the storage tank to be recirculated. Figure 3.3 provides a three-dimensional view of the testing section without the dissipation basin in place.

Some changes were made to the structure after the first phase of testing. The primary change was the addition of two floor drains to the tail box to increase the amount of flow that could be carried from the tail box to the V-notch weir. The primary purpose of this change was to reduce the tailwater levels in the tail box for high discharge flows so that tailwater influences could be eliminated in the dissipation basin.

37
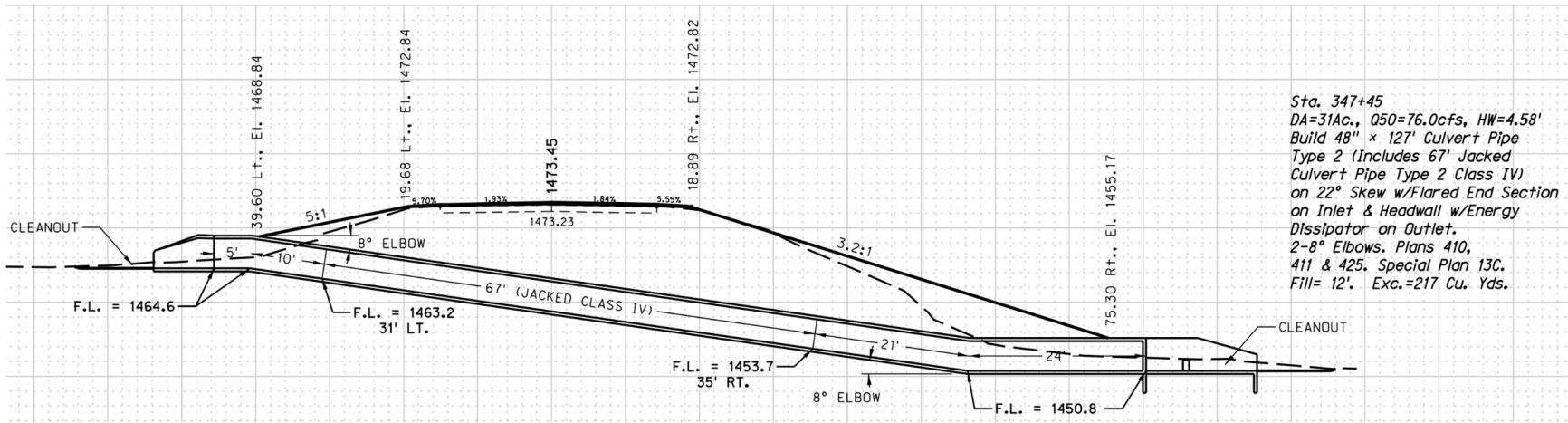
Figure 3.1 Example circular culvert designs provided by NDOT (2020). This is project culvert 11718-347.

Table 3.2 Typical circular culvert designs provided by NDOT (2020)

ID (CN: Station)	Diam. (in)	Runout Type	Design Storm (yr)	Design Q (ft³/s)	Inlet Elev. (ft-msl)	Outlet Elev. (ft-msl)	Drop Slope	Runout Slope	Runout Length (ft)
11895: 1038	24(30)†	CMP	25	11.2	1048.2	1042.0	(1048.2-1042.1)/51	0.0042	24
11718: 510	30	RCP	50	27.2	1476.0	1467.1	(1476.0-1467.1)/90	0	15
11718: 350	42	RCP	50	58.7	1467.1	1457.9	(1467.1-1457.9)/80	0	24
11718: 523	42	RCP	50	39.4	1460.5†	1452.1	(1460.5-1452.1)/92	0	16
11718: 202	48	RCP	50	83.9	1471.3	1457.2	(1471.3-1457.2)/88	0	26
11718: 347	48	RCP	50	76	1464.6	1450.8	(1464.6-1450.8)/98	0	24
11718: 584	48	RCP	50	41.8	1429.5	1424.2	(1429.5-1424.2)/79	0	15
004-127: 127	54	CMP	25	134	1490.9	1484.2	(1490.8-1484.7)/32	0.0104	48
13303: 672	54	CMP	50	126.5	1290.6	1281.00	(1290.6-1281.0)/84††	0	20
12988: 1309	60	RCP	50	177	1022.14	1000.96	(1021.17-1000.96)/48	0	30
11718: 13	60	RCP	50	149.6	1416.6	1413.1	(1416.6-1413.1)/69	0	25
11718: 256	60	RCP	50	116.2	1486.3	1481.1	(1486.3-1481.1)/67	0	22
11895: 1410	66	RCP	25	178.4	1143.0	1130.6	(1143.0-1130.8)/104	0.0033	60
11718: 341	72	RCP	50	188.6	1463.3	1459.1	(1463.3-1459.1)/65	0	26
11718: 482	72	RCP	50	230	1468.7	1466.0	(1468.7-1466.0)/66	0	25

Note: Grayed culverts appear to have horizontal bends in them (see plan views)

†Error in special plans or in originally provided information

†† Uncertain if 84 ft length includes horizontal inlet head race.
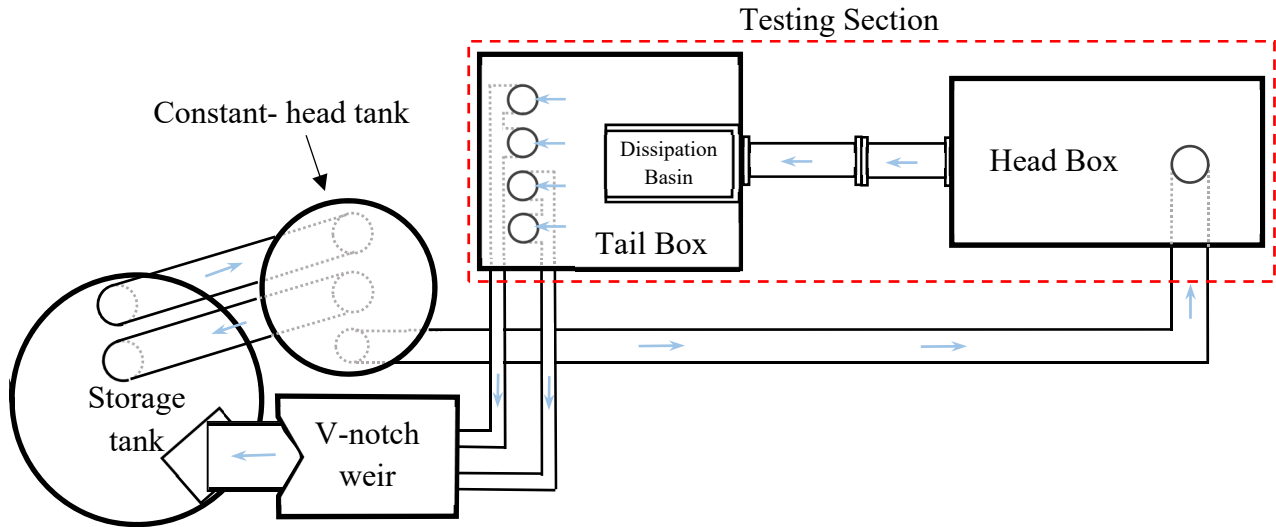
Figure 3.2 System layout plan view (including the testing section)
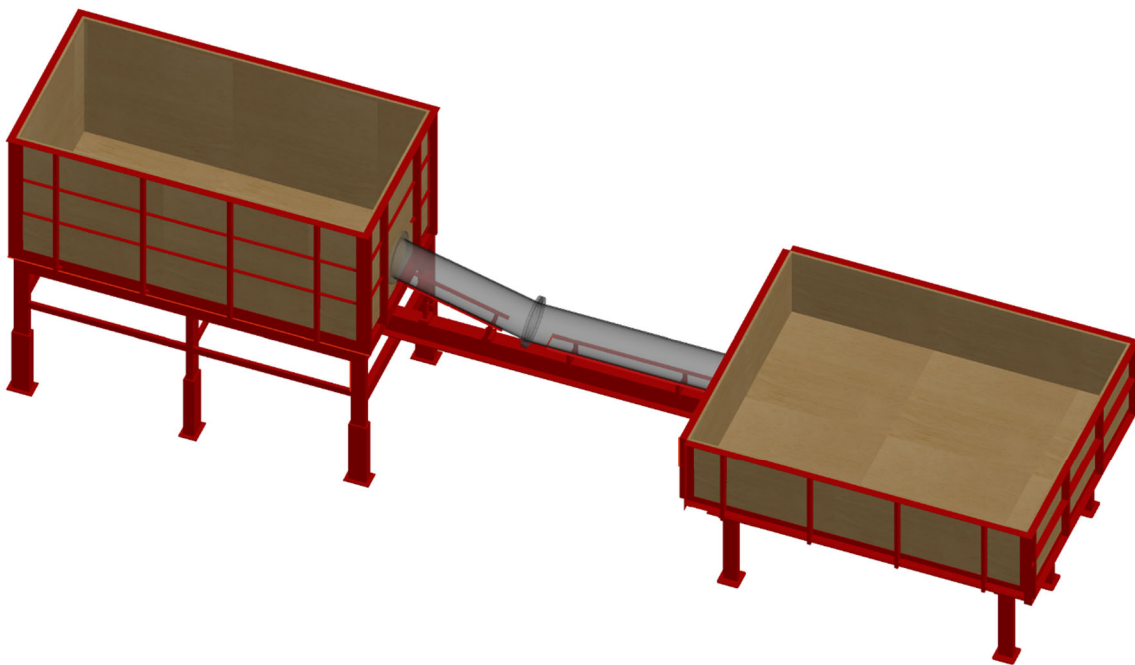
Figure 3.3 Testing section

3.5 Testing Section Description

As mentioned earlier, the model is a Froude-based model of the prototype. Aside from the energy dissipation structures, the same testing facility is used for all experiments described in this report. In this section, the testing section design is described in detail. This is followed by discussion of model scale, model geometry, the energy dissipation basin, and instrumentation.

40

3.5.1 <u>Testing section design</u>

The main testing section consists of the head tank, a pipe model, the energy dissipation basin, and the tailwater tank. A flow measurement weir is located downstream of the tailwater tank. As shown in Figure 3.4, three configurations were considered when designing the test facility:

1. An uncontrolled broken-back culvert,
2. A gate-controlled broken-back culvert, and
3. A gate-controlled straight culvert.

Each configuration has advantages and disadvantages. Table 3.3 is a side-by-side comparison of the three configurations.

Table 3.3 shows that the geometry of the Type I configuration is the most similar to real broken-back culvert geometries. However, only one drop angle can be simulated without incurring considerable increases in cost. The Type III facility is best for control of flow behavior because the gate allows selection of a wide range of inlet Froude numbers for the same discharge. The Type I configuration is controlled entirely by discharge, and with no gate, only one inflow state will be possible for each discharge. The Type II facility is also good for controlling flow behavior, but length of the drop may reduce some of that control. The Type III facility is susceptible to drowning of the inlet because the invert is horizontal; neither of the facilities with drops is susceptible to drowning of the inlet or control gate. Highest inlet Froude numbers can be achieved with the Type II facility because it has the greatest potential elevation between the head tank surface and the outlet invert. The greater elevation difference results in higher kinetic energies at the outlet. The Type III facility is the easiest to construct.

Table 3.3 Comparison of Test Facility Functionality

	Type I	Type II	Type III
Similarity to Real Geometry	Best[†]	Median[†]	Worst
Control of Flow Behavior	Worst	Median	Best
Susceptibility to Inflow Drowning	N/A	N/A	Worst
Highest Inlet Froude No.	Worst	Best	Median
Ease of Construction	Median	Worst	Best

[†]Note, however, that only one drop angle is simulated

In consultation with NDOT, it was decided to implement a gate-controlled broken-back facility with a drop angle of 15 degrees for testing dissipation structures. 15 degrees was deemed to be the greatest angle that would likely be used in typical designs. It was concluded that such a facility would provide the greatest range of testing capabilities while also being similar to typical configurations of broken-back structures.
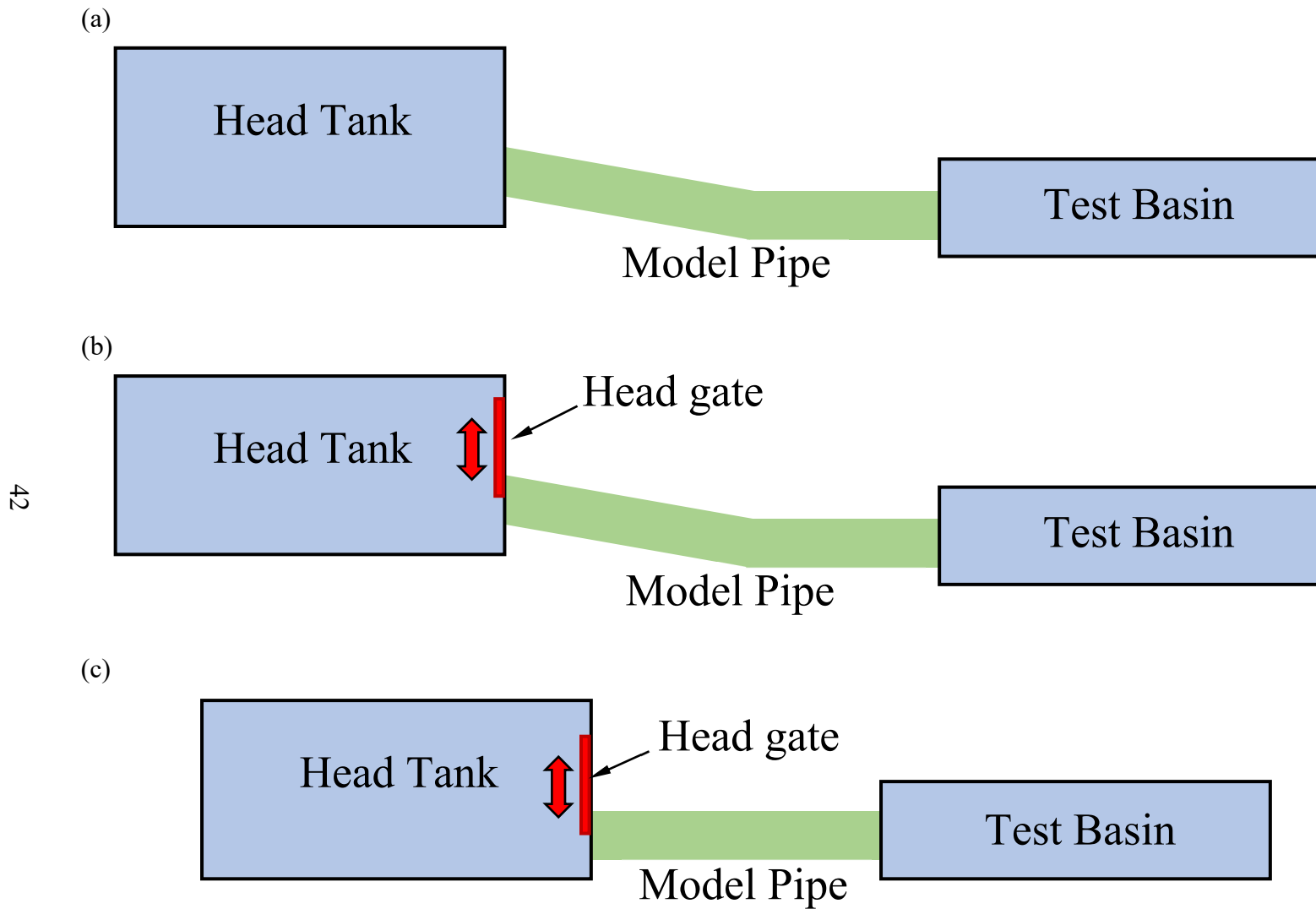
Figure 3.4 Test basin layouts considered: (a) uncontrolled broken back, (b) gate-controlled broken back, and (c) gate-controlled.

It was later found in testing that the gate-controlled configuration was not feasible as planned (Fig. 3.5). The flow coming out from the gate does not attach to the bed of the culvert. Because of this, Type I configuration was used for all tests. Modifications to the inlet may have improved inlet conditions for gate-controlled applications, but required modifications were more extensive than was possible within available time constraints.

Figure 3.5 Gate controlled flow behavior

3.5.2 Model scale

Assuming that the prototype is 48 or 60 inches in diameter with a maximum discharge of 100 to 200 ft^3/s, that the drop slope is 15 degrees, and that the runout is horizontal with a length of six to eight diameters, a reasonable design model scale can be selected. Tables 3.4 and 3.5 show model selection scales for a 48" and 60" design prototype, respectively. Each table shows model pipe diameters, discharges, and roughness for 1/4, 1/5, and 1/6 scale models.

Table 3.4 Model variables for 1/4, 1/5, and 1/6 scale models based on a 48" diameter culvert

Parameter	Prototype	Model		
		1/4 Scale	1/5 Scale	1/6 Scale
Diameter	48"	12"	9.6"	8"
Discharge 1	100 ft^3/s	3.13 ft^3/s	1.79 ft^3/s	1.13 ft^3/s
Discharge 2	200 ft^3/s	6.25 ft^3/s	3.58 ft^3/s	2.27 ft^3/s
Manning Roughness	0.012	0.010	0.009	0.009

Table 3.5 Model variables for 1/4, 1/5, and 1/6 scale models based on a 60" diameter culvert

Parameter	Prototype	Model		
		1/4 Scale	1/5 Scale	1/6 Scale
Diameter	60"	15"	12"	10"
Discharge 1	100 ft³/s	3.13 ft³/s	1.79 ft³/s	1.13 ft³/s
Discharge 2	200 ft³/s	6.25 ft³/s	3.58 ft³/s	2.27 ft³/s
Manning Roughness	0.012	0.010	0.009	0.009

The lab can provide about 3 ft³/s of water to the model using the pump that we prefer to use for this project. Thus, based on supply capabilities, 100 ft³/s can be simulated for all scales for both prototypes. That is, the model diameter can be anywhere from 8" to 12" for simulating 100 ft³/s in a 48" prototype and anywhere from 10" to 15" for simulating 100 ft³/s in a 60" prototype. For simulating 200 ft³/s, only an 8" pipe can be used to simulate flow in the 48" prototype and only a 10" pipe can be used to simulate flow in the 60" prototype. Based on design flows shown in Table 3.2, 100 ft³/s should be sufficient for studying a 48" culvert and 200 ft³/s should be sufficient for studying flow in a 60" culvert. Thus, a 10" model diameter was selected to simulate relevant flows. Although roughness is not expected to significantly affect flow behavior in the model, estimated model roughness values are similar to that of acrylic (~0.009).

3.5.3 Model geometry

Based on observations made in Section 3.5.1, a gated broken back structure (Type II) was selected for the model. In consultation with the NDOT Technical Advisory Committee (TAC), the prototype runout section length was selected to be 24-ft for a 48" diameter culvert. A drop slope of 15 degrees was also preferred by the TAC to maximize flow velocity at the outlet. The prototype material was selected to be RCP. In addition to these dimensions, a drop height of one pipe diameter was chosen to prevent flooding of the upstream forebay gate (if a gate is in use).

A diagram of the model selected for this study is shown in Figure 3.6. Important dimensions include:

- D – Culvert diameter
- L – Runout length
- ϕ – Drop angle
- Y – Drop height
- S – Drop length

The figure also shows some of the important flow dimensions, including:

- H – Head in the head tank
- T – Outlet depth
- h – Gate opening
- d – Upstream supercritical flow depth
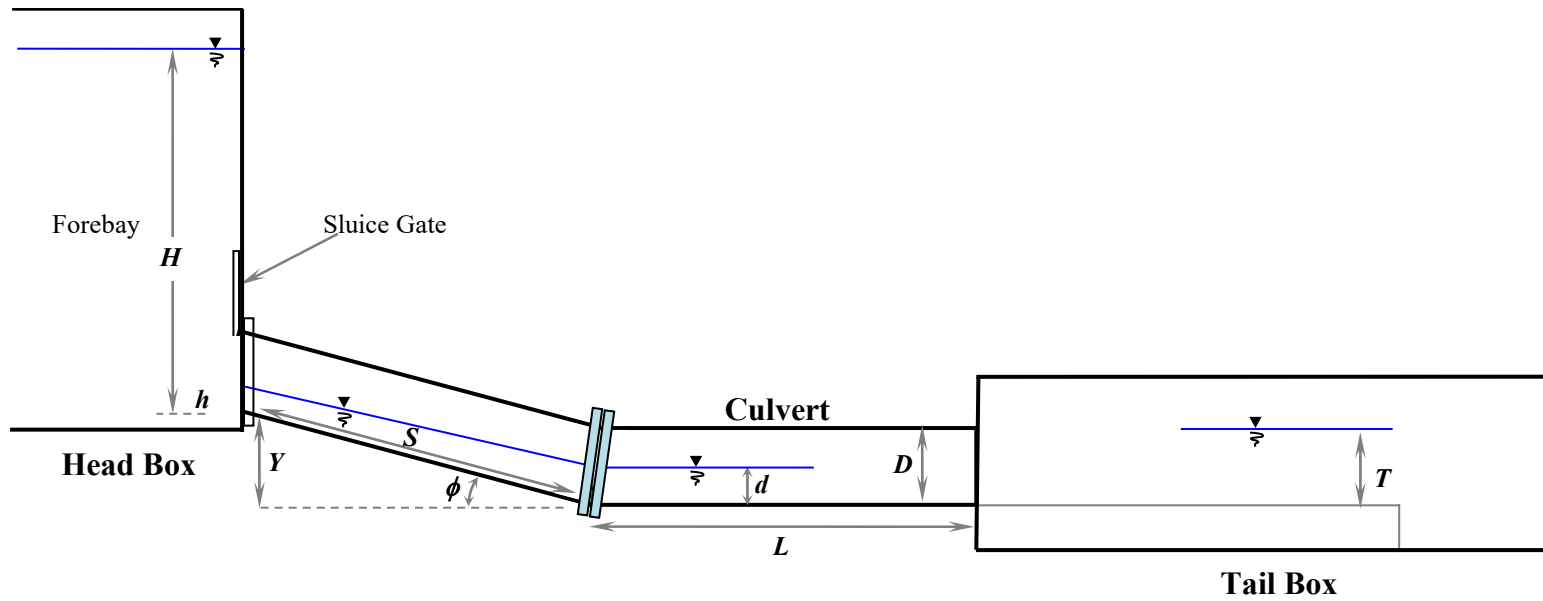
Figure 3.6 Various test facility dimensions

One dimension that is not shown in the figure that is relevant is the width of the dissipation structure inside the tailwater tank:

- w – internal width of the dissipation structure

Dimensions of the selected geometry of the model test system are provided in Table 3.6. The model made use of a 10" diameter acrylic culvert, which provided a wall roughness similar to the scaled roughness of RCP. Wall roughness effects can be checked, but are expected to be negligible for the current study. For a 48-inch diameter prototype, the 10-inch model is 1/4.8 scale.

Table 3.6 Model test system geometry.

Parameter	Prototype	Model
Diameter (D)	48"	10"
Runout Length (L)	24 ft	60"
Drop angle (ϕ)	15 degrees	15 degrees
Drop height (Y)	N/A	10" [†]
Drop length (S)	N/A	38.64"

[†]Note that the drop height selected is one culvert diameter. This was selected to prevent the control gate from being flooded during operation. The drop height dictates the drop length when combined with the drop angle.

3.5.4 Energy dissipation basin

The energy dissipation structure model was designed based on preexisting prototypes for 48-inch pipes (11718:202.1, 11718:347.45 and 11718:548.02). Figures 3.7 and 3.8 are the cross section and side view of the prototype. D is pipe diameter. W, L and H are the width, length and height of the basin respectively. W1 is the outer basin width. L1 is the length from the beginning of the basin to where the wing begins. H1 is the height from the bottom of the basin to the end of the wing. TH, TW and TB are thicknesses of the headwall, the wingwall and the bed respectively. Tables 3.7 and 3.8 show the dimensions of prototypes and 1:4.8 scale models. The shape of the constructed model was based on the scaled prototypes, but it was slightly simplified from the exact 1:4.8 scale models (see Fig. 3.9). For example, the constructed model has a uniform flat bed, whereas the prototype has chamfers near the side walls. The dimensions of TH, TW and TB for the constructed model are slightly different than those of the exact scale models. However, wall thicknesses have no bearing on the test results since flow is only affected by the internal dimensions of the structure. Moreover, H1 was set equal to H for all tests; in other words, although diagonal wings at the ends of the dissipation box sidewalls were removable, they were not removed for any of the tests. The dissipation box model had simple, rectangular side walls for all tests.
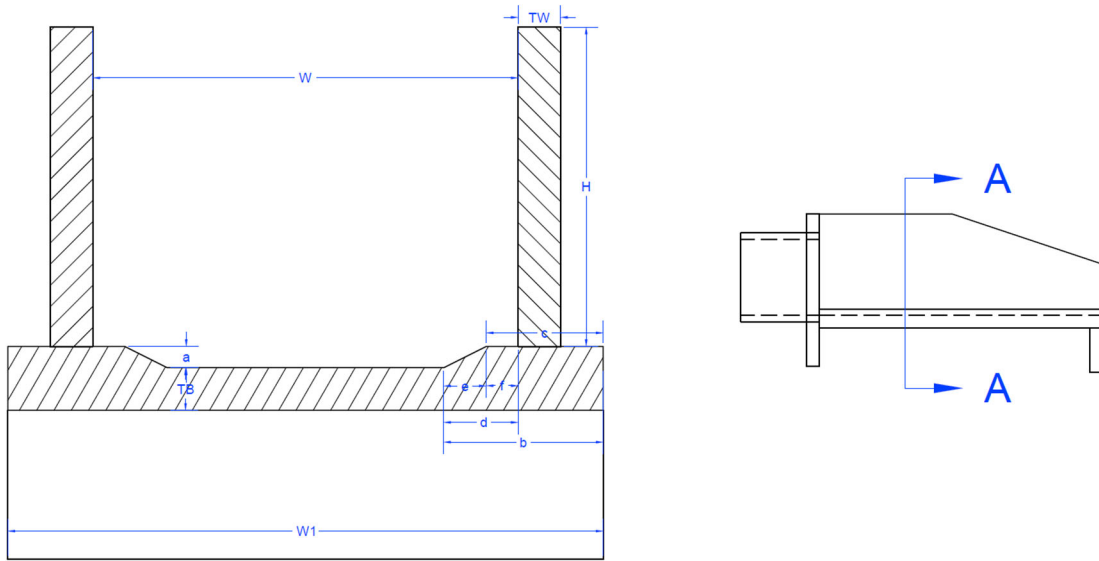
Figure 3.7 Cross section of the dissipation structure prototype
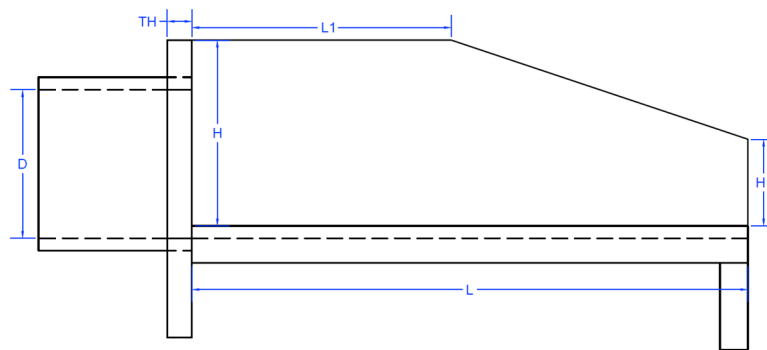
Figure 3.8 Profile of the dissipation structure prototype
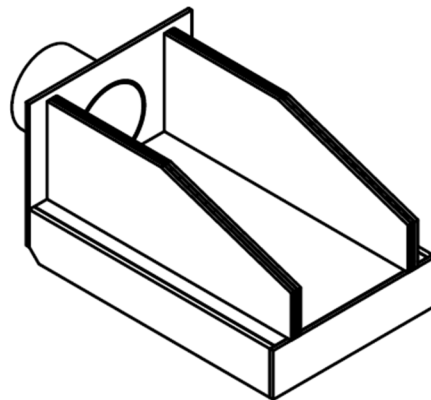
Figure 3.9 Energy dissipation box model with sloping side walls. In all testing cases, rectangular side walls were used.

Table 3.7 Dimensions of dissipation structure prototypes

Prototype	Dimensions (inches)								
	D	W	L	H	L1	H1	TH	TW	TB
11718:202.1	48	80	180	60	84	28	8	8	8
11718:347.45	48	80	180	60	84	28	8	8	8
11718:548.02	48	80	180	60	84	28	8	8	8
11718:13.80	60	92	180	78	84	46	10	10	8
11718:256.43	60	92	180	78	84	46	10	10	8
12988:1309.16	60	96	180	78	84	46	8	8	8
Hwy 4: 127.46	54	72	180	66	84	34	8	8	8

Table 3.8 Dimensions of 1:4.8 dissipation structure models

Model	Dimensions (inches)								
	D	W	L	H	L1	H1	TH	TW	TB
11718:202.1 model	10.00	16.67	37.50	12.50	17.50	5.83	1.67	1.67	1.67
11718:347.45 model	10.00	16.67	37.50	12.50	17.50	5.83	1.67	1.67	1.67
11718:548.02 model	10.00	16.67	37.50	12.50	17.50	5.83	1.67	1.67	1.67
Constructed model	10.00	16.67	37.50	13.00	17.50	6.33	0.50	1.50	2.88

At the expansion from the culvert runout section into the dissipation basin, the culvert invert is flush with the bed of the basin. The bed of the dissipation basin is 6.5 inches higher than the bed of the tailwater tank so that low tailwater conditions can be tested. The width of the dissipation basin is 1.67 times the diameter of the culvert, and the flow expands as it exits the runout section. The model dissipation box was designed such that staggered weirs and full weirs of different heights could be installed at different distances from the outlet. Only two streamwise positions were tried and only one position was tested extensively. The geometry and positions of the two types of weirs is discussed in more detail in chapter 3.6.

3.5.5 Instrumentation
Figure 3.10 shows the layout of instrumentation used for the experiments. The instrumentation included 22 piezometers (labeled 1-22), six point gauges (labeled A-F), and two Prandtl tubes (labeled P1 and P2). Later, three additional Prandtl tubes (LDB, CL, RDB) were added at the end of the dissipation box near point gauge F (Fig. 3.11). In addition to the instrumentation, a v-notch weir was used to measure the discharge passing through the testing section. Instrumentation is discussed in detail in this section.

Due to two manometer leaks and interference with some of the dissipation structures, not all of the 22 piezometers were functional for every test, but the most useful ones were. In addition to the measurement devices provided in Figures 3.10 and 3.11, the water level in the tailwater tank (TW) was recorded and flow rate was measured using a V-notch weir.
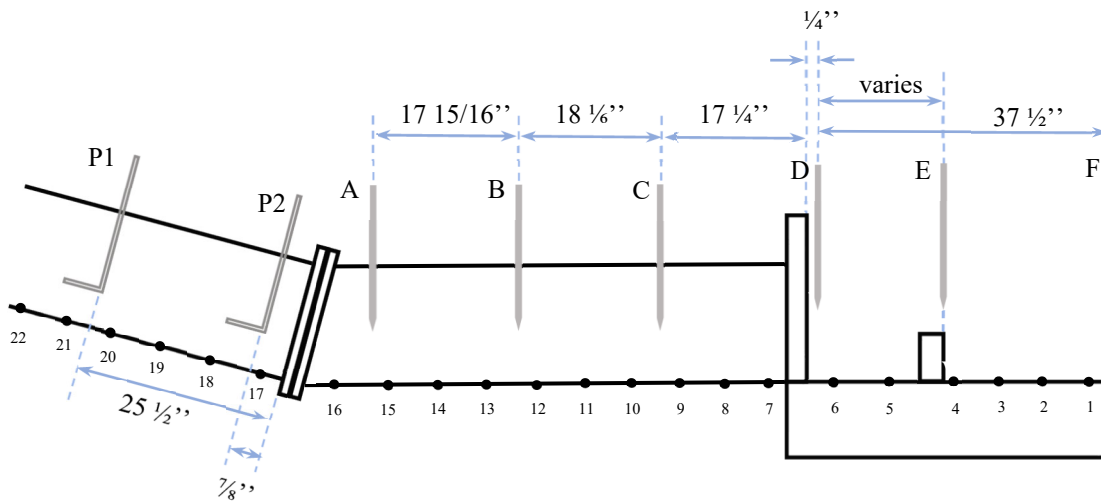
Figure 3.10 Initial layout of piezometers, point gauges, and Prandtl tubes

Figure 3.11 Three additional Prandtl tubes at the end of the dissipation structure

3.5.5.1 Point gauges

Point gauges were installed to measure the depth of water at six locations within the test facility. Three point gauges (A, B and C) were installed in the horizontal run-out section of the culvert and three point gauges (D, E and F) were installed in the weir box. Point gauges A, B, C and D are evenly spaced with nominal 18-inch spacing from A to B, B to C and C to D. The directly measured spacings are shown in Fig. 3.10. Point gauge D is located immediately downstream of the dissipation box head wall. Gauge E is located at the downstream edge of the weir or

staggered weir, so the position of gauge E is changed when the weir position is changed. Gauge F is located at the downstream edge of the weir box.

Table 3.9 provides specific information about each of the point gauges, including their positions (distance upstream of the end of the dissipation structure), their bed elevation relative to the elevation of point gauge A, and their baseline readings (the readings of the point gauges when they are at the bed elevation). The position of point gage E is for when the weir is in its upstream-most position.

Table 3.9 Point gauge information

Point Gauge	Position in (cm)	Bed Elevation (cm)	Baseline Reading (cm)
A	90.38 (229.6)	-0.04	27.76
B	72.69 (184.6)	-0.09	29.16
C	54.75 (139.1)	-0.02	28.71
D	36.94 (93.8)	0.11	67.56
E	22.94 (58.3)	-0.03	67.19
F	0.19 (0.48)	0.00	67.43

It was necessary to calibrate the point gauges because:
1. The point gauges have arbitrary scales. These scales must be translated so that water depths and bed elevations can be determined at each position.
2. The datum of the system is at the outlet of the dissipation basin, and all other bed elevations must be determined relative to this datum.

Next, the process of determining bed elevations and baseline readings for point gauge measurements is described.

Point gauge calibration
The datum for the system is the bed at point gauge F. Elevations along the culvert runout invert and the bed of the dissipation basin were nearly the same but varied slightly due to construction imperfections. Relative elevations of the bed were determined by sealing the tailwater outlets and filling the downstream end of the system with water. The depth of the non-moving water above a perfectly horizontal bed will be uniform. Thus, bed elevation can be obtained from the variation of water depth along the culvert and dissipation basin beds. Bed elevations along the length of the culvert are reported in Tables 3.9. Bed elevations in the runout section and dissipation basin had a maximum deviation of 1.1 mm. The datum at the dissipation basin outlet was the basis for all energy calculations.

Baseline point gauge readings were determined by recording the point gauge reading when the point gauge was lowered to the bed. The depth at each cross section could then be determined

for any test by subtracting the baseline reading from the point gauge reading. Baseline point gauge readings at the point gauge positions are reported in Table 3.9.

3.5.5.2 Piezometers

Like the point gages, the piezometers have arbitrary scales and rely on the fixed datum at the dissipation basin outlet. Table 3.10 provides information similar to the information provided for point gages for each of the piezometers.

Table 3.10 Piezometer Information

Piezometer	Position in (cm)	Bed Elevation (cm)	Baseline Reading (cm)
TW	N/A	N/A	N/A
1	4.44 (11.3)	0.00	0.40
2	10.44 (26.5)	-0.01	0.40
3	16.44 (41.8)	-0.02	0.40
4	22.44 (57.0)	-0.03	0.40
5	28.44 (72.2)	0.03	0.40
6	34.44 (87.5)	0.09	0.40
7	40.44 (102.7)	0.09	0.40
8	46.44 (118.0)	0.04	0.40
9	52.44 (133.2)	0.00	0.40
10	58.44 (148.4)	-0.04	0.40
11	64.44 (163.7)	-0.06	5.84
12	70.44 (178.9)	-0.08	5.77
13	76.44 (194.2)	-0.08	5.84
14	82.44 (209.4)	-0.06	5.74
15	88.44 (224.6)	-0.04	5.83
16	94.44 (239.9)	-0.04	5.75
17	103.25 (262.3)	3.86	9.53
18	109.25 (277.5)	7.76	13.46
19	115.25 (292.7)	11.65	17.27
20	121.25 (308.0)	15.55	21.21
21	127.25 (323.2)	19.45	25.02
22	133.25 (338.5)	23.35	29.08

Piezometer calibration

Piezometer calibration was necessary to obtain water depths and water surface elevations from piezometer readings. In our experimental setup, the point gauges were used to measure water depths directly. To get the water depth at a specific point gauge, the baseline point gauge reading was subtracted from the gauge reading. For piezometer calibration, the water depth at the point gauge closest to a piezometer was used as the water depth of that piezometer. The water depth at point gauge A was used for piezometers 14-16; the water depth at point gauge B was used for

51

piezometers 11-13; The water depth at point gauge C was used for piezometers 7-10; the water depth at point gauge D was used for piezometers 5-6; the water depth at point gauge E was used for piezometers 3-4; and the water depth at point gauge F was used for piezometers 1-2. Point gauge A was used to calculate water depths at piezometers 17-22 in the sloping section. Due to the inclination of the culvert upstream of the runout section, the bed elevation of the inclined culvert required additional calculation. Bed elevation differences were subtracted from the water depth at point gauge A to get the water depth in the inclined section. The design angle of inclination is 15 degrees. This exact angle was difficult to achieve during construction. The actual angle of inclination was determined by fitting a linear trendline for baseline readings of piezometers 17-22 and the distances of piezometer 17-22 from culvert break. The trendline slope represented the sine of the actual angle of inclination. It was found that the actual angle of inclination was 14.81 degrees. The actual angle of inclination was then used to calculate the bed elevations at piezometers 17-22 with respect to the bed of the culvert invert.

A trendline for piezometer readings and water depths for piezometers 1-10 was fitted. The y-intercept, 0.40 cm, was the baseline of piezometers 1-10, indicating that 0.40 cm should be subtracted from each piezometer reading to obtain actual water depth. Individual trendlines were also fitted for piezometers 11-16 since the scale lines were not the same as for piezometers 1-10. The y-intercepts were the datums for piezometers 11-16. For piezometers 17-22, the piezometer readings and water depths did not grow at the same rate due to the culvert inclination. The depth at each cross section can then be determined for any test by subtracting the baseline reading from the piezometer reading. Baseline piezometer readings at each piezometer position are reported in Table 3.10.

3.5.5.3 Prandtl tubes

Prandtl tubes are devices used to measure the velocity of water at a fixed point by utilizing the difference between the stagnation pressure and the static pressure. Stagnation pressure is the pressure at the tip of the Prandtl tube, where velocity goes to zero. Static pressure is measured by holes in the side of the Prandtl tube and is the pressure of the unimpeded flow. Applying the Bernoulli equation and using the definitions of stagnation and static pressure results in:

$$V = \sqrt{2g\left(\frac{P_0 - P}{\gamma}\right)} = \sqrt{2g\Delta h} \qquad (3.1)$$

where V is the flow velocity, g is the gravitational acceleration, P_0 is stagnation pressure, P is static pressure, and Δh is the difference between stagnation pressure head and static pressure head.

Prandtl tubes used in the experiments were permanently affixed in the same position for all tests. Initially, two Prandtl tubes (P1 and P2) were installed in the inclined section of the culvert (Fig. 3.5). P1 was located immediately downstream of the entrance to the drop and P2 immediately upstream of the break in the culvert. Both P1 and P2 were located along the center plane of the flow and were positioned 3.5 cm above the bed. Later, three Prandtl tubes (LDB, CL, and RDB) were installed across the downstream end of the dissipation box. These were positioned 1.0 cm above the bed of the box, with one Prandtl tube at the center plane of the box (CL), and two Prandtl tubes on either side (LDB and RDB) (Fig. 3.12).

Δh for Prandtl tubes P1 and P2 were measured using manometers; Δh for Prandtl tubes LDB, CL, and RDB were found using digital manometers connected to them through stilling tanks that dampen pressure fluctuations (Fig. 3.13). Air entrainment of the flow in the dissipation basin caused air bubbles to become trapped in the Prandtl tubes. To prevent the errors caused by air bubbles, the stilling tanks were filled prior to each test to flush out any air bubbles. Readings were collected after the water columns in the stilling tanks stabilized.
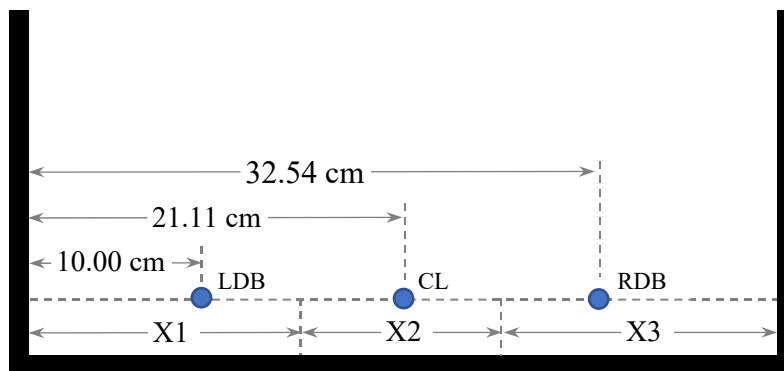
Figure 3.12 Positions of Prandtl tubes (looking downstream)
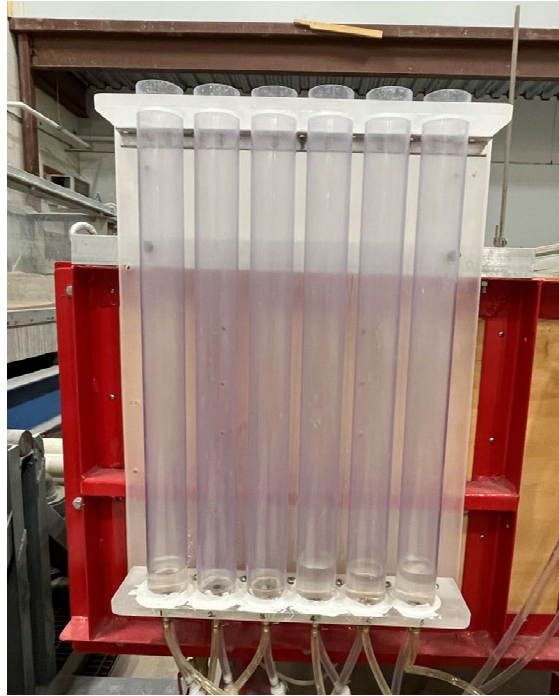
Figure 3.13 Stilling tanks for Prandtl tubes LDB, CL and RDB

3.5.5.4 V-notch weir and weir equations

A V-notch weir tank was installed downstream of the tail box to measure the discharge passing through the test section. Discharge coming from the tail box entered the weir tank through four pipes. Diffusers on the ends of the pipes helped to disperse the incoming water jets. The water then flowed through a large baffle in the center of the weir tank, which helped to break up the flow. The water traveled over a V-notch weir and was returned to the system supply tank. Figure 3.14 shows the geometry of the V-notch weir at the outlet of the weir tank.
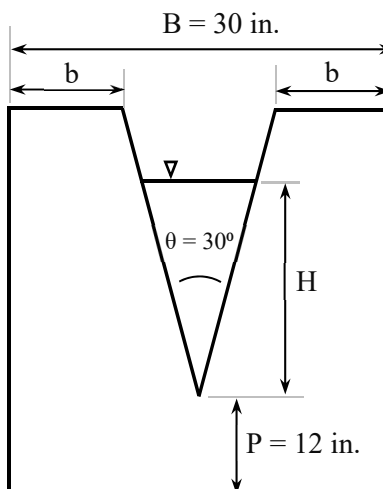
Figure 3.14 V-notch weir geometry and dimensions

A stilling tank was attached to the center of the bottom of the V-notch weir tank. A point gauge was attached to the side of the tank to measure the water surface elevation in the stilling tank (and thus in the weir tank). The water surface elevation corresponding to the crest elevation (P) was measured by reading the point gauge when there was no flow out of the weir tank and the water level in the tank was up to the crest; this measurement was used as a datum. For all tests, the flow rate through the test section was set and allowed to reach steady conditions. The water surface elevation in the weir tank was measured using the point gauge and stilling basin. Then H was found by subtracting the crest elevation from the point gauge reading. For a partially contracted V-notch weir, the discharge (Q) in ft³/s is a function of the effective discharge coefficient (C_e), the weir angle (θ), and the depth of the water above the crest of the V-notch (H) in ft (U.S. Bureau of Reclamation, 1997):

$$Q = 4.28 C_e \tan\left(\frac{\theta}{2}\right)(H + k_h)^{5/2} \qquad (3.2)$$

k_h is a function of the weir angle and is 0.007 for a 30-degree weir. The effective discharge coefficient (C_e) is a function of H/P and P/B. It can be found using Fig. 3.15.
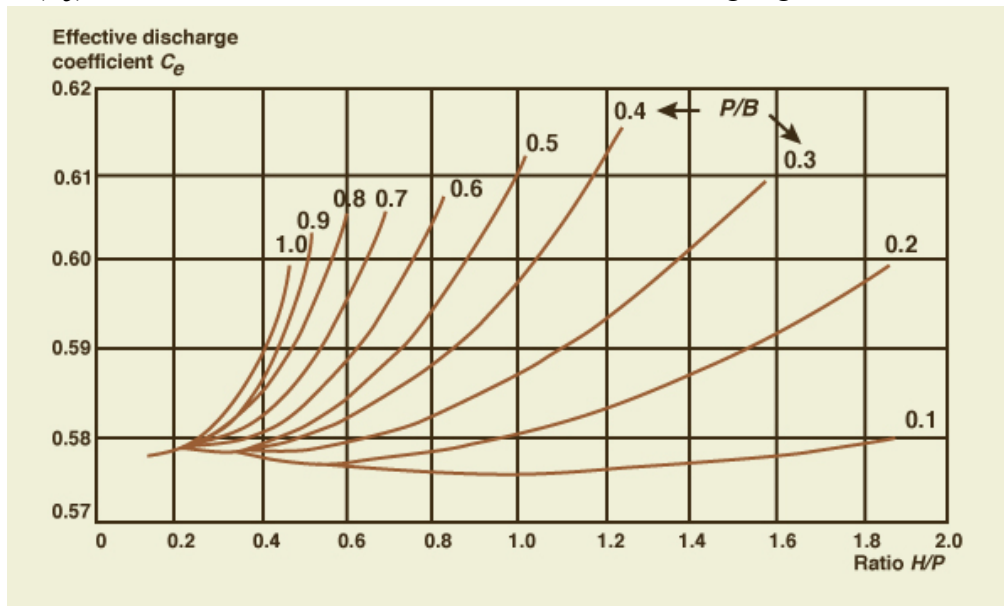
Figure 3.15 Effective discharge coefficient (C_e) as a function of H/P and P/B (British Standard 3680, part 4A, 1971)

3.6 Tested Dissipation Structures
In this section, the energy dissipation structures that were tested in the facility are described in more detail. Two types of structures were tested over the course of the project: a staggered weir, and a full-length weir. The two types of weirs were tested primarily at one streamwise position, but it would be relatively straightforward to adjust streamwise positions in future testing.

3.6.1 Energy dissipation structure 1 – staggered weir

The concept of the staggered weir wall was developed to produce the same effect as the weir wall while reducing sediment buildup and preventing the formation of a stagnant water pool when the weir was not operating. Originally, the gap between the two rows of the prototype staggered weir wall was set to six inches to reduce debris entrapment. The distance that was used in the model was scaled from the 48-inch prototype.

Figure 3.16 shows the geometry of the staggered weir in the model dissipation structure. All three weir walls (the upstream weir wall and two downstream side weir walls) have identical thicknesses of 2.08 inches. The width of the upstream weir wall is 8.33 inches and the downstream weir walls have widths of 5.42 inches. The distance between the headwall and the upstream face of the upstream weir wall is 12.50 inches. The distance between the two rows of weir walls is 1.25 inches. Four sets of staggered weirs of different heights were tested: $D/8$, $2D/8$, $3D/8$ and $4D/8$ where D is the diameter of the culvert model.

Tested Weir Heights in. (cm)
1.25 (3.18) $\left[\frac{1}{8}D\right]$
2.50 (6.35) $\left[\frac{2}{8}D\right]$
3.75 (9.53) $\left[\frac{3}{8}D\right]$
5.00 (12.70) $\left[\frac{4}{8}D\right]$
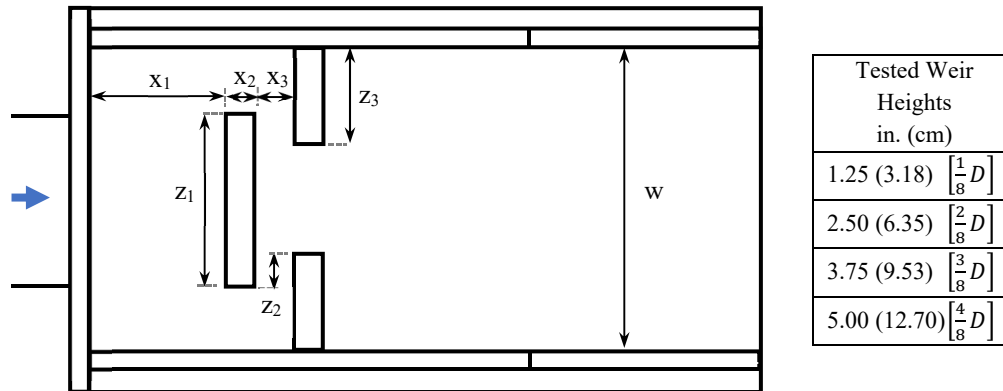
Description	Variable	Dimensions in. (cm)
Pipe diameter	D	10.0 (25.4)
Downstream placement of central baffle	x_1	12.5 (31.8)
Weir thickness	x_2	2.08 (5.3)
Baffle offset	x_3	1.25 (3.2)
Central baffle width	z_1	8.33 (21.2)
Baffle overlap	z_2	1.25 (3.2)
Downstream baffle width	z_3	5.42 (13.8)
Dissipation basin width	w	16.67 (42.3)
Dissipation basin length	L	37.5 (95.3)

Figure 3.16 Plan view of model staggered weir in the dissipation box

3.6.2 Energy dissipation structure 2 – full-length weir

The second structure tested in the test facility was a full-length weir. Figure 3.17 shows the geometry of the full-length weir in the dissipation structure model. The width of the weir is the

same as the width of the dissipation structure model, 16.67 in. The thickness of the weir is 2.08 inches, and the front face of the weir was located 12.5 inches downstream of the headwall. Like the staggered weirs, four full-length weirs with different heights were used in the tests. The heights of the full-length weirs that were tested were: 1/8D, 2/8D, 3/8D and 4/8D where D is the diameter of the culvert model. Additional geometric information is provided in Figure 3.17.

Tested Weir Heights in. (cm)
1.25 (3.18) $\left[\frac{1}{8}D\right]$
2.50 (6.35) $\left[\frac{2}{8}D\right]$
3.75 (9.53) $\left[\frac{3}{8}D\right]$
5.00 (12.70) $\left[\frac{4}{8}D\right]$
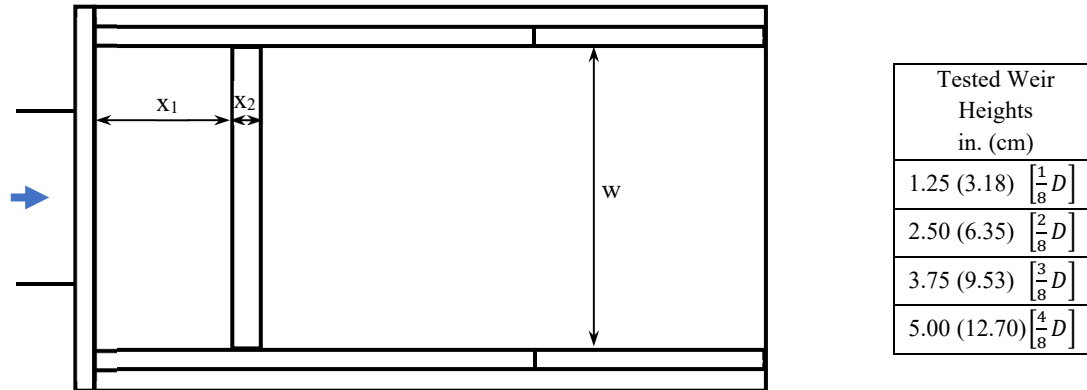
Description	Variable	Value in. (cm)
Pipe diameter	D	10.0 (25.4)
Downstream placement of weir	x_1	12.5 (31.8)
Weir thickness	x_2	2.08 (5.3)
Dissipation basin width	w	16.67 (42.3)
Dissipation basin length	L	37.5 (95.3)

Figure 3.17 Plan view of model weir in the model dissipation structure

3.7 Dimensional Considerations

A simple dimensional analysis of the present configuration is provided here for the energy dissipation structures. The most important variables in the present analysis include geometric dimensions, flow variables, and fluid properties. Geometric dimensions are depicted in Figure 3.6. A list of the most important variables, including geometric dimensions, flow variables, and fluid properties includes: culvert diameter (D), depth in the runout section (d), depth at the dissipation basin outlet (T), basin width (w), basin length (L), weir height (h), discharge (Q), kinematic viscosity (ν), density (ρ), and gravitational acceleration (g).

3.7.1.1 Dissipation basin outlet depth

The outlet depth of the dissipation structure when there is no weir is related to the discharge, the depth in the culvert, the diameter of the culvert, the width of the structure, the gravitational acceleration, the viscosity of the water, and the density of the water.

$$T = f(Q, d, D, w, g, \mu, \rho) \tag{3.3}$$

By dimensional analysis, this can be resolved into five dimensionless parameters:

$$\frac{T}{D} = f\left(\frac{Q}{g^{1/2}d^{5/2}}, \frac{d}{D}, \frac{w}{D}, \frac{\rho Q}{\mu d}\right) \tag{3.4}$$

The relation suggests that the dimensionless outlet depth (T/D) is a function of runout Froude Number (Fr), the depth to diameter ratio in the runout section, the width to diameter ratio of the dissipation basin, and the Reynolds number in the runout section. For high Reynolds numbers, flow behavior is generally independent of Reynolds number, and for the present tests, w/D is a fixed value. Thus, T/D is then a function of d/D and $Q/(g^{1/2}d^{5/2})$:

$$\frac{T}{D} = f\left(\frac{Q}{g^{1/2}d^{5/2}}, \frac{d}{D}\right) \tag{3.5}$$

The Coriolis coefficient, α, also affects the Froude number, so a standard Froude number is used in place of the one shown in equation 3.5. The standard Froude number is based on the velocity in the runout section and the hydraulic depth:

$$Fr = \frac{V}{\sqrt{g\dfrac{D_h}{\alpha}}} \tag{3.6}$$

Where $D_h = A/T_w$. A is the flow cross sectional area, and T_w is the top width. A is directly related to d^2, and D_h is directly related to d, so the Froude number defined by equation 3.6 in place of $Q/(g^{1/2}d^{5/2})$ fully captures the same important flow behavior.

3.7.1.2 Weir dimensional considerations
For the weirs, important variables also include the distance of the weir from the dissipation box head wall (x_1) and the weir height (h):

$$T = f(Q, d, D, w, g, v, \rho, h, x_1) \tag{3.7}$$

Incorporating these variables into the dimensional analysis results in the following parameter set:

$$\frac{T}{D} = f\left(Fr, \frac{d}{D}, \frac{h}{D}, \frac{x_1}{D}\right) \tag{3.8}$$

The parameter x_1/D does not change for the present experiments so:

$$\frac{T}{D} = f\left(Fr, \frac{d}{D}, \frac{h}{D}\right) \tag{3.9}$$

3.7.1.3 Energy considerations

By assessing the energy upstream and downstream of a dissipation structure, one can determine the energy absorbed by the structure for different flows. The variables required to determine change in specific energy include both inflow and outflow variables:

$$\Delta E = f(Q, d, T, \alpha_1, \alpha_2, g,) \tag{3.10}$$

Where change in specific energy is defined as:

$$\Delta E = \left(\alpha_1 \frac{Q^2}{2gA_1^2} + d \right) - \left(\alpha_2 \frac{Q^2}{2gA_2^2} + T \right) \tag{3.11}$$

α_1 and α_2 are velocity correction (Coriolis) coefficients. These are often assumed to be 1.0. However, in the present case, α_1 and α_2 are likely greater than 1 due to uneven distribution of velocity at the inflow and outflow cross sections. It may be difficult to determine the exact Coriolis coefficient, but literature provides some estimates that will likely improve results. A_1 and A_2 are cross sectional areas of the flow upstream and downstream of the dissipation structure, respectively. In the present case, A_2 is simply wT; A_1 is a more complicated function of the runout depth.

A dimensionless form of ΔE will be used in this report, $\Delta E/y_c$, where y_c is the critical depth at the dissipation box outlet, so that it is easy to estimate ΔE for scaled structures. ΔE does not add any additional variables to the dimensional analysis because it is fully dependent on the variables shown in Equations 3.3 and 3.7 (ignoring variability of α). As shown by Equation 3.11, ΔE is mostly dependent on the runout depth, the dissipation basin outlet depth, and the discharge. We can use it to replace the tailwater depth in Equation 3.9, so it can be analyzed as a function of runout Froude number, runout depth, and weir height:

$$\frac{\Delta E}{y_c} = f\left(Fr, \frac{d}{D}, \frac{h}{D} \right) \tag{3.12}$$

In similar fashion, outlet energy can also be calculated as a function of the runout section variables, and may be useful for flow behavior predictions:

$$\frac{E_2}{y_c} = f\left(Fr, \frac{d}{D}, \frac{h}{D} \right) \tag{3.13}$$

3.7.1.4 Outlet momentum considerations

The outlet momentum from the dissipation box is useful if forces on weirs are needed. No measurements of forces were done in the current research, and this section is provided primarily for reference purposes. For predicting erosion at outlets, momentum might also provide a useful substitute for specific energy because specific energy consists of both potential energy and kinetic energy, and erosion is mostly associated with kinetic energy. Momentum is a function of the discharge, outlet depth, and flow density:

$$M = f(Q, T, w, \rho, g) \tag{3.14}$$

It is defined as:

$$M = \rho\, Q^2 / A \tag{3.15}$$

Like specific energy, the outlet momentum is a function of outlet tailwater depth and can replace tailwater depth as the dependent variable. No independent variables are added to Equation 3.7 by the introduction of momentum. Thus, the outlet momentum (M_2) can be introduced as:

$$M_2 = f\left(Fr, \frac{d}{D}, \frac{h}{D} \right) \tag{3.16}$$

Following Sturm (2010), momentum can be made dimensionless using the critical depth and the width of the dissipation box:

$$\frac{M_2}{\rho g w y_c^2} = f\left(Fr, \frac{d}{D}, \frac{h}{D} \right) \tag{3.17}$$

Density cancels out because all of the flows of interest are water (assuming that density variations due to aeration are negligible).

It is also useful to consider momentum and pressure differentials on the model weirs, since these provide a measure of the forces on the weirs, but a closer look reveals that this is complicated for the present geometry. If the momentum equation is considered for a prismatic channel in which shear stresses are negligible, it can be shown that the force on a weir across the channel, F_w, is simply:

$$F_w = -\Delta(M + \gamma h_c A) \tag{3.18}$$

Where Δ is an operator that represents the difference between the downstream and upstream sections of the system (the difference in momentum and hydrostatic forces between the outlet

and the runout section). h_c is the location of the centroid of the flow cross section area below the free surface; it is simply half the depth for rectangular cross sections, but for partly filled circular culverts it is quite a bit more complex. Equation 3.18 represents a balance between changes in momentum, the hydrostatic force differential, and the force on the weir. In the present case the problem is made complex by the expansion at the outlet of the runout section. Reapplying the momentum equation between the runout section and the dissipation box outlet, the resulting force is the combined force of the flow on the weir and the head wall:

$$F_w - F_h = -\Delta(M + \gamma h_c A) \tag{3.19}$$

The force on the headwall, F_h, is associated with hydrostatic pressure since there is no momentum flux across the head wall. In this case, $F_h = \gamma h_{cw} A_w$, where h_{cw} and A_w are the centroid and cross section area of the headwall below the water surface at the weir. These two variables have very complex geometry but can be determined as a function of water depth measurements immediately upstream of the weir. Then, Equation 3.19 becomes:

$$F_w = \gamma h_{cw} A_w - \Delta(M + \gamma h_c A) \tag{3.20}$$

Direct measurements of the force on the model weir would allow examination of the accuracy of Equation 3.20; while this is outside of the scope of the present study, it is a useful topic for a future study. A dimensionless version of the force on the head wall is given by Equation 3.21.

$$\frac{F_w}{\rho g w y_c{}^2} = f\left(Fr, \frac{d}{D}, \frac{h}{D}\right) \tag{3.21}$$

3.8 Energy Calculation Details

3.8.1 Specific energy and energy calculations
Specific energy head is the summation of velocity head and streamwise depth:

$$E = \alpha \frac{V^2}{2g} + y \tag{3.22}$$

Where α is the energy coefficient, V is the bulk average velocity, and y is depth. Bulk average velocity is calculated as the ratio of flow rate and cross-sectional area.

In the present work, velocity and depth measurements are collected for analysis in relatively difficult conditions. Upstream data are collected in circular conduits flowing partly full, while downstream data are collected in a rectangular section. Flow in partly full circular conduits is

more complex than in rectangular sections, but for the present flows, data analysis is difficult for both because: (a) assessment of flow depth is necessary to determine Froude regime and specific energy, (b) depth measurements are small, leading to a high relative uncertainty of the depth, (c) the flow is highly turbulent with air entrainment, making depth measurements difficult in most locations, (d) the flow is supercritical in most sections so that much of the flow energy is contained in the velocity head term, and (e) it is only practical to collect a limited number of velocity measurements.

There are two ways to determine specific energy in the test facility: (1) Measure the depth and compute the velocity from the ratio of discharge and cross-sectional flow area, or (2) Measure the depth and velocity separately to compute the specific energy. The first method is useful in areas with no velocity measurements. The second method is useful for areas with shallow depth and high velocity, because in these areas, small error in depth measurements leads to significant error in specific energy calculations. These two methods are described here.

In some cases, it may also be necessary to determine total energy because not all bed elevations in the experimental setup are the same. In such cases, total energy is the sum of bed elevation, streamwise depth and velocity head. As a reminder, the datum used for total energy calculations is the bed of the energy dissipation basin.

3.8.2 Energy calculations from depth measurements

3.8.2.1 Streamwise water depth
For piezometers 1-16 and point gauges A-F, streamwise water depths are calculated by subtracting baseline readings from experimental readings.
For piezometers 17-22 that are located at the inclined section of the culvert, assuming that we have parallel flow in the inclined section, the pressure at the bed (p) is:

$$p = \gamma d \cos\theta \tag{3.23}$$

where γ is the specific weight of water, d is the streamwise depth, and θ is the bed slope angle. Since pressure is measured with the piezometer:

$$p = \gamma \Delta z \tag{3.24}$$

where Δz is the difference between the test piezometer reading and the piezometer reading when there is no flow in the testing section but the piezometer is still full of water. Then:

$$d = \frac{\Delta z}{\cos\theta} \tag{3.25}$$

If a point gauge is used to measure Δz, Δz is the difference between the point gauge reading for the test and the point gauge reading of the bed.

When the water level in a piezometer exceeds the top of the culvert (i.e., the pipe is full), the piezometer reading no longer reflects the depth. When the streamwise water depth reading inside the culvert exceeds the culvert diameter, the actual streamwise water depth is the same as the culvert diameter. Thus, the maximum streamwise water depth is the inner diameter of the culvert. Moreover, in the case of a full pipe, total energy calculations require the pressure head because the flow becomes closed conduit flow. The pressure head can be determined from piezometer measurements but not from point gauge measurements.

3.8.2.2 Cross-sectional area

In order to determine bulk-average velocity, it was necessary to determine the cross-sectional area at each location. There are two types of cross sections in the testing section: partially filled circular cross sections in the culvert and rectangular cross sections in the dissipation basin. Partially filled circular cross-sectional areas (corresponding to point gauges A-C and piezometers 7-22) can be found using the relation between streamwise water depth and flow cross section depicted in Figure 3.18. θ and A can be calculated as follows:

$$\theta = 2 \arccos\left(\frac{r-h}{r}\right) \tag{3.26}$$

$$A = \frac{r^2}{2}(\theta - \sin\theta) \tag{3.27}$$
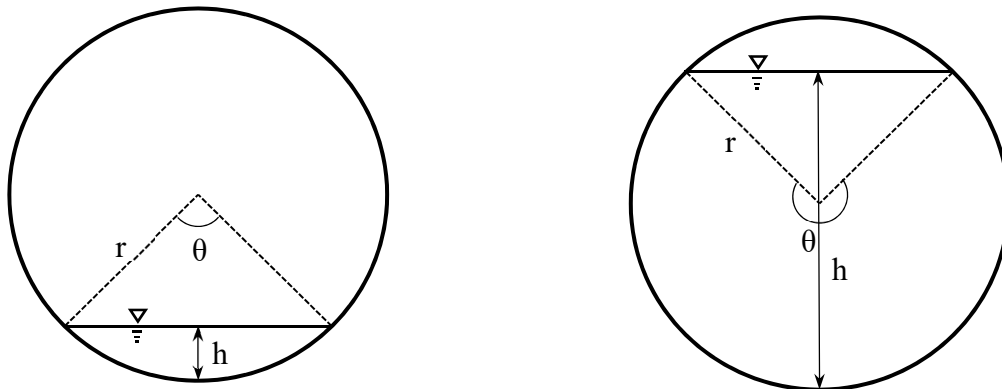
Figure 3.18 Geometric determination of flow cross section.

As shown in Figure 3.19, in the dissipation basin, the rectangular cross-sectional area (corresponding to piezometers 1-6 and point gauges D-F) is much simpler and is the product of water depth and the inside width of the dissipation basin:

$$A = w \cdot h \tag{3.28}$$

For piezometers 3 and 4 and point gauge E, the flow cross-sectional area must also take the weir type and position into account.
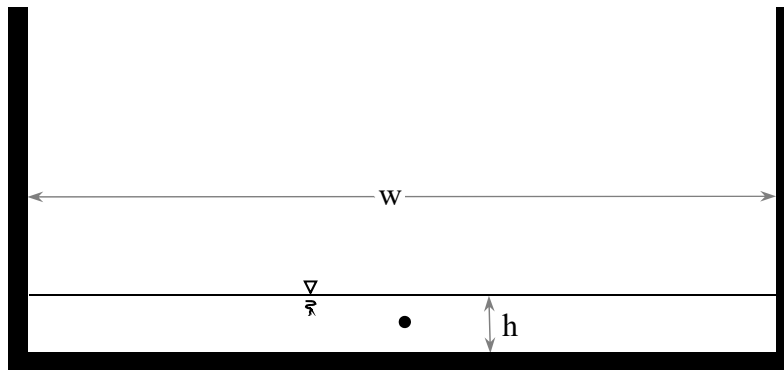
Figure 3.19 Flow cross section of dissipation box.

3.8.3 Energy calculations from depth and velocity measurements

3.8.3.1 Velocity
Flow velocity was measured using two Prandtl tubes installed in the inclined section of the culvert and three installed at the downstream end of the dissipation basin. The velocity of the flow at the Prandtl tube tip (u) is calculated as:

$$u = \sqrt{2g\Delta h} \tag{3.29}$$

Where g is gravitational acceleration and Δh is the difference of the two manometer readings.

3.8.3.2 Velocity corrections
The Prandtl tube measures velocity at a point, but the bulk average velocity is needed for specific energy calculations. Since Prandtl tube elevations were fixed, velocities measured at the dissipation basin outlet were adjusted using the power law. Originally, Nikuradse utilized a power relation to model pipe flow data (Schlichting, 1960), and the relation has been extended for use in wide open-channel flows as given by Equation 3.30.

$$\frac{u}{u_{max}} = \left(\frac{z}{H}\right)^{1/7} \tag{3.30}$$

$$V = \frac{Q}{A} = \frac{\int_0^H u_{max} \left(\frac{z}{H}\right)^{1/7} b\, dz}{bH} = \frac{7}{8} u_{max} \qquad (3.31)$$

In which u is the velocity at elevation z above the bed (measured with the Prandtl tube), and u_{max} is the velocity at the water surface where z equals the flow depth. The power relation shows that the velocity at 0.4 times the flow depth equals the bulk average velocity ($V = \frac{7}{8} u_{max}$). Furthermore, the average of the velocities measured at 0.2 and 0.8 times the depth also equals the bulk average velocity. Discharge measurements in rivers typically utilize this observation in integrating velocity measurements across a river cross section. In the present research, however, the power law is used to convert velocities measured at an arbitrary fraction of the depth to bulk average velocities in the rectangular outlet section.

An iterative method is used to calculate the streamwise depth given the measured velocity (u), the elevation of the tip of the Prandtl tube above the bed (z), and the measured flow rate (Q). Using an initial guess of the streamwise depth (H) in equation 3.30 yields maximum flow velocity, and equation 3.31 yields the bulk average velocity. Dividing the flow rate by the bulk average velocity and dissipation structure inner width yields a new streamwise depth. The process can be iterated until depth converges.

3.8.4 Additional energy calculation considerations

In most cases, for the calculation of dissipation basin outlet specific energy, the velocity head at the dissipation basin outlet was determined from the three Prandtl tubes. A weighted average of the three Prandtl tube readings was used, assuming that the LDB, CL and RDB Prandtl tubes measure the velocity heads for X1, X2 and X3, correspondingly (Fig. 3.12). Bulk average velocity and streamwise depth were calculated based the power law. Although energy (or Coriolis) coefficients are often assumed to be unity, these coefficients can be significantly higher than unity for open channel flows. For rectangular channels, energy coefficients have been reported by Chow (1959) to range from 1.10 to 1.20 with an average of α = 1.15. These values are based on the work of Kolupaila (1956). While there are insufficient spatial velocity data to verify this coefficient, we assume that α = 1.15 for determination of specific energy at the outlet.

For the calculation of specific energy in the runout section, the depths were higher and directly measured depths were used to calculate specific energy. We elected to do this in the runout section because knowledge about the velocity distribution in a partially full circular pipe is not as prevalent. Nevertheless, Table 3.11 and 3.12 show two references that discuss the Coriolis coefficient for partially filled culverts. Both references are for relatively low Froude numbers. In any case, it is not possible for α to be less than 1 and it is unlikely to be more than 1.5. Most of the runout section depths for the current experiments were in the 5 to 10 cm range, which corresponds to depths of 0.2D to 0.4D. Based primarily on this depth range and the more recent work of Sterling (1998) and a depth of about 0.333D, we elected to use a constant value of α of

1.25; this value was applied in Froude, energy and velocity head calculations in the partially filled culvert. The numbers in Tables 3.11 and 3.12 demonstrate that even with perfect local measurements of depth and velocity, there could be significant uncertainty due to error in the Coriolis coefficient. It is difficult to overcome this issue, for lack of available information.

Table 3.11 Coriolis coefficients reported by Sterling (1998)

Froude	d/D	Coriolis Coef.
0.516	0.333	1.28
0.505	0.506	1.48
0.441	0.666	1.29
0.375	0.826	1.37

Table 3.12 Coriolis coefficients reported by Replogle (1966)

Froude	d/D	Coriolis Coef.	Froude	d/D	Coriolis Coef.
0.945	0.333	1.125	0.626	0.332	1.184
0.938	0.500	1.067	0.693	0.498	1.145
0.798	0.683	1.053	1.280	0.651	1.102
			0.543	0.678	1.090

3.9 Consistency of Piezometer and Point Gauge Measurements

Water depth can be directly measured using either the point gauges or piezometers. This is useful for comparing if the two depths are consistent. There are a number of reasons that the measured depths may be different, including:

1. The piezometers are not perfectly machined. Although care was taken when the piezometers were installed, the material is acrylic, and the piezometers may not be exactly perpendicular to the bed. This can artificially elevate or reduce static pressure measurements.
2. The flow in the culvert and the dissipation box is not completely uniform. For example, at the break in slope, the momentum of the water causes spatial oscillation of the supercritical water surface. This leads to places where the piezometers may read high or low, depending on if the flow is impinging on the bed or diverging from the bed. This is especially problematic where the flow is exiting the culvert or going over a weir.
3. In some parts of the flow, there are hydraulic jumps or rapidly changing water surface conditions. In these areas, it can be difficult to use the point gauges accurately.
4. Both piezometers and point gauges are along the channel centerline, but there are parts of the culvert and dissipation basin where there is some lateral variation of the water surface. This is especially true in the dissipation basin when there are no dissipation structures installed.

In Figure 3.20, point gauge depths are directly compared with piezometer depths for a wide range of tests, some of which have weirs installed. Depths measured with piezometers 15 and 16 are interpolated for comparison with point gauge A, depths measured with piezometers 12 and 13 are interpolated for comparison with point gauge B, and depths measured with piezometers 9

and 10 are interpolated for comparison with point gauge C. The depth from piezometer 6 is directly compared with the depth from point gauge D, since it is very close to point gage D and interpolation is impractical at the sudden expansion from the circular culvert to the rectangular dissipation structure. The depth from piezometer 1 is directly compared with the depth from point gauge F, since there is no piezometer farther downstream for interpolating. Piezometer 1 and point gauge F are also in close proximity. No comparison is given for point gage E since it is situated directly above a weir during weir tests.

Figure 3.20 includes data from nine test sets: tests with no weirs, tests with staggered weirs, and tests with full weirs. Weir heights range from 1/8D to 4/8D in the tests. For each test, eight different flow rates are used, resulting in a total of 72 conditions. Most of the data points are very close to the 1:1 trendline, indicating consistency between point gauge readings and piezometer readings. Data points that fall further from the trendline indicate inconsistency between point gauge readings and piezometer readings. It is observed that the inconsistency occurs primarily at point gauges D and F for high flow rates. The inconsistency may be due to the reasons given above, but point gages D and F are also located in places where accurate measurements are more difficult – at the outlet of the culvert and at the outlet of the dissipation basin. Neither point gauges nor piezometers are as accurate in positions where there is significant aeration and nonuniformity of the flow. The piezometer and point gauge readings are more consistent at other locations and at lower flow rates, but even in these conditions, the depth measurement accuracy is on the order of about 1 cm, based on the data in figure 3.20. In general, the point gage measurements appear to be more reliable than the piezometer measurements for this facility.
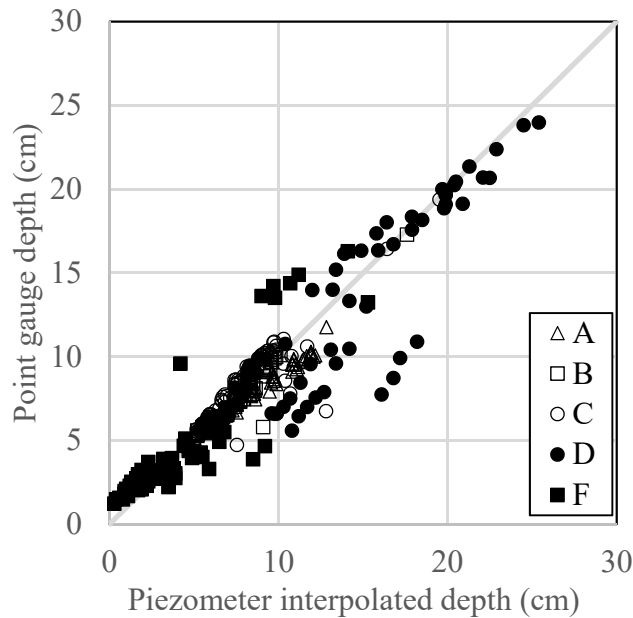
Figure 3.20 Plot of piezometer interpolated depth and point gauge depth

3.10 Overview of Tests

For the dissipation structures tested, there are three primary causes of energy loss: the dissipation basin expansion, the structures added to the dissipation basin, and the hydraulic jump and eddies that form due to tailwater. These three causes need to be isolated to get a better idea of the effectiveness and optimal geometry of targeted dissipation structures. The tests can be divided into three types:

- Baseline Tests: Because the dissipation basin is an expansion from a circular culvert to a rectangular box, there is energy loss associated with the expansion alone. Thus, in order to better understand the effect of each structure added to the basin, the basin is tested by itself before introducing any structures. Baseline tests were performed for both tailwater-independent and tailwater control tests and are included with the data.

- Tailwater-independent Tests: A problem arises when the tailwater is controlled by the outlet gate in that the energy dissipation of the dissipation structure and the energy dissipation of the hydraulic jump that forms because of the tailwater cannot be separated. Consequently, the main tests rely on keeping the tailwater as low as possible so that it does not impact the exit depth of the dissipation basin. If the flow approaching the outlet is supercritical, tailwater-independent outlet depth will be less than or equal to critical. In this case, the closer the outlet depth is to critical, the greater the energy loss caused by the weir. Alternatively, if the flow in the dissipation basin is subcritical, the water surface profile will be an H2 curve, and the depth will approach critical at the outlet. Subcritical flow is ideal because it minimizes exit velocities, but it is also unlikely that a standard weir configuration will cause this type of profile. Incidentally, subcritical flows were not observed in the dissipation basin for any of the tailwater-independent tests.

- Tailwater Control Tests: early in the testing process a large number of tests were done with all weir configurations. For these tests two parameters were varied: the discharge and the tailwater depth. As the tailwater was increased, the water in the tail tank flooded the dissipation basin and the runout section of the culvert. Although many data were collected, they are not used as extensively as the tailwater-independent tests because it is impossible to separate weir performance from tailwater influence for these tests. However, the data are used to investigate backwater heights required to force the jump into the culvert.

Results of the tests are presented in Chapter 4.

3.10.1 <u>Baseline tests</u>

To calculate energy dissipation associated with different weir geometries, the energy at the downstream end of the dissipation structure when no weir is in place is needed for different flow rates. Depths measured with piezometers 1 and 2 for eight flow rates when no weir is in place are shown in Figure 3.21. These two piezometers are located near the end of the dissipation structure. The plotted model discharges range from 0.60 to 1.79 ft³/s. Nonlinear curve fits of the depth versus discharge data are shown in Fig. 3.21. The two data points with the highest flow rate are discarded since the tailwater influences water depth in the dissipation structure at these

discharges. Fig. 3.21 shows that the depths in the dissipation are quite low – less than 0.5 cm at the outlet for the lowest discharges. We found the depths to be slightly higher than reported by the piezometers (but difficult to accurately measure). Nevertheless, the outlet velocities are swift and the depths are shallow, especially when no weirs are in place.
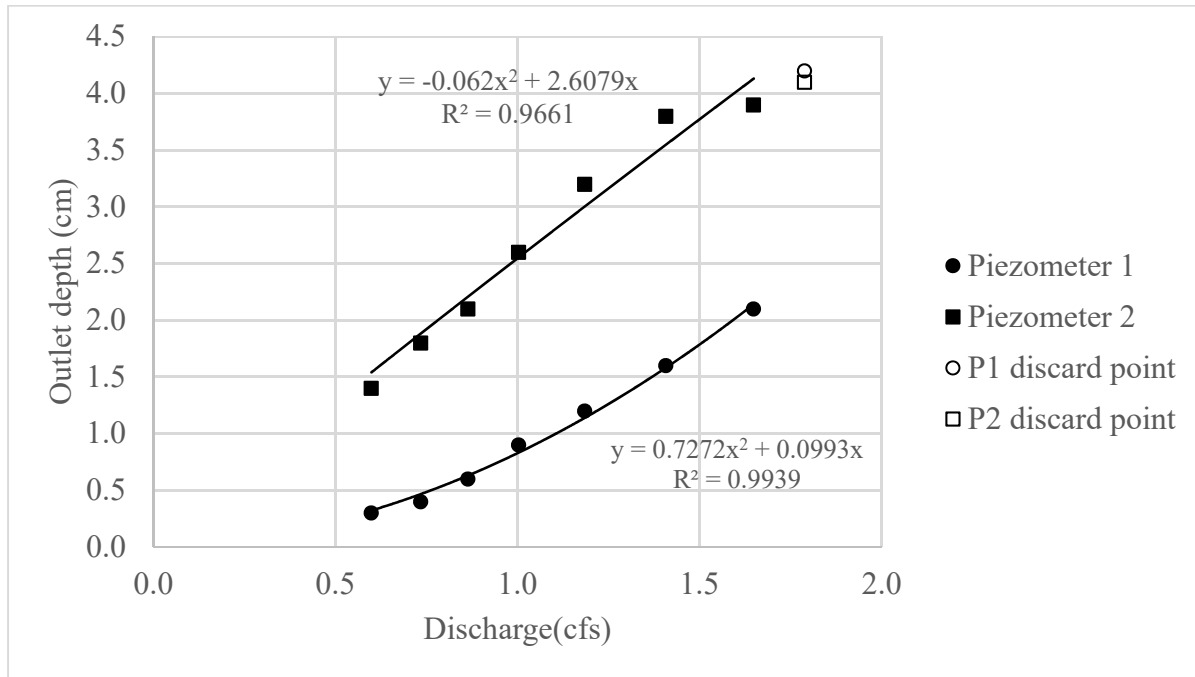
Figure 3.21 Plot of outlet depth as a function of discharge with no weir

3.10.2 Tailwater-independent tests

Table 3.13 provides conditions for the tailwater-independent tests, including baseline tests (YYA), full-length weir tests (YYB-YYE), and staggered weir tests (YZB-YZE). Eight discharges were tested for each weir type and height, for a total of 72 tests. The eight discharges ranged from 0.015 to 0.055 m³/s and were selected so that each test series had matching sets of discharges.

Table 3.13 shows the conditions of the tailwater-independent full-length weir tests. Even though the range of discharges is fairly wide, the range of Froude numbers is limited by the geometry of the system. In future studies, modifications to the experimental system can provide a wider range of both Froude numbers and discharges. These modifications are not extremely difficult, but they are substantial enough that they could not be employed in the present research; they are discussed in the conclusions section of this report. Although these tests were designed to be tailwater independent, the data collected showed that the tests with the two highest discharges had tailwater influence (this is clearly denoted in figures provided in the results).

Table 3.13 also shows the conditions of the tailwater-independent staggered weir tests. Like the full-length weir tests, the range of Froude numbers is limited by the geometry of the system. These tests are discarded in scale-independent analyses. Again, the tests with the two highest discharges did appear to be influenced by the tailwater. These tests are discarded in scale-independent analyses.

Table 3.13 Summary of tailwater-independent weir tests

Series	Weir	Weir Height	Tests	Discharges (m³/s)	Runout Froude Range	Notes
YYA	None	N/A	8	0.017 to 0.053	3.8 to 4.4	Prandtl
YYB	Full-Length	D/8	8	0.016 to 0.054	3.8 to 4.5	Prandtl
YYC	Full-Length	2D/8	8	0.017 to 0.053	4.0 to 4.8	Prandtl
YYD	Full-Length	3D/8	8	0.017 to 0.054	3.7 to 4.4	Prandtl
YYE	Full-Length	4D/8	8	0.017 to 0.054	3.9 to 4.2	Prandtl
YZB	Staggered	D/8	8	0.017 to 0.053	3.8 to 4.0	Prandtl
YZC	Staggered	2D/8	8	0.017 to 0.053	3.9 to 4.3	Prandtl
YZD	Staggered	3D/8	8	0.017 to 0.053	3.8 to 4.3	Prandtl
YZE	Staggered	4D/8	8	0.017 to 0.054	3.8 to 4.4	Prandtl

3.10.3 <u>Tailwater tests</u>

The tailwater tests are shown in Table 3.14 and consisted of many more tests (approximately 400 tests) than the tailwater-independent tests. Although baseline tests (tests without weirs in place) were collected for the tailwater tests, they are not shown in Table 3.14 because they are not used in any of the analyses presented in the report.

Each tailwater test series consisted of four discharges and eleven or twelve tailwater depths. The four discharges were carefully set so that the same four discharges were used for each test series. These four discharges are limited to a smaller range because the tailwater basin could not pass as much flow when these tests were performed.

Table 3.14 Summary of tailwater-influenced weir tests

Series	Weir	Weir Height	Tests	Discharges (m³/s)	Runout Froude Range	Notes
A	Staggered	D/8	~48	0.017 to 0.039	3.7 to 4.9	Tailwater Control
B	Staggered	2D/8	~48	0.017 to 0.039	3.7 to 4.9	Tailwater Control
C	Staggered	3D/8	~48	0.017 to 0.039	3.7 to 4.9	Tailwater Control
D	Staggered	4D/8	~48	0.017 to 0.039	3.7 to 4.9	Tailwater Control
I	Full-Length	D/8	~48	0.017 to 0.039	3.7 to 4.9	Tailwater Control
J	Full-Length	2D/8	~48	0.017 to 0.039	3.7 to 4.9	Tailwater Control
K	Full-Length	3D/8	~48	0.017 to 0.039	3.7 to 4.9	Tailwater Control
L	Full-Length	4D/8	~48	0.017 to 0.039	3.7 to 4.9	Tailwater Control

4. Results

4.1 Introduction

The results are divided into three sections: (1) staggered weir results, (2) full-length weir results, and (3) combined results for comparison purposes. Not all of the data collected were used in the analyses. Some of the data were found to be unnecessary or unreliable, and here it helped to have data redundancy to confirm measurements. In some cases, piezometers were in locations that made their outputs incorrect. For example, piezometers located immediately downstream of weirs or other abrupt changes in flow direction produced unreliable results. The high velocities and turbulent aeration observed in the system also made it difficult to read exact depths, whether by point gauge or by piezometer, in some cases.

Additional data were unused because the tests produced results that made it difficult or impossible to extract useful information. An example of this is the collection of data with large tailwaters. When tailwater was controlled, energy losses associated with the weirs could not be separated from energy losses associated with hydraulic jumps and energy absorbing eddies that were not directly produced by the weirs.

Therefore, the reported results mainly utilize depth data collected near the start of the runout section and near the outlet of the dissipation box. In the runout section, it was discovered that the point gauges were most reliable and easiest to read because of normal pressure effects induced on the piezometers by the drop structure. In the dissipation box, the two piezometers closest to the outlet were initially used because the outlet point gauge was difficult to accurately read. Ultimately, outlet depths were determined indirectly by measuring the outlet velocity using three transversely located Prandtl tubes. These velocity measurements were found to be significantly more accurate than depth measurements for the very low depths observed at the dissipation box outlet. This was not as much of a problem in the runout section, where the narrower cross-section caused larger water depths.

This chapter begins with a look at staggered weir results using directly measured runout and outlet depths. Then, using Prandtl tube measurements, staggered results are analyzed in greater detail. This process is repeated for the full-weir results. Finally, the chapter provides a comparison of staggered and full-weir performance.

4.2 Staggered Weir Results

In this section, piezometer-based energy dissipation results are presented. These results demonstrate performance of the staggered weirs based on piezometer and discharge measurements.

4.2.1 <u>Initial data</u>

Data collected for tailwater-independent tests are shown in Figure 4.1, which shows the dissipation basin outlet depth immediately upstream of the outlet (piezometer 1) and slightly farther upstream from the outlet (piezometer 2). Significant increases in the outlet depth are evident at Piezometer 1 for the highest discharge, indicating that the highest discharge tested is not tailwater-independent. The figures show that the third highest weir results in the highest outlet depths for the higher discharges. This behavior is apparent for both piezometer 1, which is at the outlet of the dissipation box, and at piezometer 2.
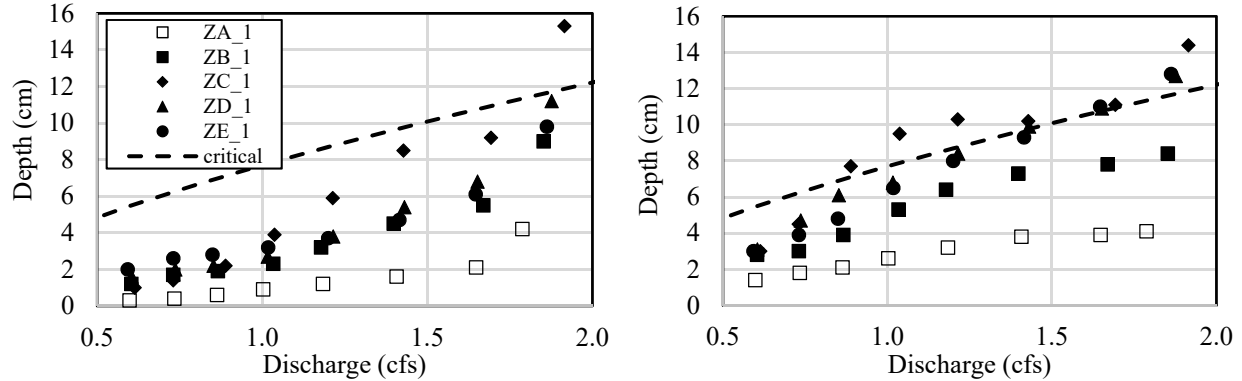
Figure 4.1 Plot of streamwise depth vs. discharge for the staggered weir at (a) Piezometer 1 and (b) Piezometer 2

4.2.1.1 Scale-independent dissipation box outlet depth

The results can be reduced to dimensionless results by appropriately scaling the data as shown in Section 3.7. This allows the results to be readily applied to structures at prototype scales. Figure 4.2 shows the scale-independent results based on outlet piezometer measurements. The dimensionless outlet depth y/D is plotted on the y axis instead of T/D because the piezometers are upstream of the outlet. Also, a Coriolis coefficient was not applied to the Froude number on the x axis. This will not affect general trends since the best available information would require application of a constant Coriolis coefficient. Figures 4.2a and 4.2b also indicate that the third highest weir performs the best.

While analyzing these data, time was spent comparing piezometer measurements to point gauge measurements near the outlet. In our estimation, both piezometer and point gauge measurements had an accuracy of about 5 to 10 mm due to the turbulent, highly aerated nature of the flow. For the shallow outlet depths of 1 to 5 cm, this accuracy led to some concern about the usefulness and reliability of the measurements. There was also some inconsistency in subsequent calculations, so Prandtl measurements were included with later tests to improve upon the results in this section.
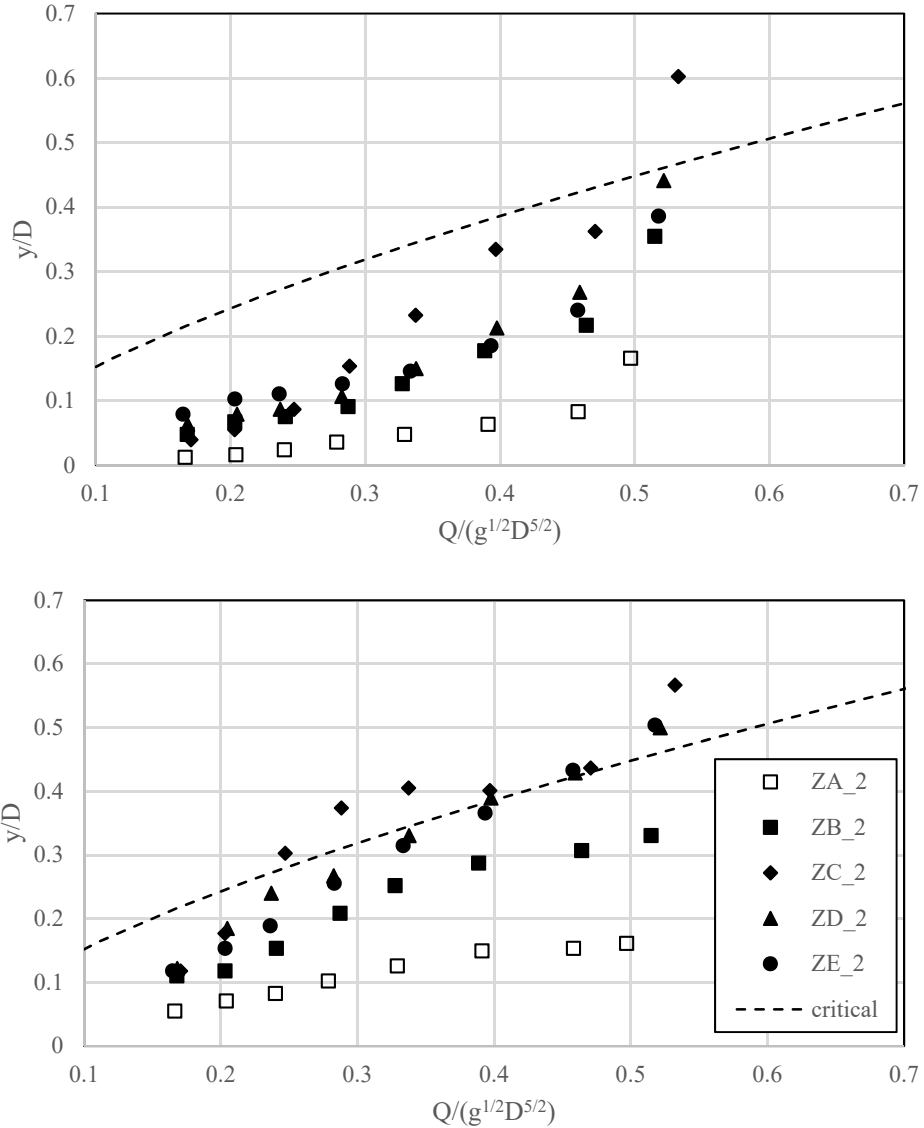
Figure 4.2 Plot of y/D as a function of $\frac{Q}{g^{1/2}D^{5/2}}$ at (a) piezometer 1 and (b) piezometer 2 for the staggered weir

4.2.1.2 Implementation of Prandtl-tube measurements

As shown in Section 3.7, the specific energy of the flow is a function of both flow velocity and depth. The flows that are most useful for analysis of weir performance are not influenced by tailwater and are supercritical at the dissipation basin outlet. For these flows, the velocity head is significantly larger than the pressure head. For example, Figure 4.3 shows the combined contributions of pressure head and velocity head for four weir types and heights over a range of flow rates. In Figure 4.3, α is set equal to 1 for comparison purposes, but it is certainly higher than this, and the velocity head plays an even more important role than is depicted in the figure.
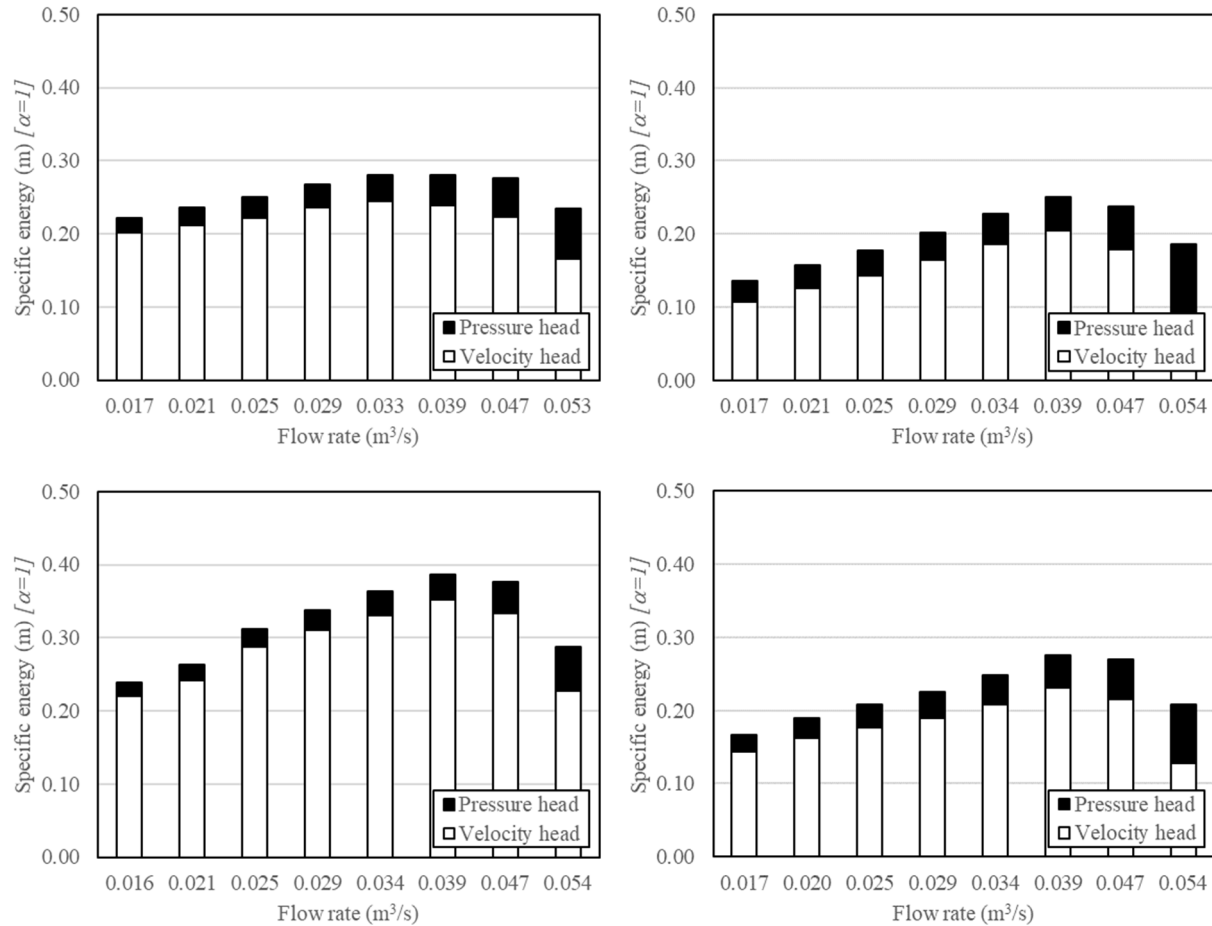
Figure 4.3 Contributions of pressure and velocity head to specific energy for staggered weir: (a) height = D/8 and (b) height = 4D/8 and full weir: (c) height = D/8 and (d) height = 4D/8.

Clearly, specific energy at the dissipation box outlet is more sensitive to velocity head than to pressure head. Therefore, in the present case, velocity head measurements are more useful than depth measurements. Often, depth measurements are used to calculate velocities and specific energies without a direct measurement of velocity. We are suggesting that for these super critical flows, it is better to measure velocity and calculate depth and specific energy from the velocity measurement.

Figure 4.4 shows a comparison of outlet depth calculated with based on Prandtl tube velocity measurements with outlet depths measured with piezometer 1 (Figure 4.4a), piezometer 2 (Figure 4.4b), and point gauge F (Figure 4.4c). The points shown in the figure are for all of the datasets collected after the outlet Prandtl tubes were installed. The open circles in the figure represent the highest discharge, which includes tailwater influence. These points are not representative of the quality of depth measurements because the rapidly varied conditions that occur at the outlet when tailwater begins to influence the outlet reduce the accuracy and reliability of point gauge, piezometer, and Prandtl-tube measurements.
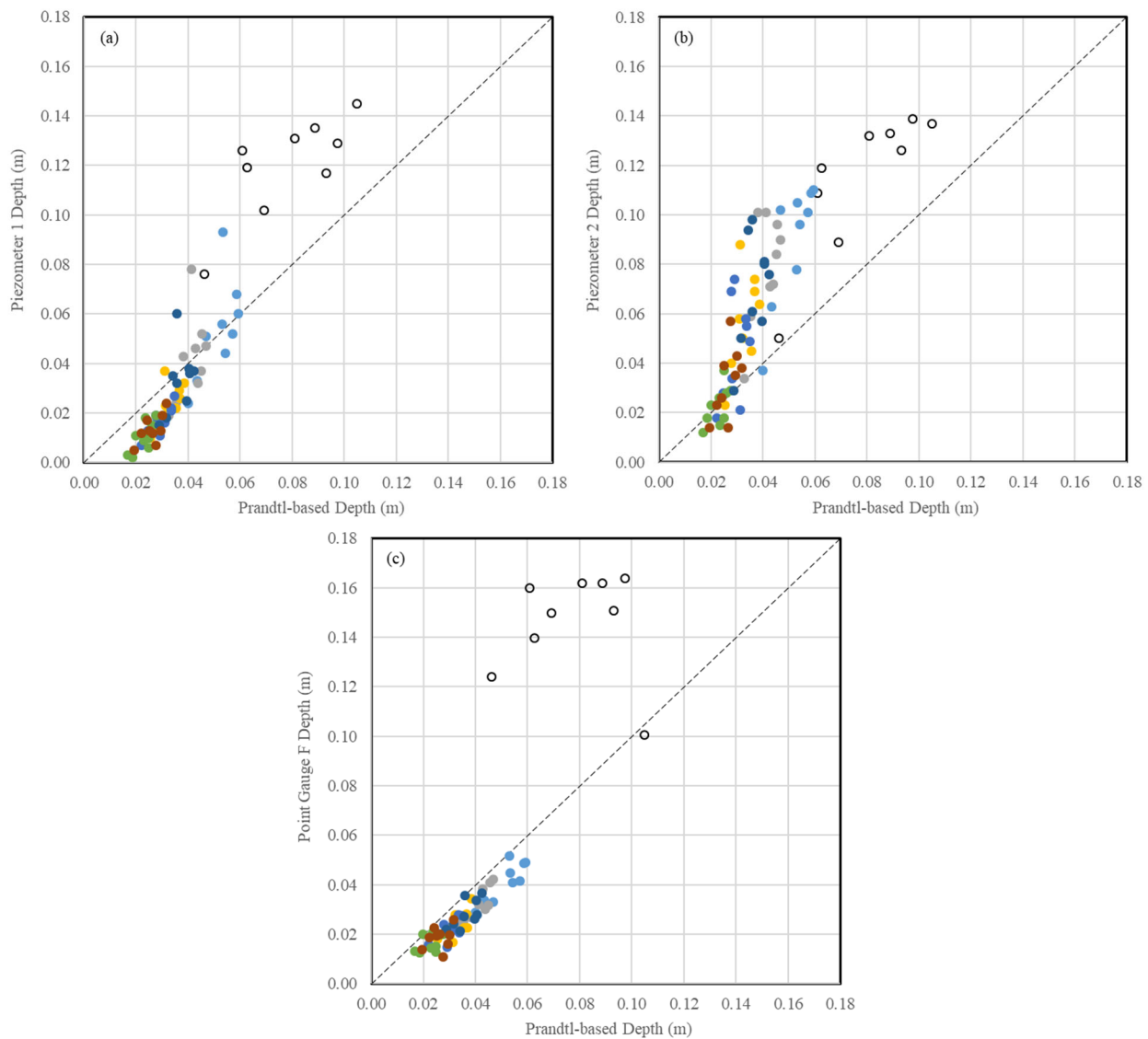
Figure 4.4 Comparison of Prandtl-based outlet depth with (a) piezometer 1 depth, (b) piezometer 2 depth, and (c) point gauge F depth.

The two piezometers show significant scatter and an unexpected upwards trend. It is not surprising that piezometer 2 has higher depths than piezometer 1 because it is 15 cm upstream of piezometer 1. The slope of both piezometer scatter plots is unexpectedly high. Excluding the highest discharge tests, depth measurements with the point gauge at F are consistent with Prandtl-based depths. The point gauge measurements are biased low – likely due to the accuracy of the point gauge, which we estimate to be about 0.5 to 1.0 cm for the present testing conditions. Even if the Prandtl-based depths are high by a centimeter, energy and velocity-based calculations will be good since velocity is directly measured.

4.2.2 <u>Tailwater-independent results – Prandtl-based results</u>

Figure 4.5 shows how outlet depth varies with discharge for the staggered weir tests. The critical depth line (denoted y_c) is the highest possible depth at the dissipation basin outlet that can occur with no tailwater influence. The closer the depth is to this line, the less kinetic energy at the outlet of the dissipation basin. For the data to the right of the tailwater influence line, the depth in the tailwater basin is high enough to begin backing up the flow in the dissipation structure. These data are ignored in the analysis because they contain additional energy dissipation beyond what the weirs provide.

Based on the Prandtl-tube measurements, the highest and second highest staggered weirs result in the lowest outlet depths.
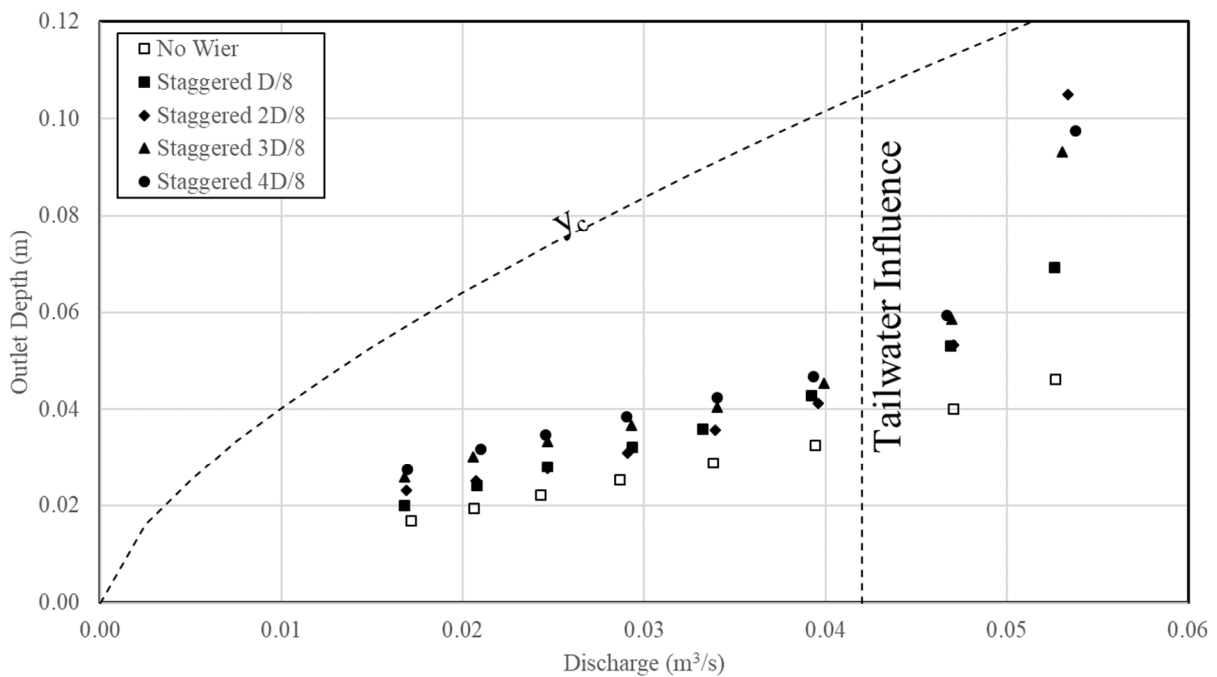
Figure 4.5 Outlet depth as a function of discharge (staggered weir tests).

Figure 4.6 shows the specific energy at the outlet of the dissipation basin as a function of discharge. The effect of tailwater is clearer in this graph, demonstrating rapid fall off in specific energy as tailwater increases. This happens as water backs up in the dissipation basin and a hydraulic jump begins to form. A Coriolis coefficient of 1.15 is applied for the velocity head at the exit of the dissipation basin.
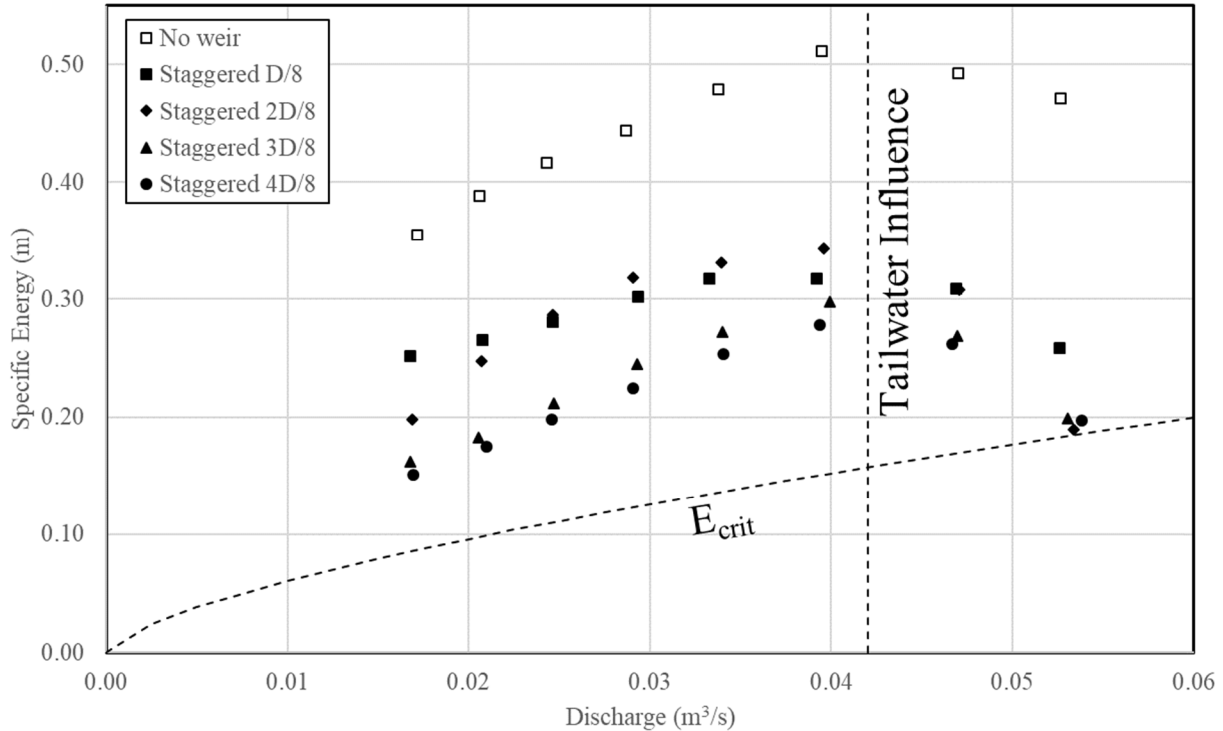
Figure 4.6 Specific energy as a function of discharge (staggered weir tests).

Flow through the dissipation basin results in head loss without the introduction of a weir. Introduction of a weir increases the total head loss. Prior to installing any weirs, eight flow rates were tested in the dissipation basin to determine head loss as a function of flow rate. The same eight flow rates were tested for all of the weirs, both staggered and full-length. In this way, the head loss associated with each weir could be determined by subtracting the head loss measured for the dissipation basin from the total head loss measured for the weir. Figure 4.7 shows additive head loss associated with each staggered weir. The maximum measurable head loss that can be added by the weir is shown by the line dE_{max}. If the head loss surpasses dE_{max}, the head loss caused by the weir is immeasurable because total head loss includes tailwater losses.

Figure 4.8 provides the total head loss resulting from the staggered weir and dissipation basin combinations. Only one dissipation basin width was tested in the experiments, but based on previous work, wider dissipation basins will result in additional energy dissipation. Figures 4.5 through 4.8 all show that the tallest staggered weir performs the best in all conditions. Energy losses are maximized and outlet energy is minimized by the weir that is half of the culvert diameter.
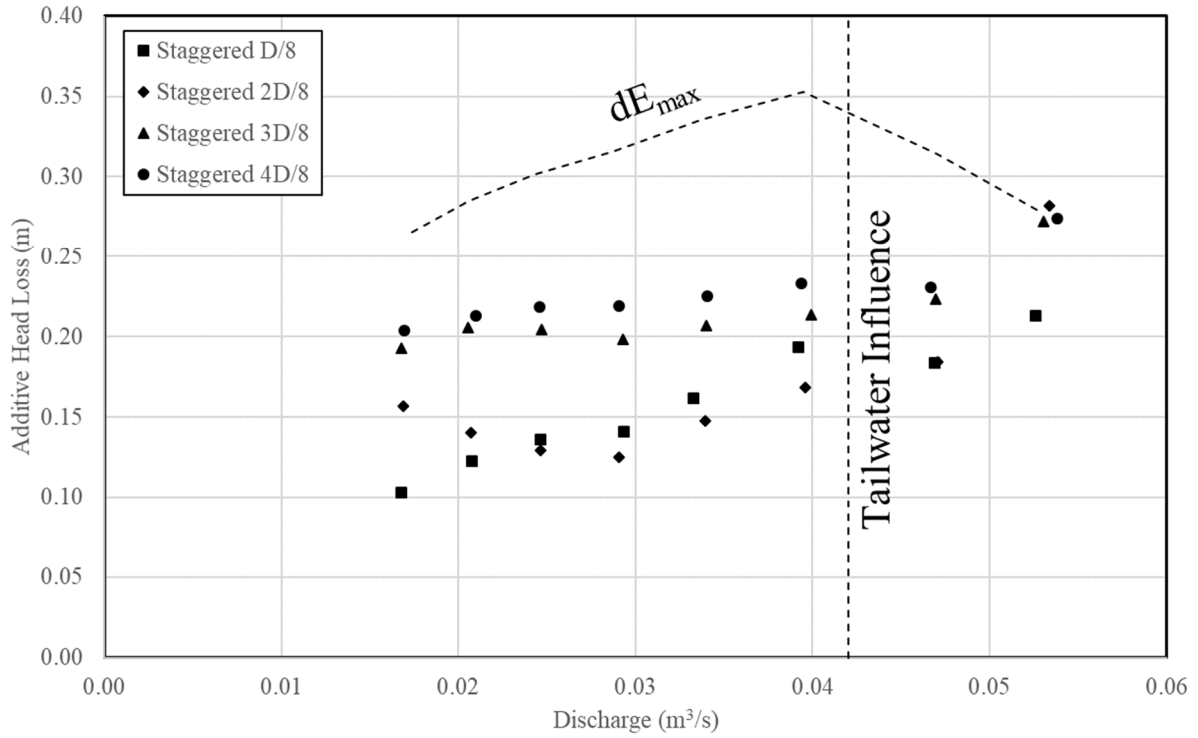
Figure 4.7 Additive head loss as a function of discharge (staggered weir tests).
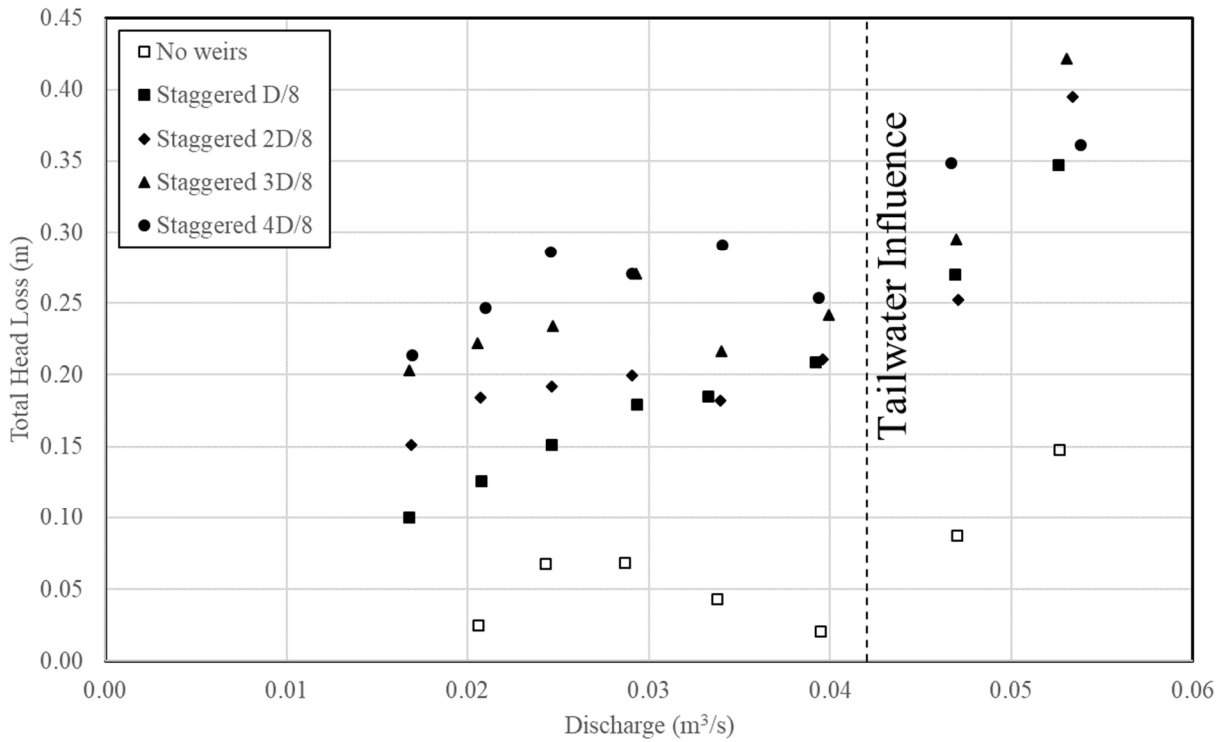
Figure 4.8 Total head loss as a function of discharge (staggered weir tests).

4.2.3 Scale-independent results

Scale-independent results are provided so that results can be easily applied to any culvert size. Figure 4.9 shows the dimensionless head loss as a function of the runout Froude number. For the calculation of runout Froude number, a Coriolis coefficient of 1.25 was used for the partially filled culvert. In the figure, only points that are unaffected by tailwater are shown. The Froude number range of the data is only from 3.8 to 4.4, due to apparatus design constraints. The Runout Froude number does not appear to increase monotonically with depth or discharge and is a function of both. As the discharge increases, so does the depth, and in the complex partially filled circular cross section, Froude number does not vary much over a wide range of discharges. The figure shows that the highest dimensionless energy losses are for the two tallest weirs.
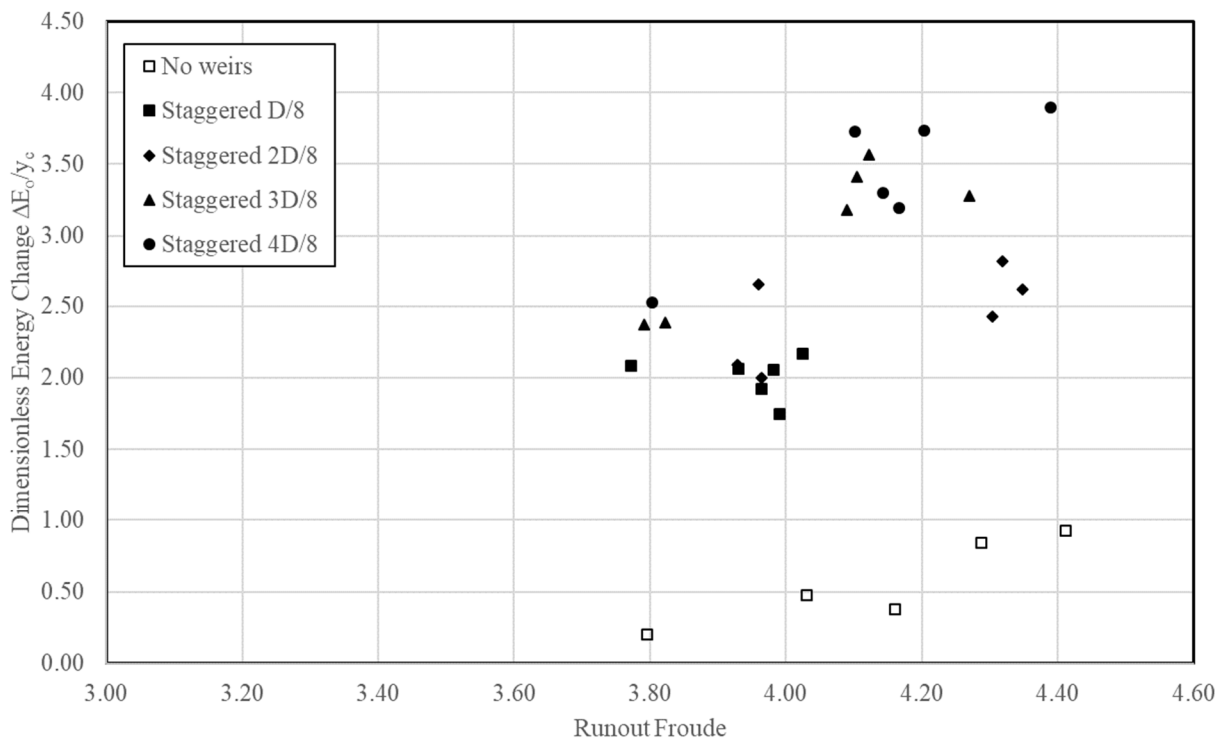
Figure 4.9 Total dimensionless head loss as a function of discharge (staggered weir tests).

In tests with the same discharge, the runout Froude numbers should be about the same, but this is not always the case in Figure 4.9. Runout Froude number is based on discharge and runout depth and the runout depth is measured as an average of the two upstream-most point gauge measurements. These measurements have considerable uncertainty because the velocities in the runout section are very high and make it difficult to identify the exact height of the water surface. There is a Prandtl tube located immediately upstream of the break in slope in the drop structure. One possibility is to use this Prandtl tube to estimate the runout Froude number, much like how the outlet depth was determined in the dissipation basin. The Prandtl tube upstream of the break will provide a runout velocity that is biased slightly low because it is slightly higher than the

runout section. Use of this Prandtl tube is also somewhat complicated because of the non-uniform velocity distribution in the partially filled circular conduit.

Figure 4.10 shows the dimensionless outlet energy for each of the staggered weir heights. The two highest staggered weirs both result in dimensionless outlet energies that are constant. For the second-highest weir, the dimensionless outlet energy is 2.9, and for the highest weir, the dimensionless outlet energy is 2.7. The other weirs do not appear to have a constant dimensionless outlet energy for the conditions tested. This may be caused by skimming for the lowest two weirs. For almost all flowrates and staggered weir heights, the runout depth remains supercritical at the upstream point gauges. Consequently, the supercritical runout depth is always between 5 and 10 cm. The weirs have heights of 3.2 cm, 6.4 cm, 9.5 cm, and 12.7 cm. The two tallest weirs have heights that are similar to the deepest runout depths, while the lowest two weirs have heights that are less than or similar in size to the shallowest runout depths.
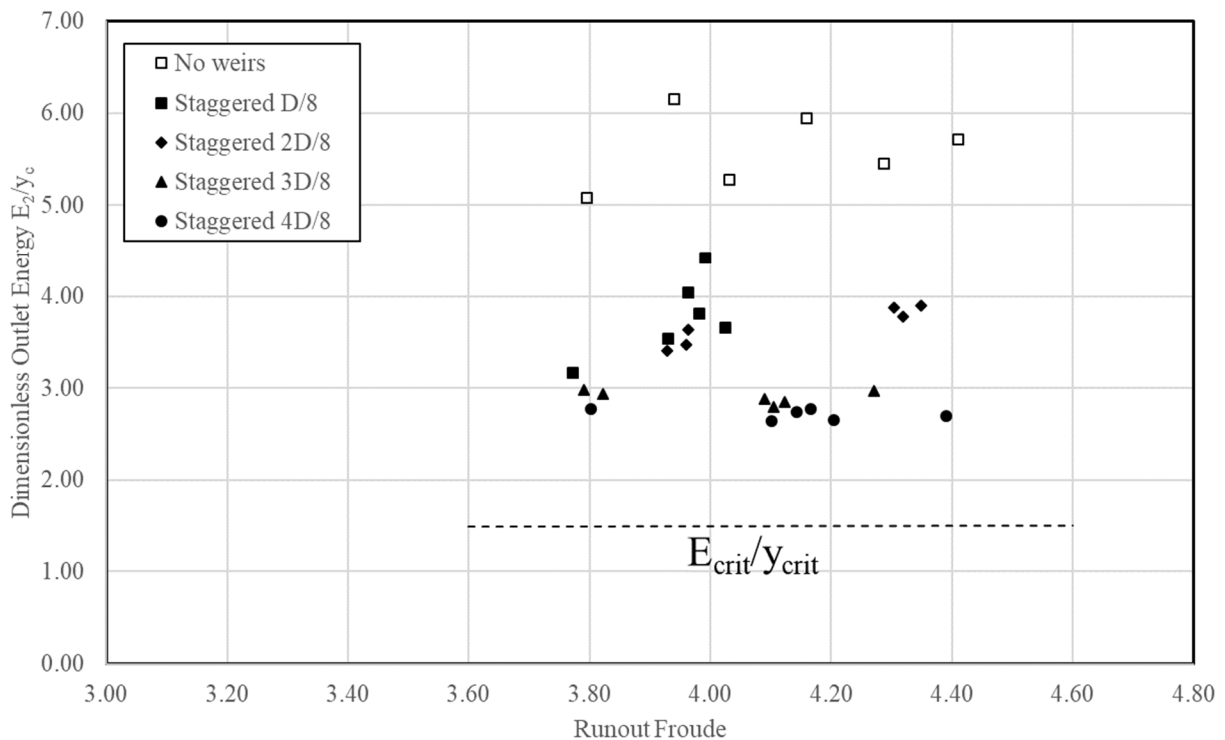
Figure 4.10 Scale-independent outlet energy as a function of outlet Froude number.

Devoid of a hydraulic jump in the runout section, parts of the high velocity flows may not directly impact the weirs with the lower heights before continuing to the outlet. Thus, it is best to ensure that the weir wall height exceeds the supercritical runout depth. This aligns with the recommendation that optimal baffle block height is 1.5 times the incoming flow depth. Also, it would be useful to have additional tests with lower runout Froude numbers (unfortunately, this does require some modification to the existing test facility). One final note about this; particularly for the two lowest staggered weirs, the relation between dimensionless outlet energy

and runout Froude number will require more data for a definitive result. The data do not show a definite trend between the two parameters.

4.3 Full Weir Results

In this section, piezometer-based energy dissipation results are presented. These results demonstrate performance of the full-length weirs based on piezometer and discharge measurements.

4.3.1 <u>Initial data</u>

Data collected for tailwater-independent tests are shown in Figure 4.11, which shows the dissipation basin outlet depth at piezometer 1 and piezometer 2. The effects of tailwater are evident at piezometer 1 for the highest discharge, as all of the outlet depths increase dramatically from those of lower discharges.   The figures show that the third tallest weir results in the highest outlet depths for the higher discharges. This behavior is apparent for both piezometer 1, which is at the outlet of the dissipation box, and at piezometer 2.
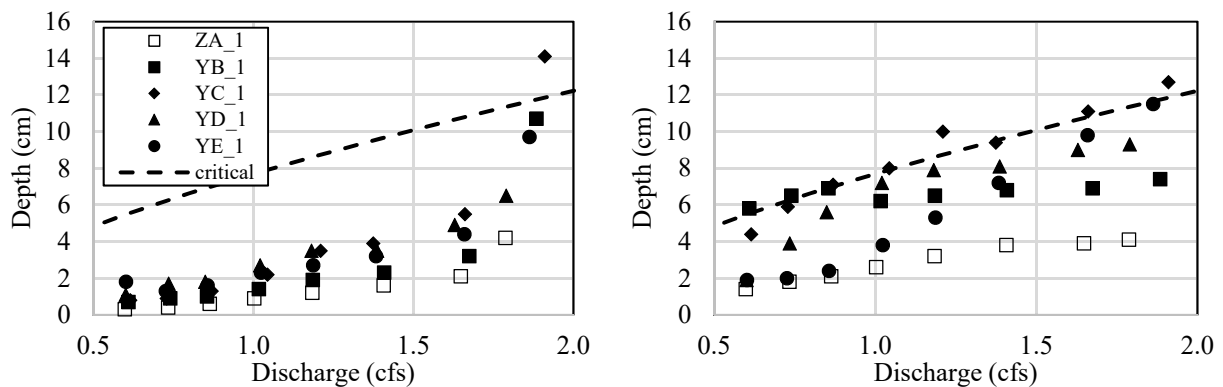
Figure 4.11 Plot of streamwise depth vs. discharge for the full-length weir at (a) Piezometer 1 and (b) Piezometer 2

4.3.1.1 Scale-independent dissipation box outlet depth

Dimensionless outlet depth y/D is plotted against Froude number in Figure 4.12. A Coriolis coefficient was not applied to the Froude numbers used for the x axis. As was the case for the staggered weir, Figures 4.12a and 4.12b indicate that the third highest full-length weir results in the lowest outlet depth.

As described for the staggered weir, Prandtl tubes were installed and tailwater-independent tests were rerun because of concerns about depth measurement accuracy near the outlet of the dissipation basin. These results are presented in the following sections.

81
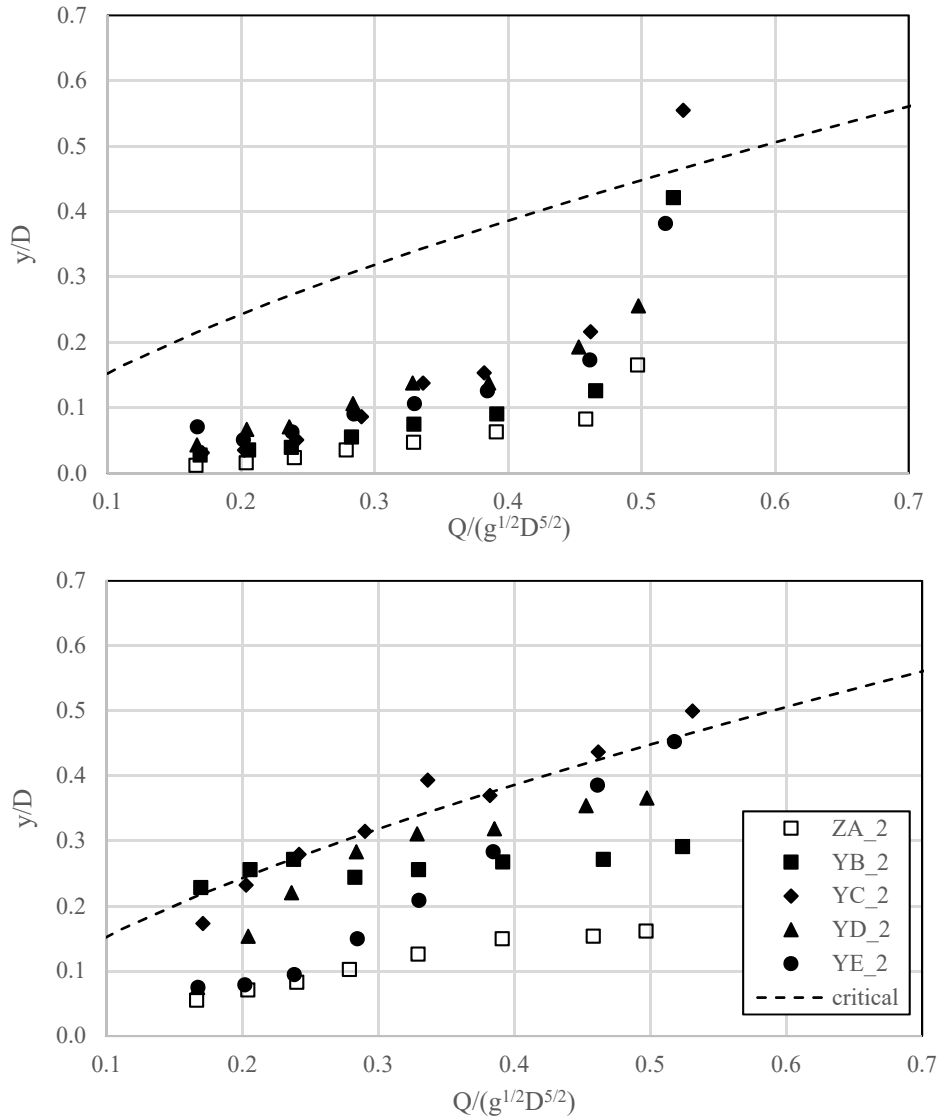
Figure 4.12 Plot of y/D as a function of $\frac{Q}{g^{1/2}D^{5/2}}$ at (a) piezometer 1 and (b) piezometer 2 for the full-length weir

4.3.2 <u>Tailwater-independent results – Prandtl-based results</u>

Figure 4.13 shows how outlet depth varies with discharge for the staggered weir tests. The critical depth line (denoted y_c) is the highest possible depth at the dissipation basin outlet that can occur with no tailwater influence. Based on the Prandtl-tube measurements, the highest and second highest staggered weirs result in the lowest outlet depths. For the full-length weir, the second highest weir performs better than the highest weir. This may be because the staggered weir does not force all of the water over the top of the weir. If two full-length weir heights have roughly the same energy dissipating capacity, the taller weir will result in more outlet energy because the potential energy of the flow over the top of the taller weir is greater. In the case of

the staggered weir, additional dissipation occurs downstream of the weir due to the flow through gaps between the offset weirs. It may be possible to optimize this behavior in future tests by adjusting the streamwise spacing between the offset weirs.
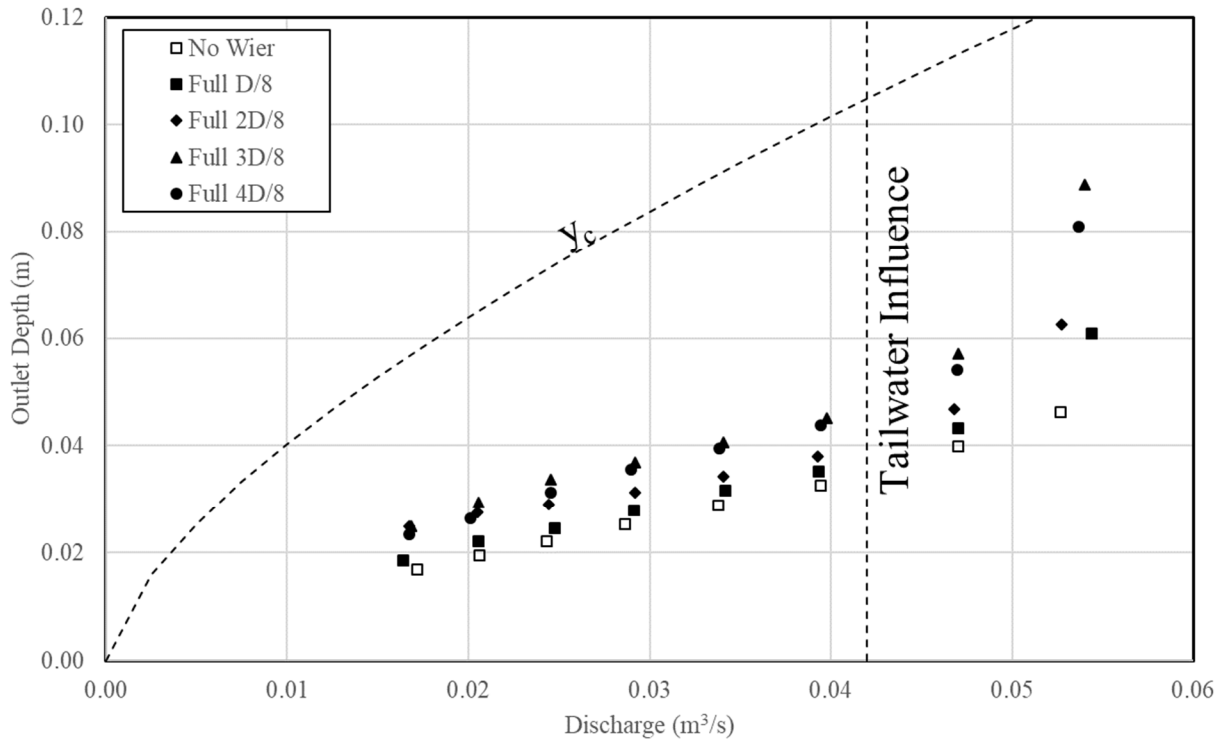
Figure 4.13 Outlet depth as a function of discharge for the full-length weir tests.

Figure 4.14 shows the specific energy at the outlet as a function of discharge for the full-length weir. As discussed for Figure 4.13, the outlet specific energy is least for the second highest full-length weir. At the lowest discharge, the third highest weir appears to become as effective as the two highest weirs. This supports the idea that the lowest full-length weir that dissipates all of the incoming kinetic energy is desirable because it creates the least potential energy for the water conveyed over the weir.
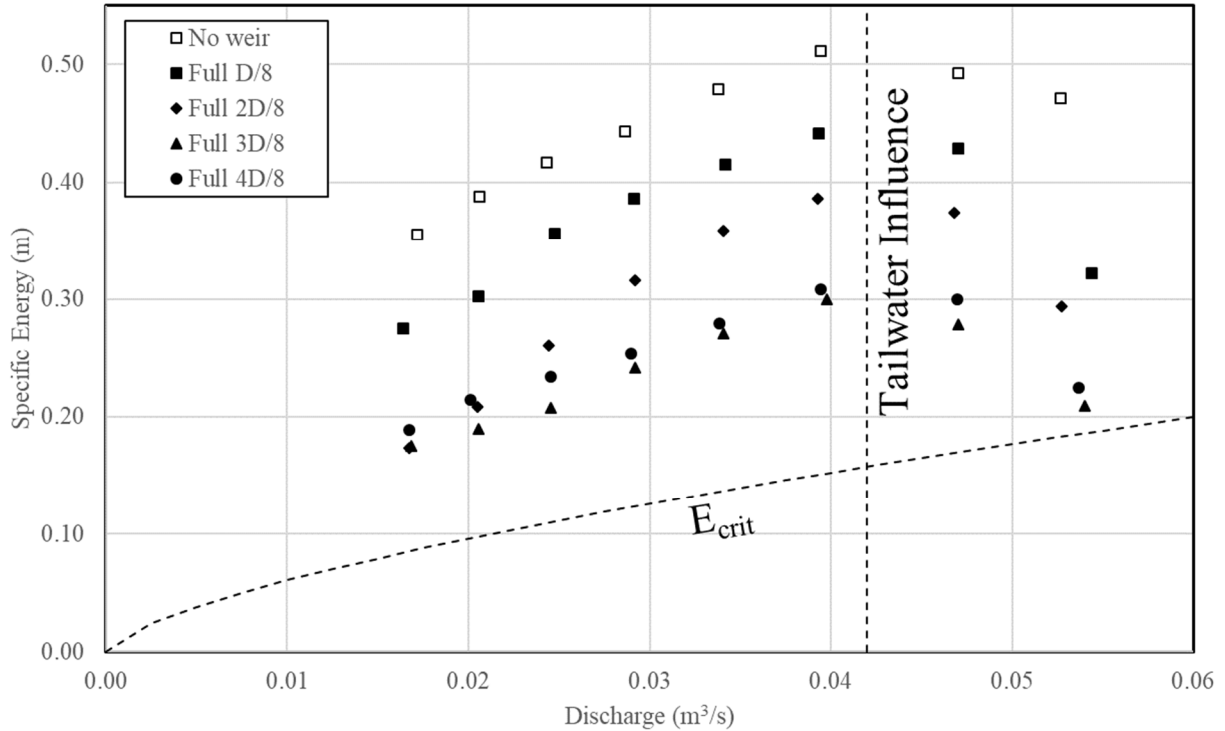
Figure 4.14 Specific energy as a function of discharge for the full-length weir tests.

Figure 4.15 shows the head loss added to the dissipation basin by installation of each full-length weir. The added head loss is remarkably constant for the second-highest weir over most of the discharge range.

The total head loss is provided as a function of discharge in Figure 4.16. There appears to be an optimal total head loss for some of the weir heights that occurs somewhere in the middle of the observed flow rate range. More measurements would be needed to confirm this.
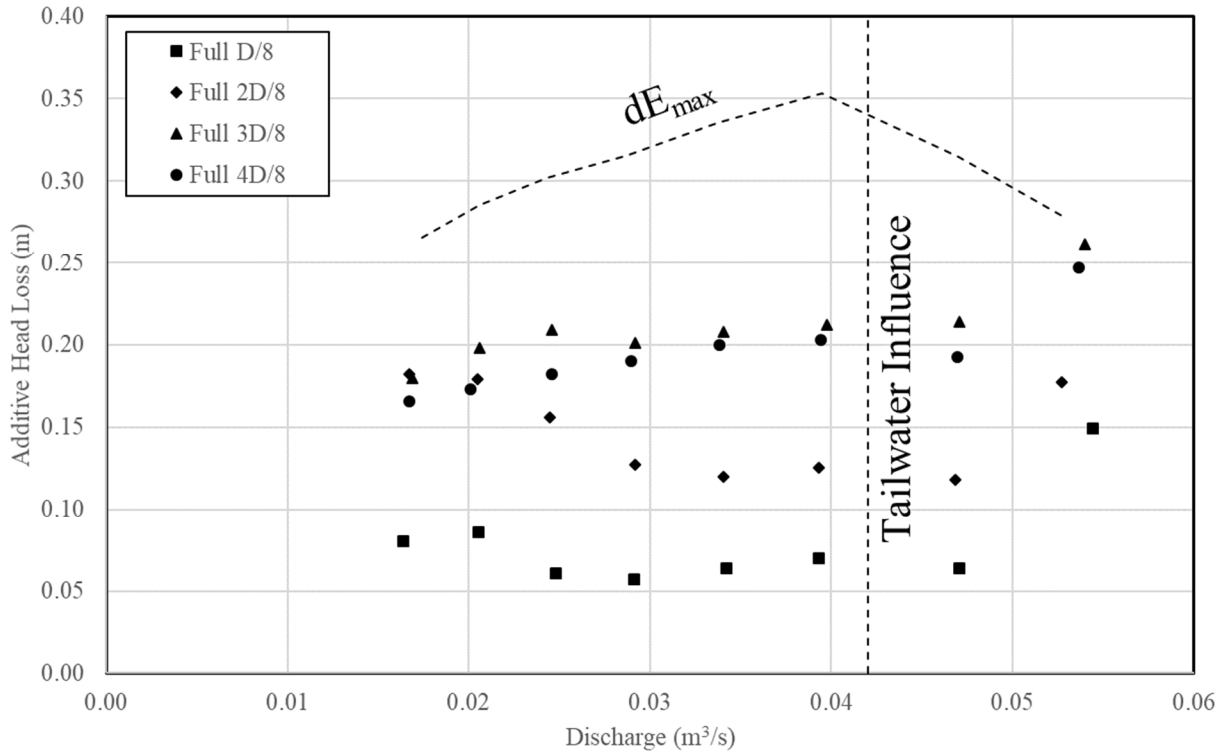
Figure 4.15 Additive head loss as a function of discharge for the full-length weir tests.
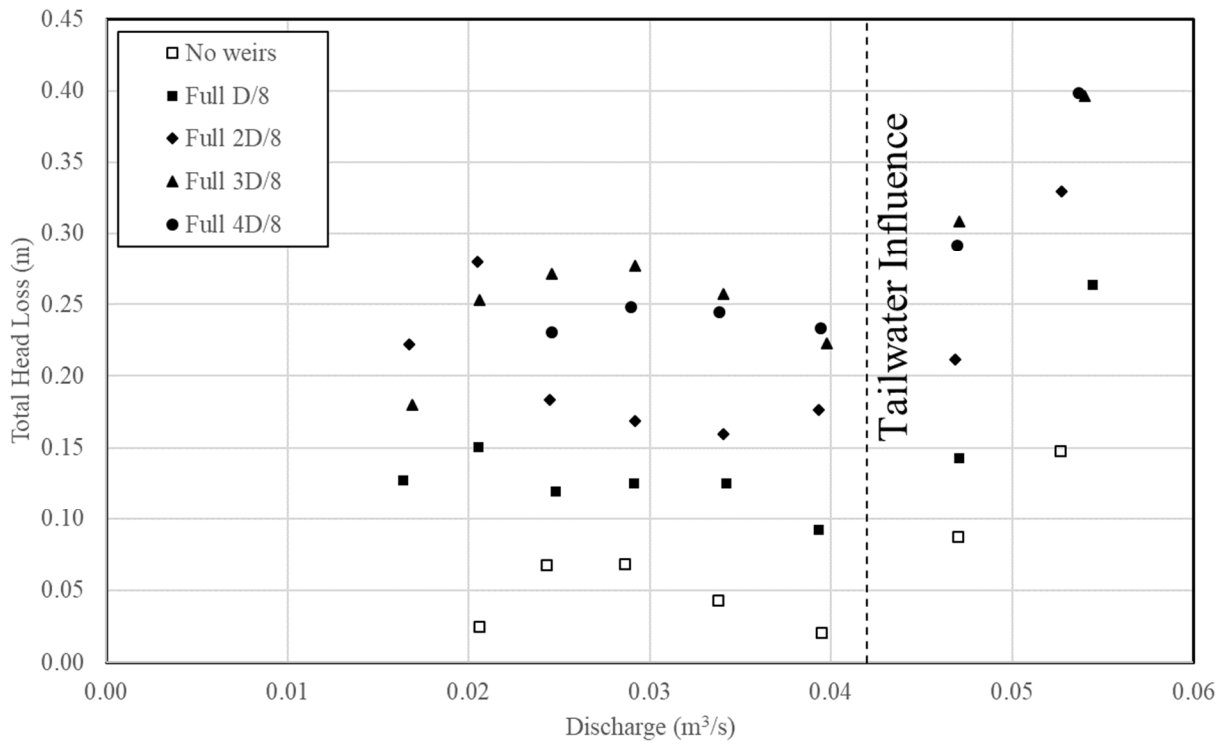
Figure 4.16 Total head loss as a function of discharge for the full-length weir tests.

4.3.3 Scale-independent results

Scale-independent change in specific energy and outlet energy are presented in this section. Figure 4.17 shows the scale-independent energy loss as a function of Runout Froude. In all cases, the energy loss increases with runout Froude number.
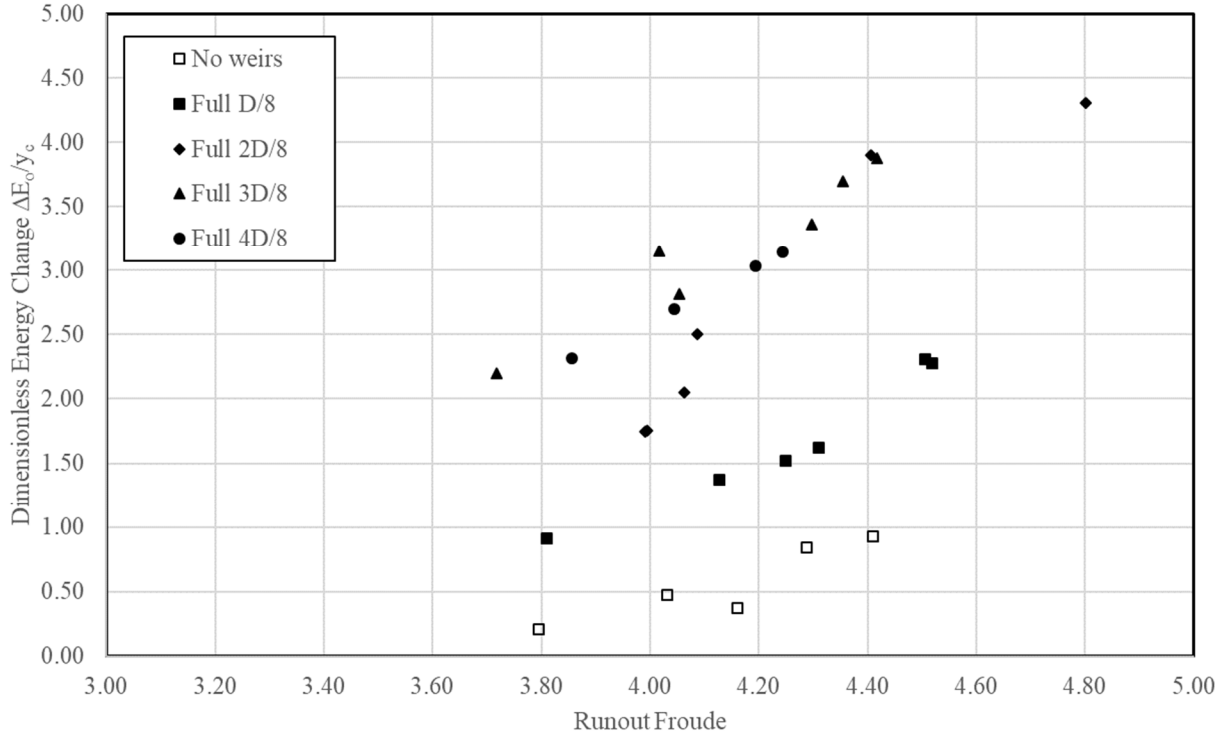
Figure 4.17 Total energy loss as a function of discharge (full-length weir tests).

Figure 4.18 demonstrates that just like for the staggered weir, the dimensionless outlet energy for the two highest full-length weirs both have dimensionless outlet energies that are constant over the range of conditions tested. For the second-highest weir, the dimensionless outlet energy is again 2.9, and for the highest weir, the dimensionless outlet energy is 3.2.
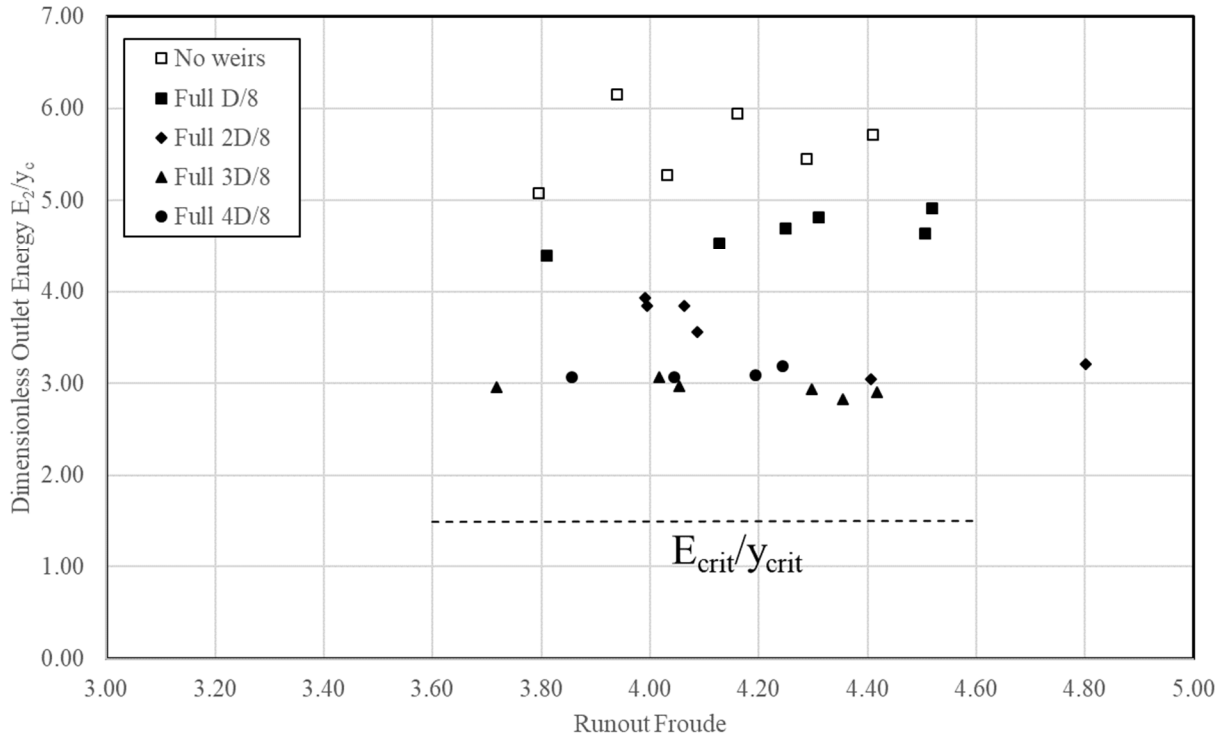
Figure 4.18 Scale-independent outlet energy as a function of outlet Froude number.

4.4 Comparative Results

In this section, results of Sections 4.2 and 4.3 are combined to compare and contrast performance of the two types of weirs. Outlet characteristics are based on Prandtl measurements.

4.4.1 Specific energy at the outlet

Figure 4.19 shows the specific energy at the outlet of the dissipation basin for the two styles of weirs that were tested. Symbols that are solid squares represent staggered weir performance, and symbols that are solid circles represent full-length weir performance. The open square symbols show performance when no weir is installed. The line identified as E_{crit} is the critical specific energy at the outlet and represents the minimum possible specific energy without tailwater control.
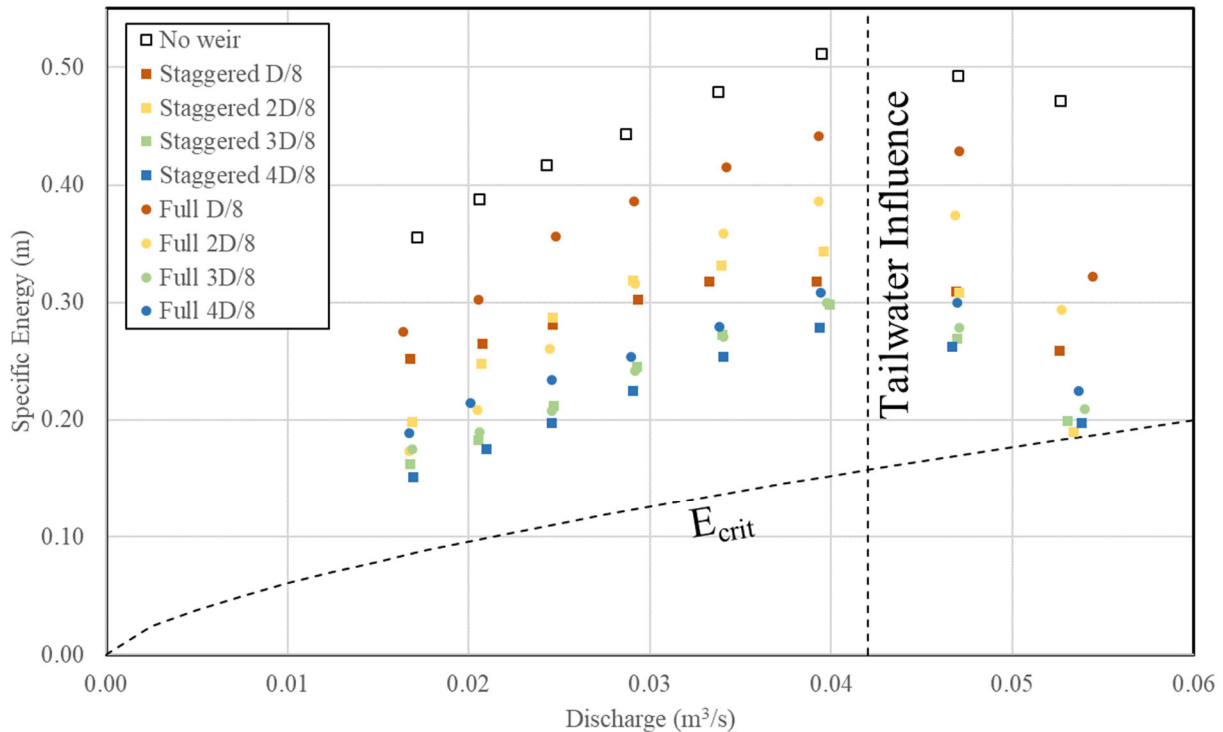
Figure 4.19 Comparison of specific energy at the outlet for the staggered and full weir

Without weirs, the dissipation basin contributes to energy loss because of flow expansion, but installation of weirs increases the total energy loss in all cases. For almost every case, the staggered weir performs at least as well as the full-length weir, and in the majority of cases it performs better. The best performing weir configuration is the staggered weir that is half as high as the culvert diameter. It is possible that a higher staggered weir will increase energy loss. The same is not true of the full-length weir, which appears to perform optimally when the weir is 3/8 of the culvert diameter. This may be because higher full-length weirs back up the flow, creating more potential energy at the weir crest and resulting in more kinetic energy at the outlet. In the case of the staggered weir, flow does not have to back up as high since there is a way for a fraction of the flow to go around the weir. This raises the question of whether larger distances between the sections of the staggered weir could improve energy dissipation by allowing more flow to travel around the weir instead of over it.

Figure 4.20 depicts a typical water surface profile in the culvert and dissipation basin. Ideally, the velocity at the outlet is minimized. Subcritical flow is preferred, but the full-length weir, which causes a hydraulic jump in many situations, forces the flow to pass back through critical, resulting in supercritical flow at the outlet for all observed test cases. The potential energy stored behind the weir is reconverted into supercritical kinetic energy as the flow travels over the weir. An optimized staggered weir may help to alleviate this problem by allowing a portion of the flow to travel around the weir instead of over it. For this very reason, most dissipation basins

use baffle blocks to dissipate energy because they do not force the flow back through critical. It should be emphasized that in all tests, both full-length and staggered weirs caused a significant reduction in the flow energy between the runout and the basin outlet. The point here is one of optimization.
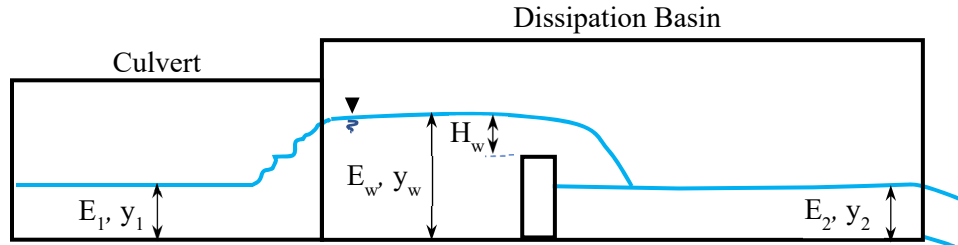
Figure 4.20 Profile of the water surface as it passes through a hydraulic jump, discharges over a full-length weir and reestablishes itself as supercritical flow at the outlet.

In order to better demonstrate the energy storage provided by the weir, the specific energy was calculated upstream of the weir for varying discharges and weir heights. Several assumptions were made, including:
   1. The specific energy upstream of the weir is the sum of the depth and the velocity head, using a velocity coefficient of 1.15 for the rectangular dissipation basin.
   2. Energy losses from flow over the weir are negligible.
   3. The sharp-crested rectangular weir equation is applicable, and a weir coefficient of 0.61 is reasonable across the range of flows and weir heights.

Following these assumptions, the outlet depth can be determined based on the specific energy upstream of the weir, E_w, and the discharge. More details about this calculation, along with a closed form solution to the equation for alternate depths, are provided in Appendix B.

Figure 4.21 shows measured dissipation basin outlet depth as a function of discharge for both types of weirs. Four subfigures are provided; one for each of the four different weir heights. The line in the figure is the calculated supercritical alternate depth calculated using the weir equation to calculate the upstream depth, y_w, and specific energy, E_w, and following the assumptions outlined above. Considering only flows that are not influenced by tailwater (to the left of the dashed line), these figures demonstrate several characteristics of flow over the weirs: (1) at higher discharges, the alternate depth line consistently overpredicts the outlet depth – especially at lower weir heights, (2) at low discharges over the highest weirs, the measured data approach the predicted supercritical outlet depth, and (3) only the staggered weir has any points that are above the calculated alternate depth line.

The first observation is likely because the weirs are not behaving like weirs at low weir heights and high discharges. Instead they are sills, and the weir equation is not ideal. Flow is not backed up behind them and the velocity is not distributed equally across them (α is higher than 1.15).

For these conditions, the total energy upstream of the weir is likely higher than predicted by the weir equation. It would be best to avoid these low weir heights in the prototype because the lower weirs are not dissipating as much energy as is possible. The second observation is because at low discharges and high weir heights, the velocities are low and the weir behaves much more like traditional weirs. Further increases in weir height beyond those tested will likely result in higher energy at the basin outlet (although some energy dissipation will result from additional head losses caused by the increased drop height). The third observation is probably because the staggered weir provides additional head losses beyond those caused by the full-length weir. Again, it would be worth investigating if different geometries can improve performance of the staggered weir.
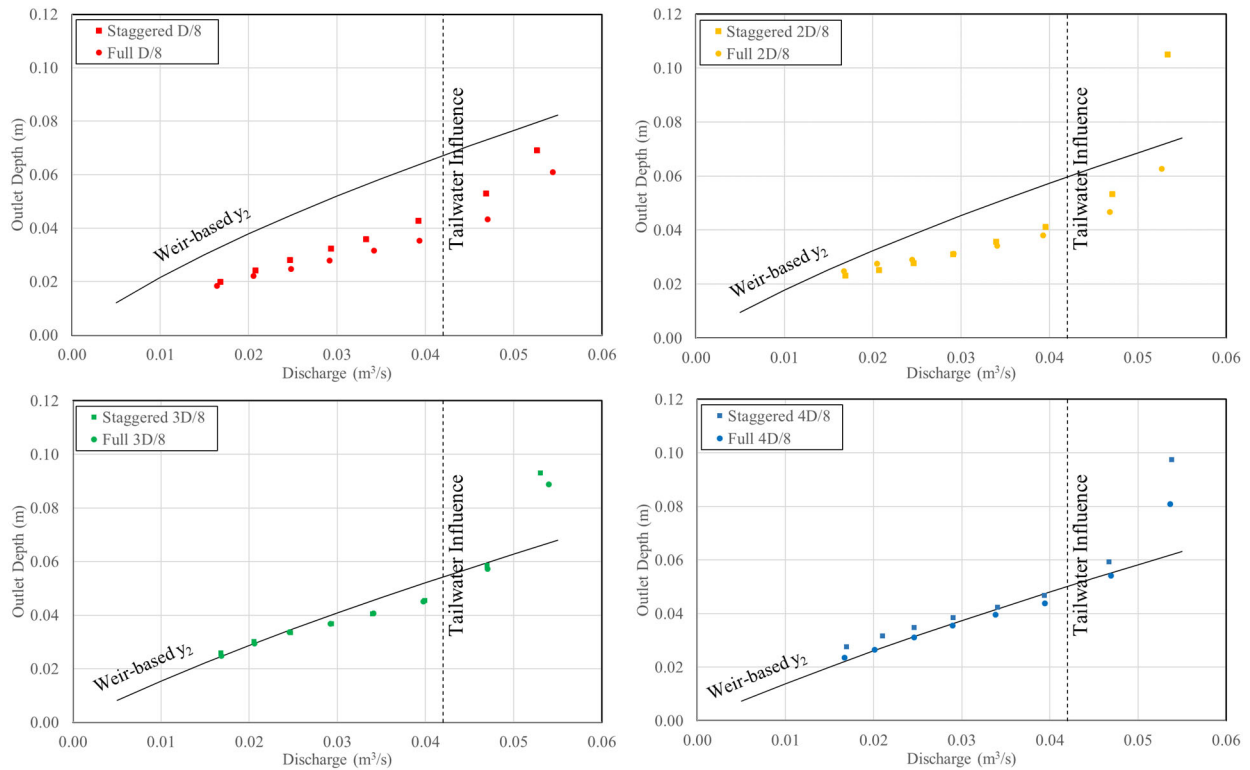
Figure 4.21 Comparison of outlet depths determined from Prandtl measurements with outlet depth predicted from discharge and weir equation for all four sizes of weirs.

It is worth considering the case of lower Froude numbers in the runout section (for the same discharge). In this case, the runout depth will increase and runout velocity will decrease. Due to the lower kinetic energy, assumptions about the inflow velocity distribution will be more accurate, and it appears likely that the taller weirs will behave similar to what is shown by Figure 4.21. A reasonable upper limit for the runout depth in this case is y_w, the sum of the weir height and the height of the water surface above the weir crest. Tests with lower Froude numbers would be useful to verify this prediction.

Flows with higher Froude numbers will likely result in higher energy dissipation and outlet depths similar to those observed in the figures for the taller weirs. Again, verification of this prediction would be helpful by performing tests with higher Froude numbers. The description of the Type VI dissipation basin provided in Chapter 2 implies that these types of basins result in similar outlet conditions for a wide range of outlet velocities – a behavior that may also be true for the taller weirs.

4.4.2 <u>Tailwater-influenced results</u>

A large amount of data were collected for a range of tailwaters. For the most part, these data are not extensively analyzed in this report because energy losses in such cases are independent of weir performance. For tailwater control, the exit velocity depends primarily on the tailwater depth and the discharge. Energy losses are associated with the weir, the expansion, and one or more jumps. The flow always adjusts so that the combined losses are defined by the incoming energy and the tailwater elevation. These losses cannot be separated, but they do not necessarily need to be separated for all forms of analysis. The primary benefit of a full-length weir in this case is to ensure that a jump occurs well upstream of the outlet.

The tailwater tests allowed us to consider jump position as a function of tailwater depth. In this section, the position of the jump upstream of the weir is examined for different tailwaters in order to predict what weir heights are needed if it is necessary to force the jump to occur at the break in culvert slope. Keep in mind that the behavior of a jump in a circular culvert with an expansion at the outlet will be very different from the behavior of a classical jump. The recommendation provided by Forster and Skrinde (1950) that jump length be at least five times the downstream sequent depth is likely not applicable, because a classical jump cannot form in the present conditions. Instead, if it is necessary to retain the jump within the culvert, the recommendation of Larson et al. (2005) to locate the toe of the jump to the break in slope might be better. However, if the height of the weir is selected to force the jump into the culvert, it could easily result in reduced overall energy dissipation and higher dissipation basin outlet velocities. Additional tests with taller weirs could be done to confirm this.

Figure 4.22 shows how jump length varies with tailwater depth for the staggered weir tests. Four discharges were tested for each staggered weir height, and for each discharge, ten to twelve tailwater elevations were tested. Figures 4.22a – d show the results for the four different weir heights. Each graph contains four discharges, and the discharges do not change from weir to weir (they were carefully set to be the same four discharges for all four test sets). L/D is the dimensionless distance of the jump from the upstream face of the weir, where D is the culvert diameter. The position of the break is also shown on the graph. It is always 72.5 inches upstream of the weir. Notice that there are very few jumps with lengths between 3D and 7D. The culvert is smooth and offers very little resistance to jump movement. Once a jump clears the culvert entrance it is very likely to reposition at the culvert break.

For the lowest two weirs, some tailwaters and discharges do not cause a jump within the culvert. These are shown on the graph as L/D = 0. The two highest weirs always produce a jump, both with and without tailwater, which is why L/D never drops to zero for these two weirs. To force the jump toe to occur at the break requires a dimensionless tailwater depth of about T/D = 1.1. It looks like the required T/D could be more than 1.1 for higher discharges. To cause the same effect as the tailwater when no tailwater is present, the staggered weir has to be tall enough to drown the culvert. Additional variation of discharge and runout Froude would help to expand this result.
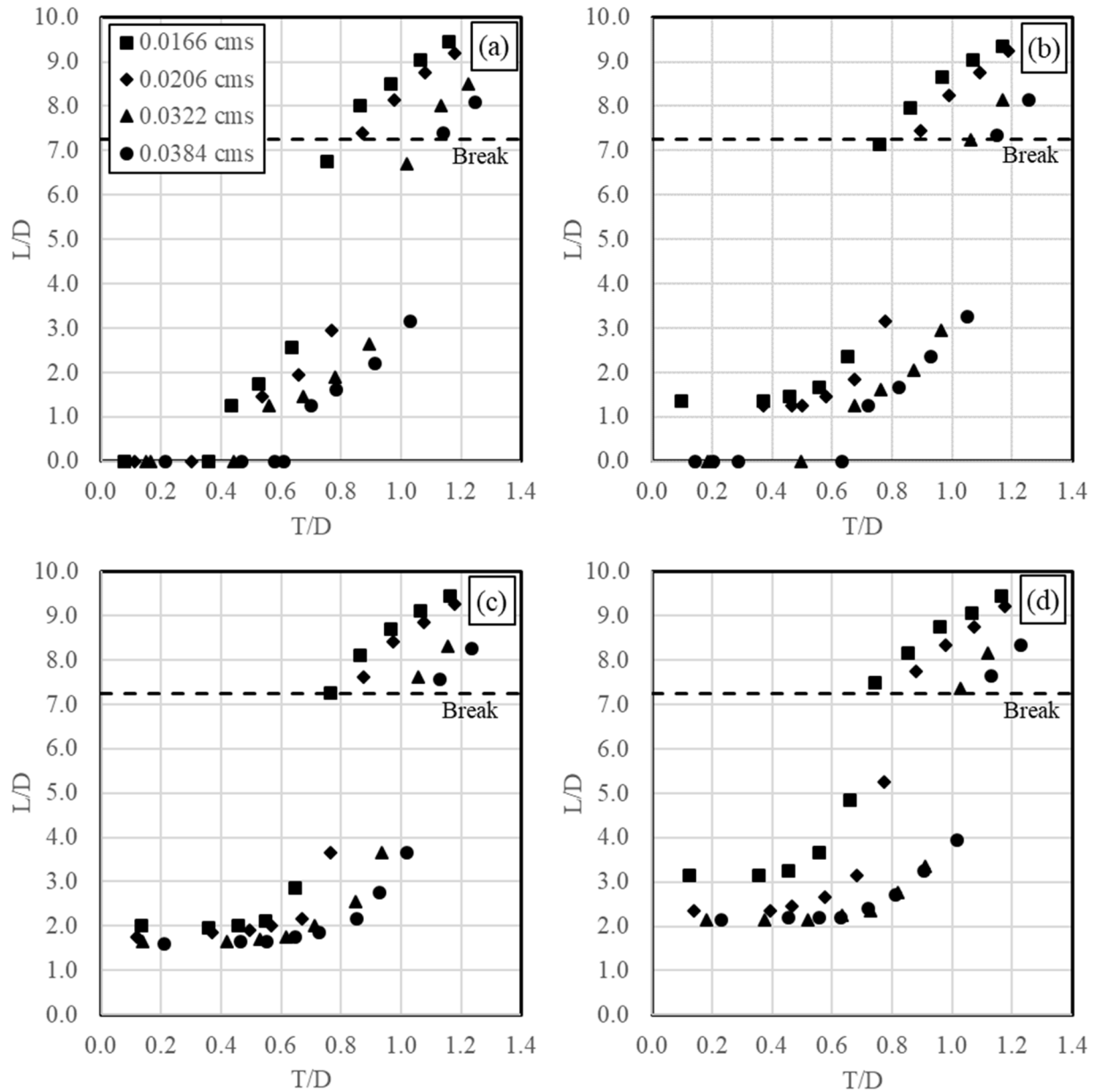
Figure 4.22 Dimensionless jump length as a function of the dimensionless tailwater depth for staggered weir heights of: (a) D/8, (b) 2D/8, (c) 3D/8, and (d) 4D/8.

The tests were repeated with full-length weirs with similar outcomes. The two tallest full-length weirs cause longer jumps than the two tallest staggered weirs because they force all of the flow to go up and over them. However, the dimensionless tailwater depth required to force the jump to the break is still about 1.1. The highest flow rate over the tallest weir tested results in a culvert outlet depth that is equivalent to a dimensionless tailwater depth (T/D) of about 0.8. Thus, the tallest weir tested would have to be raised by about 0.3D to raise the dimensionless depth to 1.1. That could raise the dissipation basin outlet velocity considerably since the flow over the top of the weir will have more potential energy.
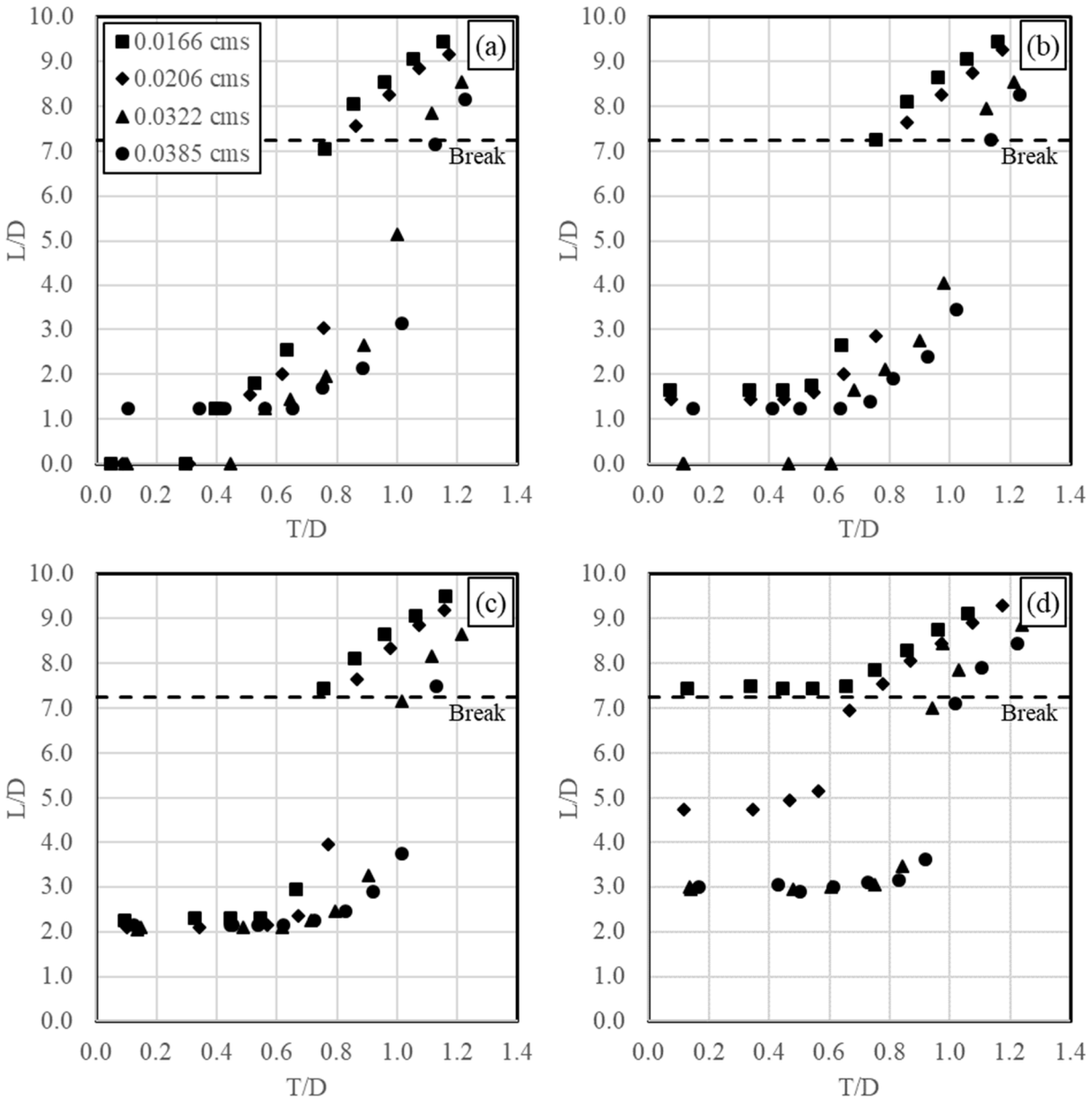
Figure 4.23 Dimensionless jump length as a function of the dimensionless tailwater depth for full-length weir heights of: (a) D/8, (b) 2D/8, (c) 3D/8, and (d) 4D/8.

5. Conclusions and Suggestions for Future Work

5.1 Conclusions

A study of two weir types, staggered and full-length, was completed in an experimental dissipation basin. Three data sets were collected: two tailwater-independent data sets and one data set with tailwater influence. The first of the tailwater-independent data sets is not reported here because the range of discharges that the tailwater tank could convey was found to be limited and because outlet depth measurements were not found to be accurate enough to complete all of the analyses. The second tailwater-independent data set was collected after the tailwater tank was modified to increase discharge measurement range and after Prandtl tubes were installed at the dissipation basin outlet to improve energy measurements.

In the tailwater-independent tests, data were collected for eight discharges, two weir types and four weir heights. Initially, the primary measurements included discharge, numerous water depths using both piezometers and point gages, and drop velocities using two Prandtl tubes. Data were also collected when no weirs were installed.

It was found that outlet energy could not be accurately determined using depth measurements because of depth measurement accuracy limitations. These limitations were a result of the highly turbulent, aerated flow at the outlet and the very small outlet depths. In addition, a large fraction of the specific energy at the outlet is kinetic. Therefore, tests were repeated after three Prandtl tubes were installed at the outlet. There were some difficulties associated with using the Prandtl tubes in the aerated flows, but these were overcome by flushing air bubbles out of the tubes prior to each velocity measurement.

Comparisons of outlet depths with depths predicted with a simple weir equation and some general assumptions about the flow upstream of the weir showed that the weir equation does a reasonably good job of predicting outlet depth for taller full-length weirs for the range of discharges tested. For shorter weirs, the flow appears to skim the weir and the weir equation greatly overestimates energy dissipation, especially for high discharges.

Taller weirs are needed to force the upstream development of hydraulic jumps and prevent skimming over the weir; however, the taller the weir, the more potential energy that is stored upstream of the weir, energy that is converted back into supercritical kinetic energy as the water flows over the weir. The optimal full-length weir is one that is just tall enough to back up the flow into the culvert for the highest flow rate. Although the currently tested staggered weirs had performance that was similar to full-length weirs, an advantage of the staggered weir is that it behaves more like a baffle, allowing some of the flow to go around it instead of over it. The result of this behavior is observed in the slightly lower specific energies observed at the outlet for the staggered weirs. The staggered weirs had specific energies at the outlet that were equal to or

less than those observed for the equivalent full-length weir in nearly all cases. Due to time constraints, staggered weirs tested in the present research were not optimized to take full advantage of this behavior.

Although hydraulic jumps can be induced in the model culvert, hydraulic jumps in the circular culvert are dissimilar to those in prismatic, rectangular culverts. When installing weirs for dissipation in rectangular channels, it is recommended that the length of the jump upstream of the weir is long enough to ensure that the jump is fully formed – roughly five times the upper sequent depth of the jump. The present configuration, however, is complicated by the circular culvert cross section and the expansion into the dissipation basin, and forcing a jump to form within the runout section may not always be optimal. Instead, the staggered weir can provide good energy dissipation if it is used as an impact wall like a Type VI dissipation basin.

In the tailwater-influenced tests, data were collected for four discharges, ten to twelve tailwater depths, two weir types, and four weir heights. The primary measurements included discharge, numerous water depths using both piezometers and point gages, the position of the toe of the hydraulic jump caused by the tailwater and/or weir, and drop velocities using two Prandtl tubes.

Forcing the toe of the jump to approach the culvert break upstream of the runout section for all tested discharges required the outlet of the culvert to be submerged to about 1.1D. This result was independent of the weirs that were tested because at this submergence, the weirs have little influence on the flow. The result was not independent of discharge, and lower discharges required lower outlet depths to achieve the same jump position. In fact, for the tallest full-length weir, the lowest discharge resulted in a hydraulic jump toe at the culvert break, independent of tailwater depth. For the full range of discharges, weir height could be increased to cause the culvert outlet to be submerged to 1.1D to ensure that the jump toe reaches the break, but this is not advisable based on the present observations since taller weirs will lead to higher basin outlet velocities.

5.2 Recommendations

Based on experimental observations, our recommendations include:
1. Staggered weirs are preferred over full-length weirs, not only because of their ability to pass debris and fully drain, but because they provide enhanced energy dissipation. The improved dissipation is only slight for the tested geometries (as evidenced in Appendix C), but could be improved in future work.
2. For the tested geometries and conditions, the optimal observed dimensionless outlet energy was about three times the critical depth. In this context, the staggered weir showed a slight improvement over the full-length weir.
3. Reconsider the spacing of the second row of the staggered weir so that there is more flow area. Six inches is not sufficient for some debris, but more importantly, additional space will reduce the depth upstream of the weir, reducing the amount of energy left over after

weir impact. Additional testing is recommended to optimize the spacing and impact wall height.

4. For the range of conditions tested, optimal wall height was 3D/8 for the full-length weir and 4D/8 for the staggered weir. Raising the height of the full-length weir to 4D/8 resulted in a small, but noticeable increase in the specific energy at the outlet. This could be because increasing the weir height above what is needed to dissipate the runout energy raises the total energy of the flow before it passes over the weir. Additional testing would benefit this conclusion.

5. Avoid using weirs that are lower than 3D/8 – at least for the current test range. Skimming over the tops of the shorter weirs leads to reduced energy dissipation.

6. Forcing the jump into the culvert requires the culvert outlet to be submerged for the full range of discharges tested. However, this is not advisable and will likely result in an unnecessary increase in outlet energy.

5.3 Future Work

Upon completion of the present research, several potential improvements to the experimental setup and future energy dissipation structure tests were identified. The experimental setup was selected early in the project based on a desire to simulate the extreme conditions of broken-back culverts. In this case, a 15 degree drop angle was selected and a drop height of one pipe diameter was chosen. The range of runout Froude numbers was about 3.8 to 4.4 for the present set of experiments. Installation of a gate control was not successful, though relatively straightforward modifications to the system may be possible to increase the runout Froude number by another means. In any case, choices in system geometry made it impractical to simulate low Froude numbers in the runout section and no simple modifications were found to achieve lower Froude numbers. The following provisions might be considered in future research:

1. Culvert inlet depth controls can be added to the present experimental culvert to increase Froude numbers for the same flow rate, thereby making it possible to separate the effects of runout Froude number from those of runout depth.

2. The range of Froude numbers can be increased by modifying the system so that it does not include a sloped section. By reducing the drop between the head tank and the tail tank, lower Froude numbers can be achieved. By constructing a better inlet to the test section, higher Froude numbers are also possible.

3. The outlet basin can be modified to convey more flow without tailwater influencing the flow in the dissipation basin. This modification is relatively straightforward but will require effort to change the height of the dissipation basin and runout pipe. The modification will result in an increased discharge range for simulating more flows.

4. In future work, it may be possible to directly measure forces on the staggered weirs. Any design of force measurement techniques will require careful thought.

Future research may help to answer additional questions about improving the staggered weir system. One important question is if additional geometries, such as increasing the spacing between the staggered weir sections can increase conveyance and reduce outlet energy. Another important question is how well the weirs perform when the runout section has a much higher depth. Finally, it may be beneficial to examine existing designs such as the Type VI design basin to see if it can be an effective tool for storm water culverts, which operate at relatively low outlet velocities.

6. References

Abt, S. R., Thompson, P. L. & Lewis, T. M. (1996), "Enhancement of the culvert outlet scour estimation equations", *Transportation Research Record*, **No. 1523**, pp. 178-185.

ASCE-97 (2000) <u>Hydraulic modeling: concepts and practice</u>, Eds.: R. Ettema, R. Arndt, P. Roberts, and T. Wahl. *ASCE Manuals and Reports on Engineering Practice No. 97*. 390 pp.

Bradley, J.N., and Peterka, A.J. (1957a) "Hydraulic design of stilling basins: hydraulic jumps on a horizontal apron (Basin I)", *J. Hydraulics Division, ASCE*, **83(5)**.

Bradley, J.N., and Peterka, A.J. (1957b) "Hydraulic design of stilling basins: short stilling basin for canal structures, small outlet works and small spillways (Basin III)," *J. Hydraulics Division*, ASCE, **83(5)**.

Bremen, R. (1990) Expanding stilling basin. Thesis 850, presented to the Ecole Polytechnique Federale de Lausanne (EPFL), Switzerland, in partial fulfillment for the requirements of Doctor of Technical Sciences.

Bremen, R. and Hager, W.H. (1993) "T-jump in abruptly expanding channel," *J. Hydraulic Research*, **31(1)**, 61-78.

British Standard 3680, part 4A and ISO/TC 113/GT 2 (France-10) 1971

Chaudhry, M. H. (2007). <u>Open-channel flow</u>. Springer Science & Business Media, NY. 523 pp.

Chow, V.T. (1959) <u>Open channel hydraulics</u>, McGraw-Hill, NY. 680 pp.

Emami, S. and Schleiss, A. (2010) "Prediction of localized scour hole on natural mobile bed at culvert outlets," *Geotechnical Special Publication. International Conference on Scour and Erosion.* 844-853. 10.1061/41147(392)84
https://www.researchgate.net/publication/269084525

Forster, J.W., and Skrinde, R.A. (1950) "Control of the hydraulic jump by sills" *Trans., Amer. Soc. Civil Engrs.*, **115(1)**, 973-1022.

Hager, W. H., Bremen, R., & Kawagoshi, N. (1990) "Classical hydraulic jump: length of roller," *Journal of Hydraulic Research*, **28(5)**, 591-608.

Hagar, W.H. (1992). <u>Energy dissipators and hydraulic jump</u>, Kluwer Academic Publishers, Dordrecht, The Netherlands. 288 pp.

Hagar, W. (2010) <u>Wastewater Hydraulics – Theory and Practice, 2nd Ed.</u>, Springer, Zurich, Switzerland. 652 pp.

HEC-14 (2006) <u>Hydraulic design of energy dissipators for culverts and channels</u>, HEC Circular No. 14, 3rd Ed., U.S. Department of Transportation – Federal Highway Administration, Pub. No. FHWA-NHI-06-086.

Hotchkiss, R. and Larson, E., (2005) "Simple methods for energy dissipation at culvert outlets", Proceedings of Impacts of Global Climate Change: pp.1-12, DOI: 10.1061/40792(173)443.

Jesudhas, V., Balachandar, R., Roussinova, V., and Barron, R., (2018) "Turbulence characteristics of classical hydraulic jump using DES." *Journal of Hydraulic Engineering,* **144(6)**. https://doi.org/10.1061/(ASCE)HY.1943-7900.0001427.

Larson, E. A. (2004) <u>Energy dissipation in culverts by forcing a hydraulic jump at the outlet</u>. Master's thesis. Washington State University

Larson, E., Hotchkiss, R., and Admiraal, D. (2005) "Energy dissipation in culverts by forcing a hydraulic jump within the barrel," *Transportation Research Record - Journal of the Transportation Research Board, **1904**, 124-132.*

Lowe, N. Hotchkiss, R., Nelson, E.J. (2011) "Theoretical determination of sequent depths in closed conduits," *Journal of Irrigation and Drainage Engineering*, **137(12)**, 801-810.

NDOT (2020) Personal Communication.

Novak, P., Moffat, A.I.B., Nalluri, C., and Narayanan, R. (2001) <u>Hydraulic structures, 3rd Ed.</u>, Spon Press, London, 666 pp.

Peterka, A. J. (1978) <u>Hydraulic design of stilling basins and energy dissipator, Engineering Monograph</u>, No. 25. Bureau of Reclamation, United States Department of the Interior. Washington, D.C.

Rajaratnam, N. (1964) "The forced hydraulic jump," *Water Power*, **16 (Jan)** 14-19: **16 (Feb)** 61-65.

Rand, W. (1966) "Flow over a dentated sill in an open channel," *Proc. ASCE, J. Hydraulics Division*, **92(HY5)**, 135-153.

Rand, W. (1970) "Sill-controlled flow transitions and extent of erosion," *Proc. ASCE, J. hydraulics division*, **96(HY4)**, 927-939.

Replogle, J. and Chow, V. (1966) "Tractive-force distribution in open channels," *Journal of the Hydraulics Division*, **92(HY2)**, 169-191.

Silberman, E. (1970), "Effect of helix angle on flow in corrugated pipes," *Journal of the Hydraulics Division*, ASCE, **96(11)**, 2253-2263.

Stahl, H. and Hager, W. H. (1999) "Hydraulic jump in circular pipes," *Canadian Journal of Civil Engineering*, *26*, 368-373.

Sterling, M. (1998), A study of boundary shear stress, flow resistance, and the free overfall in open channels with a circular cross-section, PhD Thesis, School of Civil Engineering, University of Birmingham, UK.

Sturm, T.W. (2010) Open channel hydraulics, 2nd Ed., McGraw-Hill Education, NY, 546 pp.

U.S. Bureau of Reclamation (1987) Design of small dams, 3rd Ed., U.S. Department of the Interior, Bureau of Reclamation, Water Resources Technical Publication, 860 pp.

U.S. Bureau of Reclamation (1997) Water Measurement Manual, 3rd Ed., U.S. Department of the Interior, Bureau of Reclamation, Water Resources Technical Publication. http://www.usbr.gov/tsc/techreferences/mands/wmm/index.htm

Vischer, D.L. (1995) Energy dissipators, Eds. D.L. Vischer and W.H. Hager, Chapter 2, pgs 9-21.

Appendix A Communications

Dr. Admiraal,

Based on our discussion last week, I've attached a spreadsheet that Ben Fischer started. The spreadsheet lists size, material, and design discharges. You mentioned headwater, tailwater, slopes, exit slopes, etc. last week. I can continuing collecting that data, but this may give you a start. Based on the original research completed for the weir wall energy dissipator, which is only applicable for broken back boxes, this spreadsheet includes weir wall energy dissipators which were applied to broken back culverts, both round pipe and boxes. There are actually quite a few characteristics we can pull from HY-8 (FHWA's free culvert analysis program), so I want to make sure that we collect what you want for each of the pipes listed in the attached spreadsheet. See a basic screen shot of the culvert summary table and water surface profile below:

Discharge Names	Total Discharge (cfs)	Culvert Discharge (cfs)	Headwater Elevation (ft)	Inlet Control Depth(ft)	Outlet Control Depth(ft)	Flow Type	Outlet Depth (ft)	Tailwater Depth (ft)	Outlet Velocity (ft/s)	Tailwater Velocity (ft/s)
10 year	105.50	105.50	1495.47	**4.57**	-4.75	5-S2n	2.28	1.95	13.07	1.84
25 year	133.80	133.80	1496.77	5.63	**5.87**	7-M2c	2.57	2.16	14.28	1.96
50 year	162.90	162.90	1497.82	**6.92**	6.78	7-M2c	2.86	2.36	15.25	2.06

Water Surface Profile

Crossing - HWY 004 RP 127.46 (Post-feield visit adjustments) (Copy) (Copy), Design Discharge - 0.0 cfs
Culvert - ****Proposed 4.5' Double BB, updated lengths and elvations, Culvert Discharge - 133.8 cfs
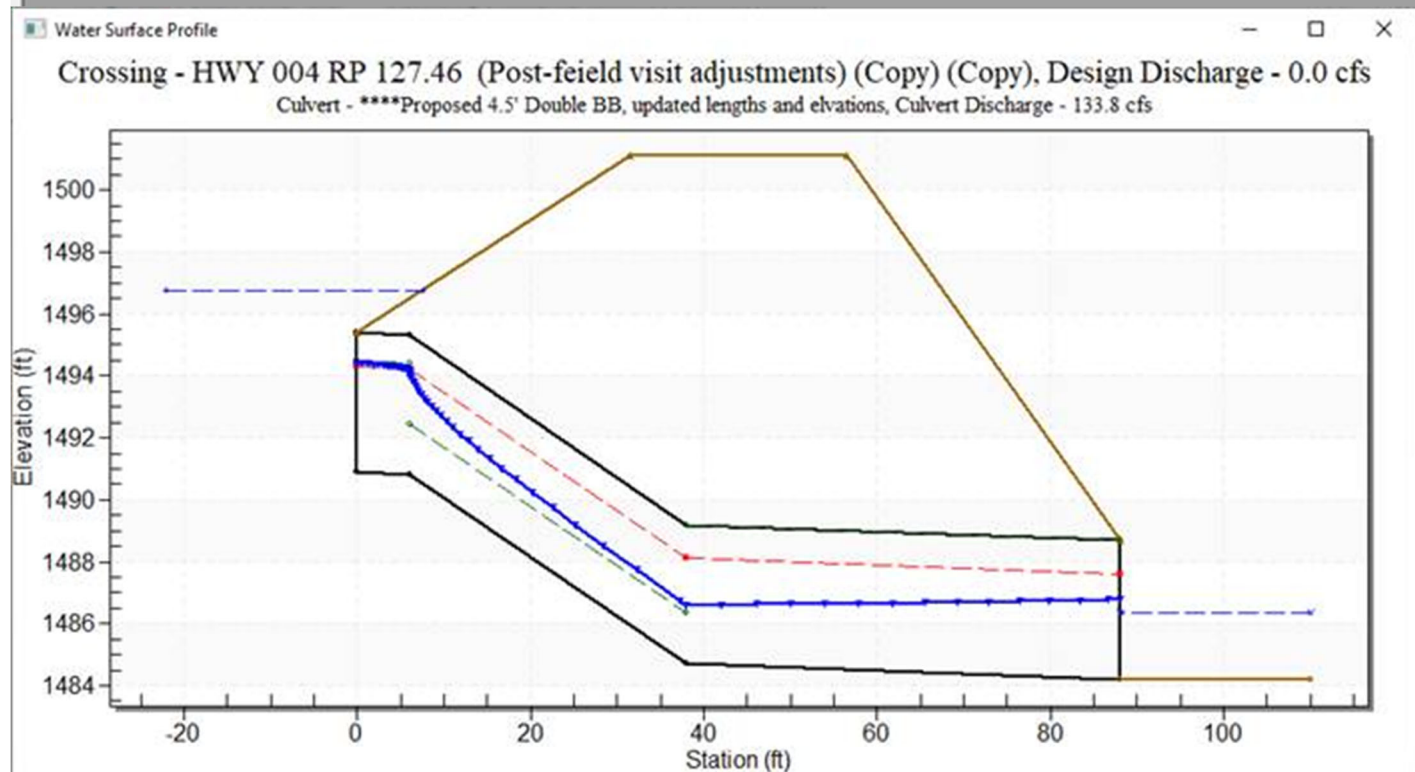
We can also pull the Froude Number, or calculate it based on the diameter and velocity, which I think will be useful. For the weir wall energy dissipator research completed for the broken back boxes, the design was only applicable for Froude numbers between 2 and 7, which are referenced in the research and FHWA's HEC-14 (https://www.fhwa.dot.gov/engineering/hydraulics/pubs/06086/hec14.pdf).

The design files can be obtained, but it can take some searching, and not all design characteristics are provided on the construction plans. Construction plans include the design discharge, headwater depth, and drainage area. The new estimated outlet velocities after the energy dissipator are obtained from the calculation spreadsheet put together to analyze the weir wall.

Let me know if the spreadsheet contains exactly what you want, or what we can remove or add. We could add in the flow types identified as well.

To answer your questions below, it seems like the most popular pipe size is the 48" with a discharge of around 80 cfs. Pertaining to most commonly used material, we use RCP and CMP depending on whether we need to jack the pipe under the highway. If we are able to open cut, then we prefer the CMP due to the increased roughness. I prefer that we look at both types of material, due to the changes in roughness. If we had to prioritize, I'd prefer to look at RCP because that will give us a worst case scenario which lead to higher outlet velocities.

The current design of the weir wall structure allows for the weir walls to be placed completely perpendicular to the direction of flow. For simulation of length of pipe upstream, this depends on the hydraulic jump that may or may not occur because of the introduced tailwater. I'd have to go through the weir wall spreadsheet calculations to determine the minimum length from the lower break that was specified in each case. Let me add that to the spreadsheet, as well as weir wall heights. And finally last question about broken back and straight, can we do both?

I'll set up a webex meeting to walk through this after you've had a chance to read through this email.

Julie Ramirez

Appendix B Calculating Alternate Depths with No Head Losses

It is useful to consider how the weirs may affect outlet depths in the dissipation basin. If it is assumed that energy losses associated with flow over the weir are negligible, the energy equation can be applied to determine the supercritical outlet depth. This appendix shows how specific energy can be used to find alternate depths in a rectangular channel when head losses are negligible. Equation B.1 shows the specific energy (E) as a function of depth (y), discharge (Q), and the channel width (w):

$$E = \alpha \frac{V^2}{2g} + y = \alpha \frac{\left(\frac{Q}{wy}\right)^2}{2g} + y \tag{B.1}$$

Equation B.1 can be modified to form a cubic equation:

$$y^3 - Ey^2 + \alpha \frac{Q^2}{2gw^2} = 0 \tag{B.2}$$

The coefficients in this cubic equation are, $a = 1$, $b = -E$, $c = 0$, and $d = \alpha \frac{Q^2}{2gw^2}$

As long as the specific energy corresponds to a real open-channel flow, all solutions to Equation B.2 are real, and Cardano's formula can be used to solve it. First the equation is changed to the depressed cubic form, defined as:

$$t^3 + pt + q = 0 \tag{B.3}$$

Where p and q are defined by:

$$p = \frac{3ac - b^2}{3a^2} = -\frac{E^2}{3} \tag{B.4}$$

$$q = \frac{2b^3 - 9abc + 27a^2d}{27a^3} = \alpha \frac{Q^2}{2gw^2} - \frac{2E^3}{27} \tag{B.5}$$

The three roots for the depressed cubic form are then given by:

$$t_k = 2\sqrt{-\frac{p}{3}} \cos\left[\frac{1}{3} arccos\left(\frac{3q}{2p}\sqrt{\frac{-3}{p}}\right) - \frac{2\pi k}{3}\right]_{k=1,2,3} \tag{B.6}$$

$$t_k = \frac{2E}{3} \cos\left[\frac{1}{3}\left(arccos\left(1 - \alpha\frac{27Q^2}{4gw^2E^3}\right) - 2\pi k\right)\right]_{k=1,2,3} \tag{B.7}$$

Finally, the roots are converted to roots of the original equation:

$$y_k = \left(t_k - \frac{b}{3a} \right)\Big|_{k=1,2,3} = \left(t_k + \frac{E}{3} \right)\Big|_{k=1,2,3}$$

(B.8)

Equation B.7 can be introduced into Equation B.8 to find the roots of the original cubic equation:

$$y_k = \frac{E}{3} + \frac{2E}{3} \cos\left[\frac{1}{3}\left(arccos\left(1 - \alpha \frac{27Q^2}{4gw^2E^3} \right) - 2\pi k \right) \right]\Big|_{k=1,2,3}$$

(B.9)

Equation B.9 can be used to find the alternate depths by entering the appropriate value of k (1, 2, or 3). Only two of the depths are physically possible, the third will be negative. Equation B.9 is solved by entering the upstream specific energy in Equation B.9 along with the discharge and section width. Then, k is cycled to determine the two possible flow depths.

Appendix C Calculation of Dissipation Basin Outlet Depth and Velocity

This appendix is intended to expand the utility of observed model results. The key equation for the conversions discussed in this appendix is the conversion from specific energy to depth or velocity for the rectangular cross section of the outlet of the dissipation basin:

$$E = \alpha\frac{V^2}{2g} + T = \alpha\frac{Q^2}{2gw^2T^2} + T \qquad\qquad (C.1)$$

Where E is specific energy at the outlet, V is bulk average velocity, g is gravitational acceleration, T is the depth inside the dissipation basin at its outlet, w is the width of the dissipation basin and Q is discharge. Also recall that α is the Coriolis coefficient and is assumed to be 1.15 for the rectangular outlet section of the dissipation basin. A second equation that is helpful is the relation between bulk average velocity and discharge:

$$Q = VwT \qquad\qquad (C.2)$$

Finally, the equation for the critical depth in a rectangular channel is useful for the purpose of converting dimensionless specific energy to dimensional form:

$$y_c = \sqrt[3]{\frac{q^2\alpha}{g}} \qquad\qquad (C.3)$$

Figure 4.10 and 4.18 provide a good summation of the observed results for this research and indicate that dimensionless specific energy at the dissipation basin outlet is roughly constant over the range of Froude numbers observed in the culvert runout section (Approx. 3.8 to 4.4). I would prefer a wider range of Froude numbers, but the range was limited by our decision to simulate a drop angle of 15 degrees, something that was not easily adjusted in the facility. Nevertheless, the baseline dimensionless specific energy for critical depth at the outlet is a constant (1.5) and the data collected appear to repeat that behavior but at higher values.

For the staggered weir, the minimum value of E/y_c was found to be 2.7, while for the full weir, the minimum value of E/y_c was 2.9. In comparison, E/y_c was about 5.5 without any weir, and E/y_c is 1.5 if the outlet depth is critical. We can use these measurements to determine equivalent depths and velocities at the dissipation basin outlet.

As an example, let us select a model discharge of 0.03 m³/s, which is within our range of tested data. The dissipation basin width (w) is 0.0423 meters. This yields a discharge per unit width (q) of 0.071 m²/s. The corresponding critical depth is found using C.3 to be 0.08 m (8 cm). Now we can use equations C.1 and C.2 to find the depth and velocity for all four of the conditions described in the previous paragraph. For example, if E/y_c equals 2.7, E is 0.216 m. Based on simultaneous solution of equation C.1 and C.2, this results in a depth and velocity of 4.1 cm and 1.72 m/s. Note that C.1 is a cubic equation, the solution of which is discussed in Appendix B. Repeating this for all four conditions, the results are shown in Table C.1.

Table C.1 Examples of basin outlet velocity and depth for a model discharge of 0.03 m³/s.

Condition	Outlet Depth (m)	Outlet Velocity (m/s)	Prototype (48 in) Outlet Depth (m)	Prototype (48 in) Outlet Velocity (m/s)
E/y_c = 2.7 (opt. Stag.)	0.040	1.78	0.19	3.91
E/y_c = 2.9 (opt. Full)	0.038	1.87	0.18	4.10
E/y_c = 5.5 (no weir)	0.026	2.72	0.12	5.97
E/y_c = 1.5 (critical)	0.084	0.85	0.40	1.85

The results shown in Table C.1 are for the optimal staggered weir condition (as tested), the optimal full weir condition (as tested), when no weir is installed, and if the outlet is at critical depth. Prototype equivalent values for a 48-inch pipe are determined by scaling the results using a Froude model approach with the scale at 4.8 (since the model has a 10-inch diameter and the prototype has a 48-inch diameter). Results will be different for different prototype diameters.

However, the beauty of the dimensionless approach is that the model conditions do not have to be calculated first. The E/y_c parameter is the same for the model and the prototype since it is dimensionless. If the critical depth at the prototype outlet is found, it can be used to find E for the prototype and then T and V for the prototype without requiring the extra scaling step. This can be applied to the prototype values in Table C.1 by first computing the equivalent discharge of the model (0.03 m³/s in the model is 1.51 m³/s in a 48-inch prototype according to Froude scaling laws). Scaling everything first and then applying the conditions in the first column of Table C.1 results in the same prototype depths and velocities as shown in the table.

Appendix D Point Gauge and Piezometer Datums

Bed readings and crest readings (zero points) for point gages and piezometers

V-Notch Weir Reading

Datum (cm)	Description
47.45	Crest Elevation

Point Gages

Point Gage	Datum (cm)	Description
A	27.76	Bed Elevation
B	29.16	Bed Elevation
C	28.71	Bed Elevation
D	67.56	Bed Elevation
E	67.19	Bed Elevation
F	67.43	Bed Elevation

Piezometers

Piezometer	Datum	Description
1	0.40 cm	Bed Elevation
2	0.40 cm	Bed Elevation
3	0.40 cm	Bed Elevation
4	0.40 cm	Bed Elevation
5	0.40 cm	Bed Elevation
6	0.40 cm	Bed Elevation
7	0.40 cm	Bed Elevation
8	0.40 cm	Bed Elevation
9	0.40 cm	Bed Elevation
10	0.40 cm	Bed Elevation
11	2.30 in	Bed Elevation
12	2.27 in	Bed Elevation
13	2.30 in	Bed Elevation
14	2.26 in	Bed Elevation
15	2.30 in	Bed Elevation
16	2.26 in	Bed Elevation
17	3.75 in	Bed Elevation
18	5.30 in	Bed Elevation
19	6.80 in	Bed Elevation
20	8.35 in	Bed Elevation
21	9.85 in	Bed Elevation
22	11.45 in	Bed Elevation

Appendix E Data - Tailwater Tests – No Weirs

Four Discharges
Approximately 12 Tailwaters for Each Discharge

Test: Weir Height N/A - Streamwise Position N/A　　　　　　　**Date:** 4/15/2022

Run	Z-1-1	Z-1-2	Z-1-3	Z-1-4	Z-1-5	Z-1-6	Z-1-7	Z-1-8	Z-1-9	Z-1-10	Z-1-11	Z-1-12
Time	10:12	10:32	10:46	10:59	11:17	11:44	12:03	12:20	12:35	12:48	13:04	13:18
V-notch gauge (cm)	78.35	78.40	78.39	78.37	78.37	78.39	78.39	78.40	78.38	78.36	78.37	78.38
	78.39	78.37	78.35	78.37	78.37	78.39	78.37	78.36	78.38	78.36	78.38	78.37
Temp (C)	20.9	20.9	21.0	21.1	21.1	21.2	21.3	21.4	21.4	21.5	21.6	21.6
Prandtl U1 (ft)	1.03	1.03	1.03	1.03	1.03	1.04	1.04	1.04	1.04	1.04	1.03	1.01
Prandtl U2 (ft)	0.55	0.55	0.55	0.56	0.56	0.56	0.57	0.56	0.57	0.57	0.59	0.61
Prandtl D1 (ft)	1.15	1.15	1.15	1.15	1.15	1.15	1.12	0.99	0.92	0.86	0.78	0.75
Prandtl D2 (ft)	0.15	0.15	0.15	0.15	0.15	0.15	0.19	0.32	0.40	0.47	0.56	0.60
Pt. Gauge A (cm)	33.46	33.93	33.75	33.81	33.44	33.45	43.22	48.73	52.29	full	full	full
Pt. Gauge B (cm)	34.69	34.72	34.80	34.89	34.80	34.87	49.44	52.68	53.60	full	full	full
Pt. Gauge C (cm)	34.24	34.29	34.23	34.36	34.38	39.91	50.24	52.92	53.62	full	full	full
Pt. Gauge D (cm)	73.58	73.60	73.66	79.05	83.05	86.39	89.81	92.00	94.87	97.41	99.80	N/A
Pt. Gauge E (cm)	71.57	71.54	71.40	80.24	81.90	85.96	89.35	91.97	94.58	97.03	99.71	N/A
Pt. Gauge F (cm)	68.74	73.10	78.55	80.85	83.83	87.28	89.83	92.35	94.91	97.45	N/A	N/A
Tailwater Depth (cm)	5.1	8.6	11.8	14.4	17.2	20	22.5	25.1	27.7	30.2	32.8	33.8
Piezo 1 (cm)	1	2.7	7.6	13.2	16.5	19.8	22.4	25	27.6	30.1	32.7	33.7
Piezo 2 (cm)	2.6	2.6	4.7	12.9	16	19.7	22.4	25	27.6	30.1	32.7	33.7
Piezo 3 (cm)	3.4	3.4	3.4	12.3	15	19.4	22.3	24.9	27.5	30	32.6	33.6
Piezo 4 (cm)												
Piezo 5 (cm)												
Piezo 6 (cm)	6.6	6.5	6.5	12.1	14.5	18.2	22	24.7	27.3	29.8	32.4	33.4
Piezo 7 (cm)	5.8	5.8	5.8	8.6	13.2	16.2	22.1	24.8	27.3	29.8	32.4	33.4
Piezo 8 (cm)	5.6	5.7	5.7	5.9	10.1	13.9	21.9	24.7	27.3	29.8	32.4	33.4
Piezo 9 (cm)	5.7	5.6	5.7	5.6	6	12	21.8	24.7	27.2	29.8	32.4	33.4
Piezo 10 (cm)	6.2	6.2	6.2	6.2	6.2	10	21.5	24.6	27.2	29.7	32.4	33.4
Piezo 11 (in)	4.5	4.5	4.5	4.5	4.5	4.8	10.5	11.8	12.8	13.9	14.9	15.3
Piezo 12 (in)	4.6	4.6	4.6	4.6	4.6	4.6	10.2	11.7	12.8	13.9	14.9	15.3
Piezo 13 (in)	4.3	4.3	4.3	4.3	4.3	4.4	9.7	11.4	12.6	13.7	14.8	15.3
Piezo 14 (in)	4.1	4.1	4.1	4.1	4.1	4.1	9	11.1	12.5	13.7	14.8	15.3
Piezo 15 (in)	4.1	4.1	4.1	4.1	4.1	4.1	8.5	10.7	12.4	13.6	14.8	15.3
Piezo 16 (in)	5.3	5.3	5.3	5.3	5.3	5.3	7.9	10.2	12.1	13.4	14.7	15.3
Piezo 17 (in)	6.1	6.1	6.1	6.1	6.1	6.1	6.8	9.7	11.3	12.9	14.3	15
Piezo 18 (in)	7.7	7.7	7.7	7.7	7.7	7.7	7.7	8.9	10.9	12.5	14	14.7
Piezo 19 (in)	9.2	9.2	9.2	9.2	9.2	9.2	9.2	9.3	10.1	11.8	13.6	14.3
Piezo 20 (in)	10.7	10.7	10.7	10.7	10.7	10.7	10.7	10.7	10.7	11.2	12.9	13.7
Piezo 21 (in)	12.9	12.9	12.9	12.9	12.9	12.9	12.9	12.9	12.9	12.9	13.1	13.5
Piezo 22 (in)	15.1	15.1	15.1	15.1	15.1	15.1	15.1	15.1	15.1	15.1	15.1	15.1
Jump Location (in)	N/A	33.5±1.5	25±2	2±2	7.5±2.5	16±3	62±2	70±2	75±2	79±2	83.5±2	85.5±2

Notes: Baseline discharge tests - no weirs in place

Test: Weir Height N/A - Streamwise Position N/A   **Date:** 4/18/2022

Run	Z-2-1	Z-2-2	Z-2-3	Z-2-4	Z-2-5	Z-2-6	Z-2-7	Z-2-8	Z-2-9	Z-2-10	Z-2-11	Z-2-12
Time	11:11	11:30	11:44	12:01	12:19	12:38	12:54	13:09	13:24	13:40	13:53	14:05
V-notch gauge (cm)	75.89	75.90	75.91	75.84	75.82	75.77	75.78	75.80	75.73	75.74	75.70	75.71
	75.86	75.91	75.89	75.80	75.82	75.73	75.79	75.78	75.76	75.73	75.72	75.80
Temp (C)	20.5	20.6	20.7	20.8	20.9	21.0	21.0	21.1	21.2	21.3	21.3	21.4
Prandtl U1 (ft)	1.18	1.20	1.20	1.21	1.20	1.21	1.21	1.21	1.21	1.21	1.16	1.13
Prandtl U2 (ft)	0.74	0.72	0.72	0.72	0.72	0.72	0.72	0.72	0.72	0.72	0.77	0.80
Prandtl D1 (ft)	1.18	1.18	1.18	1.17	1.17	1.17	1.06	0.91	0.86	0.82	0.76	0.74
Prandtl D2 (ft)	0.18	0.18	0.18	0.18	0.18	0.18	0.30	0.46	0.51	0.56	0.63	0.65
Pt. Gauge A (cm)	32.49	32.35	32.35	32.38	32.40	38.67	44.98	50.07	full	full	full	full
Pt. Gauge B (cm)	34.52	34.52	34.51	34.55	34.52	46.16	50.03	52.87	full	full	full	full
Pt. Gauge C (cm)	33.07	33.10	33.13	33.12	33.39	41.61	50.14	52.80	full	full	full	full
Pt. Gauge D (cm)	73.64	73.68	77.20	80.67	83.60	86.82	89.10	91.98	94.80	97.16	99.82	N/A
Pt. Gauge E (cm)	70.82	70.85	78.45	79.52	82.20	86.24	88.92	91.70	94.25	96.75	99.33	N/A
Pt. Gauge F (cm)	68.45	74.73	77.90	80.94	83.91	86.75	89.36	92.12	94.60	97.16	99.62	N/A
Tailwater Depth (cm)	6.1	8.6	11.4	14.2	17.1	19.7	22.2	24.8	27.3	29.8	32.4	33.3
Piezo 1 (cm)	1.7	3.5	10.1	13.4	16.8	19.6	22.1	24.7	27.2	29.7	32.3	33.2
Piezo 2 (cm)	2.2	2.2	10	12.9	16.6	19.6	22.1	24.7	27.2	29.7	32.3	33.2
Piezo 3 (cm)	2.9	2.8	9.8	12.7	16.3	19.5	22	24.7	27.1	29.7	32.2	33.2
Piezo 4 (cm)												
Piezo 5 (cm)												
Piezo 6 (cm)	6	6.1	9.4	12.2	14.9	19.2	21.8	24.5	27	29.5	32.1	33.1
Piezo 7 (cm)	5.3	5.3	6.9	10.6	13	19.3	21.9	24.6	27.1	29.5	32.2	33.1
Piezo 8 (cm)	5.1	5.1	5.2	8.3	11.5	19.1	21.9	24.5	27	29.6	32.1	33.1
Piezo 9 (cm)	4.7	4.7	4.7	4.8	8.8	19	21.8	24.5	27	29.6	32.1	33.1
Piezo 10 (cm)	5.3	5.3	5.3	5.2	5.7	18.7	21.7	24.5	27	29.6	32.1	33.1
Piezo 11 (in)	4.3	4.3	4.3	4.3	4.3	9.3	10.6	11.8	12.8	13.8	14.8	15.2
Piezo 12 (in)	4.3	4.3	4.3	4.3	4.3	8.9	10.4	11.7	12.8	13.8	14.8	15.2
Piezo 13 (in)	4.1	4.1	4.1	4.1	4.1	8.4	10	11.5	12.6	13.7	14.8	15.2
Piezo 14 (in)	3.8	3.8	3.8	3.8	3.8	7.6	9.7	11.4	12.6	13.7	14.8	15.2
Piezo 15 (in)	3.9	3.9	3.9	3.9	3.9	6.8	9.4	11.1	12.4	13.6	14.8	15.2
Piezo 16 (in)	4.6	4.6	4.6	4.6	4.6	6.2	9.1	10.8	12.3	13.5	14.7	15.2
Piezo 17 (in)	5.8	5.8	5.8	5.8	5.8	5.9	8.3	10.2	11.8	13	14.5	15
Piezo 18 (in)	7.4	7.4	7.4	7.4	7.4	7.4	7.9	9.9	11.4	12.8	14.3	14.8
Piezo 19 (in)	9	9	9	9	9	9	9	9.4	10.9	12.5	13.9	14.6
Piezo 20 (in)	10.3	10.4	10.4	10.3	10.3	10.4	10.3	10.4	10.5	11.8	13.5	14.2
Piezo 21 (in)	12.4	12.4	12.4	12.4	12.4	12.4	12.4	12.4	12.4	12.4	12.9	13.6
Piezo 22 (in)	15	15	15	15	15	15	15	15	15	15	15	15
Jump Location (in)	N/A	31.5±1	N/A	5±3	14±3	59±1	66±1	73±2	77.5±1.5	82±1	86±1	87.5±1

Notes: Baseline discharge tests - no weirs in place. Z-2-4 downstream pitot tube was off due to debris blockage

Test: Weir Height N/A - Streamwise Position N/A   **Date:** 4/18/2022

Run	Z-3-1	Z-3-2	Z-3-3	Z-3-4	Z-3-5	Z-3-6	Z-3-7	Z-3-8	Z-3-9	Z-3-10	Z-3-11	Z-3-12
Time	15:18	15:32	15:46	15:59	16:13	16:25	16:37	16:50	17:06	17:20	17:35	17:46
V-notch gauge (cm)	84.14	84.13	84.12	84.09	84.10	84.12	84.11	84.11	84.15	84.13	84.13	84.14
	84.14	84.16	84.15	84.14	84.19	84.13	84.13	84.15	84.14	84.17	84.13	84.13
Temp (C)	21.5	21.5	21.6	21.7	21.7	21.7	21.8	21.8	21.8	21.8	21.9	21.9
Prandtl U1 (ft)	1.19	1.20	1.20	1.20	1.20	1.20	1.21	1.21	1.21	1.21	1.22	1.20
Prandtl U2 (ft)	0.76	0.76	0.76	0.76	0.77	0.76	0.76	0.76	0.76	0.77	0.77	0.78
Prandtl D1 (ft)	1.20	1.20	1.20	1.20	1.20	1.20	1.20	1.20	1.11	1.02	0.93	0.90
Prandtl D2 (ft)	0.17	0.16	0.16	0.16	0.16	0.16	0.16	0.16	0.27	0.37	0.46	0.50
Pt. Gauge A (cm)	35.96	35.35	34.93	34.98	35.00	35.45	35.37	34.89	49.60	full	full	full
Pt. Gauge B (cm)	36.47	36.47	36.43	36.41	36.42	36.45	36.46	49.42	53.15	full	full	full
Pt. Gauge C (cm)	37.18	37.05	36.98	36.94	37.04	37.00	37.06	51.88	53.03	full	full	full
Pt. Gauge D (cm)	74.43	74.44	74.50	74.30	78.82	83.53	88.21	93.26	96.10	98.55	N/A	N/A
Pt. Gauge E (cm)	73.53	73.54	73.35	73.51	85.08	86.72	89.61	92.90	95.34	98.17	N/A	N/A
Pt. Gauge F (cm)	69.30	69.40	77.22	82.54	85.20	87.82	90.85	93.69	96.20	98.66	N/A	N/A
Tailwater Depth (cm)	5.9	9.3	11.9	15.2	17.9	20.5	23.5	26.3	28.9	31.4	34	34.9
Piezo 1 (cm)	2.8	2.8	6.1	11.1	15.8	19.5	23.1	26.1	28.8	31.3	33.9	34.7
Piezo 2 (cm)	3.9	4	4	8.5	15	18.4	22.8	26	28.7	31.2	33.8	34.7
Piezo 3 (cm)	5.1	5	4.9	5.8	14.7	17	22.2	25.8	28.5	31.1	33.7	34.6
Piezo 4 (cm)												
Piezo 5 (cm)												
Piezo 6 (cm)	7.7	7.7	7.7	7.6	14.3	16.9	20.7	25.2	27.9	30.5	33.3	34.3
Piezo 7 (cm)	6.8	6.7	6.7	6.8	9.2	12	18.3	25	27.9	30.5	33.2	34.2
Piezo 8 (cm)	7.7	7.7	7.6	7.6	7.7	8.3	13.7	24.6	27.8	30.4	33.1	34.2
Piezo 9 (cm)	7.8	7.8	7.8	7.8	7.7	7.8	9.4	24.2	27.6	30.3	33.1	34.2
Piezo 10 (cm)	7.8	7.8	7.8	7.8	7.8	7.8	8	22.5	27.4	30.3	33	34.1
Piezo 11 (in)	5.3	5.3	5.3	5.3	5.3	5.3	5.3	10.4	12.9	14	15.2	15.6
Piezo 12 (in)	5.2	5.2	5.2	5.2	5.2	5.2	5.2	9.1	12.6	13.9	15.1	15.5
Piezo 13 (in)	5	5	5	5	5	5	5	7.5	12.1	13.6	15	15.4
Piezo 14 (in)	4.8	4.7	4.7	4.7	4.7	4.7	4.7	5.1	11.4	13.5	14.8	15.3
Piezo 15 (in)	4.9	4.9	4.9	4.9	4.9	4.9	4.9	4.9	11.1	13.3	14.7	15.2
Piezo 16 (in)	6.6	6.6	6.6	6.6	6.6	6.7	6.7	6.7	10.9	12.9	14.6	15.2
Piezo 17 (in)	7	7	7	7	7	7	7	7	9.6	11.8	13.7	14.5
Piezo 18 (in)	8.4	8.4	8.4	8.4	8.4	8.4	8.4	8.4	9	10.9	13.1	13.9
Piezo 19 (in)	10	10	10	10	10	10	10	10	10	10.5	12.3	13
Piezo 20 (in)	11.8	11.7	11.8	11.7	11.7	11.7	11.7	11.7	11.8	11.8	12	12.6
Piezo 21 (in)	14.4	14.4	14.4	14.4	14.4	14.4	14.4	14.4	14.4	14.4	14.4	14.5
Piezo 22 (in)	15.1	15.1	15.1	15.1	15.2	15.2	15.2	15.2	15.2	15.2	15.2	15.1
Jump Location (in)	0	0	29±1.5	22±2	0	5±2	12±3	43±2	67±2	72.5±1.5	78±1.5	80±2

Notes: Baseline discharge tests - no weirs in place

Test: <u>Weir Height N/A - Streamwise Position N/A</u>　　　　　　**Date:** <u>4/19/2022</u>

Run	Z-4-1	Z-4-2	Z-4-3	Z-4-4	Z-4-5	Z-4-6	Z-4-7	Z-4-8	Z-4-9	Z-4-10	Z-4-11	Z-4-12
Time	10:20	10:40	10:54	11:05	11:20	11:35	11:50	12:06	12:20	12:36	12:49	13:00
V-notch gauge (cm)	86.73	86.71	86.69	86.69	86.70	86.74	86.71	86.70	86.74	86.75	86.73	86.75
	86.71	86.71	86.71	86.71	86.73	86.73	86.73	86.75	86.75	86.75	86.73	86.76
Temp (C)	21.1	21.0	21.1	21.1	21.1	21.1	21.2	21.2	21.2	21.3	21.3	21.3
Prandtl U1 (ft)	0.91	0.92	0.91	0.91	0.90	0.91	0.91	0.91	0.91	0.90	0.91	0.90
Prandtl U2 (ft)	1.31	1.31	1.31	1.31	1.32	1.31	1.31	1.31	1.31	1.32	1.31	1.32
Prandtl D1 (ft)	0.30	0.30	0.30	0.30	0.30	0.30	0.29	0.29	0.31	0.42	0.53	0.58
Prandtl D2 (ft)	1.35	1.35	1.35	1.35	1.35	1.34	1.35	1.35	1.33	1.22	1.12	1.08
Pt. Gauge A (cm)	35.84	35.47	35.69	35.59	35.59	35.59	35.59	35.59	45.55	52.17	full	full
Pt. Gauge B (cm)	37.34	37.30	37.30	37.30	37.29	37.23	37.20	37.23	52.25	full	full	full
Pt. Gauge C (cm)	37.84	37.85	37.85	37.86	37.86	37.84	37.65	42.86	Full	full	full	full
Pt. Gauge D (cm)	75.09	75.14	75.11	75.25	75.91	82.53	86.09	91.41	96.20	98.75	N/A	N/A
Pt. Gauge E (cm)	73.68	73.70	73.75	73.86	83.52	87.19	88.90	92.83	95.76	98.24	N/A	N/A
Pt. Gauge F (cm)	76.55	77.16	78.55	81.20	84.86	87.95	90.62	93.44	96.48	99.11	N/A	N/A
Tailwater Depth (cm)	11.1	11.7	12.7	15	18	20.8	23.7	26.5	29.3	31.8	34.4	35.4
Piezo 1 (cm)	4.6	5.5	6.6	9.4	16	19.1	22.8	26.2	29.1	31.7	34.2	35.2
Piezo 2 (cm)	4.4	4.5	4.6	6.7	15.1	17.9	20.8	26	29	31.5	34.1	35.1
Piezo 3 (cm)	5.3	5.3	5.4	5.4	14.4	16.4	2.02	25.2	28.8	31.2	33.9	35
Piezo 4 (cm)												
Piezo 5 (cm)												
Piezo 6 (cm)	8.3	8.2	8.1	8.1	13.5	16	19.9	24	27.9	30.6	33.4	34.7
Piezo 7 (cm)	7.5	7.7	7.7	7.6	9.9	10.8	15	22.2	27.8	30.4	33.3	34.6
Piezo 8 (cm)	8.7	8.7	8.8	8.7	8.9	9	10.4	19.1	27.6	30.3	33.2	34.5
Piezo 9 (cm)	8.7	8.7	8.7	8.7	8.7	8.7	8.8	14.8	27.2	30.1	33.1	34.4
Piezo 10 (cm)	8.8	8.7	8.7	8.7	8.7	8.7	8.7	10.9	26.7	30	33	34.3
Piezo 11 (in)	5.6	5.6	5.6	5.6	5.6	5.6	5.6	5.8	12.4	13.9	15.1	15.6
Piezo 12 (in)	5.5	5.5	5.5	5.5	5.5	5.5	5.5	5.5	12	13.7	15	15.6
Piezo 13 (in)	5.4	5.4	5.4	5.4	5.4	5.4	5.4	5.4	11.3	13.3	14.9	15.5
Piezo 14 (in)	5.1	5.1	5.1	5.1	5.1	5.1	5.1	5.1	10.4	12.9	14.7	15.4
Piezo 15 (in)	5.4	5.4	5.4	5.4	5.4	5.4	5.4	5.4	9.5	12.3	14.4	15.2
Piezo 16 (in)	7.3	7.3	7.3	7.3	7.3	7.3	7.3	7.3	9.4	12.1	14.4	15.3
Piezo 17 (in)	7.5	7.4	7.5	7.5	7.5	7.5	7.5	7.5	7.9	10.5	13.3	14.2
Piezo 18 (in)	8.8	8.8	8.8	8.8	8.8	8.8	8.8	8.8	8.8	9.8	12.2	13.4
Piezo 19 (in)	10.3	10.3	10.3	10.3	10.3	10.3	10.3	10.3	10.3	10.4	11.4	12.5
Piezo 20 (in)	12.4	12.4	12.3	12.3	12.3	12.3	12.3	12.3	12.3	12.3	12.4	12.6
Piezo 21 (in)	15.1	15.2	15.2	15.2	15.2	15.2	15.2	15.2	15.2	15.2	15.2	15.2
Piezo 22 (in)	15.1	15.1	15.1	15.1	15.1	15.1	15.1	15.1	15.1	15.1	15.1	15.1
Jump Location (in)	33±2	31.5±1.5	30±2	26±2	0	3±2	7±2	17.5±2.5	60±2	68±2	74±2	77±2

Notes: Baseline discharge tests - no weirs in place

Appendix F Data - Tailwater Tests – Staggered Weirs
Four Discharges for Each Weir Height
Approximately 12 Tailwaters for Each Discharge

Test: <u>Weir Height 1/8D - Streamwise Position A</u> **Date:** <u>4/25/2022</u>

Run	A-1-1	A-1-2	A-1-3	A-1-4	A-1-5	A-1-6	A-1-7	A-1-8	A-1-9	A-1-10	A-1-11	A-1-12
Time	13:17	13:30	13:45	14:13	14:32	14:59	15:21	15:41	15:55	16:07	16:20	16:29
V-notch gauge (cm)	78.39	78.44	78.4	78.4	78.41	78.4	78.39	78.45	78.43	78.42	78.42	78.43
	78.39	78.39	78.44	78.41	78.38	78.43	78.45	78.43	78.41	78.41	78.44	78.42
Temp (C)	16.7	16.9	17	17.3	17.5	17.7	17.9	18	18.1	18.2	18.3	18.3
Prandtl U1 (ft)	1.32	1.31	1.31	1.31	1.31	1.31	1.31	1.31	1.31	1.31	1.3	1.28
Prandtl U2 (ft)	0.82	0.83	0.83	0.83	0.83	0.83	0.83	0.83	0.83	0.83	0.84	0.86
Prandtl D1 (ft)	1.27	1.27	1.27	1.27	1.3	1.3	1.23	1.13	1.05	1	0.92	0.89
Prandtl D2 (ft)	0.31	0.31	0.31	0.31	0.28	0.28	0.35	0.46	0.56	0.62	0.7	0.74
Pt. Gauge A (cm)	33.1	33.1	32.96	33.22	33.22	33.18	43.38	48.99	52.41	full	full	full
Pt. Gauge B (cm)	35	35.03	35.11	35.11	35.11	35	49.01	52.61	full	full	full	full
Pt. Gauge C (cm)	34.33	34.32	34.38	34.38	34.38	34.59	50.32	53.03	full	full	full	full
Pt. Gauge D (cm)	74.22	73.93	73.96	79.83	83.9	86.52	89.23	91.96	94.52	97.3	99.7	N/A
Pt. Gauge E (cm)	75.09	75.62	79.11	81.34	82.39	86.05	89.38	91.9	94.62	96.92	99.42	N/A
Pt. Gauge F (cm)	70.25	75.07	78.45	81.04	84.11	86.93	89.58	92.23	94.81	97.35	99.95	N/A
Tailwater Depth (cm)	6.3	8.9	11.6	14.3	17.1	19.9	22.5	25	27.6	30.1	32.6	33.6
Piezo 1 (cm)	2.8	7.7	10.5	13	16.5	19.7	22.4	24.9	27.5	30	32.5	33.5
Piezo 2 (cm)	3.4	6.7	10.3	12.8	16	19.5	22.4	24.9	27.5	30	32.5	33.5
Piezo 3 (cm)	7.4	8	11.7	13.4	14.9	18.3	20.2	21.7	23.4	25	26.9	27.8
Piezo 4 (cm)												
Piezo 5 (cm)												
Piezo 6 (cm)	6.5	7.1	9.4	11.9	13.7	17.9	22	24.6	27.2	29.7	32.2	33.3
Piezo 7 (cm)	6.1	6.2	6.7	8.9	12.7	16.1	22	24.6	27.2	29.7	32.3	33.3
Piezo 8 (cm)	5.7	5.7	5.6	5.7	7.8	13.8	22	24.6	27.2	29.7	32.3	33.3
Piezo 9 (cm)	5.7	5.6	5.6	5.7	5.7	10.6	21.9	24.5	27.1	29.7	32.3	33.3
Piezo 10 (cm)	6.3	6.2	6.2	6.2	6.2	7.5	21.7	24.5	27.1	29.7	32.3	33.3
Piezo 11 (in)	4.5	4.5	4.5	4.5	4.5	4.7	10.6	11.8	12.8	13.9	14.9	15.3
Piezo 12 (in)	4.6	4.6	4.6	4.6	4.6	4.6	10.2	11.6	12.8	13.8	14.9	15.3
Piezo 13 (in)	4.4	4.4	4.4	4.4	4.4	4.4	9.8	11.3	12.6	13.7	14.8	15.3
Piezo 14 (in)	4.1	4.1	4.1	4.1	4.1	4.1	9.1	11	12.5	13.7	14.8	15.3
Piezo 15 (in)	4.1	4.1	4.2	4.2	4.2	4.2	8.5	10.6	12.3	13.5	14.8	15.2
Piezo 16 (in)	5.3	5.3	5.3	5.3	5.3	5.3	8.1	10.2	12.1	13.3	14.7	15.2
Piezo 17 (in)	6.2	6.2	6.2	6.2	6.2	6.2	6.8	9.5	11.3	12.9	14.3	14.9
Piezo 18 (in)	7.7	7.7	7.7	7.7	7.7	7.7	7.7	8.8	10.8	12.5	13.9	14.6
Piezo 19 (in)	9.3	9.3	9.3	9.3	9.3	9.3	9.3	9.3	10.1	11.8	13.4	14.2
Piezo 20 (in)	10.7	10.7	10.7	10.7	10.7	10.7	10.7	10.7	10.7	11.2	12.9	13.7
Piezo 21 (in)	12.9	12.9	12.9	12.9	12.9	12.9	12.9	12.9	12.9	12.9	13.1	13.4
Piezo 22 (in)	15.1	15.1	15.1	15.1	15.1	15.1	15.1	15.1	15.1	15.1	15.1	15.1
Jump Location (in)			0±2	2±2	7±4	17±5	61.5±2	69±2	75±2	79.5±1.5	84±1.5	85.5±1.5

Notes: Debris was caught on downstream pitot tube during A-1-4 and A-1-5

Test: Weir Height 1/8D - Streamwise Position A   **Date:** 4/27/2022

Run	A-2-1	A-2-2	A-2-3	A-2-4	A-2-5	A-2-6	A-2-7	A-2-8	A-2-9	A-2-10	A-2-11	A-2-12
Time	11:05	11:22	11:34	11:49	12:06	12:22	12:40	12:59	13:29	13:47	14:03	14:12
V-notch gauge (cm)	84.15	84.16	84.14	84.16	84.13	84.14	84.17	84.22	84.16	84.15	84.18	84.21
	84.14	84.14	84.14	84.17	84.16	84.14	84.17	84.21	84.13	84.19	84.14	84.22
Temp (C)	19.5	19.6	19.7	19.8	19.9	19.9	20	20.1	20.3	20.4	20.5	20.5
Prandtl U1 (ft)	1.3	1.29	1.3	1.29	1.3	1.3	1.3	1.3	1.3	1.29	1.3	1.27
Prandtl U2 (ft)	0.86	0.86	0.86	0.86	0.86	0.85	0.86	0.86	0.85	0.86	0.85	0.87
Prandtl D1 (ft)	1.35	1.35	1.35	1.35	1.35	1.35	1.35	1.35	1.22	1.16	1.09	1.05
Prandtl D2 (ft)	0.31	0.31	0.31	0.31	0.31	0.31	0.31	0.31	0.46	0.53	0.62	0.67
Pt. Gauge A (cm)	35.4	35.43	35.53	35.34	35.36	35.26	35.46	39.85	50.07	full	full	full
Pt. Gauge B (cm)	36.2	36.24	36.28	36.33	36.33	36.33	36.42	50.75	full	full	full	full
Pt. Gauge C (cm)	36.91	36.93	36.92	36.85	36.93	36.93	36.92	52.85	full	full	full	full
Pt. Gauge D (cm)	74.42	74.42	74.43	74.89	80.3	84.17	87.83	92.91	95.15	97.92	N/A	N/A
Pt. Gauge E (cm)	77.12	77.16	78.71	82.2	85.21	86.7	89.24	92.81	95.4	97.85	N/A	N/A
Pt. Gauge F (cm)	71.25	71.6	78.64	81.61	84.5	87.2	90.1	93.34	96.18	98.49	N/A	N/A
Tailwater Depth (cm)	6.7	9.6	12.2	14.9	17.6	20.5	23.4	26.2	28.8	31.3	33.8	34.9
Piezo 1 (cm)	3.9	4.1	11.2	13.5	15.9	19.3	23.1	26.1	28.6	31.1	33.7	34.8
Piezo 2 (cm)	6.2	6.4	10.9	12.7	15.1	18.1	22.1	25.3	27.9	30.3	32.8	33.9
Piezo 3 (cm)	7	6.9	9.4	10.6	12	13.8	17.4	21.1	25.5	27.8	30.5	31.9
Piezo 4 (cm)												
Piezo 5 (cm)												
Piezo 6 (cm)	7.5	7.5	9.3	11.6	14	16.9	20.7	25.1	27.8	30.4	33.1	34.4
Piezo 7 (cm)	7.1	7	7.6	8.3	9.8	13.2	18.6	25	27.8	30.4	33.1	34.4
Piezo 8 (cm)	7.6	7.6	7.6	7.7	7.6	8.9	13.7	24.7	27.7	30.4	33.1	34.4
Piezo 9 (cm)	7.8	7.8	7.8	7.8	7.8	7.8	9.4	24.3	27.6	30.3	33	34.3
Piezo 10 (cm)	7.9	7.9	7.9	7.9	7.9	7.9	8.1	23.4	27.4	30.2	32.9	34.3
Piezo 11 (in)	5.3	5.3	5.3	5.3	5.3	5.3	5.3	11.1	12.8	14	15.1	15.6
Piezo 12 (in)	5.2	5.2	5.2	5.2	5.2	5.2	5.2	10.4	12.6	13.9	15	15.6
Piezo 13 (in)	5.1	5.1	5.1	5.1	5.1	5.1	5.1	9.6	12.2	13.7	14.9	15.5
Piezo 14 (in)	4.8	4.8	4.8	4.8	4.8	4.7	4.8	8.4	11.7	13.5	14.8	15.4
Piezo 15 (in)	4.9	4.9	4.9	4.9	4.9	4.9	4.9	6.9	11.2	13.1	14.7	15.3
Piezo 16 (in)	6.7	6.6	6.7	6.7	6.7	6.7	6.7	7.1	11	12.9	14.6	15.4
Piezo 17 (in)	7	7	7	7	7	7	7	7	9.5	11.8	13.8	14.6
Piezo 18 (in)	8.4	8.4	8.4	8.4	8.4	8.4	8.4	8.4	9	10.9	13	13.9
Piezo 19 (in)	9.9	9.9	9.9	9.9	9.9	9.9	9.9	9.9	9.9	10.3	12.1	13.2
Piezo 20 (in)	11.8	11.8	11.8	11.8	11.7	11.7	11.7	11.7	11.7	11.7	12	12.7
Piezo 21 (in)	14.4	14.4	14.4	14.4	14.4	14.4	14.4	14.4	14.4	14.4	14.4	14.4
Piezo 22 (in)	15.2	15.2	15.2	15.2	15.2	15.2	15.2	15.2	15.2	15.2	15.2	15.2
Jump Location (in)				0±2	2±1.5	6.5±2.5	14±3	54.5±2.5	67.5±1.5	72.5±1.5	78.5±1.5	80.5±1.5

Test: <u>Weir Height 1/8D - Streamwise Position A</u>   **Date:** <u>4/29/2022</u>

Run	A-3-1	A-3-2	A-3-3	A-3-4	A-3-5	A-3-6	A-3-7	A-3-8	A-3-9	A-3-10	A-3-11	A-3-12
Time	10:27	10:41	10:57	11:10	11:24	11:42	11:59	12:14	12:29	12:42	12:52	13:03
V-notch gauge (cm)	75.93	75.95	75.93	75.88	75.84	75.89	75.89	75.86	75.86	75.86	75.87	75.82
	75.93	75.86	75.87	75.85	75.82	75.89	75.86	75.86	75.86	75.86	75.82	75.86
Temp (C)	20.8	20.9	21	21.1	21.2	21.3	21.4	21.5	21.6	21.7	21.8	21.8
Prandtl U1 (ft)	1.26	1.25	1.25	1.25	1.25	1.26	1.25	1.25	1.25	1.25	1.22	1.18
Prandtl U2 (ft)	0.76	0.76	0.76	0.76	0.76	0.76	0.76	0.76	0.76	0.76	0.79	0.83
Prandtl D1 (ft)	1.24	1.23	1.23	1.24	1.23	1.23	1.11	0.99	0.92	0.88	0.82	0.8
Prandtl D2 (ft)	0.24	0.24	0.24	0.24	0.24	0.24	0.37	0.49	0.57	0.62	0.69	0.71
Pt. Gauge A (cm)	32.73	32.54	32.54	32.49	32.49	38.06	45.63	50.2	full	full	full	full
Pt. Gauge B (cm)	34.56	34.56	34.56	34.57	34.55	46.25	49.94	52.71	full	full	full	full
Pt. Gauge C (cm)	33.1	33.1	33.13	33.14	33.2	47.68	50.38	52.99	full	full	full	full
Pt. Gauge D (cm)	73.88	73.77	74.22	80.45	83.45	86.21	89.06	91.68	94.32	96.83	99.4	N/A
Pt. Gauge E (cm)	75	75.72	78.71	79.95	82.16	86.29	88.92	91.6	94.15	96.57	99.15	N/A
Pt. Gauge F (cm)	69.35	76.5	78.45	80.82	83.6	86.6	89.38	91.94	94.42	96.9	99.51	N/A
Tailwater Depth (cm)	6.1	8.5	11.2	14	16.9	19.5	22.1	24.6	27.1	29.6	32.1	33.3
Piezo 1 (cm)	2.5	7.7	10.3	13.4	16.5	19.4	22	24.5	27	29.5	32	33.2
Piezo 2 (cm)	3.3	7	10.3	12.5	16.4	19.4	22	24.5	27	29.5	32	33.2
Piezo 3 (cm)	6.6	7.5	10.3	12.2	15.9	19.3	21.9	24.5	27	29.5	32	33.1
Piezo 4 (cm)												
Piezo 5 (cm)												
Piezo 6 (cm)	6.2	6.9	9.3	11.5	14.1	19.1	21.8	24.4	26.9	29.4	31.9	33.1
Piezo 7 (cm)	5.7	5.7	6.8	10.1	12.9	19.1	21.8	24.4	26.9	29.4	31.9	33.1
Piezo 8 (cm)	5.3	5.2	5.2	6.2	11.1	19	21.8	24.4	26.9	29.4	31.9	33.1
Piezo 9 (cm)	4.7	4.7	4.7	4.7	7.4	18.7	21.8	24.4	26.9	29.4	31.9	33.1
Piezo 10 (cm)	5.4	5.4	5.4	5.4	5.4	18.4	21.6	24.3	26.9	29.4	31.9	33.1
Piezo 11 (in)	4.3	4.3	4.3	4.3	4.3	9.2	10.6	11.7	12.8	13.7	14.8	15.2
Piezo 12 (in)	4.3	4.3	4.3	4.3	4.3	8.7	10.5	11.7	12.7	13.7	14.8	15.2
Piezo 13 (in)	4.2	4.2	4.2	4.2	4.2	8	10.1	11.5	12.6	13.6	14.7	15.2
Piezo 14 (in)	3.8	3.8	3.8	3.8	3.8	7.3	9.7	11.3	12.5	13.6	14.7	15.2
Piezo 15 (in)	4	4	4	4	4	6.4	9.4	11.1	12.4	13.5	14.7	15.2
Piezo 16 (in)	4.6	4.7	4.6	4.6	4.6	5.6	9	10.6	12.3	13.4	14.6	15.2
Piezo 17 (in)	5.8	5.8	5.8	5.8	5.8	5.8	8.3	10	11.6	12.9	14.4	15
Piezo 18 (in)	7.4	7.4	7.4	7.4	7.4	7.4	7.9	9.7	11.3	12.7	14.1	14.8
Piezo 19 (in)	9	9	9	9	9	9	9	9.3	10.7	12.3	13.8	14.6
Piezo 20 (in)	10.4	10.4	10.4	10.4	10.4	10.4	10.4	10.4	10.5	11.6	13.3	14.2
Piezo 21 (in)	12.4	12.4	12.4	12.4	12.4	12.4	12.4	12.4	12.4	12.4	12.9	13.5
Piezo 22 (in)	15	15	15	15	15	15	15	15	15	15	15	15
Jump Location (in)			0±2	5±3	13±4	55±2	67.5±1.5	72.5±1.5	78±1	82±1	86±1	87.5±1

Notes: A-3-2 debris on downstream pitot tube. Adjusted flow rate at A-3-6

Test: Weir Height 1/8D - Streamwise Position A   **Date:** 4/29/2022

Run	A-4-1	A-4-2	A-4-3	A-4-4	A-4-5	A-4-6	A-4-7	A-4-8	A-4-9	A-4-10	A-4-11	A-4-12
Time	14:48	15:05	15:19	15:34	15:46	15:58	16:14	16:29	16:44	16:59	17:12	17:20
V-notch gauge (cm)	86.69	86.68	86.71	86.7	86.71	86.75	86.77	86.74	86.73	86.74	86.74	86.8
	86.72	86.71	86.73	86.76	86.77	86.75	86.71	86.74	86.74	86.74	86.75	86.77
Temp (C)	22.3	22.4	22.4	22.5	22.5	22.6	22.7	22.8	22.8	22.9	22.9	23
Prandtl U1 (ft)	1.21	1.21	1.21	1.22	1.21	1.21	1.22	1.22	1.2	1.21	1.21	1.2
Prandtl U2 (ft)	0.81	0.81	0.81	0.8	0.81	0.81	0.8	0.8	0.81	0.81	0.81	0.81
Prandtl D1 (ft)	1.29	1.29	1.29	1.29	1.29	1.29	1.29	1.28	1.25	1.15	1.02	1
Prandtl D2 (ft)	0.22	0.22	0.22	0.22	0.22	0.22	0.23	0.22	0.26	0.37	0.52	0.54
Pt. Gauge A (cm)	35.89	36.05	35.83	35.92	36.21	36.27	36.68	36.54	46.72	full	full	full
Pt. Gauge B (cm)	37.31	37.28	37.27	37.28	37.28	37.3	37.3	37.3	full	full	full	full
Pt. Gauge C (cm)	37.98	38.01	38	38	38	38	38	38.18	full	full	full	full
Pt. Gauge D (cm)	75	75.26	75.2	75.5	75.51	83.14	87.37	91.37	95.31	97.97	N/A	N/A
Pt. Gauge E (cm)	77.57	77.7	77.89	82.2	85.39	87.85	90.22	92.78	95.88	98.3	N/A	N/A
Pt. Gauge F (cm)	72.84	79.33	82.15	82.9	85.25	87.32	90.62	93.6	96.41	99.08	N/A	N/A
Tailwater Depth (cm)	10.8	11.5	13.3	15.7	17.9	20.7	23.6	26.6	29.3	31.9	34.4	35.4
Piezo 1 (cm)	5.8	6.4	12	14.3	16.2	19.1	22.9	26.3	29.1	31.7	34.3	35.3
Piezo 2 (cm)	7.6	7.4	9.6	13.9	15.8	18.2	22.1	26	29	31.6	34.2	35.3
Piezo 3 (cm)	6.4	6.6	6.8	13.7	15.7	17.8	21.4	25.6	28.7	31.4	33.9	35
Piezo 4 (cm)												
Piezo 5 (cm)												
Piezo 6 (cm)	8.3	8.4	8.3	11.8	14.2	16.6	19.8	24	27.9	30.6	33.6	34.8
Piezo 7 (cm)	7.6	7.5	7.5	9.1	10	12.4	15.8	22.2	27.9	30.6	33.5	34.7
Piezo 8 (cm)	8.6	8.6	8.6	8.6	8.8	8.9	11.1	19.1	27.8	30.4	33.4	34.7
Piezo 9 (cm)	8.6	8.6	8.7	8.6	8.7	8.6	9	15.1	27.5	30.3	33.3	34.6
Piezo 10 (cm)	8.9	8.9	8.9	8.9	8.9	8.9	8.9	11.4	26.9	30	33.2	34.5
Piezo 11 (in)	5.6	5.6	5.6	5.6	5.6	5.6	5.6	5.8	12.5	13.9	15.2	15.7
Piezo 12 (in)	5.5	5.5	5.5	5.5	5.5	5.5	5.5	5.5	12.1	13.7	15.1	15.6
Piezo 13 (in)	5.4	5.4	5.4	5.4	5.4	5.4	5.4	5.4	11.5	13.3	15	15.5
Piezo 14 (in)	5.1	5.1	5.1	5.1	5.1	5.1	5.1	5.1	10.6	12.9	14.8	15.4
Piezo 15 (in)	5.4	5.4	5.4	5.4	5.4	5.4	5.4	5.4	9.6	12.5	14.6	15.3
Piezo 16 (in)	7.2	7.2	7.2	7.2	7.2	7.3	7.3	7.3	9.6	12.3	14.5	15.3
Piezo 17 (in)	7.4	7.4	7.5	7.4	7.5	7.5	7.5	7.5	8	10.7	13.4	14.3
Piezo 18 (in)	8.8	8.8	8.8	8.8	8.8	8.8	8.8	8.8	8.8	9.9	12.4	13.5
Piezo 19 (in)	10.3	10.3	10.3	10.3	10.3	10.3	10.3	10.3	10.3	10.4	11.6	12.7
Piezo 20 (in)	12.3	12.3	12.3	12.3	12.3	12.3	12.3	12.3	12.3	12.3	12.4	12.7
Piezo 21 (in)	15.2	15.2	15.1	15.1	15.1	15.1	15.1	15.2	15.2	15.1	15.2	15.2
Piezo 22 (in)	15.1	15.1	15.1	15.1	15.1	15.1	15.1	15.1	15.2	15.1	15.2	15.1
Jump Location (in)					0±2	3.5±2	9.5±2.5	19±3	61.5±1.5	68.5±1.5	75±1.5	78±1

Test: Weir Height 2/8D - Streamwise Position A   **Date:** 4/6/2022

Run	B-1-1	B-1-2	B-1-3	B-1-4	B-1-5	B-1-6	B-1-7	B-1-8	B-1-9	B-1-10	B-1-11	B-1-12
Time	11:14	11:50	12:11	12:30	12:47	1:03		1:16	1:40	2:04	2:22	2:47
V-notch gauge (cm)	84.26	84.20	84.11	84.20	84.16	84.14		84.05	84.12	84.13	84.13	84.16
	84.20	84.19	84.14	84.20	84.15	84.14		84.05	84.20	84.17	84.17	84.16
Temp (C)	16.3	16.7	16.9	17.1	17.3	17.5		17.6	17.7	17.9	18.1	18.3
Prandtl U1 (ft)	0.33	0.35	0.35	0.33	0.29	0.29		0.92	0.94	0.92	0.93	0.92
Prandtl U2 (ft)	1.29	1.26	1.26	1.29	1.32	1.32		0.49	0.43	0.49	0.48	0.50
Prandtl D1 (ft)	0.49	0.49	0.49	0.49	0.48	0.50		1.32	1.29	1.19	1.11	1.01
Prandtl D2 (ft)	0.92	0.92	0.92	0.93	0.93	0.92		0.29	0.33	0.43	0.52	0.63
Pt. Gauge A (cm)	35.40	34.50	35.10	34.80	34.40	35.10		34.34	44.60	52.50	full	full
Pt. Gauge B (cm)	36.25	36.50	36.40	36.40	36.40	36.30		36.40	53.67	full	full	full
Pt. Gauge C (cm)	36.62	36.90	36.80	36.80	37.40	37.20		41.30	full	full	full	full
Pt. Gauge D (cm)	74.78	74.90	75.00	75.50	82.80	86.20		91.02	94.50	96.90	99.90	0.00
Pt. Gauge E (cm)	82.90	82.80	83.20	83.70	85.50	87.60		91.20	94.11	96.51	99.16	0.00
Pt. Gauge F (cm)	72.30	72.10	80.00	84.60	86.80	89.60		91.90	94.35	97.10	0.00	0.00
Tailwater Depth (cm)	7.9	10.6	13.3	16	18.9	21.7		24.5	27.3	29.9	32.4	35
Piezo 1 (cm)	6.4	6.7	11.5	14.6	18.2	21.2		24.2	27.1	29.6	32.2	34.8
Piezo 2 (cm)	10.2	10.1	11.5	13.4	17.4	20.6		23.9	26.9	29.5	32	34.7
Piezo 3 (cm)	7.7	7.7	10	12.2	16.4	20		23.5	26.7	29.3	31.8	34.4
Piezo 4 (cm)												
Piezo 5 (cm)												
Piezo 6 (cm)	11.1	11.1	11.6	12.5	15.3	18.4		22.3	26.4	29	31.6	34.5
Piezo 7 (cm)	8.3	8.2	8.5	8.7	10.8	16.2		21	26.3	29	31.6	34.4
Piezo 8 (cm)	8.3	8.2	8.4	8.3	8.5	11.2		18.1	26.1	28.9	31.5	34.5
Piezo 9 (cm)	7.9	7.9	7.9	7.9	8	8.2		14.2	25.9	28.8	31.4	34.4
Piezo 10 (cm)	7.9	8	8	7.9	7.9	7.9		10.2	25.7	28.6	31.4	34.4
Piezo 11 (in)	5.3	5.3	5.3	5.3	5.3	5.3		5.4	12	13.3	14.5	15.7
Piezo 12 (in)	5.2	5.2	5.2	5.2	5.2	5.2		5.2	11.7	13.1	14.4	15.6
Piezo 13 (in)	5.1	5.1	5.2	5.2	5.1	5.1		5.1	11	12.8	14.1	15.5
Piezo 14 (in)	4.7	4.7	4.7	4.7	4.8	4.8		4.8	10.3	12.5	14	15.4
Piezo 15 (in)	4.9	4.9	4.9	4.9	4.9	4.9		4.9	9.5	12	13.9	15.3
Piezo 16 (in)	6.7	6.7	6.8	6.8	6.7	6.7		6.7	9.3	11.7	13.6	15.4
Piezo 17 (in)	7	7.1	7.1	7.1	7	7		7	7.7	10.4	12.6	14.6
Piezo 18 (in)	8.5	8.5	8.5	8.5	8.4	8.4		8.5	8.5	9.6	11.7	13.9
Piezo 19 (in)	9.9	9.9	9.9	9.9	9.9	9.9		9.9	9.9	10	10.9	13.2
Piezo 20 (in)	11.7	11.7	11.6	11.6	11.7	11.7		11.7	11.6	11.6	11.7	12.7
Piezo 21 (in)	14.4	14.4	14.4	14.4	14.4	14.4		14.4	14.5	14.4	14.4	14.5
Piezo 22 (in)	15.2	15.2	15.1	15.2	15.2	15.2		15.2	15.1	15.1	15.1	15.1
Jump Location (in)	0	0	0	0±0	3.5±2	8±2		17±3	60±2	69±2	74.5±2	80±2

Test: <u>Weir Height 2/8D - Streamwise Position A</u>   **Date:** <u>4/12/2022</u>

Run	B-2-1	B-2-2	B-2-3	B-2-4	B-2-5	B-2-6	B-2-7	B-2-8	B-2-9	B-2-10	B-2-11	B-2-12
Time	9:26	9:59	10:18	10:49	11:06	11:21	11:40	12:02	12:19	12:36	12:49	1:01
V-notch gauge (cm)	78.47	78.46	78.35	78.30	78.35	78.40	78.40	78.40	78.39	78.37	78.37	78.38
	78.47	78.43	78.41	78.46	78.41	78.43	78.40	78.40	78.41	78.41	78.40	78.40
Temp (C)	19.4	19.6	19.7	19.9	20.0	20.1	20.3	20.4	20.5	20.6	20.7	20.8
Prandtl U1 (ft)	1.11	1.11	1.11	1.10	1.10	1.11	1.11	1.11	1.10	1.10	1.09	1.07
Prandtl U2 (ft)	0.62	0.62	0.62	0.63	0.63	0.62	0.62	0.62	0.62	0.63	0.64	0.66
Prandtl D1 (ft)	1.29	1.29	1.29	1.29	1.29	1.29	1.29	1.21	1.18	1.23	1.18	1.17
Prandtl D2 (ft)	0.29	0.29	0.29	0.30	0.30	0.30	0.41	0.57	0.70	0.84	0.98	1.03
Pt. Gauge A (cm)	33.17	33.52	33.30	33.85	33.82	33.93	43.10	49.87	52.44	full	full	full
Pt. Gauge B (cm)	34.71	34.73	34.64	34.60	34.66	34.78	49.93	53.64	53.90	full	full	full
Pt. Gauge C (cm)	34.25	34.27	34.22	34.15	34.53	43.20	50.60	53.47	53.90	full	full	full
Pt. Gauge D (cm)	74.02	74.21	75.10	78.70	83.72	87.33	90.21	92.47	95.00	97.31	99.90	0.00
Pt. Gauge E (cm)	79.71	78.98	79.71	80.69	82.50	86.91	89.69	92.32	94.84	97.28	99.80	0.00
Pt. Gauge F (cm)	79.30	76.80	80.12	82.13	84.55	87.15	90.19	92.55	95.18	97.59	100.10	0.00
Tailwater Depth (cm)	6.7	9.5	12	14.9	17.6	20.2	22.8	25.4	27.8	30.4	32.9	33.8
Piezo 1 (cm)	2.5	6.4	11.1	14.2	17.1	20	22.7	25.3	27.7	30.3	32.8	33.7
Piezo 2 (cm)	4.8	5.1	9.8	13.4	16.4	19.8	22.6	25.2	27.6	30.2	32.8	33.6
Piezo 3 (cm)	7.1	7.2	8.9	12	15.8	19.6	22.5	25.1	27.5	30.1	32.7	33.5
Piezo 4 (cm)												
Piezo 5 (cm)												
Piezo 6 (cm)	10.2	10	10.4	11.9	13.7	18.9	22.4	25	27.4	30	32.6	33.5
Piezo 7 (cm)	7.1	6.9	7.1	8.5	13.3	17.2	22.4	25	27.4	30	32.6	33.5
Piezo 8 (cm)	5.8	5.7	5.7	5.8	7.9	16.1	22.4	25	27.4	30	32.6	33.5
Piezo 9 (cm)	6.9	6.9	6.9	6.9	7.1	14.2	22.3	24.9	27.4	30	32.6	33.5
Piezo 10 (cm)	6.8	6.7	6.8	6.8	6.8	11.6	22	24.8	27.3	30	32.6	33.5
Piezo 11 (in)	4.6	4.6	4.6	4.6	4.6	4.9	10.7	11.9	12.9	13.9	15	15.4
Piezo 12 (in)	4.6	4.6	4.6	4.6	4.6	4.6	10.3	11.7	12.8	13.9	15	15.4
Piezo 13 (in)	4.4	4.4	4.4	4.4	4.4	4.4	10	11.5	12.7	13.8	14.9	15.3
Piezo 14 (in)	4.1	4.1	4.1	4.1	4.1	4.1	9.2	11.2	12.6	13.7	14.9	15.3
Piezo 15 (in)	4.1	4.1	4.1	4.1	4.1	4.1	8.8	10.7	12.4	13.6	14.8	15.3
Piezo 16 (in)	5.3	5.3	5.3	5.3	5.3	5.2	8.4	10.5	12.1	13.5	14.8	15.2
Piezo 17 (in)	6.2	6.2	6.1	6.1	6.1	6.1	7.1	9.8	11.4	12.9	14.5	15
Piezo 18 (in)	7.7	7.7	7.7	7.7	7.7	7.7	7.7	9.1	10.9	12.6	14.1	14.7
Piezo 19 (in)	9.3	9.3	9.3	9.3	9.3	9.3	9.3	9.3	10.2	11.9	13.7	14.2
Piezo 20 (in)	10.7	10.7	10.7	10.7	10.7	10.7	10.7	10.7	10.7	11.3	13.1	13.7
Piezo 21 (in)	12.9	12.9	12.9	12.9	12.9	12.9	12.9	12.9	12.9	12.9	13.2	13.4
Piezo 22 (in)	15.1	15.1	15.1	15.1	15.1	15.1	15.1	15.1	15.1	15.1	15.1	15.1
Jump Location (in)	0±0	0±0	0±0	2±2	6±2	19±4	62±2	70±2	75±2	80±2	84±2	85±2

Notes: downstream pitot tube came off at B-2-3

Test: Weir Height 2/8D - Streamwise Position A **Date:** 4/13/2022

Run	B-3-1	B-3-2	B-3-3	B-3-4	B-3-5	B-3-6	B-3-7	B-3-8	B-3-9	B-3-10	B-3-11	B-3-12
Time	10:42	11:00	11:17	11:44	12:01	12:17	12:31	12:48	13:04	13:20	13:34	13:45
V-notch gauge (cm)	86.71	86.63	86.71	86.69	86.72	86.70	86.72	86.67	86.72	86.70	86.70	86.71
	86.71	86.74	86.67	86.67	86.71	86.70	86.73	86.74	86.73	86.72	86.76	86.76
Temp (C)	20.5	20.5	20.6	20.7	20.8	20.8	20.9	20.9	21.0	21.0	21.1	21.1
Prandtl U1 (ft)	1.33	1.34	1.33	1.34	1.34	1.34	1.34	1.33	1.34	1.33	1.33	1.34
Prandtl U2 (ft)	0.93	0.93	0.93	0.93	0.93	0.93	0.93	0.93	0.93	0.94	0.94	0.92
Prandtl D1 (ft)	0.38	0.39	0.42	0.39	0.39	0.39	0.40	0.39	0.43	0.55	0.67	0.70
Prandtl D2 (ft)	1.49	1.48	1.46	1.48	1.49	1.49	1.47	1.49	1.44	1.33	1.22	1.18
Pt. Gauge A (cm)	35.19	35.52	35.67	35.09	35.30	35.07	35.28	35.59	47.53	52.35	full	full
Pt. Gauge B (cm)	37.22	37.01	36.90	37.17	37.25	37.06	36.95	36.72	53.58	full	full	full
Pt. Gauge C (cm)	37.92	37.77	37.78	37.92	37.76	37.70	37.85	44.40	full	full	full	full
Pt. Gauge D (cm)	75.77	75.96	75.67	75.88	81.90	84.43	88.45	92.59	96.55	99.35	N/A	N/A
Pt. Gauge E (cm)	83.13	82.89	83.13	83.90	85.47	86.64	89.90	93.24	96.25	98.71	N/A	N/A
Pt. Gauge F (cm)	71.10	72.65	74.70	83.46	85.69	88.34	91.00	94.12	96.66	99.28	N/A	N/A
Tailwater Depth (cm)	11.2	11.8	13.4	15.6	18.3	21.2	24	26.8	29.6	32.1	34.7	35.4
Piezo 1 (cm)	9.4	9.9	11.9	14.1	17.1	20.6	23.5	26.5	29.4	31.9	34.6	35.3
Piezo 2 (cm)	10.5	10.9	11.9	13.3	16.1	20	22.8	26.2	29.1	31.6	34.3	35.2
Piezo 3 (cm)	8.4	8.7	9.8	11.8	14.8	18.9	22.2	25.7	28.8	31.3	33.9	34.7
Piezo 4 (cm)												
Piezo 5 (cm)												
Piezo 6 (cm)	11.8	11.7	12.1	12.6	14.6	17.5	20.8	24.5	28.3	31	33.9	34.8
Piezo 7 (cm)	9.1	9.1	9.1	9.4	10.1	13.3	17.8	23.2	28.2	30.8	33.8	34.7
Piezo 8 (cm)	8.8	8.7	8.7	8.7	8.8	9.4	13.1	20.2	28	30.7	33.7	34.6
Piezo 9 (cm)	8.8	8.8	8.8	8.7	8.8	8.8	9.5	17.1	27.8	30.6	33.6	34.6
Piezo 10 (cm)	8.7	8.7	8.7	8.7	8.7	8.7	8.7	13.4	27.5	30.3	33.6	34.5
Piezo 11 (in)	5.6	5.6	5.6	5.6	5.6	5.6	5.6	6	12.7	14	15.4	15.8
Piezo 12 (in)	5.5	5.5	5.5	5.5	5.5	5.5	5.5	5.5	12.3	13.9	15.3	15.7
Piezo 13 (in)	5.4	5.4	5.4	5.4	5.4	5.4	5.4	5.4	11.6	13.5	15	15.5
Piezo 14 (in)	5.1	5.1	5.1	5.1	5.1	5.1	5.1	5.1	11	13.2	14.9	15.4
Piezo 15 (in)	5.4	5.3	5.3	5.4	5.4	5.4	5.4	5.4	10.1	12.6	14.7	15.4
Piezo 16 (in)	7.2	7.3	7.3	7.3	7.2	7.3	7.2	7.3	10	12.5	14.7	15.5
Piezo 17 (in)	7.5	7.5	7.4	7.5	7.4	7.5	7.5	7.5	8.2	11	13.5	14.5
Piezo 18 (in)	8.7	8.7	8.7	8.7	8.7	8.7	8.7	8.7	8.8	10	12.6	13.5
Piezo 19 (in)	10.3	10.3	10.3	10.3	10.3	10.3	10.3	10.3	10.3	10.4	11.7	12.6
Piezo 20 (in)	12.2	12.2	12.2	12.2	12.2	12.2	12.3	12.2	12.2	12.2	12.4	12.7
Piezo 21 (in)	15.1	15.2	15.1	15.1	15.2	15.1	15.1	15.2	15.2	15.2	15.2	15.2
Piezo 22 (in)	15.1	15.1	15.1	15.1	15.2	15	15.1	15.1	15.1	15.2	15.1	15.1
Jump Location (in)	0	0	0	0	0±0	4±2	11±2	20±3	61±2	69±2	74±2	77±2

Test: <u>Weir Height 2/8D - Streamwise Position A</u>   **Date:** <u>4/13/2022</u>

Run	B-4-1	B-4-2	B-4-3	B-4-4	B-4-5	B-4-6	B-4-7	B-4-8	B-4-9	B-4-10	B-4-11	B-4-12
Time	14:30	14:48	15:02	15:18	15:32	16:03	16:20	16:37	16:56	17:10	17:22	17:33
V-notch gauge (cm)	76.03	75.93	75.91	75.95	75.91	75.91	75.91	75.89	75.85	75.87	75.87	75.91
	75.92	75.94	75.93	75.92	75.90	75.91	75.91	75.89	75.90	75.90	75.90	75.93
Temp (C)	21.2	21.3	21.4	21.4	21.5	21.6	21.7	21.7	21.8	21.8	21.9	21.9
Prandtl U1 (ft)	1.38	1.38	1.37	1.37	1.37	1.37	1.37	1.37	1.37	1.36	1.32	1.29
Prandtl U2 (ft)	0.88	0.88	0.88	0.88	0.87	0.88	0.88	0.87	0.88	0.88	0.92	0.95
Prandtl D1 (ft)	0.42	0.42	0.42	0.42	0.42	0.25	0.47	0.58	0.73	0.86	0.99	1.03
Prandtl D2 (ft)	1.44	1.44	1.44	1.44	1.42	1.25	1.22	1.02	1.08	1.13	1.11	1.11
Pt. Gauge A (cm)	32.57	32.50	32.58	32.62	32.41	39.06	45.92	50.44	52.46	full	full	full
Pt. Gauge B (cm)	34.50	34.51	34.56	34.66	34.43	45.85	50.62	53.30	full	full	full	full
Pt. Gauge C (cm)	33.06	33.29	33.08	33.01	33.36	47.40	50.49	53.12	full	full	full	full
Pt. Gauge D (cm)	77.86	78.41	78.58	80.77	83.34	86.68	89.17	91.77	94.54	97.00	99.70	N/A
Pt. Gauge E (cm)	79.14	79.17	79.09	80.15	82.31	86.73	89.06	91.70	94.32	96.83	99.35	N/A
Pt. Gauge F (cm)	69.90	76.86	79.03	81.55	83.95	86.66	89.32	92.00	94.55	97.10	99.55	N/A
Tailwater Depth (cm)	6.5	9.2	11.8	14.6	17.1	19.7	22.3	24.8	27.3	29.9	32.3	33.4
Piezo 1 (cm)	2	8.5	11.4	14.1	16.8	19.6	22.2	24.7	27.2	29.8	32.3	33.3
Piezo 2 (cm)	3.4	6.8	10.8	13.3	16.4	19.6	22.1	24.7	27.2	29.8	32.2	33.3
Piezo 3 (cm)	6.5	6.9	8.9	12.4	16	19.4	22	24.6	27.1	29.7	32.2	33.2
Piezo 4 (cm)												
Piezo 5 (cm)												
Piezo 6 (cm)	10	10.2	10.4	11.3	14.1	19.4	22	24.5	27.1	29.6	32.1	33.2
Piezo 7 (cm)	7	7.1	7.9	10.7	13.2	19.4	22	24.6	27.1	29.6	32.1	33.2
Piezo 8 (cm)	5.2	5.2	5.3	6	11.2	19.3	22	24.6	27.1	29.6	32.1	33.2
Piezo 9 (cm)	4.8	4.8	4.7	4.7	7.9	19.1	21.9	24.6	27.1	29.6	32.1	33.2
Piezo 10 (cm)	5.5	5.5	5.4	5.4	5.8	18.9	21.8	24.6	27.1	29.6	32.1	33.2
Piezo 11 (in)	4.3	4.3	4.3	4.3	4.3	9.3	10.7	11.8	12.8	13.8	14.8	15.2
Piezo 12 (in)	4.3	4.3	4.3	4.3	4.3	9	10.5	11.7	12.8	13.8	14.8	15.2
Piezo 13 (in)	4.2	4.2	4.2	4.2	4.2	8.4	10.4	11.6	12.6	13.7	14.8	15.2
Piezo 14 (in)	3.8	3.8	3.8	3.8	3.8	7.6	9.8	11.4	12.5	13.7	14.8	15.2
Piezo 15 (in)	4	4	4	4	4	6.9	9.4	11.1	12.5	13.6	14.7	15.2
Piezo 16 (in)	4.6	4.6	4.6	4.6	4.6	6	8.9	10.6	12.3	13.5	14.7	15.2
Piezo 17 (in)	5.8	5.8	5.8	5.8	5.8	5.8	8.4	10.1	11.7	13	14.4	15
Piezo 18 (in)	7.4	7.4	7.4	7.4	7.4	7.4	8	9.8	11.4	12.8	14.2	14.9
Piezo 19 (in)	9	9	9	9	9	9	9	9.3	10.8	12.4	13.9	14.6
Piezo 20 (in)	10.4	10.4	10.4	10.4	10.4	10.4	10.4	10.4	10.5	11.6	13.5	14.2
Piezo 21 (in)	12.4	12.4	12.4	12.4	12.4	12.4	12.4	12.4	12.4	12.4	12.9	13.6
Piezo 22 (in)	15	15	15	15	15	15	15	15	15	15	15	15
Jump Location (in)	1±2	1±2	2±2	4±2	11±4	59±2	67±2	74±2	78±2	81±2	86±2	88±2

Notes: Downstream pitot tube had bubble during B-4-5. Drained.

Test: Weir Height 3/8D - Streamwise Position A   **Date:** 5/3/2022

Run	C-1-1	C-1-2	C-1-3	C-1-4	C-1-5	C-1-6	C-1-7	C-1-8	C-1-9	C-1-10	C-1-11	C-1-12
Time	10:10	10:29	10:49	11:08	11:25	11:40	12:06	12:20	12:32	12:44	12:55	13:02
V-notch gauge (cm)	78.43	78.44	78.44	78.42	78.40	78.42	78.40	78.44	78.41	78.41	78.41	78.40
	0.00	78.44	78.42	78.40	78.40	78.43	78.41	78.44	78.41	78.41	78.39	78.40
Temp (C)	20.9	21.0	21.1	21.2	21.2	21.3	21.4	21.5	21.5	21.6	21.7	21.7
Prandtl U1 (ft)	1.30	1.29	1.30	1.29	1.29	1.30	1.29	1.29	1.29	1.30	1.28	1.26
Prandtl U2 (ft)	0.81	0.81	0.81	0.81	0.81	0.81	0.81	0.81	0.81	0.81	0.84	0.88
Prandtl D1 (ft)	1.29	1.29	1.29	1.29	1.29	1.29	1.24	1.02	1.04	0.99	0.91	0.88
Prandtl D2 (ft)	0.29	0.29	0.29	0.29	0.29	0.29	0.34	0.47	0.55	0.62	0.71	0.74
Pt. Gauge A (cm)	34.01	34.13	34.13	34.10	34.09	34.12	44.70	49.59	full	full	full	full
Pt. Gauge B (cm)	35.16	35.07	35.00	34.96	34.97	34.96	50.21	52.90	full	full	full	full
Pt. Gauge C (cm)	34.41	34.40	34.40	34.39	34.40	44.41	51.11	53.11	full	full	full	full
Pt. Gauge D (cm)	82.65	82.82	83.12	83.86	84.94	87.32	89.83	92.25	94.91	97.43	99.90	N/A
Pt. Gauge E (cm)	84.16	84.15	84.17	83.97	84.36	87.03	89.62	92.12	94.59	97.15	99.55	N/A
Pt. Gauge F (cm)	70.50	76.85	80.00	81.85	84.41	86.84	89.65	92.20	94.77	97.35	99.85	N/A
Tailwater Depth (cm)	6.7	9.5	12.2	14.7	17.3	19.9	22.5	25	27.6	30	32.6	33.6
Piezo 1 (cm)	2.2	7.6	11.2	13.3	15.6	18.5	21.7	24.5	27	29.6	32.3	33.3
Piezo 2 (cm)	5	5.8	10.9	13.6	16.2	19.4	22.2	24.8	27.3	29.8	32.3	33.4
Piezo 3 (cm)	6.8	6.8	9.4	12.6	15.8	19.2	22.2	24.7	27.3	29.8	32.4	33.4
Piezo 4 (cm)												
Piezo 5 (cm)												
Piezo 6 (cm)	13.3	13.5	13.6	13.9	14.9	18.9	22.5	25	27.5	29.9	32.4	33.5
Piezo 7 (cm)	11.3	11.2	11.7	12.8	13.8	18	22.4	24.9	27.4	29.9	32.4	33.5
Piezo 8 (cm)	6.4	6.3	6.4	7.4	10.4	16.3	22.3	24.9	27.4	29.9	32.4	33.5
Piezo 9 (cm)	5.7	5.6	5.7	5.7	6.1	14.4	22.2	24.9	27.4	29.9	32.4	33.5
Piezo 10 (cm)	6.2	6.2	6.2	6.2	6.2	11.8	22.1	24.8	27.3	29.9	32.4	33.5
Piezo 11 (in)	4.5	4.5	4.5	4.5	4.5	6.7	10.8	11.9	12.9	13.9	14.9	15.4
Piezo 12 (in)	4.6	4.6	4.6	4.6	4.6	5.9	10.5	11.8	12.8	13.9	14.9	15.4
Piezo 13 (in)	4.3	4.3	4.3	4.3	4.3	4.4	10	11.5	12.7	13.8	14.9	15.3
Piezo 14 (in)	4.1	4.1	4.1	4.1	4.1	4.1	9.5	11.3	12.7	13.7	14.8	15.3
Piezo 15 (in)	4.1	4.1	4.1	4.1	4.1	4.1	9	10.9	12.5	13.6	14.8	15.3
Piezo 16 (in)	5.3	5.3	5.3	5.3	5.3	5.3	8.4	10.3	12.2	13.4	14.7	15.3
Piezo 17 (in)	6.2	6.2	6.2	6.2	6.2	6.2	7.1	9.8	11.4	12.9	14.3	15
Piezo 18 (in)	7.7	7.7	7.7	7.7	7.7	7.7	7.8	9.1	11	12.5	14	14.7
Piezo 19 (in)	9.3	9.3	9.3	9.3	9.3	9.3	9.3	9.3	10.1	11.8	13.6	14.3
Piezo 20 (in)	10.7	10.7	10.7	10.7	10.7	10.7	10.7	10.7	10.8	11.3	13	13.8
Piezo 21 (in)	12.9	12.9	12.9	12.9	12.9	12.9	12.9	12.9	13	12.9	13.1	13.4
Piezo 22 (in)	15.1	15.1	15.1	15.1	15.1	15.1	15.1	15.1	15.1	15.1	15.1	15.1
Jump Location (in)	5±2	6±2	6.5±2	7.5±2.5	9±3	24±7	63.5±1.5	71.5±1.5	76±1	80±1	84±1	85.5±1

Test: Weir Height 3/8D - Streamwise Position A   **Date:** 5/4/2022

Run	C-2-1	C-2-2	C-2-3	C-2-4	C-2-5	C-2-6	C-2-7	C-2-8	C-2-9	C-2-10	C-2-11	C-2-12
Time	10:07	10:27	10:41	11:00	11:28	11:46	12:02	12:19	12:40	12:54	13:05	0:00
V-notch gauge (cm)	84.15	84.14	84.14	84.16	84.18	84.16	84.22	84.20	84.21	84.22	84.22	0.00
	84.16	84.16	84.16	84.20	84.19	84.19	84.22	84.19	84.17	84.21	84.23	0.00
Temp (C)	21.2	21.3	21.4	21.5	21.6	21.6	21.7	21.8	21.9	21.9	22.0	0.0
Prandtl U1 (ft)	1.30	1.31	1.30	1.31	1.30	1.30	1.30	1.30	1.30	1.29	1.30	0.00
Prandtl U2 (ft)	0.87	0.86	0.86	0.86	0.86	0.86	0.86	0.86	0.86	0.87	0.86	0.00
Prandtl D1 (ft)	1.35	1.35	1.35	1.42	1.42	1.41	1.41	1.36	1.27	1.18	1.10	0.00
Prandtl D2 (ft)	0.35	0.35	0.34	0.37	0.37	0.37	0.37	0.43	0.53	0.63	0.72	0.00
Pt. Gauge A (cm)	35.90	36.19	35.95	36.10	36.10	36.10	36.15	46.92	full	full	full	0.00
Pt. Gauge B (cm)	36.33	36.32	36.32	36.32	36.32	36.32	36.34	53.79	full	full	full	0.00
Pt. Gauge C (cm)	36.81	36.81	36.82	36.87	36.86	36.87	44.24	full	full	full	full	0.00
Pt. Gauge D (cm)	82.46	82.57	82.72	83.64	85.24	88.23	92.02	94.12	96.76	99.06	N/A	0.00
Pt. Gauge E (cm)	86.71	86.69	86.75	87.05	87.90	89.70	91.67	94.04	96.50	98.94	N/A	0.00
Pt. Gauge F (cm)	70.90	78.09	80.90	83.14	85.50	88.95	91.20	94.30	96.74	99.41	N/A	0.00
Tailwater Depth (cm)	7.1	9.9	12.9	15.7	18.3	21.9	24.5	27.1	29.6	32.2	34.7	0
Piezo 1 (cm)	4.2	5.1	11.8	14.9	17.6	21.4	24.1	26.8	29.4	31.9	34.5	0
Piezo 2 (cm)	8	8.1	10.5	13.7	16.7	20.9	23.8	26.6	29.2	31.7	34.2	0
Piezo 3 (cm)	9.4	9.3	10.1	12.6	15.9	20.4	23.6	26.5	29.1	31.7	34.3	0
Piezo 4 (cm)												
Piezo 5 (cm)												
Piezo 6 (cm)	15.9	15.9	16.1	16.4	17.6	19.9	23.1	26.7	29.2	31.8	34.5	0
Piezo 7 (cm)	10.2	10.4	10.4	11.4	12.9	17.6	21.6	26.5	29	31.6	34.4	0
Piezo 8 (cm)	7.7	7.8	7.9	7.9	8.6	12.7	18.6	26.4	29	31.5	34.4	0
Piezo 9 (cm)	7.9	7.9	7.8	7.9	7.9	8.9	15.4	26.2	28.9	31.5	34.3	0
Piezo 10 (cm)	7.9	7.9	7.8	7.8	7.8	7.9	11.7	25.9	28.8	31.4	34.2	0
Piezo 11 (in)	5.2	5.2	5.3	5.2	5.2	5.2	5.7	12.2	13.4	14.5	15.7	0
Piezo 12 (in)	5.2	5.2	5.2	5.2	5.2	5.2	5.3	11.9	13.3	14.5	15.6	0
Piezo 13 (in)	5	5	5	5	5	5	5	11.4	12.9	14.3	15.5	0
Piezo 14 (in)	4.7	4.8	4.8	4.8	4.8	4.7	4.8	10.7	12.6	14.1	15.5	0
Piezo 15 (in)	4.9	4.9	4.9	4.9	4.9	4.9	4.9	9.9	12.3	13.9	15.4	0
Piezo 16 (in)	6.6	6.6	6.6	6.6	6.6	6.6	6.6	9.7	12	13.7	15.4	0
Piezo 17 (in)	7	7	7	7	7	7	7	8.1	10.7	12.6	14.6	0
Piezo 18 (in)	8.4	8.4	8.4	8.4	8.4	8.4	8.4	8.5	9.8	11.9	14	0
Piezo 19 (in)	9.9	9.9	9.9	9.9	9.9	9.9	9.9	9.9	10	11.1	13.2	0
Piezo 20 (in)	11.7	11.7	11.7	11.7	11.7	11.7	11.7	11.7	11.7	11.8	12.8	0
Piezo 21 (in)	14.4	14.4	14.4	14.4	14.4	14.4	14.4	14.4	14.4	14.4	14.4	0
Piezo 22 (in)	15.2	15.2	15.1	15.2	15.2	15.2	15.1	15.2	15.1	15.1	15.1	0
Jump Location (in)	4±1.5	4±1.5	4.5±2.5	5±2	7.5±2.5	13±3	24±5	63.5±2	70.5±1.5	76±1.5	81±1	0

Notes: C-2-4 downstream pitot tube caught debris

Test: Weir Height 3/8D - Streamwise Position A   **Date:** 5/6/2022

Run	C-3-1	C-3-2	C-3-3	C-3-4	C-3-5	C-3-6	C-3-7	C-3-8	C-3-9	C-3-10	C-3-11	C-3-12
Time	11:02	11:19	11:42	11:59	12:15	12:30	12:52	13:05	13:22	13:35	13:48	13:56
V-notch gauge (cm)	86.68	86.71	86.71	86.71	86.73	86.70	86.70	86.71	86.72	86.70	86.76	86.73
	86.67	86.67	86.70	86.72	86.72	86.71	86.74	86.70	86.73	86.73	86.71	86.74
Temp (C)	21.3	21.4	21.4	21.5	21.6	21.6	21.7	21.8	21.8	21.9	22.0	22.0
Prandtl U1 (ft)	1.35	1.34	1.34	1.33	1.34	1.34	1.34	1.33	1.33	1.34	1.33	1.32
Prandtl U2 (ft)	0.93	0.94	0.94	0.94	0.93	0.94	0.94	0.94	0.94	0.93	0.94	0.95
Prandtl D1 (ft)	1.28	1.29	1.29	1.29	1.33	1.37	1.41	1.42	1.39	1.30	1.22	1.19
Prandtl D2 (ft)	0.34	0.34	0.34	0.34	0.34	0.35	0.34	0.35	0.41	0.53	0.67	0.74
Pt. Gauge A (cm)	36.24	36.37	36.34	36.42	36.35	36.34	36.34	36.21	48.19	full	full	full
Pt. Gauge B (cm)	37.20	37.18	37.17	37.19	37.19	37.17	37.16	37.16	full	full	full	full
Pt. Gauge C (cm)	37.87	37.88	37.88	37.88	37.88	37.86	37.91	46.80	full	full	full	full
Pt. Gauge D (cm)	83.00	83.45	83.62	83.48	84.20	86.80	89.78	93.04	96.25	98.22	N/A	N/A
Pt. Gauge E (cm)	87.90	87.94	87.85	88.19	89.04	90.05	91.59	93.55	95.94	98.29	N/A	N/A
Pt. Gauge F (cm)	72.73	79.24	81.42	83.84	85.85	89.07	91.02	93.36	96.07	98.83	N/A	N/A
Tailwater Depth (cm)	10.6	11.6	13.6	16	18.6	21.3	23.8	26.4	29.1	31.7	34.3	35.4
Piezo 1 (cm)	6.1	7.3	11.7	15.1	17.9	20.8	23.4	26.1	28.9	31.3	33.9	35.1
Piezo 2 (cm)	9.6	9.7	10.8	13.7	16.8	20	22.8	25.8	28.5	31	33.6	34.7
Piezo 3 (cm)	10.4	10.4	10.6	12.5	15.9	19.1	22.2	25.5	28.4	31	33.6	34.6
Piezo 4 (cm)												
Piezo 5 (cm)												
Piezo 6 (cm)	16.7	16.9	16.9	17.2	18.5	20.1	22.1	24.9	28.5	31	33.8	35.2
Piezo 7 (cm)	11.9	11.9	11	11.5	12.6	15.6	19.6	23.3	28.2	30.8	33.5	34.9
Piezo 8 (cm)	8.9	8.9	8.8	8.9	9.2	11	15.3	20.8	28.1	30.7	33.5	34.9
Piezo 9 (cm)	8.7	8.7	8.7	8.7	8.7	8.9	11.1	17.5	27.8	30.6	33.4	34.8
Piezo 10 (cm)	8.7	8.7	8.7	8.7	8.7	8.7	9.2	13.2	27.5	30.4	33.3	34.7
Piezo 11 (in)	5.6	5.6	5.6	5.6	5.6	5.6	5.6	6	12.8	14.1	15.3	15.9
Piezo 12 (in)	5.5	5.5	5.5	5.5	5.5	5.5	5.5	5.6	12.5	13.9	15.2	15.8
Piezo 13 (in)	5.4	5.4	5.4	5.4	5.4	5.4	5.4	5.4	11.8	13.5	15	15.6
Piezo 14 (in)	5.1	5.1	5.1	5.1	5.1	5.1	5.1	5.1	11.1	13.3	14.8	15.5
Piezo 15 (in)	5.4	5.4	5.4	5.4	5.4	5.4	5.4	5.3	10.3	12.8	14.6	15.4
Piezo 16 (in)	7.2	7.2	7.2	7.2	7.2	7.2	7.2	7.2	10	12.5	14.6	15.4
Piezo 17 (in)	7.4	7.4	7.4	7.4	7.5	7.5	7.4	7.4	8.3	11	13.4	14.6
Piezo 18 (in)	8.7	8.7	8.7	8.7	8.7	8.7	8.7	8.7	8.8	10.1	12.4	13.6
Piezo 19 (in)	10.3	10.3	10.3	10.3	10.3	10.3	10.3	10.3	10.3	10.4	11.6	12.7
Piezo 20 (in)	12.3	12.3	12.3	12.3	12.3	12.3	12.4	12.4	12.3	12.3	12.5	12.8
Piezo 21 (in)	15.1	15.1	15.1	15.1	15.1	15.1	15.1	15.1	15.1	15.1	15.1	15.2
Piezo 22 (in)	15.1	15.1	15.1	15.1	15.1	15.1	15.2	15.1	15.1	15.1	15.1	15.1
Jump Location (in)	3.5±1.5	4±1.5	4±2	5±2	6±2	9±3	15±4	24±5	63±2	70±2	75.5±1.5	78.5±1.5

Notes: big bubble in downstream pitot tube at C-3-6, downstream velocity data might be wrong till C-3-6

Test: Weir Height 3/8D - Streamwise Position A   **Date:** 5/6/2022

Run	C-4-1	C-4-2	C-4-3	C-4-4	C-4-5	C-4-6	C-4-7	C-4-8	C-4-9	C-4-10	C-4-11	C-4-12
Time	14:59	15:14	15:27	15:42	15:55	16:10	16:21	16:35	16:48	17:00	17:10	17:19
V-notch gauge (cm)	75.90	75.92	75.90	75.90	75.91	75.90	75.90	75.91	75.91	75.86	75.89	75.88
	75.92	75.90	75.90	75.89	75.88	75.90	75.88	75.88	75.89	75.87	75.90	75.86
Temp (C)	22.2	22.2	22.3	22.4	22.4	22.5	22.6	22.7	22.7	22.8	22.9	22.9
Prandtl U1 (ft)	1.38	1.38	1.38	1.37	1.37	1.37	1.37	1.37	1.37	1.37	1.34	1.30
Prandtl U2 (ft)	0.88	0.88	0.88	0.88	0.88	0.88	0.88	0.88	0.88	0.88	0.92	0.96
Prandtl D1 (ft)	1.38	1.36	1.35	1.34	1.33	1.31	1.18	1.05	0.99	0.95	0.90	0.88
Prandtl D2 (ft)	0.38	0.36	0.35	0.34	0.33	0.34	0.44	0.57	0.65	0.70	0.78	0.81
Pt. Gauge A (cm)	32.85	32.78	32.86	32.85	32.87	40.28	46.27	50.12	full	full	full	full
Pt. Gauge B (cm)	34.71	34.60	34.60	34.62	34.58	47.19	50.25	53.09	full	full	full	full
Pt. Gauge C (cm)	33.36	33.35	33.32	33.30	33.32	48.25	50.27	53.34	full	full	full	full
Pt. Gauge D (cm)	82.81	82.62	82.66	83.15	84.21	87.21	89.56	92.00	94.75	97.19	99.64	N/A
Pt. Gauge E (cm)	82.42	82.17	82.21	82.28	83.61	86.61	89.17	91.72	94.22	96.82	99.32	N/A
Pt. Gauge F (cm)	70.89	76.54	79.05	81.35	83.90	86.84	89.38	92.00	94.44	97.00	99.53	N/A
Tailwater Depth (cm)	6.6	9.3	11.9	14.4	17	19.5	22.1	24.6	27.1	29.7	32.2	33.2
Piezo 1 (cm)	2.3	9	11.7	14	16.6	19.5	22	24.5	27	29.6	32.1	33.1
Piezo 2 (cm)	3.3	7.7	10.9	13.5	16.3	19.4	21.9	24.5	26.9	29.5	32	33.1
Piezo 3 (cm)	6.2	6.7	9.8	12.9	16.1	19.2	21.9	24.5	26.9	29.5	32	33.1
Piezo 4 (cm)												
Piezo 5 (cm)												
Piezo 6 (cm)	12.4	12.3	12.4	13.1	15.4	19.6	22.1	24.6	27	29.6	32.1	33.1
Piezo 7 (cm)	11.5	11.5	11.4	12	13.8	19.6	22	24.6	27	29.6	32.1	33.1
Piezo 8 (cm)	7.1	7.3	7.5	9.1	11.9	19.5	22	24.6	27	29.6	32.1	33.1
Piezo 9 (cm)	4.8	4.8	4.8	5.1	8.5	19.4	22	24.6	27	29.6	32.1	33.1
Piezo 10 (cm)	5.4	5.4	5.4	5.4	6.6	19.2	21.9	24.6	27	29.6	32.1	33.1
Piezo 11 (in)	4.3	4.3	4.3	4.3	4.4	9.6	10.8	11.8	12.8	13.8	14.8	15.2
Piezo 12 (in)	4.3	4.3	4.3	4.3	4.3	9.3	10.6	11.8	12.7	13.8	14.8	15.2
Piezo 13 (in)	4.2	4.2	4.2	4.2	4.2	8.7	10.3	11.6	12.6	13.7	14.8	15.2
Piezo 14 (in)	3.9	3.9	3.8	3.8	3.8	7.9	10	11.4	12.6	13.7	14.8	15.2
Piezo 15 (in)	4	4	4	4	4	7.3	9.6	11.2	12.4	13.6	14.8	15.2
Piezo 16 (in)	4.6	4.6	4.6	4.7	4.7	6.6	9.1	10.8	12.3	13.5	14.7	15.2
Piezo 17 (in)	5.8	5.8	5.8	5.8	5.8	6	8.5	10.2	11.7	13	14.5	15
Piezo 18 (in)	7.4	7.4	7.4	7.4	7.4	7.4	8	9.9	11.4	12.8	14.2	14.8
Piezo 19 (in)	9	9	9	9	9	9	9	9.4	10.8	12.4	13.9	14.6
Piezo 20 (in)	10.5	10.5	10.5	10.5	10.5	10.5	10.4	10.4	10.6	11.7	13.4	14.2
Piezo 21 (in)	12.4	12.4	12.4	12.4	12.4	12.4	12.4	12.4	12.4	12.4	12.8	13.6
Piezo 22 (in)	15	15	15	15	15	15	15	15	15	15	15	15
Jump Location (in)	7.5±2.5	7±3	7.5±2.5	8.5±2.5	16±5	60±1.5	68.5±1.5	74.5±1.5	78.5±1.5	82±1.5	86±1.5	87.5±1

Test: Weir Height 4/8D - Streamwise Position A   **Date:** 4/20/2022

Run	D-1-1	D-1-2	D-1-3	D-1-4	D-1-5	D-1-6	D-1-7	D-1-8	D-1-9	D-1-10	D-1-11	D-1-12
Time	10:21	10:45	11:01	11:16	11:30	11:44	11:58	12:13	12:30	12:45	12:57	13:08
V-notch gauge (cm)	84.19	84.22	84.19	84.23	84.22	84.23	84.20	84.20	84.20	84.20	84.21	84.21
	84.21	84.22	84.23	84.24	84.24	84.23	84.26	84.24	84.23	84.24	84.27	84.25
Temp (C)	20.9	21.1	21.1	21.2	21.3	21.4	21.5	21.5	21.6	21.7	21.7	21.8
Prandtl U1 (ft)	1.26	1.25	1.25	1.26	1.25	1.25	1.26	1.25	1.26	1.26	1.26	1.25
Prandtl U2 (ft)	0.81	0.81	0.82	0.81	0.81	0.82	0.80	0.81	0.81	0.81	0.81	0.82
Prandtl D1 (ft)	1.37	1.36	1.37	1.37	1.37	1.37	1.37	1.33	1.25	1.16	1.09	1.06
Prandtl D2 (ft)	0.33	0.33	0.33	0.33	0.33	0.33	0.33	0.37	0.46	0.56	0.65	0.68
Pt. Gauge A (cm)	34.98	34.78	34.78	34.78	34.78	34.54	34.79	46.00	51.74	full	full	full
Pt. Gauge B (cm)	36.60	36.47	36.46	36.46	36.46	36.46	36.49	52.64	full	full	full	full
Pt. Gauge C (cm)	36.83	36.80	36.80	36.90	36.90	36.91	45.20	53.46	full	full	full	full
Pt. Gauge D (cm)	87.63	87.66	87.81	88.26	88.55	90.22	92.25	94.52	97.21	99.33	N/A	N/A
Pt. Gauge E (cm)	89.50	89.75	89.75	89.79	90.00	90.50	92.04	93.70	96.02	98.62	N/A	N/A
Pt. Gauge F (cm)	72.02	76.99	80.59	83.50	85.90	88.25	90.55	93.50	95.85	98.38	N/A	N/A
Tailwater Depth (cm)	7.2	10.1	13.2	15.9	18.5	21.1	23.6	26.2	28.8	31.3	33.8	34.8
Piezo 1 (cm)	4.5	5.3	12.2	15.5	18.1	20.4	23.2	25.8	28.4	31	33.6	34.5
Piezo 2 (cm)	7.7	8	10.6	14.6	17.4	20.1	22.8	25.7	28.3	30.9	33.5	34.5
Piezo 3 (cm)	10.3	10.2	11.3	13.7	16.5	19.7	22.6	25.5	28.2	30.8	33.4	34.4
Piezo 4 (cm)												
Piezo 5 (cm)												
Piezo 6 (cm)	19.4	19.4	19.7	19.7	20.4	21.9	23.4	26.5	28.9	31.4	34	35
Piezo 7 (cm)	15.9	15.7	16	16.4	17.2	19.4	21.9	26.2	28.6	31.2	33.6	34.6
Piezo 8 (cm)	10.8	10.7	10.8	11.2	12.4	16.1	20	26.2	28.6	31.1	33.6	34.6
Piezo 9 (cm)	8.2	8.3	8.2	8.3	8.7	11.7	16.6	25.9	28.5	31	33.5	34.6
Piezo 10 (cm)	7.9	7.9	7.9	7.9	8	8.6	13.4	25.6	28.4	30.9	33.5	34.6
Piezo 11 (in)	5.3	5.3	5.3	5.3	5.3	5.3	6	12.1	13.2	14.3	15.3	15.8
Piezo 12 (in)	5.2	5.2	5.2	5.2	5.2	5.2	5.4	11.7	13	14.3	15.3	15.7
Piezo 13 (in)	5.1	5.1	5.1	5.1	5.1	5.1	5.1	11.1	12.7	14.1	15.2	15.6
Piezo 14 (in)	4.8	4.8	4.8	4.8	4.8	4.8	4.8	10.4	12.2	13.9	15.1	15.5
Piezo 15 (in)	5.5	5.5	5.5	5.5	5.5	5.5	5.4	9.7	11.7	13.7	14.9	15.4
Piezo 16 (in)	6.7	6.7	6.7	6.7	6.7	6.7	6.8	9.4	11.5	13.3	14.9	15.5
Piezo 17 (in)	7.1	7	7.1	7.1	7.1	7.1	7.1	7.7	10.3	12.3	14.1	14.9
Piezo 18 (in)	8.4	8.4	8.4	8.4	8.4	8.4	8.4	8.5	9.5	11.4	13.4	14.1
Piezo 19 (in)	10	10	9.9	10	10	10	10	10	10	10.7	12.6	13.4
Piezo 20 (in)	11.8	11.7	11.7	11.8	11.7	11.8	11.8	11.8	11.8	11.8	12.3	13
Piezo 21 (in)	14.4	14.4	14.4	14.5	14.4	14.5	14.4	14.5	14.5	14.4	14.4	14.5
Piezo 22 (in)	15.1	15.1	15.1	15.1	15.1	15.1	15.2	15.1	15.1	15.1	15.1	15.2
Jump Location (in)	9±2	9±2	9±2	10±2	11±2	15±2	21±3	61±2	69±2	73±1.5	79.5±1.5	81±1.5

Test: Weir Height 4/8D - Streamwise Position A   **Date:** 4/20/2022

Run	D-2-1	D-2-2	D-2-3	D-2-4	D-2-5	D-2-6	D-2-7	D-2-8	D-2-9	D-2-10	D-2-11	D-2-12
Time	14:00	14:18	14:34	12:00	15:06	15:25	15:43	15:59	16:16	16:28	16:40	16:50
V-notch gauge (cm)	78.41	78.40	78.40	78.40	78.39	78.37	78.38	78.40	78.40	78.42	78.36	78.37
	78.40	78.41	78.40	78.39	78.42	78.41	78.40	78.40	78.40	78.37	78.39	78.40
Temp (C)	22.0	22.0	22.1	22.2	22.3	22.4	22.5	22.5	22.6	22.7	22.7	22.8
Prandtl U1 (ft)	1.27	1.27	1.26	1.27	1.27	1.27	1.28	1.28	1.28	1.27	1.26	1.23
Prandtl U2 (ft)	0.79	0.79	0.79	0.79	0.79	0.79	0.79	0.79	0.78	0.79	0.81	0.83
Prandtl D1 (ft)	1.35	1.35	1.35	1.35	1.35	1.35	1.27	1.16	1.10	1.05	0.97	0.93
Prandtl D2 (ft)	0.35	0.35	0.35	0.35	0.35	0.35	0.43	0.55	0.62	0.68	0.72	0.80
Pt. Gauge A (cm)	33.48	33.52	33.51	33.52	33.31	32.87	45.34	50.82	full	full	full	full
Pt. Gauge B (cm)	34.77	34.82	34.82	34.86	34.86	44.13	50.55	53.37	full	full	full	full
Pt. Gauge C (cm)	34.42	34.38	34.33	34.33	39.54	48.90	51.25	53.37	full	full	full	full
Pt. Gauge D (cm)	86.54	86.06	86.06	86.07	87.16	88.54	90.56	93.27	95.25	97.91	N/A	N/A
Pt. Gauge E (cm)	85.65	85.86	85.75	85.75	86.10	87.57	89.66	92.54	94.75	97.20	99.78	N/A
Pt. Gauge F (cm)	70.97	77.40	79.27	82.04	84.76	87.10	89.79	92.30	94.70	97.30	99.90	N/A
Tailwater Depth (cm)	6.8	9.6	12.3	14.9	17.4	19.9	22.6	25.1	27.5	30	32.6	33.7
Piezo 1 (cm)	3.2	8.8	12	14.7	17.2	19.7	22.4	25	27.4	29.9	32.5	33.6
Piezo 2 (cm)	4.4	6.2	11.2	14.3	17	19.6	22.3	24.9	27.3	29.9	32.4	33.6
Piezo 3 (cm)	7.7	7.8	10.4	13.4	16.3	19.3	22.1	24.8	27.2	29.8	32.4	33.5
Piezo 4 (cm)												
Piezo 5 (cm)												
Piezo 6 (cm)	15.9	16.1	16	16.6	17.9	20.7	23.1	25.4	27.6	30.2	32.6	33.8
Piezo 7 (cm)	14.4	14.5	14.5	14.8	16.7	20.4	23	25.3	27.6	30.1	32.6	33.7
Piezo 8 (cm)	11.9	11.8	11.9	12.7	14.6	19.9	23	25.2	27.6	30.1	32.6	33.7
Piezo 9 (cm)	6.8	6.9	7.1	7.7	11.9	18.9	22.9	25.2	27.6	30.1	32.6	33.6
Piezo 10 (cm)	6.4	6.3	6.4	6.4	7.5	17.6	22.8	25.1	27.5	30.1	32.6	33.6
Piezo 11 (in)	4.6	4.6	4.6	4.6	4.6	7.8	10.9	12	13	14	15	15.4
Piezo 12 (in)	4.6	4.6	4.6	4.6	4.6	7	10.7	11.9	12.9	14	15	15.4
Piezo 13 (in)	4.4	4.4	4.4	4.4	4.4	5.9	10.4	11.7	12.8	13.9	14.9	15.4
Piezo 14 (in)	4.1	4.1	4.1	4.1	4.1	4.2	9.9	11.4	12.7	13.8	14.9	15.4
Piezo 15 (in)	4.2	4.1	4.1	4.1	4.1	4.1	9.4	11	12.4	13.6	14.9	15.4
Piezo 16 (in)	5.3	5.3	5.3	5.3	5.3	5.3	9	10.7	12.2	13.4	14.8	15.4
Piezo 17 (in)	6.2	6.2	6.2	6.2	6.2	6.2	7.9	10	11.5	12.9	14.5	15.1
Piezo 18 (in)	7.7	7.7	7.7	7.7	7.7	7.7	7.9	9.4	11.1	12.6	14.1	14.8
Piezo 19 (in)	9.3	9.3	9.3	9.3	9.3	9.3	9.3	9.4	10.4	12	13.7	14.5
Piezo 20 (in)	10.7	10.8	10.8	10.8	10.8	10.7	10.7	10.7	10.8	11.3	13.1	14
Piezo 21 (in)	12.9	12.9	12.9	12.9	12.9	12.9	12.9	12.9	12.9	12.9	13.1	13.6
Piezo 22 (in)	15.1	15.1	15.1	15.1	15.1	15.1	15.1	15.1	15.2	15.1	13.1	15.1
Jump Location (in)	11±2.5	11±2.5	12±2	14±3	19±4	40±3	65±2	71±2	75±1.5	79.5±1.5	84.5±1.5	85.5±1.5

Notes: D-2-3 debris was caught on downstream pitot tube

Test: Weir Height 4/8D - Streamwise Position A   **Date:** 4/21/2022

Run	D-3-1	D-3-2	D-3-3	D-3-4	D-3-5	D-3-6	D-3-7	D-3-8	D-3-9	D-3-10	D-3-11	D-3-12
Time	10:12	10:47	11:07	11:30	11:48	12:05	12:18	12:33	12:47	13:00	13:11	13:21
V-notch gauge (cm)	75.93	75.91	75.91	75.91	75.89	75.89	75.93	75.91	75.89	75.91	75.94	75.94
	75.91	75.91	75.91	75.91	75.90	75.94	75.91	75.95	75.93	75.93	75.94	75.93
Temp (C)	22.2	22.4	22.4	22.5	22.7	22.7	22.8	22.9	22.9	23.0	23.0	23.1
Prandtl U1 (ft)	1.24	1.24	1.24	1.24	1.24	1.24	1.24	1.24	1.23	1.23	1.19	1.16
Prandtl U2 (ft)	0.75	0.75	0.74	0.75	0.75	0.75	0.75	0.74	0.75	0.75	0.80	0.83
Prandtl D1 (ft)	1.21	1.21	1.20	1.21	1.20	1.16	1.05	0.94	0.91	0.85	0.79	0.77
Prandtl D2 (ft)	0.20	0.21	0.21	0.21	0.21	0.26	0.37	0.49	0.53	0.59	0.66	0.68
Pt. Gauge A (cm)	32.56	32.56	32.54	32.54	32.54	41.91	46.14	50.94	full	full	full	full
Pt. Gauge B (cm)	34.62	34.48	34.52	34.49	40.81	47.81	50.47	53.30	full	full	full	full
Pt. Gauge C (cm)	33.40	33.44	41.41	42.76	45.12	48.68	50.67	53.25	full	full	full	full
Pt. Gauge D (cm)	85.25	85.00	85.36	85.56	86.54	87.95	89.61	92.24	94.96	97.37	99.76	N/A
Pt. Gauge E (cm)	84.50	84.47	84.61	84.72	85.34	86.75	89.27	91.85	94.40	96.94	99.50	N/A
Pt. Gauge F (cm)	70.61	76.44	78.95	81.56	84.18	86.31	89.14	91.84	94.46	97.02	99.62	N/A
Tailwater Depth (cm)	6.5	9.2	11.8	14.5	16.9	19.5	22.1	24.6	27.2	29.7	32.3	33.3
Piezo 1 (cm)	2.9	8.8	11.6	14.3	16.8	19.5	22	24.5	27.1	29.6	32.2	33.2
Piezo 2 (cm)	3.7	7.7	11.1	14.2	16.6	19.4	21.9	24.5	27	29.6	32.2	33.2
Piezo 3 (cm)	6.7	7.8	11.3	14	16.2	19.1	21.8	24.4	27	29.6	32.2	33.2
Piezo 4 (cm)												
Piezo 5 (cm)												
Piezo 6 (cm)	16.3	16.4	16.6	17.3	18.2	20.4	22.5	24.9	27.2	29.8	32.4	33.4
Piezo 7 (cm)	14.2	14.9	15.7	16.3	17.9	20.3	22.5	24.9	27.2	29.7	32.3	33.3
Piezo 8 (cm)	12.6	12.4	13.3	14.6	17.2	20.2	22.5	24.9	27.2	29.7	32.3	33.3
Piezo 9 (cm)	10.1	10.7	11.7	12.6	15.8	20.1	22.4	24.9	27.2	29.7	32.3	33.3
Piezo 10 (cm)	6.7	7.1	9.4	10.6	14.1	20	22.3	24.8	27.2	29.7	32.3	33.3
Piezo 11 (in)	4.4	4.5	4.6	5.5	7	9.9	10.9	11.9	12.9	13.9	14.9	15.3
Piezo 12 (in)	4.4	4.4	4.4	4.6	6.2	9.7	10.8	11.9	12.8	13.9	14.9	15.3
Piezo 13 (in)	4.2	4.2	4.2	4.2	5.4	9.2	10.5	11.7	12.7	13.8	14.9	15.3
Piezo 14 (in)	3.8	3.8	3.8	3.8	4.1	8.6	10.1	11.5	12.7	13.7	14.9	15.3
Piezo 15 (in)	3.9	4	4	3.9	3.9	8	9.7	11.3	12.6	13.6	14.8	15.3
Piezo 16 (in)	4.6	4.6	4.6	4.7	4.7	7.6	9.3	10.9	12.4	13.5	14.8	15.3
Piezo 17 (in)	5.8	5.8	5.8	5.8	5.8	6.6	8.8	10.3	11.8	13.1	14.6	15.1
Piezo 18 (in)	7.4	7.4	7.4	7.4	7.4	7.4	8.2	10	11.4	12.9	14.4	14.9
Piezo 19 (in)	9	9	9	9	9	9	9	9.5	10.9	12.5	14.1	14.7
Piezo 20 (in)	10.4	10.4	10.4	10.4	10.4	10.4	10.4	10.4	10.5	11.8	13.6	14.3
Piezo 21 (in)	12.4	12.5	12.5	12.5	12.5	12.5	12.5	12.4	12.4	12.5	13	13.8
Piezo 22 (in)	15	15	15	15	15	15	15	15	15	15	15	15
Jump Location (in)	19±5	19±5	20±5	24±6	36±5	62.5±1	69±1.5	75±1	78±1	82±1	86±1	87.5±1

Test: Weir Height 4/8D - Streamwise Position A　　　　　　　　**Date:** 4/22/2022

Run	D-4-1	D-4-2	D-4-3	D-4-4	D-4-5	D-4-6	D-4-7	D-4-8	D-4-9	D-4-10	D-4-11	D-4-12
Time	14:15	14:34	14:53	15:10	15:25	15:40	15:55	16:14	16:30	16:48	16:59	17:07
V-notch gauge (cm)	86.69	86.67	86.67	86.69	86.70	86.68	86.72	86.74	86.76	86.76	86.72	86.74
	86.69	86.68	86.68	86.69	86.72	86.71	86.76	86.78	86.75	86.77	86.75	86.76
Temp (C)	22.6	22.7	22.8	22.8	22.9	23.0	23.1	23.1	23.2	23.3	23.4	23.4
Prandtl U1 (ft)	1.34	1.35	1.34	1.34	1.34	1.34	1.34	1.33	1.33	1.33	1.33	1.34
Prandtl U2 (ft)	0.94	0.94	0.94	0.93	0.93	0.93	0.93	0.94	0.94	0.94	0.94	0.93
Prandtl D1 (ft)	1.48	1.47	1.48	1.48	1.48	1.48	1.48	1.47	1.40	1.32	1.23	1.19
Prandtl D2 (ft)	0.41	0.41	0.40	0.40	0.41	0.40	0.41	0.41	0.48	0.59	0.68	0.74
Pt. Gauge A (cm)	35.08	35.10	35.10	35.44	35.38	35.31	35.31	35.31	49.72	full	full	full
Pt. Gauge B (cm)	37.28	37.27	37.27	37.30	37.30	37.30	37.19	37.25	full	full	full	full
Pt. Gauge C (cm)	37.90	37.92	37.95	38.02	38.01	38.03	38.04	48.91	full	full	full	full
Pt. Gauge D (cm)	88.45	88.45	88.45	88.50	88.88	90.14	91.87	94.44	97.35	99.41	N/A	N/A
Pt. Gauge E (cm)	90.59	90.62	90.68	90.81	91.10	92.00	92.69	93.92	96.60	98.87	N/A	N/A
Pt. Gauge F (cm)	73.26	78.95	81.54	83.43	85.75	88.00	90.44	93.21	96.10	98.60	N/A	N/A
Tailwater Depth (cm)	11.2	12	14	16.2	18.8	21.4	24	26.5	29.2	31.7	34.2	35.4
Piezo 1 (cm)	6.3	7.6	12.3	15.3	18.2	20.7	23.4	26.1	28.7	31.3	33.9	34.9
Piezo 2 (cm)	9.2	9.3	11.1	14.4	17.4	20	22.9	25.7	28.5	31.1	33.8	34.9
Piezo 3 (cm)	12.1	11.9	12.4	14	16.6	19.4	22.7	25.6	28.4	31	33.7	34.8
Piezo 4 (cm)												
Piezo 5 (cm)												
Piezo 6 (cm)	21.1	21.1	21.2	21.3	21.7	22.9	24.3	26.4	29.3	31.9	34.4	35.7
Piezo 7 (cm)	16.2	16.1	16.2	16.6	17.5	20.1	22.2	25.2	28.8	31.4	33.8	35.1
Piezo 8 (cm)	11.5	11.8	12.1	12	12.9	16.1	19.5	23.2	28.7	31.3	33.8	35.1
Piezo 9 (cm)	9.2	9.1	9.1	9.2	9.4	11.4	15.2	20.4	28.6	31.1	33.7	35
Piezo 10 (cm)	8.8	8.7	8.8	8.8	8.8	9.1	11.4	17.5	28.3	31	33.6	34.9
Piezo 11 (in)	5.6	5.6	5.6	5.6	5.6	5.6	5.9	7.7	13	14.3	15.4	15.9
Piezo 12 (in)	5.5	5.5	5.5	5.5	5.5	5.5	5.5	6	12.8	14.2	15.3	15.8
Piezo 13 (in)	5.4	5.4	5.4	5.4	5.4	5.4	5.4	5.4	12.2	13.9	15.1	15.7
Piezo 14 (in)	5.1	5.1	5.1	5.1	5.1	5.1	5.1	5.1	11.7	13.6	14.9	15.6
Piezo 15 (in)	5.4	5.4	5.4	5.4	5.4	5.4	5.4	5.4	10.9	13.2	14.8	15.5
Piezo 16 (in)	7.2	7.2	7.3	7.3	7.3	7.3	7.3	7.3	10.8	12.9	14.7	15.5
Piezo 17 (in)	7.5	7.5	7.5	7.5	7.5	7.5	7.5	7.5	9.2	11.6	13.7	14.6
Piezo 18 (in)	8.8	8.8	8.8	8.8	8.8	8.8	8.7	8.8	9	10.4	12.7	13.7
Piezo 19 (in)	10.3	10.3	10.3	10.3	10.3	10.3	10.3	10.3	10.3	10.6	11.8	13
Piezo 20 (in)	12.3	12.3	12.3	12.3	12.3	12.3	12.3	12.4	12.3	12.3	12.5	12.8
Piezo 21 (in)	15.2	15.2	15.2	15.2	15.2	15.2	15.2	15.2	15.2	15.2	15.2	15.2
Piezo 22 (in)	15.1	15.1	15.2	15.1	15.1	15.2	15.1	15.1	15.1	15.1	15.1	15.1
Jump Location (in)	9±2	9.5±2.5	9.5±2.5	9.5±2.5	11.5±3.5	14.5±2.5	20±4	27±5	64±2	71±2	76±1	79.5±1.5

Appendix G Data - Tailwater Tests – Full Weirs

Four Discharges for Each Weir Height

Approximately 12 Tailwaters for Each Discharge

Test: Full Weir Height 1/8D - Streamwise Position A   **Date:** 6/6/2022

Run	I-1-1	I-1-2	I-1-3	I-1-4	I-1-5	I-1-6	I-1-7	I-1-8	I-1-9	I-1-10	I-1-11	I-1-12
Time	13:30	13:41	13:54	14:04	14:16	14:27	14:44	14:59	15:09	15:22	15:34	15:43
V-notch gauge (cm)	78.40	78.37	78.41	78.41	78.39	78.36	78.35	78.33	78.39	78.35	78.37	78.36
	78.36	78.34	78.37	78.37	78.38	78.34	78.34	78.35	78.40	78.33	78.35	78.37
Temp (C)	21.5	21.6	21.7	21.7	21.8	21.9	22.0	22.1	22.1	22.2	22.3	22.3
Prandtl U1 (ft)	1.28	1.29	1.28	1.28	1.29	1.28	1.28	1.28	1.29	1.28	1.28	1.25
Prandtl U2 (ft)	0.80	0.80	0.80	0.80	0.80	0.80	0.80	0.80	0.79	0.80	0.80	0.83
Prandtl D1 (ft)	1.28	1.29	1.29	1.29	12.90	1.13	1.24	1.12	1.05	0.98	0.92	0.89
Prandtl D2 (ft)	0.27	0.27	0.27	0.27	0.27	0.42	0.31	0.44	0.53	0.61	0.70	0.75
Pt. Gauge A (cm)	33.85	33.85	33.74	33.77	33.76	33.75	43.38	48.63	full	full	full	full
Pt. Gauge B (cm)	34.86	34.86	34.86	34.86	34.86	34.86	48.97	52.61	full	full	full	full
Pt. Gauge C (cm)	34.24	34.24	34.25	34.26	34.27	34.30	50.04	53.03	full	full	full	full
Pt. Gauge D (cm)	73.93	73.93	74.08	74.12	82.21	85.70	89.14	91.92	94.63	96.90	99.50	N/A
Pt. Gauge E (cm)	75.02	75.04	78.47	80.28	81.96	85.33	89.02	91.74	94.22	96.80	99.30	N/A
Pt. Gauge F (cm)	69.60	75.30	78.04	80.40	83.15	86.60	89.35	92.17	94.72	97.23	99.80	N/A
Tailwater Depth (cm)	6.1	8.8	11.6	14.1	16.9	19.8	22.4	24.9	27.4	29.9	32.4	33.5
Piezo 1 (cm)	2.4	3.9	10.3	13	16.3	19.6	22.3	24.8	27.3	29.8	32.4	33.5
Piezo 2 (cm)	3.2	3.3	10.2	12.6	15.8	19.4	22.3	24.8	27.3	29.7	32.3	33.4
Piezo 3 (cm)												
Piezo 4 (cm)												
Piezo 5 (cm)	11	11	10.7	12	13.4	18.4	22.1	24.7	27.2	29.7	32.2	33.3
Piezo 6 (cm)	6.8	6.8	9.2	11.8	13.8	17.8	22	24.5	27	29.5	32.1	33.2
Piezo 7 (cm)	6.2	6.2	6.6	8.5	12.8	15.7	21.9	24.5	27	29.5	32.1	33.2
Piezo 8 (cm)	5.5	5.5	5.5	5.6	8.1	13.3	21.9	24.5	27	29.5	32.1	33.2
Piezo 9 (cm)	5.6	5.6	5.6	5.6	5.7	10	21.8	24.5	27	29.5	32.1	33.2
Piezo 10 (cm)	6.1	6.1	6.2	6.2	6.2	7	21.7	24.4	26.9	29.5	32.1	33.2
Piezo 11 (in)	4.5	4.5	4.5	4.5	4.5	4.5	10.6	11.7	12.8	13.8	14.8	15.2
Piezo 12 (in)	4.5	4.5	4.5	4.5	4.5	4.5	10.2	11.5	12.7	13.8	14.8	15.2
Piezo 13 (in)	4.3	4.3	4.3	4.3	4.3	4.3	9.7	11.4	12.5	13.6	14.7	15.2
Piezo 14 (in)	4	4	4	4	4	4	9.1	11	12.4	13.5	14.7	15.2
Piezo 15 (in)	4.1	4.1	4.1	4.1	4.1	4.1	8.5	10.5	12.3	13.4	14.6	15.2
Piezo 16 (in)	5.3	5.2	5.2	5.2	5.2	5.2	8.1	10.2	12	13.2	14.5	15.1
Piezo 17 (in)	6.1	6.1	6.1	6.2	6.2	6.2	6.9	9.5	11.2	12.7	14.2	14.9
Piezo 18 (in)	7.7	7.7	7.7	7.7	7.7	7.7	7.7	8.8	10.7	12.4	13.9	14.6
Piezo 19 (in)	9.3	9.3	9.3	9.3	9.3	9.3	9.3	9.3	10.1	11.7	13.4	14.2
Piezo 20 (in)	11.1	11	11.1	11.1	11	11	11.1	11.1	11.1	11.4	12.9	13.7
Piezo 21 (in)	12.8	12.8	12.8	12.9	12.8	12.9	12.9	12.9	12.8	12.9	13.1	13.4
Piezo 22 (in)	15.1	15.1	15.1	15.1	15.1	15.1	15.1	15.1	15.1	15.1	15.1	15.1
Jump Location (in)	0	0	0±0	3±2	7.5±3.5	18±6	63±2	70±2	76±1.5	79±1.5	84±1.5	85.5±1.5

Notes: turned valve up after I-1-2

Test: <u>Full Weir Height 1/8D - Streamwise Position A</u>   **Date:** <u>6/8/2022</u>

Run	I-2-1	I-2-2	I-2-3	I-2-4	I-2-5	I-2-6	I-2-7	I-2-8	I-2-9	I-2-10	I-2-11	I-2-12
Time	14:06	14:25	14:36	14:46	14:59	15:12	15:29	15:42	15:54	16:03	16:10	16:18
V-notch gauge (cm)	75.91	75.91	75.86	75.87	75.88	75.90	75.91	75.94	75.92	75.90	75.90	75.89
	75.90	75.88	75.84	75.88	75.88	75.89	75.87	75.93	75.90	75.91	75.89	75.91
Temp (C)	21.8	21.9	22.0	22.0	22.1	22.2	22.3	22.4	22.4	22.5	22.5	22.6
Prandtl U1 (ft)	1.26	1.26	1.26	1.26	1.26	1.26	1.26	1.26	1.26	1.26	1.24	1.19
Prandtl U2 (ft)	0.76	0.76	0.76	0.76	0.76	0.76	0.76	0.76	0.76	0.76	0.78	0.84
Prandtl D1 (ft)	1.24	1.24	1.24	1.24	1.24	1.22	1.12	0.98	0.92	0.88	0.82	0.80
Prandtl D2 (ft)	0.23	0.23	0.23	0.22	0.22	0.24	0.35	0.49	0.56	0.61	0.67	0.70
Pt. Gauge A (cm)	32.61	32.50	32.50	32.47	32.47	38.07	44.99	49.57	full	full	full	full
Pt. Gauge B (cm)	34.47	34.45	34.45	34.45	34.45	45.24	50.14	52.80	full	full	full	full
Pt. Gauge C (cm)	33.17	33.17	33.17	33.18	33.18	47.09	50.15	52.90	full	full	full	full
Pt. Gauge D (cm)	73.75	73.75	73.70	79.72	82.83	86.48	88.71	91.62	94.14	96.55	98.65	N/A
Pt. Gauge E (cm)	75.00	75.00	77.40	79.20	81.60	86.01	88.47	91.45	93.94	96.46	98.46	N/A
Pt. Gauge F (cm)	68.63	75.03	77.47	80.84	83.55	86.77	89.10	91.79	94.23	96.75	98.80	N/A
Tailwater Depth (cm)	6.1	8.7	11.2	13.9	16.8	19.5	22	24.5	26.9	29.4	31.5	33.1
Piezo 1 (cm)	1.4	7.1	10.1	12.9	16.5	19.4	22	24.4	26.9	29.4	31.4	33
Piezo 2 (cm)	1.8	5.7	9.7	12.1	15.6	19.2	21.2	24.3	26.6	29.1	31.1	32.7
Piezo 3 (cm)												
Piezo 4 (cm)												
Piezo 5 (cm)	10.1	9.8	10	11.3	14.4	19.3	21.8	24.4	26.8	29.3	31.3	32.9
Piezo 6 (cm)	6.7	7	9.3	11.5	14.2	19.1	21.7	24.3	26.7	29.2	31.2	32.8
Piezo 7 (cm)	5.7	5.7	6.7	10.4	12.8	19.1	21.7	24.3	26.7	29.2	31.2	32.8
Piezo 8 (cm)	5.1	5	5.1	6.6	11	19	21.7	24.3	26.7	29.2	31.2	32.8
Piezo 9 (cm)	4.7	4.6	4.6	4.7	7	18.8	21.6	24.3	26.7	29.2	31.2	32.8
Piezo 10 (cm)	5.3	5.3	5.3	5.3	5.5	18.4	21.5	24.3	26.7	29.2	31.2	32.8
Piezo 11 (in)	4.2	4.2	4.2	4.2	4.3	9.2	10.6	11.7	12.7	13.7	14.5	15.1
Piezo 12 (in)	4.3	4.3	4.3	4.3	4.3	8.8	10.5	11.6	12.6	13.6	14.5	15.1
Piezo 13 (in)	4.1	4.1	4.1	4.1	4.2	8.1	10.1	11.5	12.5	13.6	14.4	15.1
Piezo 14 (in)	3.8	3.8	3.8	3.8	3.8	7.2	9.7	11.3	12.4	13.5	14.4	15.1
Piezo 15 (in)	3.9	3.9	3.9	3.9	3.9	6.1	9.3	10.9	12.3	13.4	14.3	15.1
Piezo 16 (in)	4.6	4.7	4.6	4.7	4.7	5.4	9	10.5	12.2	13.3	14.2	15.1
Piezo 17 (in)	5.9	5.9	5.9	5.9	5.9	5.9	8.2	10	11.6	12.9	14	14.9
Piezo 18 (in)	7.4	7.4	7.4	7.4	7.4	7.4	7.9	9.6	11.1	12.7	13.7	14.7
Piezo 19 (in)	9	9	9	9	9	9	9	9.3	10.6	12.2	13.4	14.5
Piezo 20 (in)	10.4	10.4	10.3	10.4	10.4	10.4	10.4	10.4	10.5	11.5	12.9	14
Piezo 21 (in)	12.4	12.4	12.4	12.4	12.4	12.4	12.4	12.4	12.4	12.4	12.6	13.4
Piezo 22 (in)	14.9	15	14.9	15	14.9	14.9	14.9	15	15	14.9	14.9	15
Jump Location (in)	0	0	0±2	5.5±3.5	13±5	58±2	68±2	73±1.5	78±1.5	82±1.5	85±1.5	87±1.5

Notes: debris caught on downstream PT at I-2-6

Test: <u>Full Weir Height 1/8D - Streamwise Position A</u>　　　　　　　**Date:** <u>6/9/2022</u>

Run	I-3-1	I-3-2	I-3-3	I-3-4	I-3-5	I-3-6	I-3-7	I-3-8	I-3-9	I-3-10	I-3-11	I-3-12
Time	14:15	14:24	14:32	14:39	14:49	15:09	15:19	15:31	15:48	15:58	16:21	16:27
V-notch gauge (cm)	84.20	84.14	84.18	84.15	84.15	84.18	84.20	84.15	84.16	84.18	84.21	84.21
	84.16	84.17	84.16	84.15	84.14	84.18	84.20	84.18	84.21	84.16	84.23	84.21
Temp (C)	22.1	22.2	22.2	22.2	22.3	22.4	22.4	22.5	22.5	22.6	22.7	22.7
Prandtl U1 (ft)	1.34	1.33	1.33	1.35	1.35	1.34	1.34	1.34	1.34	1.34	1.34	1.34
Prandtl U2 (ft)	0.89	0.90	0.89	0.88	0.88	0.89	0.89	0.89	0.89	0.89	0.89	0.89
Prandtl D1 (ft)	0.36	0.36	0.36	0.36	0.37	0.37	0.37	0.37	0.37	1.39	1.31	1.26
Prandtl D2 (ft)	1.41	1.41	1.41	1.41	1.38	1.38	1.38	1.38	1.38	0.74	0.82	0.88
Pt. Gauge A (cm)	35.37	35.14	35.18	35.27	35.33	35.28	35.33	35.33	49.03	full	full	full
Pt. Gauge B (cm)	36.50	36.40	36.40	36.40	36.40	36.38	36.37	43.17	full	full	full	full
Pt. Gauge C (cm)	36.98	36.97	36.97	37.03	37.03	37.02	36.93	51.33	full	full	full	full
Pt. Gauge D (cm)	74.42	74.38	74.41	74.73	74.93	82.94	87.64	91.92	95.20	97.66	N/A	N/A
Pt. Gauge E (cm)	76.94	76.95	77.00	81.57	83.63	85.42	88.90	92.60	95.15	97.70	N/A	N/A
Pt. Gauge F (cm)	70.00	69.87	78.80	81.69	83.81	86.81	90.02	92.87	95.72	98.30	N/A	N/A
Tailwater Depth (cm)	6.1	9.3	12	14.7	17.4	20.2	23.2	25.9	28.5	31	33.6	34.7
Piezo 1 (cm)	2.9	2.8	7.2	13.3	15.7	19.2	22.8	25.8	28.4	31	33.4	34.6
Piezo 2 (cm)	5.4	5.4	5.5	12.8	15.3	18	22.4	25.7	28.3	30.9	33.3	34.5
Piezo 3 (cm)												
Piezo 4 (cm)												
Piezo 5 (cm)	13.9	13.9	13.9	13.2	14.8	16.9	20.5	25.3	28	30.5	33.1	34.5
Piezo 6 (cm)	7.9	7.9	7.9	11.2	13.7	16.3	20.8	24.9	27.6	30.1	32.8	34.2
Piezo 7 (cm)	7.5	7.5	7.5	8.3	9.6	13	17.8	24.5	27.5	30.1	32.7	34.1
Piezo 8 (cm)	7.5	7.5	7.5	7.6	7.6	8.5	12.8	23.6	27.4	30.1	32.7	34.1
Piezo 9 (cm)	7.8	7.8	7.8	7.8	7.8	7.8	8.9	22.1	27.2	30	32.7	34.1
Piezo 10 (cm)	7.8	7.8	7.8	7.8	7.8	7.8	7.9	19.6	27	29.9	32.6	34
Piezo 11 (in)	5.2	5.2	5.2	5.2	5.2	5.2	5.2	8.8	12.8	13.9	15	15.6
Piezo 12 (in)	5.2	5.2	5.2	5.2	5.2	5.2	5.2	7.5	12.6	13.8	14.9	15.5
Piezo 13 (in)	5	5	5	5	5	5	5	5.6	11.9	13.5	14.8	15.4
Piezo 14 (in)	4.7	4.7	4.7	4.7	4.7	4.7	4.7	4.8	11.5	13.3	14.7	15.3
Piezo 15 (in)	4.9	4.9	4.9	4.9	4.9	4.9	4.9	4.9	11	13	14.5	15.2
Piezo 16 (in)	6.6	6.6	6.6	6.6	6.6	6.6	6.6	6.6	10.7	12.8	14.4	15.2
Piezo 17 (in)	7	7	7	7	7	7	7	7	9.2	11.6	13.4	14.7
Piezo 18 (in)	8.4	8.4	8.4	8.4	8.4	8.4	8.4	8.4	8.8	10.8	12.7	14
Piezo 19 (in)	10	9.9	9.9	10	10	10	9.9	9.9	10	10.3	12	13.1
Piezo 20 (in)	11.7	11.7	11.7	11.7	11.7	11.7	11.7	11.6	11.8	11.7	12	12.7
Piezo 21 (in)	14.4	14.4	14.3	14.4	14.4	14.4	14.4	14.4	14.4	14.4	14.4	14.4
Piezo 22 (in)	15.1	15.1	15.2	15.1	15.1	15.2	15.2	15.1	15.2	15.1	15.2	15.2
Jump Location (in)	0	0	0	0±2	2±2	7±3	14±3	39±5	66±2	73±2	77.5±2	80.5±1.5

Notes: I-3-5 air trapped in downstream PT

Test: <u>Full Weir Height 1/8D - Streamwise Position A</u>   **Date:** <u>6/10/2022</u>

Run	I-4-1	I-4-2	I-4-3	I-4-4	I-4-5	I-4-6	I-4-7	I-4-8	I-4-9	I-4-10	I-4-11	I-4-12
Time	13:30	13:41	13:50	13:58	14:10	14:27	14:38	14:49	15:02	15:13	15:21	15:30
V-notch gauge (cm)	86.73	86.71	86.70	86.71	86.73	86.78	86.79	86.80	86.81	86.77	86.73	86.81
	86.75	86.74	86.72	86.78	86.80	86.75	86.81	86.80	86.82	86.75	86.79	86.77
Temp (C)	22.4	22.4	22.5	22.6	22.6	22.7	22.8	22.8	22.9	22.9	23.0	23.0
Prandtl U1 (ft)	1.33	1.33	1.32	1.33	1.33	1.32	1.33	1.32	1.33	1.32	1.32	1.33
Prandtl U2 (ft)	0.91	0.90	0.91	0.90	0.90	0.91	0.90	0.91	0.91	0.92	0.91	0.90
Prandtl D1 (ft)	0.37	0.37	0.37	0.36	1.47	1.47	1.47	1.47	1.46	1.35	1.25	1.20
Prandtl D2 (ft)	1.46	1.46	1.46	1.46	0.39	0.39	0.39	0.39	0.41	0.53	0.64	0.70
Pt. Gauge A (cm)	36.12	35.97	36.29	36.16	35.75	36.26	35.55	35.86	43.67	51.17	full	full
Pt. Gauge B (cm)	37.35	37.35	37.35	37.35	37.30	37.30	37.30	37.30	53.30	full	full	full
Pt. Gauge C (cm)	38.46	38.37	38.37	38.36	38.33	38.30	38.27	38.30	full	full	full	full
Pt. Gauge D (cm)	75.54	75.46	75.46	75.52	75.55	81.22	86.27	90.53	95.01	97.83	N/A	N/A
Pt. Gauge E (cm)	77.95	77.95	77.92	81.15	83.63	85.65	88.10	91.82	95.10	97.84	N/A	N/A
Pt. Gauge F (cm)	70.12	76.15	78.30	81.64	84.00	86.50	89.93	93.21	96.00	98.59	N/A	N/A
Tailwater Depth (cm)	10.8	11.4	12.3	15.4	17.7	20.4	23.4	26.3	28.9	31.5	34	35.3
Piezo 1 (cm)	3.7	4.4	5.7	13.7	16	18.6	22.4	26	28.8	31.3	33.9	35.1
Piezo 2 (cm)	6.5	6.4	6.5	13.2	15.4	17.9	21.8	25.6	28.6	31.1	33.6	35
Piezo 3 (cm)												
Piezo 4 (cm)												
Piezo 5 (cm)	15.4	15.3	15.4	13.7	15.2	17	20	23.9	28	30.7	33.5	35
Piezo 6 (cm)	8.6	8.5	8.6	11.1	13.1	16.2	19.6	23.6	27.5	30.2	33	34.6
Piezo 7 (cm)	8.3	8.4	8.4	8.9	9.6	12.1	16.3	21.7	27.4	30.1	32.9	34.5
Piezo 8 (cm)	8.6	8.5	8.6	8.6	8.6	9	11.3	18.2	27.2	30	32.8	34.4
Piezo 9 (cm)	8.7	8.7	8.7	8.7	8.7	8.7	9.1	14	26.9	29.9	32.7	34.3
Piezo 10 (cm)	8.7	8.7	8.7	8.7	8.7	8.7	8.7	10.1	26.3	29.6	32.6	34.3
Piezo 11 (in)	5.5	5.5	5.5	5.5	5.5	5.5	5.5	5.6	12.2	13.7	15	15.7
Piezo 12 (in)	5.5	5.5	5.5	5.5	5.5	5.5	5.5	5.5	11.8	13.4	14.9	15.6
Piezo 13 (in)	5.3	5.4	5.3	5.3	5.3	5.3	5.3	5.3	11.1	13.1	14.7	15.5
Piezo 14 (in)	5.1	5.1	5.1	5.1	5.1	5.1	5.1	5.1	10	12.7	14.5	15.4
Piezo 15 (in)	5.7	5.7	5.7	5.7	5.7	5.7	5.7	5.7	9.2	12.3	14.2	15.3
Piezo 16 (in)	7.2	7.2	7.2	7.2	7.2	7.2	7.2	7.2	8.9	12	14.1	15.2
Piezo 17 (in)	7.5	7.5	7.5	7.5	7.5	7.5	7.5	7.5	7.6	10.4	12.8	14.2
Piezo 18 (in)	8.8	8.8	8.8	8.8	8.8	8.8	8.8	8.8	8.8	9.5	11.9	13.3
Piezo 19 (in)	10.3	10.3	10.3	10.3	10.3	10.3	10.3	10.3	10.3	10.4	11.2	12.4
Piezo 20 (in)	12.3	12.3	12.3	12.3	12.3	12.3	12.4	12.4	12.4	12.4	12.4	12.6
Piezo 21 (in)	15.2	15.1	15.1	15.1	15.1	15.1	15.1	15.2	15.1	15.1	15.1	15.1
Piezo 22 (in)	15.2	15.2	15.2	15.2	15.2	15.2	15.2	15.2	15.1	15.1	15.1	15.1
Jump Location (in)	0±2	0±2	0±2	0±2	0±2	4.5±2.5	9±3	19±4	59±2	69±2	74.5±1.5	78±2

Notes: I-4-4 downstream PT reading off. Drained. I-4-5 downstream PT has air bubbles. Drained.

Test: Full Weir Height 2/8D - Streamwise Position A   **Date:** 6/14/2022

Run	J-1-1	J-1-2	J-1-3	J-1-4	J-1-5	J-1-6	J-1-7	J-1-8	J-1-9	J-1-10	J-1-11	J-1-12
Time	10:01	10:14	10:24	10:34	10:45	10:56	11:08	11:20	11:30	11:40	11:50	12:01
V-notch gauge (cm)	78.40	78.40	78.40	78.42	78.40	78.39	78.41	78.39	78.41	78.43	78.40	78.40
	78.42	78.42	78.40	78.43	78.42	78.38	78.42	78.37	78.41	78.42	78.43	78.40
Temp (C)	21.9	22.0	22.1	22.1	22.2	22.3	22.3	22.4	22.4	22.5	22.6	22.7
Prandtl U1 (ft)	1.30	1.29	1.29	1.29	1.30	1.29	1.29	1.30	1.29	1.29	1.28	1.25
Prandtl U2 (ft)	0.80	0.80	0.80	0.80	0.79	0.81	0.81	0.79	0.80	0.80	0.81	0.85
Prandtl D1 (ft)	0.27	0.27	0.27	0.27	0.27	0.27	0.32	0.44	0.53	0.59	0.67	0.71
Prandtl D2 (ft)	1.29	1.29	1.29	1.29	1.29	1.29	1.24	1.12	0.99	0.97	0.90	0.87
Pt. Gauge A (cm)	34.08	34.16	34.22	34.13	33.95	34.19	42.87	48.89	52.36	full	full	full
Pt. Gauge B (cm)	35.04	35.04	34.91	34.91	34.91	34.93	49.25	53.12	full	full	full	full
Pt. Gauge C (cm)	34.16	34.16	34.26	34.24	34.31	34.37	50.38	53.22	full	full	full	full
Pt. Gauge D (cm)	77.96	77.95	77.95	78.31	82.90	86.12	89.36	92.03	94.72	97.13	99.60	N/A
Pt. Gauge E (cm)	81.15	81.11	80.50	80.85	82.61	85.59	88.75	91.70	94.41	97.00	99.35	N/A
Pt. Gauge F (cm)	69.29	76.04	78.84	81.40	83.85	86.64	89.24	92.13	94.74	97.27	99.80	N/A
Tailwater Depth (cm)	6.5	9.3	12	14.6	17.2	19.8	22.4	24.9	27.4	29.9	32.5	33.6
Piezo 1 (cm)	1.4	5.3	10.9	13.9	16.5	19.2	22	24.7	27.2	29.7	32.3	33.5
Piezo 2 (cm)	2.8	2.5	6.5	9.9	12.2	16	18.4	21	27.2	29.7	32.3	33.4
Piezo 3 (cm)												
Piezo 4 (cm)												
Piezo 5 (cm)	15.2	15.3	15.2	16.1	15.6	18.5	22.4	25	27.5	30	32.5	33.7
Piezo 6 (cm)	10.9	10.9	10.8	11.6	13.7	17.9	22.1	24.7	27.2	29.6	32.2	33.3
Piezo 7 (cm)	7.3	7.5	7.4	8.3	12.9	16.4	22.1	24.6	27.1	29.6	32.2	33.3
Piezo 8 (cm)	5.5	5.5	5.5	5.6	7.3	14.2	22.1	24.6	27.1	29.6	32.2	33.3
Piezo 9 (cm)	5.5	5.6	5.6	5.6	5.6	11.7	22	24.6	27.1	29.6	32.2	33.3
Piezo 10 (cm)	6.1	6.1	6.1	6.1	6.1	8.1	21.8	24.5	27.1	29.6	32.2	33.3
Piezo 11 (in)	4.4	4.4	4.4	4.4	4.4	4.6	10.7	11.8	12.8	13.9	14.9	15.3
Piezo 12 (in)	4.5	4.5	4.5	4.5	4.5	4.6	10.4	11.7	12.7	13.8	14.8	15.3
Piezo 13 (in)	4.3	4.3	4.3	4.3	4.3	4.3	9.8	11.4	12.5	13.7	14.7	15.3
Piezo 14 (in)	4	4	4	4	4.1	4.1	9.2	11.2	12.4	13.6	14.6	15.2
Piezo 15 (in)	4.1	4.1	4.1	4.1	4.1	4.1	8.7	10.7	12.3	13.5	14.6	15.2
Piezo 16 (in)	5.2	5.3	5.2	5.3	5.3	5.3	8.2	10.2	12.1	13.4	14.6	15.2
Piezo 17 (in)	6.1	6.1	6.1	6.1	6.1	6.1	7.1	9.7	11.3	12.8	14.3	14.9
Piezo 18 (in)	7.7	7.7	7.7	7.7	7.7	7.7	7.7	8.9	10.8	12.5	13.9	14.6
Piezo 19 (in)	9.3	9.3	9.3	9.3	9.3	9.3	9.3	9.3	10.1	11.8	13.5	14.3
Piezo 20 (in)	10.7	10.7	10.7	10.7	10.7	10.7	10.7	10.7	10.7	11.2	12.9	13.8
Piezo 21 (in)	12.8	12.9	12.9	12.8	12.8	12.9	12.9	12.9	12.9	12.8	13.1	13.4
Piezo 22 (in)	15.1	15.1	15.1	15.1	15.1	15.1	15.1	15.1	15.1	15.1	15.1	15.2
Jump Location (in)	2±1	2±2	2±1	3.5±1.5	7.5±2.5	16±4	64±2	70±2	75±1.5	80±1.5	84±1.5	85.5±1.5

Test: Full Weir Height 2/8D - Streamwise Position A   **Date:** 6/14/2022

Run	J-2-1	J-2-2	J-2-3	J-2-4	J-2-5	J-2-6	J-2-7	J-2-8	J-2-9	J-2-10	J-2-11	J-2-12
Time	12:40	12:53	13:01	13:11	13:20	13:33	13:41	13:51	13:59	14:08	14:17	14:24
V-notch gauge (cm)	75.93	75.89	75.90	75.93	75.86	75.90	75.87	75.86	75.83	75.85	75.90	75.87
	75.88	75.93	75.89	75.87	75.86	75.87	75.87	75.87	75.89	75.88	75.85	75.87
Temp (C)	22.8	22.8	22.9	23.0	23.0	23.1	23.1	23.2	23.2	23.3	23.3	23.4
Prandtl U1 (ft)	1.29	1.30	1.30	1.30	1.30	1.29	1.29	1.30	1.29	1.29	1.26	1.22
Prandtl U2 (ft)	0.80	0.79	0.80	0.79	0.80	0.80	0.80	0.79	0.79	0.80	0.84	0.87
Prandtl D1 (ft)	0.28	0.28	0.28	0.29	0.27	0.28	0.40	0.52	0.60	0.65	0.72	0.74
Prandtl D2 (ft)	1.29	1.29	1.29	1.28	1.29	1.29	1.16	1.04	0.97	0.92	0.86	0.84
Pt. Gauge A (cm)	32.60	32.63	32.63	32.63	32.68	38.30	45.41	49.43	full	full	full	full
Pt. Gauge B (cm)	34.48	34.50	34.50	34.49	34.51	45.86	49.67	52.72	full	full	full	full
Pt. Gauge C (cm)	33.00	33.11	33.10	33.12	33.12	47.35	49.87	53.20	full	full	full	full
Pt. Gauge D (cm)	79.27	79.12	79.15	80.05	82.87	86.47	89.05	91.57	94.25	96.70	99.35	N/A
Pt. Gauge E (cm)	79.77	79.81	79.17	79.55	82.24	85.90	88.67	91.35	93.91	96.61	98.95	N/A
Pt. Gauge F (cm)	69.19	75.90	78.74	81.20	83.70	86.60	89.22	91.81	94.24	96.84	99.32	N/A
Tailwater Depth (cm)	6.4	9.1	11.7	14.3	16.8	19.4	22	24.5	26.9	29.5	32	33.1
Piezo 1 (cm)	1.8	8.1	11.2	13.8	16.4	19.3	21.8	24.3	26.8	29.3	31.8	32.9
Piezo 2 (cm)	3.9	6	10.9	13.4	16.2	19.3	21.9	24.4	26.9	29.3	31.9	32.9
Piezo 3 (cm)												
Piezo 4 (cm)												
Piezo 5 (cm)	14.8	14.9	14.7	14.1	14.4	19.6	22.1	24.6	27	29.5	32	33.1
Piezo 6 (cm)	10.6	10.7	10.6	11.1	13.8	19.3	21.8	24.4	26.8	29.3	31.8	32.9
Piezo 7 (cm)	8.8	8.9	8.6	10.7	12.6	19.2	21.8	24.3	26.8	29.3	31.8	32.9
Piezo 8 (cm)	5.3	5.2	5.2	6.2	11.1	19.1	21.8	24.3	26.8	29.3	31.8	32.9
Piezo 9 (cm)	4.6	4.7	4.7	4.7	6	19	21.8	24.3	26.7	29.3	31.8	32.9
Piezo 10 (cm)	5.3	5.4	5.4	5.3	5.4	18.7	21.7	24.3	26.7	29.3	31.8	32.9
Piezo 11 (in)	4.2	4.2	4.2	4.2	4.2	9.3	10.6	11.7	12.7	13.7	14.7	15.2
Piezo 12 (in)	4.3	4.3	4.3	4.3	4.3	9	10.5	11.7	12.6	13.7	14.7	15.2
Piezo 13 (in)	4.2	4.2	4.2	4.2	4.2	8.4	10.1	11.5	12.5	13.6	14.7	15.1
Piezo 14 (in)	3.8	3.8	3.8	3.8	3.8	7.7	9.8	11.4	12.5	13.6	14.7	15.1
Piezo 15 (in)	4	4	4	4	4	6.7	9.4	11	12.4	13.5	14.6	15.1
Piezo 16 (in)	4.7	4.7	4.7	4.7	4.7	5.9	8.9	10.6	12.3	13.4	14.5	15.1
Piezo 17 (in)	5.8	5.8	5.8	5.8	5.8	5.9	8.3	10	11.6	12.9	14.3	15
Piezo 18 (in)	7.4	7.4	7.4	7.4	7.4	7.4	7.9	9.7	11.2	12.7	14.1	14.8
Piezo 19 (in)	9.1	9.1	9.1	9.1	9.1	9.1	9.1	9.3	10.7	12.3	13.8	14.5
Piezo 20 (in)	10.5	10.4	10.5	10.4	10.4	10.4	10.5	10.5	10.6	11.6	13.3	14.1
Piezo 21 (in)	12.4	12.4	12.4	12.3	12.4	12.4	12.4	12.3	12.4	12.4	12.8	13.5
Piezo 22 (in)	15	15	15	15	14.9	15	15	15	15	15	15	15
Jump Location (in)	4±2	4±2	4±2	5±2	14±4	60±2	68.5±1.5	74±1.5	78±1.5	82±1.5	85.5±1.5	87±1.5

Test: <u>Full Weir Height 2/8D - Streamwise Position A</u>　　　　　　　　　**Date:** <u>6/15/2022</u>

Run	J-3-1	J-3-2	J-3-3	J-3-4	J-3-5	J-3-6	J-3-7	J-3-8	J-3-9	J-3-10	J-3-11	J-3-12
Time	13:59	14:08	14:17	14:26	14:35	14:44	14:54	15:02	15:18	15:36	15:51	15:59
V-notch gauge (cm)	84.17	84.16	84.16	84.19	84.20	84.21	84.18	84.15	84.22	84.18	84.24	84.21
	84.14	84.19	84.18	84.17	84.20	84.20	84.18	84.16	84.20	84.16	84.21	84.23
Temp (C)	22.7	22.8	22.8	22.8	22.9	22.9	23.0	23.0	23.0	23.1	23.2	23.3
Prandtl U1 (ft)	1.32	1.34	1.34	1.34	1.33	1.33	1.33	1.33	1.33	1.33	1.34	1.34
Prandtl U2 (ft)	0.89	0.87	0.87	0.88	0.88	0.88	0.89	0.88	0.88	0.88	0.88	0.88
Prandtl D1 (ft)	1.41	1.41	1.41	1.41	1.41	1.41	1.41	1.41	1.31	1.22	1.14	1.09
Prandtl D2 (ft)	0.36	0.35	0.35	0.35	0.35	0.35	0.35	0.35	0.47	0.56	0.66	0.71
Pt. Gauge A (cm)	34.83	34.72	34.41	34.72	34.78	34.79	34.78	34.78	49.41	full	full	full
Pt. Gauge B (cm)	36.41	36.41	36.41	36.41	36.41	36.41	36.41	36.41	full	full	full	full
Pt. Gauge C (cm)	37.23	37.16	37.15	37.14	37.13	37.13	37.13	47.90	full	full	full	full
Pt. Gauge D (cm)	74.80	74.80	74.80	74.80	80.64	84.35	87.63	91.75	95.50	97.96	N/A	N/A
Pt. Gauge E (cm)	84.31	84.33	83.80	83.72	84.40	85.80	89.02	91.86	94.95	97.53	N/A	N/A
Pt. Gauge F (cm)	70.34	70.42	79.25	82.84	84.78	87.38	90.24	92.27	95.88	98.22	N/A	N/A
Tailwater Depth (cm)	6.6	9.4	12.2	14.9	17.7	20.5	23.3	25.4	28.5	31	33.5	34.7
Piezo 1 (cm)	4.2	4.2	10.1	13.5	16.8	20	22.8	25.2	28.4	31	33.5	34.7
Piezo 2 (cm)	7.7	7.4	7.8	10.6	14.4	17.4	19.6	18	28.2	30.7	33.2	34.5
Piezo 3 (cm)												
Piezo 4 (cm)												
Piezo 5 (cm)	15.7	15.7	15.9	15.8	17.5	20.7	22.1	24.7	28.5	31.1	33.9	35.2
Piezo 6 (cm)	12.4	12.4	12.1	12.5	14.1	17.1	20.4	24	27.7	30.3	32.9	34.3
Piezo 7 (cm)	8.5	8.5	8.4	8.4	9.7	13.8	18.7	22.9	27.6	30.2	32.9	34.3
Piezo 8 (cm)	7.5	7.6	7.4	7.5	7.6	8.9	14.4	20.8	27.5	30.2	32.9	34.3
Piezo 9 (cm)	7.7	7.7	7.7	7.7	7.8	7.8	10	17.8	27.4	30.1	32.9	34.3
Piezo 10 (cm)	7.8	7.8	7.8	7.8	7.8	7.8	8	14.8	27.2	29.9	32.8	34.2
Piezo 11 (in)	5.2	5.1	5.1	5.1	5.1	5.2	5.2	7	12.7	13.9	15.1	15.7
Piezo 12 (in)	5.2	5.2	5.2	5.2	5.2	5.2	5.2	5.7	12.5	13.8	15	15.6
Piezo 13 (in)	5	5	5	4.9	4.9	5	5	5	12.2	13.6	14.8	15.5
Piezo 14 (in)	4.7	4.7	4.7	4.7	4.7	4.7	4.7	4.7	11.7	13.4	14.7	15.4
Piezo 15 (in)	4.9	4.9	4.9	4.9	4.9	4.9	4.9	4.9	11.2	13.2	14.5	15.3
Piezo 16 (in)	6.6	6.6	6.6	6.6	6.6	6.6	6.6	6.6	10.8	12.9	14.4	15.3
Piezo 17 (in)	7.7	7.6	7.6	7.6	7.6	7.6	7.6	7.6	9.5	11.7	13.7	14.6
Piezo 18 (in)	8.4	8.4	8.4	8.4	8.4	8.4	8.4	8.4	8.9	10.9	12.9	13.9
Piezo 19 (in)	10	10	10	10	10	10	10	10	10	10.4	12.1	13.2
Piezo 20 (in)	11.8	11.8	11.8	11.8	11.8	11.7	11.7	11.7	11.7	11.7	12	12.7
Piezo 21 (in)	14.4	14.4	14.4	14.4	14.4	14.4	14.4	14.4	14.4	14.4	14.4	14.4
Piezo 22 (in)	15.2											
Jump Location (in)	0	0	0	0	4±2	8.5±3	15±3	28±5	67±2	73±2	78.5±2	82±2

Test: <u>Full Weir Height 2/8D - Streamwise Position A</u>　　　　　　　　**Date:** <u>6/15/2022</u>

Run	J-4-1	J-4-2	J-4-3	J-4-4	J-4-5	J-4-6	J-4-7	J-4-8	J-4-9	J-4-10	J-4-11	J-4-12
Time	13:21	13:34	13:45	13:55	14:07	14:17	14:29	14:43	15:00	15:09	15:25	15:31
V-notch gauge (cm)	86.66	86.64	86.64	86.61	86.67	86.71	86.69	86.66	86.72	86.67	86.67	86.64
	86.66	86.62	86.64	86.68	86.68	86.64	86.72	86.72	86.68	86.71	86.65	86.69
Temp (C)	22.8	22.8	22.8	22.9	22.9	23.0	23.0	23.1	23.2	23.2	23.3	23.3
Prandtl U1 (ft)	1.35	1.34	1.34	1.35	1.35	1.34	1.33	1.34	1.33	1.34	1.35	1.34
Prandtl U2 (ft)	0.92	0.93	0.93	0.92	0.92	0.93	0.93	0.93	0.94	0.93	0.92	0.93
Prandtl D1 (ft)	0.39	0.39	0.39	0.39	0.39	0.39	0.40	0.39	0.42	0.53	0.64	0.70
Prandtl D2 (ft)	1.47	1.47	1.47	1.47	1.47	1.47	1.46	1.47	1.43	1.33	1.22	1.17
Pt. Gauge A (cm)	35.71	35.89	35.70	35.89	36.03	36.28	35.88	35.95	46.02	51.74	full	full
Pt. Gauge B (cm)	37.01	37.03	37.06	37.07	37.07	37.08	37.07	37.07	53.17	full	full	full
Pt. Gauge C (cm)	37.77	37.77	37.81	37.81	37.81	37.81	37.81	43.66	full	full	full	full
Pt. Gauge D (cm)	75.68	75.71	75.71	75.70	75.70	82.97	87.25	91.23	95.50	98.20	N/A	N/A
Pt. Gauge E (cm)	84.62	84.61	84.62	84.69	84.85	86.31	88.58	92.33	95.40	97.65	N/A	N/A
Pt. Gauge F (cm)	71.20	77.84	80.18	83.60	86.07	88.08	91.00	93.40	96.33	98.76	N/A	N/A
Tailwater Depth (cm)	6.3	6.5	7.3	8.2	9.2	10.3	11.4	12.6	13.6	14.6	15.6	16
Piezo 1 (cm)	5.7	5.8	10.2	13.9	16.8	20.2	23	26	28.9	31.4	34	35.2
Piezo 2 (cm)	11.3	11.2	11.7	13.3	15.5	18.7	20.3	21.8	23.3	31.3	33.9	35.1
Piezo 3 (cm)												
Piezo 4 (cm)												
Piezo 5 (cm)	17.4	17.3	17.5	17.4	17.4	21.1	22.8	25.1	28.9	31.7	34.5	36
Piezo 6 (cm)	13	12.8	13	13.1	14.3	17	20.2	23.9	27.8	30.5	33.3	34.9
Piezo 7 (cm)	9.3	9.4	9.5	9.4	10.2	12.9	17	22.1	27.7	30.4	33.2	34.8
Piezo 8 (cm)	8.4	8.5	8.6	8.5	8.6	9.2	12.2	18.9	27.5	30.3	33.1	34.7
Piezo 9 (cm)	8.6	8.6	8.6	8.6	8.6	8.6	9.2	15.2	27.2	30.2	33.1	34.7
Piezo 10 (cm)	8.6	8.6	8.6	8.6	8.6	8.6	8.6	11	26.9	30	33	34.6
Piezo 11 (in)	5.5	5.5	5.5	5.5	5.5	5.5	5.5	5.6	12.5	13.9	15.1	15.8
Piezo 12 (in)	5.5	5.5	5.4	5.4	5.4	5.4	5.4	5.5	12.1	13.7	15	15.7
Piezo 13 (in)	5.3	5.3	5.3	5.3	5.3	5.3	5.3	5.3	11.5	13.3	14.8	15.6
Piezo 14 (in)	5	5.1	5.1	5.1	5.1	5.1	5.1	5.1	10.7	13	14.7	15.4
Piezo 15 (in)	5.3	5.3	5.3	5.3	5.4	5.3	5.3	5.3	9.7	12.5	14.6	15.3
Piezo 16 (in)	7.2	7.2	7.2	7.2	7.2	7.2	7.2	7.2	9.6	12.2	14.5	15.4
Piezo 17 (in)	7.5	7.4	7.4	7.4	7.4	7.4	7.4	7.4	8	10.7	13.2	14.5
Piezo 18 (in)	8.7	8.8	8.7	8.7	8.7	8.7	8.7	8.7	8.8	9.8	12.2	13.5
Piezo 19 (in)	10.3	10.3	10.3	10.3	10.3	10.3	10.3	10.3	10.3	10.4	11.5	12.6
Piezo 20 (in)	12.2	12.2	12.2	12.2	12.2	12.3	12.3	12.3	12.3	12.3	12.4	12.8
Piezo 21 (in)	15.1	15.1	15.1	15	15.1	15.1	15.1	15.1	15.1	15.1	15.1	15.1
Piezo 22 (in)	15.2	0	0	0	0	0	0	0	0	0	0	0
Jump Location (in)	0±2	0±2	0±2	0±2	1.5±1.5	6.5±2.5	11.5±3.5	22±5	60±2	70±2	75.5±1.5	79±1.5

Notes: 1 2 3 4 5　　22 is read once in the beginning then T is plugged into 22

Test: Full Weir Height 3/8D - Streamwise Position A   **Date:** 6/20/2022

Run	K-1-1	K-1-2	K-1-3	K-1-4	K-1-5	K-1-6	K-1-7	K-1-8	K-1-9	K-1-10	K-1-11	K-1-12
Time	11:57	12:27	12:37	12:47	12:57	13:07	13:24	13:34	13:43	13:52	14:01	14:10
V-notch gauge (cm)	78.40	78.35	78.35	78.37	78.40	78.35	78.34	78.35	78.37	78.36	78.34	78.34
	78.35	78.36	78.38	78.39	78.36	78.38	78.37	78.38	78.37	78.35	78.39	78.35
Temp (C)	21.9	22.1	22.1	22.2	22.3	22.3	22.5	22.5	22.6	22.7	22.7	22.8
Prandtl U1 (ft)	1.27	1.27	1.28	1.27	1.27	1.27	1.24	1.27	1.27	1.27	1.25	1.23
Prandtl U2 (ft)	0.78	0.78	0.78	0.78	0.78	0.78	0.81	0.79	0.78	0.78	0.80	0.82
Prandtl D1 (ft)	0.18	0.19	0.21	0.21	0.22	0.22	0.30	0.43	0.53	0.60	0.71	0.77
Prandtl D2 (ft)	1.20	1.21	1.23	1.23	1.24	1.24	1.19	1.08	0.98	0.99	0.93	0.92
Pt. Gauge A (cm)	34.25	33.97	34.07	34.05	34.05	34.05	44.21	49.92	51.88	full	full	full
Pt. Gauge B (cm)	34.80	34.80	34.80	34.80	34.80	34.80	49.89	53.42	full	full	full	full
Pt. Gauge C (cm)	34.30	34.29	34.29	34.30	34.29	44.12	50.90	53.34	full	full	full	full
Pt. Gauge D (cm)	83.62	83.61	83.64	83.64	84.21	86.83	89.71	92.50	94.75	96.98	99.82	N/A
Pt. Gauge E (cm)	83.70	83.70	83.50	83.45	83.85	86.51	89.15	91.79	94.29	96.60	99.45	N/A
Pt. Gauge F (cm)	70.01	76.10	78.96	81.90	84.45	87.01	89.44	92.26	94.65	96.84	99.80	N/A
Tailwater Depth (cm)	4.8	5.9	7	8	9	10	11	12	13	13.9	15	15.4
Piezo 1 (cm)	2.3	8.4	11.8	14.7	17	19.7	22.3	24.9	27.3	29.5	32.4	33.5
Piezo 2 (cm)	3.9	5.6	11.2	14.3	16.5	19.4	22	24.5	27	29.2	32.1	33.1
Piezo 3 (cm)												
Piezo 4 (cm)												
Piezo 5 (cm)	16.3	16.3	16.3	16.3	17.1	19.8	23	25.4	27.8	29.8	32.7	33.8
Piezo 6 (cm)	14.2	14.2	14.2	14.2	15.5	19.4	22.6	25	27.4	29.5	32.4	33.5
Piezo 7 (cm)	13.4	13.4	13.3	13.4	14.1	18.6	22.5	24.9	27.4	29.5	32.4	33.4
Piezo 8 (cm)	8.4	8.4	8.5	8.6	10.9	16.8	22.5	24.9	27.3	29.4	32.3	33.4
Piezo 9 (cm)	5.7	5.7	5.8	5.7	6.2	14.5	22.4	24.9	27.3	29.4	32.3	33.4
Piezo 10 (cm)	6.1	6.1	6.1	6.1	6.2	12.2	22.2	24.8	27.2	29.4	32.3	33.4
Piezo 11 (in)	4.4	4.4	4.4	4.4	4.4	6.1	10.8	11.9	12.9	13.8	14.9	15.3
Piezo 12 (in)	4.5	4.5	4.5	4.5	4.5	5.4	10.5	11.8	12.8	13.7	14.9	15.3
Piezo 13 (in)	4.3	4.3	4.3	4.3	4.3	4.4	10.1	11.5	12.7	13.6	14.8	15.3
Piezo 14 (in)	4	4.1	4.1	4	4.1	4.1	9.6	11.3	12.6	13.5	14.8	15.3
Piezo 15 (in)	4.1	4.1	4.1	4.1	4.1	4.1	9.1	11	12.4	13.4	14.7	15.2
Piezo 16 (in)	5.2	5.3	5.2	5.3	5.3	5.2	8.7	10.5	12.2	13.3	14.6	15.2
Piezo 17 (in)	6.1	6.2	6.2	6.2	6.2	6.2	7.5	9.8	11.4	12.7	14.3	14.9
Piezo 18 (in)	7.7	7.7	7.7	7.7	7.7	7.7	7.9	9.2	10.9	12.4	14	14.7
Piezo 19 (in)	9.3	9.3	9.3	9.3	9.3	9.3	9.3	9.4	10.2	11.7	13.6	14.3
Piezo 20 (in)	10.7	10.7	10.7	10.7	10.7	10.7	10.7	10.7	10.7	11.2	13	13.7
Piezo 21 (in)	12.9	12.9	12.9	12.9	12.9	12.9	12.8	12.8	12.8	12.8	13.1	13.4
Piezo 22 (in)	15.1											
Jump Location (in)	8.5±3.5	8.5±3.5	9±4	9±4	11±3	27±6	64±2	71±2	76±1.5	79.5±1.5	84.5±1.5	86±1.5

Notes: 1 2 4 5 manometer 22 is used for tailwater depth after first measurement.

Test: Full Weir Height 3/8D - Streamwise Position A   **Date:** 6/20/2022

Run	K-2-1	K-2-2	K-2-3	K-2-4	K-2-5	K-2-6	K-2-7	K-2-8	K-2-9	K-2-10	K-2-11	K-2-12
Time	14:42	14:56	15:08	15:19	15:30	15:42	15:55	16:04	16:15	16:25	16:33	16:41
V-notch gauge (cm)	75.91	75.94	75.90	75.90	75.92	75.87	75.90	75.86	75.88	75.93	75.90	75.91
	75.93	75.91	75.89	75.90	75.88	75.88	75.87	75.89	75.90	75.90	75.92	75.90
Temp (C)	22.9	23.0	23.0	23.1	23.2	23.3	23.4	23.4	23.5	23.5	23.6	23.6
Prandtl U1 (ft)	1.27	1.27	1.27	1.27	1.27	1.27	1.28	1.27	1.27	1.27	1.23	1.20
Prandtl U2 (ft)	0.77	0.78	0.78	0.78	0.78	0.78	0.77	0.77	0.78	0.78	0.81	0.85
Prandtl D1 (ft)	0.31	0.30	0.29	0.28	0.28	0.30	0.42	0.56	0.61	0.68	0.76	0.80
Prandtl D2 (ft)	1.33	1.32	1.31	1.30	1.29	1.25	1.14	1.00	0.97	0.93	0.89	0.89
Pt. Gauge A (cm)	32.63	32.63	32.63	32.63	32.63	40.43	45.10	50.05	full	full	full	full
Pt. Gauge B (cm)	34.50	34.55	34.55	34.55	34.56	47.38	50.04	52.92	full	full	full	full
Pt. Gauge C (cm)	33.32	33.30	33.26	33.28	33.28	48.02	50.17	52.62	full	full	full	full
Pt. Gauge D (cm)	82.61	82.65	82.65	82.66	83.95	87.16	89.38	92.17	94.60	96.92	99.51	N/A
Pt. Gauge E (cm)	81.70	81.69	81.70	81.70	83.18	86.30	88.62	91.58	94.07	96.60	99.14	N/A
Pt. Gauge F (cm)	69.80	75.79	78.74	81.32	84.25	86.63	89.22	91.80	94.35	96.91	99.42	N/A
Tailwater Depth (cm)	4.8	5.8	6.9	7.8	8.9	9.8	10.8	11.9	12.9	13.9	14.8	15.2
Piezo 1 (cm)	2	8.8	11.7	14.3	16.8	19.5	22	24.6	27.1	29.5	32	33.1
Piezo 2 (cm)	2.5	7.7	11.3	14	16.5	19.3	21.8	24.4	27	29.4	32	33
Piezo 3 (cm)												
Piezo 4 (cm)												
Piezo 5 (cm)	15.4	15.1	15.1	15.1	16.9	20.2	22.6	24.9	27.3	29.7	32.3	33.3
Piezo 6 (cm)	13.5	13.3	13.4	14	16.6	19.9	22.3	24.7	27.1	29.5	32	33
Piezo 7 (cm)	12.1	12.3	12	12.5	15.7	19.8	22.2	24.6	27.1	29.5	32	33
Piezo 8 (cm)	10	10.2	10.2	10.9	14.2	19.8	22.2	24.6	27.1	29.5	32	33
Piezo 9 (cm)	5.2	5.2	5.3	6.5	12.1	19.7	22.1	24.6	27.1	29.5	32	33
Piezo 10 (cm)	5.3	5.3	5.4	5.4	10.4	19.5	22	24.6	27	29.5	32	33
Piezo 11 (in)	4.2	4.2	4.2	4.2	4.9	9.8	10.8	11.9	12.8	13.8	14.8	15.2
Piezo 12 (in)	4.3	4.3	4.3	4.3	4.3	9.5	10.7	11.8	12.8	13.8	14.8	15.2
Piezo 13 (in)	4.2	4.2	4.2	4.2	4.2	9	10.5	11.6	12.7	13.7	14.7	15.2
Piezo 14 (in)	3.8	3.8	3.8	3.8	3.8	8.4	9.9	11.5	12.7	13.7	14.7	15.2
Piezo 15 (in)	4	4	4	4	4	7.7	9.5	11.2	12.5	13.6	14.7	15.2
Piezo 16 (in)	4.6	4.7	4.7	4.7	4.6	7.2	9.2	10.8	12.3	13.5	14.6	15.2
Piezo 17 (in)	5.9	5.9	5.9	5.9	5.9	6.3	8.6	10.3	11.7	13	14.4	15
Piezo 18 (in)	7.4	7.4	7.4	7.4	7.4	7.5	8.1	9.9	11.4	12.9	14.2	14.8
Piezo 19 (in)	9.1	9.1	9.1	9.1	9.1	9.1	9.1	9.5	10.9	12.4	13.9	14.5
Piezo 20 (in)	10.5	10.5	10.5	10.5	10.5	10.5	10.5	10.5	10.6	11.8	13.4	14.2
Piezo 21 (in)	12.4	12.4	12.4	12.4	12.4	12.4	12.3	12.4	12.3	12.4	13	13.6
Piezo 22 (in)	15											
Jump Location (in)	10±3	10.5±4.5	10.5±4.5	10.5±4.5	17±5	62±2	68.5±2	74±2	78±1.5	82.5±1.5	86±1.5	87.5±1.5

Test: Full Weir Height 3/8D - Streamwise Position A   **Date:** 7/20/2022

Run	K-3-1	K-3-2	K-3-3	K-3-4	K-3-5	K-3-6	K-3-7	K-3-8	K-3-9	K-3-10	K-3-11	K-3-12
Time	14:00	14:13	14:26	14:39	14:51	15:04	15:17	15:32	15:46	15:56	16:07	16:15
V-notch gauge (cm)	84.14	84.17	84.16	84.21	84.19	84.15	84.14	84.17	84.15	84.13	84.17	84.14
	84.14	84.16	84.18	84.14	84.16	84.18	84.16	84.11	84.14	84.13	84.18	84.16
Temp (C)	21.6	21.7	21.7	21.8	21.9	22.0	22.0	22.1	22.2	22.2	22.3	22.3
Prandtl U1 (ft)	1.33	1.33	1.33	1.32	1.32	1.32	1.33	1.33	1.33	1.32	1.32	1.32
Prandtl U2 (ft)	0.87	0.87	0.87	0.88	0.89	0.88	0.87	0.88	0.88	0.88	0.88	0.88
Prandtl D1 (ft)	1.31	1.31	1.31	1.31	1.31	1.31	1.31	1.38	1.29	1.22	1.14	1.09
Prandtl D2 (ft)	0.33	0.33	0.33	0.33	0.33	0.33	0.34	0.38	0.48	0.56	0.65	0.70
Pt. Gauge A (cm)	34.93	35.13	35.19	35.10	35.16	34.93	35.02	42.45	51.11	Full	Full	Full
Pt. Gauge B (cm)	36.23	36.22	36.20	36.20	36.20	36.20	36.23	52.17	Full	Full	Full	Full
Pt. Gauge C (cm)	36.85	36.85	36.85	36.85	36.85	36.85	36.93	52.83	Full	Full	Full	Full
Pt. Gauge D (cm)	84.51	84.52	84.52	84.52	85.38	87.09	89.50	93.08	95.95	98.24	N/A	N/A
Pt. Gauge E (cm)	86.70	86.58	86.49	86.50	86.80	88.28	89.81	92.60	95.21	97.90	N/A	N/A
Pt. Gauge F (cm)	70.94	71.20	79.83	83.15	85.52	87.60	90.36	93.20	95.74	98.23	N/A	N/A
Tailwater Depth (cm)	5	6.1	7.3	8.3	9.4	10.4	11.4	12.4	13.4	14.4	15.4	15.8
Piezo 1 (cm)	3.7	4.5	11.8	15.2	18	20.4	23.1	25.8	28.3	30.8	33.4	34.6
Piezo 2 (cm)	7.6	7.6	10.2	14.2	16.8	19.6	22.5	25.2	27.8	30.3	32.9	34.1
Piezo 3 (cm)												
Piezo 4 (cm)												
Piezo 5 (cm)	18.5	18.6	18.6	18.6	20	21.4	23.6	26.8	28.9	31.6	34	35.2
Piezo 6 (cm)	17.7	17.7	17.5	17.5	18.2	19.4	21.7	25.8	28.2	30.7	33.2	34.6
Piezo 7 (cm)	13.9	13.8	14.1	14.1	14.7	16.9	20.3	25.7	28.1	30.6	33.1	34.5
Piezo 8 (cm)	9.1	9	9.1	9.1	9.6	12.1	17.4	25.6	28	30.5	33.1	34.5
Piezo 9 (cm)	7.8	7.8	7.8	7.8	7.9	8.7	13.3	25.3	27.9	30.4	33	34.5
Piezo 10 (cm)	7.7	7.7	7.7	7.7	7.7	7.8	9.3	24.9	27.7	30.3	32.9	34.4
Piezo 11 (in)	5.1	5.1	5.1	5.1	5.1	5.1	5.2	11.6	12.9	14.1	15.2	15.7
Piezo 12 (in)	5.1	5.1	5.1	5.1	5.1	5.1	5.2	11.2	12.7	14	15.1	15.7
Piezo 13 (in)	4.9	4.9	4.9	4.9	4.9	4.9	4.9	10.5	12.3	13.7	15	15.6
Piezo 14 (in)	4.7	4.7	4.7	4.7	4.7	4.7	4.7	9.6	11.9	13.5	14.9	15.5
Piezo 15 (in)	4.9	4.9	4.9	4.9	4.9	4.9	4.9	8.6	11.4	13.3	14.7	15.4
Piezo 16 (in)	6.6	6.6	6.6	6.6	6.6	6.6	6.6	8.4	11.2	13.1	14.6	15.4
Piezo 17 (in)	7	7	7	7	7	7	7	7.3	9.9	11.9	13.8	14.8
Piezo 18 (in)	8.4	8.4	8.4	8.4	8.4	8.4	8.4	8.4	9.2	11	13.2	14
Piezo 19 (in)	10	9.9	10	9.9	9.9	10	10	9.9	10	10.5	12.3	13.3
Piezo 20 (in)	11.8	11.8	11.7	11.7	11.7	11.7	11.7	11.7	11.7	11.7	12.1	12.9
Piezo 21 (in)	14.3	14.4	14.4	14.3	14.3	14.3	14.3	14.4	14.3	14.3	14.4	14.4
Piezo 22 (in)	15.1											
Jump Location (in)	8±3	8.5±2.5	8.5±2.5	8.5±2.5	10±3	12±3	20±5	59±2	69±2	74±2	79±2	81.5±1.5

Test: Full Weir Height 3/8D - Streamwise Position A   **Date:** 7/25/2022

Run	K-4-1	K-4-2	K-4-3	K-4-4	K-4-5	K-4-6	K-4-7	K-4-8	K-4-9	K-4-10	K-4-11	K-4-12
Time	13:33	13:46	13:56	14:09	14:20	14:32	14:43	14:55	15:06	15:17	15:27	15:36
V-notch gauge (cm)	86.75	86.75	86.75	86.77	86.76	86.76	86.81	86.75	86.77	86.78	86.77	86.72
	86.74	86.76	86.74	86.80	86.77	86.78	86.79	86.79	86.80	86.86	86.78	86.83
Temp (C)	22.0	22.1	22.2	22.2	22.3	22.4	22.4	22.5	22.6	22.7	22.7	22.8
Prandtl U1 (ft)	1.30	1.31	1.31	1.30	1.30	1.30	1.30	1.30	1.30	1.30	1.31	1.30
Prandtl U2 (ft)	0.89	0.88	0.88	0.89	0.89	0.89	0.89	0.89	0.89	0.89	0.88	0.89
Prandtl D1 (ft)	1.46	1.46	1.46	1.46	1.46	1.46	1.46	1.46	1.44	1.39	1.31	1.22
Prandtl D2 (ft)	0.37	0.37	0.37	0.37	0.37	0.37	0.37	0.37	0.39	0.45	0.54	0.65
Pt. Gauge A (cm)	36.45	36.28	36.24	36.15	36.09	36.09	36.09	36.09	36.09	46.98	Full	Full
Pt. Gauge B (cm)	37.11	37.11	37.11	37.11	37.12	37.09	37.09	37.09	37.09	Full	Full	Full
Pt. Gauge C (cm)	37.64	37.67	37.68	37.68	37.84	37.85	37.87	37.85	44.92	Full	Full	Full
Pt. Gauge D (cm)	85.71	85.71	85.90	85.96	86.11	87.27	87.93	90.01	92.26	96.06	98.74	N/A
Pt. Gauge E (cm)	86.95	86.95	87.00	86.93	86.97	87.46	88.35	90.00	93.17	95.83	98.14	N/A
Pt. Gauge F (cm)	70.64	78.76	78.92	81.14	83.26	85.85	88.50	90.75	93.26	96.15	98.73	N/A
Tailwater Depth (cm)	6.9	7	6.9	7.6	8.5	9.6	10.6	11.6	12.6	13.7	14.6	15.6
Piezo 1 (cm)	5	6.7	6.7	12.2	15.3	18.4	20.9	23.6	26.1	28.8	31.3	34
Piezo 2 (cm)	8.6	8.5	8.6	10.8	14.5	17.6	20.3	23.1	25.8	28.4	30.9	33.6
Piezo 3 (cm)												
Piezo 4 (cm)												
Piezo 5 (cm)	19.1	19.6	19.6	19.5	19.5	19.6	21.5	24.2	26.5	29.5	32.2	34.8
Piezo 6 (cm)	18.8	18.8	18.8	18.8	18.9	19.5	20.8	22.4	24.9	28.5	31.1	33.9
Piezo 7 (cm)	14.1	14.1	14.5	14.3	14.4	15.2	17.1	20.5	23.6	28.4	30.9	33.7
Piezo 8 (cm)	9.7	9.8	10.1	9.8	10.1	10.8	12.5	16.7	21	28.2	30.8	33.6
Piezo 9 (cm)	8.7	8.7	8.7	8.7	8.7	8.8	9.5	12.3	18.3	28.1	30.6	33.5
Piezo 10 (cm)	8.8	8.8	8.8	8.8	8.8	8.8	8.9	9.5	14.7	27.7	30.3	33.4
Piezo 11 (in)	5.4	5.4	5.4	5.4	5.4	5.4	5.4	5.4	6.1	12.9	14	15.3
Piezo 12 (in)	5.4	5.4	5.4	5.4	5.4	5.4	5.4	5.4	5.5	12.5	13.9	15.2
Piezo 13 (in)	5.3	5.3	5.3	5.3	5.3	5.3	5.3	5.3	5.3	11.9	13.5	15.1
Piezo 14 (in)	5.1	5.1	5.1	5.1	5.1	5.1	5.1	5.1	5.1	11.3	13.2	15
Piezo 15 (in)	5.3	5.3	5.3	5.3	5.3	5.3	5.3	5.4	5.3	10.5	12.8	14.7
Piezo 16 (in)	7.2	7.2	7.2	7.1	7.2	7.2	7.2	7.2	7.2	10.2	12.5	14.7
Piezo 17 (in)	7.4	7.4	7.4	7.4	7.4	7.4	7.4	7.4	7.4	8.6	11.2	13.5
Piezo 18 (in)	8.8	8.8	8.8	8.8	8.8	8.8	8.8	8.8	8.8	8.9	10.2	12.6
Piezo 19 (in)	10.3	10.3	10.3	10.3	10.3	10.3	10.3	10.3	10.3	10.3	10.5	11.8
Piezo 20 (in)	12.3	12.3	12.3	12.3	12.3	12.3	12.3	12.3	12.3	12.3	12.3	12.4
Piezo 21 (in)	15.1	15.1	15.1	15.1	15.1	15.2	15.1	15.1	15.1	15.1	15.2	15.1
Piezo 22 (in)	15.2											
Jump Location (in)	9±4	9±4	9±3.5	9±4	9±4	10±4	12±3	16.5±5.5	25±6	62.5±2.5	70±2	76±2

Test: <u>Full Weir Height 4/8D - Streamwise Position A</u>　　　　　**Date:** <u>7/27/2022</u>

Run	L-1-1	L-1-2	L-1-3	L-1-4	L-1-5	L-1-6	L-1-7	L-1-8	L-1-9	L-1-10	L-1-11	L-1-12
Time	13:02	13:14	13:23	13:35	13:46	13:55	14:04	14:14	14:24	14:33	14:41	14:49
V-notch gauge (cm)	78.42	78.41	78.39	78.40	78.35	78.43	78.37	78.39	78.39	78.33	78.39	78.38
	78.40	78.38	78.36	78.35	78.39	78.37	78.38	78.42	78.33	78.39	78.43	78.40
Temp (C)	22.3	22.4	22.4	22.5	22.5	22.6	22.6	22.7	22.7	22.8	22.8	22.9
Prandtl U1 (ft)	1.26	1.26	1.26	1.27	1.26	1.26	1.26	1.26	1.26	1.27	1.25	1.21
Prandtl U2 (ft)	0.77	0.77	0.77	0.77	0.78	0.77	0.77	0.78	0.77	0.77	0.78	0.82
Prandtl D1 (ft)	0.27	0.27	0.27	0.27	0.27	0.30	0.38	0.48	0.55	0.60	0.69	0.72
Prandtl D2 (ft)	1.29	1.29	1.29	1.29	1.28	1.25	1.17	1.08	1.02	0.96	0.88	0.86
Pt. Gauge A (cm)	33.48	33.50	33.51	33.50	38.81	42.73	46.18	49.83	Full	Full	Full	Full
Pt. Gauge B (cm)	35.01	35.01	40.84	40.76	46.73	49.47	51.05	53.38	Full	Full	Full	Full
Pt. Gauge C (cm)	45.80	45.80	46.80	46.80	49.26	50.51	51.86	53.60	Full	Full	Full	Full
Pt. Gauge D (cm)	87.67	87.67	88.03	88.03	88.12	89.42	90.94	92.76	95.20	97.53	N/A	N/A
Pt. Gauge E (cm)	85.83	85.80	85.81	85.82	86.20	87.82	89.35	91.84	94.42	97.11	99.62	N/A
Pt. Gauge F (cm)	70.40	76.24	79.32	81.70	84.41	87.13	89.50	92.09	94.71	97.24	99.90	N/A
Tailwater Depth (cm)	4.8	5.9	7	8	9	10	11	12	13	13.9	15	15.4
Piezo 1 (cm)	2.2	5.4	11.5	14.1	17.1	19.7	22.2	24.7	27.2	29.7	32.4	33.5
Piezo 2 (cm)	2.5	2.6	10.4	13.4	17.1	19.1	21.8	24.5	27.1	29.6	32.2	33.4
Piezo 3 (cm)												
Piezo 4 (cm)												
Piezo 5 (cm)	20.1	20.5	20.5	20.5	21.5	22.2	23.8	25.9	28	30.3	32.8	33.8
Piezo 6 (cm)	20.1	20.2	20	20.4	21	21.9	23.6	25.6	27.8	30.1	32.7	33.7
Piezo 7 (cm)	19.7	19.8	19.7	20	20.8	21.8	23.5	25.5	27.8	30	32.6	33.7
Piezo 8 (cm)	18.7	19.1	18.8	19.6	20.8	21.8	23.5	25.5	27.7	30	32.6	33.7
Piezo 9 (cm)	17.1	17.6	17.6	18.3	20.4	21.7	23.5	25.5	27.7	30	32.6	33.7
Piezo 10 (cm)	14.6	15.6	15.1	16.3	20	21.6	23.5	25.4	27.6	29.9	32.5	33.6
Piezo 11 (in)	7.2	7.4	7.2	7.6	9.8	10.6	11.3	12.1	13.1	14	15	15.4
Piezo 12 (in)	6.8	6.8	6.8	7	9.3	10.4	11.2	12	13	14	15	15.4
Piezo 13 (in)	5	5.4	5.4	5.4	8.8	9.7	10.8	11.8	12.9	13.9	14.9	15.4
Piezo 14 (in)	4.1	4.2	4.2	4.1	7.9	9	10.2	11.6	12.8	13.8	14.9	15.4
Piezo 15 (in)	4.1	4.1	4.1	4.1	6.9	8.4	9.9	11.3	12.7	13.7	14.8	15.4
Piezo 16 (in)	5.2	5.2	5.2	5.2	6.5	7.8	9.4	11	12.5	13.6	14.8	15.4
Piezo 17 (in)	6.1	6.1	6.1	6.1	6.2	6.7	8.6	10.2	11.7	13.1	14.5	15.1
Piezo 18 (in)	7.7	7.7	7.7	7.7	7.7	7.8	8.3	9.6	11.1	12.8	14.1	14.9
Piezo 19 (in)	9.2	9.2	9.2	9.2	9.3	9.2	9.3	9.5	10.5	12.1	13.7	14.5
Piezo 20 (in)	10.7	10.7	10.7	10.7	10.7	10.7	10.7	10.7	10.8	11.6	13.2	13.9
Piezo 21 (in)	13.1	13.1	13.1	13.1	13.2	13.2	13.1	13.1	13.1	13.2	13.4	13.8
Piezo 22 (in)	15											
Jump Location (in)	35±5	35±5	37±5	39±4	57±2	63±2	68±2	72±2	76.5±2	80.5±2	84±2	86±1.5

Test: Full Weir Height 4/8D - Streamwise Position A   **Date:** 7/28/2022

Run	L-2-1	L-2-2	L-2-3	L-2-4	L-2-5	L-2-6	L-2-7	L-2-8	L-2-9	L-2-10	L-2-11	L-2-12
Time	14:47	15:01	15:10	15:18	15:28	15:41	15:51	16:01	16:10	16:18	16:27	16:33
V-notch gauge (cm)	84.15	84.18	84.16	84.16	84.17	84.19	84.16	84.15	84.15	84.12	84.14	84.17
	84.18	84.14	84.13	84.17	84.18	84.16	84.18	84.18	84.20	84.16	84.21	84.14
Temp (C)	22.5	22.5	22.6	22.6	22.7	22.7	22.8	22.8	22.9	22.9	22.9	23.0
Prandtl U1 (ft)	1.32	1.30	1.31	1.32	1.31	1.31	1.30	1.32	1.31	1.31	1.30	1.30
Prandtl U2 (ft)	0.85	0.86	0.86	0.85	0.86	0.86	0.86	0.85	0.86	0.85	0.86	0.86
Prandtl D1 (ft)	0.31	0.32	0.32	0.32	0.32	0.32	0.32	0.41	0.49	0.57	0.66	0.68
Prandtl D2 (ft)	1.37	1.36	1.37	1.37	1.37	1.37	1.36	1.28	1.20	1.13	1.05	1.03
Pt. Gauge A (cm)	35.00	35.00	35.00	35.00	35.00	35.00	41.34	48.55	Full	Full	Full	Full
Pt. Gauge B (cm)	36.47	36.47	36.47	36.47	36.47	36.47	50.63	Full	Full	Full	Full	Full
Pt. Gauge C (cm)	37.38	37.37	37.37	37.35	37.35	37.35	53.27	Full	Full	Full	Full	Full
Pt. Gauge D (cm)	89.30	88.84	88.85	88.85	89.51	91.13	92.93	95.03	97.11	99.36	N/A	N/A
Pt. Gauge E (cm)	89.00	88.86	88.80	88.75	89.31	90.02	91.30	93.59	96.10	98.56	N/A	N/A
Pt. Gauge F (cm)	70.96	70.90	79.65	82.80	86.45	88.79	91.30	93.60	92.26	98.87	N/A	N/A
Tailwater Depth (cm)	5	6.2	7.3	8.4	9.7	10.7	11.7	12.7	13.6	14.7	15.7	15.9
Piezo 1 (cm)	3.1	4	11.4	14.9	18.7	21.3	23.6	26.2	28.7	31.3	34	34.4
Piezo 2 (cm)	5.4	5	9.7	14.5	18.5	20.6	23.1	25.7	28.5	31.1	33.7	34.1
Piezo 3 (cm)												
Piezo 4 (cm)												
Piezo 5 (cm)	22.5	22.5	22.5	22.5	22.6	23.6	25.9	28.1	30	32.2	34.6	35.1
Piezo 6 (cm)	21.5	21.2	21.3	21.3	22.1	22.5	25.6	27.5	29.6	32	34.5	35.1
Piezo 7 (cm)	19.8	19.6	19.6	19.6	20.3	20.9	25.4	27.3	29.4	31.7	34.2	34.7
Piezo 8 (cm)	16.9	16.3	16.5	16.6	17	18.5	25.2	27.2	29.4	31.6	34.2	34.7
Piezo 9 (cm)	12.8	12.3	12.2	12.5	13.5	15.2	24.9	27	29.3	31.6	34.2	34.7
Piezo 10 (cm)	9.1	8.8	8.8	8.9	9.9	11.5	24.2	26.7	29.2	31.5	34.1	34.6
Piezo 11 (in)	5.2	5.2	5.2	5.2	5.3	5.5	11.4	12.6	13.6	14.5	15.6	15.8
Piezo 12 (in)	5.1	5.1	5.1	5.1	5.2	5.3	11	12.3	13.5	14.5	15.5	15.8
Piezo 13 (in)	5	5	5	5	5	5	10.2	11.9	13.2	14.3	15.4	15.7
Piezo 14 (in)	4.7	4.7	4.7	4.7	4.7	4.7	9.3	11.4	13	14.1	15.3	15.6
Piezo 15 (in)	4.8	4.8	4.8	4.8	4.9	4.8	8.4	10.8	12.6	13.9	15.2	15.5
Piezo 16 (in)	6.6	6.6	6.6	6.6	6.6	6.6	8.1	10.5	12.4	13.8	15.2	15.5
Piezo 17 (in)	7	7	7	7	7	7	7.2	9.1	11.1	12.9	14.5	14.8
Piezo 18 (in)	8.4	8.4	8.4	8.4	8.4	8.4	8.4	8.8	10.2	12	13.8	14.2
Piezo 19 (in)	9.9	9.9	9.9	9.9	9.9	9.9	9.9	9.9	10.2	11.1	13.1	13.5
Piezo 20 (in)	11.8	11.8	11.8	11.8	11.8	11.8	11.7	11.7	11.7	11.8	12.6	12.9
Piezo 21 (in)	14.3	14.3	14.3	14.4	14.4	14.3	14.3	14.3	14.4	14.4	14.4	14.4
Piezo 22 (in)	15.2											
Jump Location (in)	17±4	17.5±4.5	17±4	17.5±4.5	18±5	22±6	57.5±2.5	66±2	72±2	76±2	81±2	82±2

Test: Full Weir Height 4/8D - Streamwise Position A   **Date:** 7/30/2022

Run	L-3-1	L-3-2	L-3-3	L-3-4	L-3-5	L-3-6	L-3-7	L-3-8	L-3-9	L-3-10	L-3-11	L-3-12
Time	9:20	9:31	9:41	9:51	9:59	10:08	10:19	10:38	10:48	10:56	11:04	11:10
V-notch gauge (cm)	86.70	86.66	86.66	86.68	86.70	86.70	86.69	86.74	86.79	86.71	86.73	86.64
	86.67	86.69	86.67	86.67	86.72	86.69	86.73	86.74	86.73	86.78	86.69	86.66
Temp (C)	22.4	22.4	22.5	22.5	22.5	22.6	22.7	22.7	22.8	22.8	22.9	22.9
Prandtl U1 (ft)	1.32	1.32	1.34	1.32	1.32	1.33	1.33	1.33	1.32	1.32	1.32	1.33
Prandtl U2 (ft)	0.88	0.92	0.91	0.92	0.92	0.91	0.92	0.91	0.92	0.92	0.92	0.92
Prandtl D1 (ft)	1.47	1.47	1.47	1.47	1.47	1.47	1.47	1.43	1.37	1.28	1.20	1.17
Prandtl D2 (ft)	0.39	0.39	0.39	0.39	0.39	0.39	0.39	0.42	0.48	0.58	0.68	0.72
Pt. Gauge A (cm)	35.89	35.79	35.79	35.79	35.79	35.79	35.79	43.36	51.20	Full	Full	Full
Pt. Gauge B (cm)	37.00	37.00	37.01	37.01	37.02	37.02	37.02	53.06	Full	Full	Full	Full
Pt. Gauge C (cm)	38.17	38.17	38.17	38.17	38.17	38.17	44.38	Full	Full	Full	Full	Full
Pt. Gauge D (cm)	90.40	90.35	90.35	90.35	90.35	90.90	92.23	94.85	96.91	99.10	N/A	N/A
Pt. Gauge E (cm)	90.12	90.10	90.05	90.05	90.10	90.60	91.51	93.70	96.12	98.20	N/A	N/A
Pt. Gauge F (cm)	71.68	78.30	80.22	83.01	85.92	88.50	90.74	93.25	95.55	98.53	N/A	N/A
Tailwater Depth (cm)	6.4	6.8	7.5	8.4	9.5	10.5	11.5	12.6	13.6	14.6	15.6	16
Piezo 1 (cm)	4.6	5.7	11.5	14.8	18.1	21	23.4	25.8	28.5	31	33.6	34.8
Piezo 2 (cm)	7.7	7.5	9.2	14.1	17.6	20.4	22.3	24.9	27.6	30.3	32.9	33.8
Piezo 3 (cm)												
Piezo 4 (cm)												
Piezo 5 (cm)	22.7	21.5	21.5	21.5	22	23.8	24.8	28.3	29.8	32.3	34.7	35.7
Piezo 6 (cm)	22.7	23.1	22.8	23	22.8	23.9	24.5	27.5	29.6	31.9	34.4	35.5
Piezo 7 (cm)	21	21	20.8	20.8	21	21.9	23	27.2	29.2	31.5	34	35.1
Piezo 8 (cm)	17.3	17.4	17.2	17.2	17.4	19	20.2	26.9	29	31.4	33.9	35
Piezo 9 (cm)	13	13.3	13.1	13.2	13.1	15.6	16.6	26.5	28.9	31.3	33.8	34.9
Piezo 10 (cm)	9.5	9.7	9.5	9.6	9.7	11.5	12.4	26	28.6	31.2	33.7	34.8
Piezo 11 (in)	5.5	5.5	5.5	5.5	5.5	5.6	5.8	12.1	13.4	14.4	15.4	15.9
Piezo 12 (in)	5.4	5.4	5.4	5.4	5.4	5.5	5.5	11.6	13.1	14.3	15.3	15.8
Piezo 13 (in)	5.3	5.3	5.3	5.3	5.3	5.4	5.3	10.6	12.4	14	15.2	15.7
Piezo 14 (in)	5	5.1	5.1	5.1	5.1	5.2	5.1	9.5	11.8	13.6	15.1	15.6
Piezo 15 (in)	5.3	5.3	5.3	5.3	5.4	5.3	5.4	8.2	11.2	13.3	14.9	15.5
Piezo 16 (in)	7.2	7.2	7.2	7.2	7.2	7.2	7.2	8.2	11.1	13.2	14.8	15.6
Piezo 17 (in)	7.4	7.4	7.4	7.4	7.5	7.4	7.5	7.5	9.6	11.7	13.6	14.7
Piezo 18 (in)	8.8	8.8	8.8	8.8	8.8	8.8	8.8	8.8	9.2	10.8	12.8	13.8
Piezo 19 (in)	10.3	10.3	10.3	10.3	10.3	10.3	10.3	10.3	10.3	10.6	12.1	12.9
Piezo 20 (in)	12.3	12.3	12.3	12.3	12.3	12.3	12.3	12.3	12.3	12.3	12.5	12.9
Piezo 21 (in)	15.1	15.1	15.1	15.2	15.2	15.1	15.1	15.1	15.1	15.1	15.1	15.2
Piezo 22 (in)	15.1											
Jump Location (in)	17.5±4.5	18±5	16.5±4.5	17.5±4.5	18.5±4.5	19±5	23.5±5.5	58.5±2.5	66.5±2.5	72±2	77±2	79±2

Test: <u>Full Weir Height 4/8D - Streamwise Position A</u> **Date:** <u>8/2/2022</u>

Run	L-4-1	L-4-2	L-4-3	L-4-4	L-4-5	L-4-6	L-4-7	L-4-8	L-4-9	L-4-10	L-4-11	L-4-12
Time	13:54	14:04	14:14	14:22	14:31	14:39	14:51	14:59	15:09	15:16	15:26	15:35
V-notch gauge (cm)	75.95	75.92	75.85	75.85	75.94	75.84	75.87	75.94	75.88	75.88	75.84	75.84
	75.89	75.84	75.84	75.91	75.93	75.88	75.94	75.93	75.88	75.88	75.82	75.87
Temp (C)	22.4	22.4	22.5	22.5	22.6	22.6	22.7	22.7	22.8	22.8	22.9	22.9
Prandtl U1 (ft)	1.26	1.27	1.27	1.26	1.26	1.26	1.26	1.26	1.26	1.26	1.21	1.18
Prandtl U2 (ft)	0.76	0.76	0.76	0.77	0.76	0.76	0.77	0.76	0.76	0.76	0.82	0.85
Prandtl D1 (ft)	1.23	1.24	1.24	1.23	1.22	1.17	1.06	0.97	0.94	0.89	0.84	0.83
Prandtl D2 (ft)	0.28	0.28	0.28	0.28	0.29	0.35	0.46	0.56	0.60	0.66	0.73	0.75
Pt. Gauge A (cm)	40.33	40.38	40.40	40.46	40.90	43.84	47.47	50.78	full	full	full	full
Pt. Gauge B (cm)	48.15	47.91	47.91	47.91	48.05	48.78	51.28	53.70	full	full	full	full
Pt. Gauge C (cm)	48.65	48.65	48.60	48.60	48.60	49.68	51.48	full	full	full	full	full
Pt. Gauge D (cm)	87.25	87.25	87.25	87.24	87.32	88.51	90.26	92.48	94.62	97.12	99.70	N/A
Pt. Gauge E (cm)	84.90	84.90	84.90	84.90	85.01	86.42	89.14	91.61	94.10	96.63	99.32	N/A
Pt. Gauge F (cm)	70.73	76.06	78.72	81.23	84.10	86.52	89.25	91.80	94.35	96.89	99.52	N/A
Tailwater Depth (cm)	4.7	5.8	6.9	7.9	8.9	9.9	10.8	11.8	12.8	13.8	14.8	15.2
Piezo 1 (cm)	2.3	7.7	11.4	13.9	16.9	19.3	21.9	24.4	27	29.6	32	33
Piezo 2 (cm)	2.3	3.5	10.6	13.3	16.8	18.9	21.7	24.3	26.8	29.5	32	32.9
Piezo 3 (cm)												
Piezo 4 (cm)												
Piezo 5 (cm)	20.2	20.3	20.3	20.2	20.6	21.5	23.3	25.3	27.5	30	32.4	33.3
Piezo 6 (cm)	20	20	20	20.1	20.3	21.3	23.1	25.2	27.4	29.8	32.3	33.2
Piezo 7 (cm)	19.9	19.9	19.9	20	20.2	21.2	23	25.1	27.3	29.8	32.2	33.2
Piezo 8 (cm)	19.8	19.8	19.8	19.9	20.2	21.2	23	25.1	27.3	29.8	32.2	33.2
Piezo 9 (cm)	19.7	19.7	19.7	19.8	20.1	21.1	23	25.1	27.3	29.8	32.2	33.2
Piezo 10 (cm)	19.6	19.6	19.6	19.7	20	20.9	22.9	25	27.3	29.7	32.2	33.2
Piezo 11 (in)	9.8	9.8	9.8	9.8	9.9	10.3	11.2	12	12.9	13.9	14.9	15.2
Piezo 12 (in)	9.5	9.5	9.5	9.6	9.6	10.2	11.1	12	12.9	13.9	14.9	15.2
Piezo 13 (in)	8.9	9	9	9.1	9.1	9.8	10.8	11.9	12.8	13.8	14.8	15.2
Piezo 14 (in)	8.4	8.4	8.4	8.4	8.6	9.4	10.5	11.7	12.7	13.7	14.8	15.2
Piezo 15 (in)	7.7	7.8	7.8	7.8	8	9	10.2	11.5	12.6	13.6	14.8	15.2
Piezo 16 (in)	7.1	7.2	7.2	7.3	7.6	8.6	9.7	11.2	12.5	13.4	14.8	15.2
Piezo 17 (in)	6.2	6.3	6.3	6.3	6.6	7.7	9.3	10.5	11.9	13.1	14.6	15
Piezo 18 (in)	7.4	7.4	7.4	7.5	7.5	7.7	8.6	10.2	11.5	12.9	14.3	14.8
Piezo 19 (in)	9	9	9	9	9	9	9.1	9.7	11	12.5	14.1	14.6
Piezo 20 (in)	10.4	10.4	10.4	10.4	10.4	10.4	10.4	10.4	10.6	11.9	13.6	14.2
Piezo 21 (in)	12.4	12.4	12.4	12.4	12.4	12.4	12.4	12.4	12.4	12.4	13.1	13.5
Piezo 22 (in)	15.1											
Jump Location (in)	62±2.5	62.5±2.5	62±2.5	62±2.5	62.5±2.5	66±2	70.5±2.5	75±2	78.5±2	83±2	86±2	87.5±1.5

Appendix H Data – Uncontrolled Outlet – No Weirs
Eight Discharges

Run	ZA-X-1	ZA-X-2	ZA-X-3	ZA-X-4	ZA-X-5	ZA-X-6	ZA-X-7	ZA-X-8
Time	13:08	13:34	13:53	14:17	14:46	15:15	15:37	16:11
V-notch gauge (cm)	90.98	89.67	87.28	84.75	82.47	80.50	78.54	76.16
Temp (C)	20.5	20.7	20.7	20.8	20.9	21.0	21.1	21.3
Prandtl U1 (ft)	0.78	0.79	0.77	0.76	0.74	0.73	0.73	0.72
Prandtl U2 (ft)	1.15	1.14	1.16	1.18	1.19	1.20	1.21	1.21
Prandtl D1 (ft)	0.44	0.45	0.52	0.47	0.47	0.47	0.47	0.46
Prandtl D2 (ft)	1.58	1.57	1.49	1.53	1.51	1.50	1.49	1.48
Pt. Gauge A (cm)	37.63	37.55	36.41	35.70	34.55	34.12	33.73	32.90
Pt. Gauge B (cm)	38.83	38.35	37.50	36.50	35.93	35.30	34.86	34.46
Pt. Gauge C (cm)	39.06	38.75	38.02	37.02	36.03	35.27	34.20	33.33
Pt. Gauge D (cm)	77.02	76.46	75.71	74.43	73.75	73.51	73.58	73.57
Pt. Gauge E (cm)	74.27	74.03	73.63	73.40	73.13	72.65	71.62	70.72
Pt. Gauge F (cm)	77.01	70.31	69.92	69.56	69.21	69.00	68.90	68.65
Tailwater Depth (in)	7.4	5.7	3.7	2	0.9	0	N/A	N/A
Piezo 1 (cm)	4.6	2.5	2	1.6	1.3	1	0.8	0.7
Piezo 2 (cm)	4.5	4.3	4.2	3.6	3	2.5	2.2	1.8
Piezo 3 (cm)								
Piezo 4 (cm)								
Piezo 5 (cm)	8.2	7.6	6.9	6.2	5.5	5.1	4.7	4.5
Piezo 6 (cm)	8.7	8.5	7.8	7.4	7.1	6.8	6.4	5.9
Piezo 7 (cm)	8.4	8.2	7.5	6.9	6.2	5.9	5.6	5.3
Piezo 8 (cm)	9.8	9.5	8.6	7.7	6.7	6	5.4	5
Piezo 9 (cm)	9.8	9.4	8.7	7.9	7	6.2	5.4	4.6
Piezo 10 (cm)	9.8	9.3	8.7	7.9	7.2	6.6	6	5.3
Piezo 11 (in)	6	5.8	5.6	5.3	5	4.7	4.5	4.2
Piezo 12 (in)	6.1	5.9	5.6	5.3	5.1	4.9	4.7	4.4
Piezo 13 (in)	6	5.8	5.5	5.1	4.8	4.6	4.4	4.2
Piezo 14 (in)	5.8	5.7	5.3	5	4.7	4.5	4.2	4
Piezo 15 (in)	6.1	5.9	5.5	5	4.6	4.4	4.2	4
Piezo 16 (in)	8.3	8	7.5	6.9	6.3	5.9	5.4	4.8
Piezo 17 (in)	8.4	8.1	7.7	7.3	6.9	6.6	6.3	6
Piezo 18 (in)	9.4	9.2	8.9	8.6	8.3	8	7.8	7.5
Piezo 19 (in)	11.1	10.8	10.4	10.1	9.7	9.5	9.3	9.1
Piezo 20 (in)	13.3	13	12.5	11.9	11.5	11.2	10.8	10.5
Piezo 21 (in)	16.5	16.1	15.5	14.5	13.9	13.2	12.8	12.5
Piezo 22 (in)	14.9	15.1	15.2	15.1	15.1	15.1	15.1	14.9
Jump Location (in)								

Notes: TW is measured using manometer 22

Appendix I Data – Uncontrolled Outlet – Staggered Weirs

Eight Discharges for Each Weir Height

Test: <u>Weir Height 1/8D - Streamwise Position A</u> **Date:** <u>9/30/2022</u>

Run	YB-X-1	YB-X-2	YB-X-3	YB-X-4	YB-X-5	YB-X-6	YB-X-7	YB-X-8
Time	13:39	14:10	14:27	14:47	15:07	15:24	15:44	16:07
V-notch gauge (cm)	91.84	89.92	87.26	84.77	82.66	80.43	78.60	76.34
Temp (C)	20.6	20.7	20.7	20.7	20.7	20.8	20.8	20.9
Prandtl U1 (ft)	1.35	1.35	1.36	1.38	1.39	1.39	1.40	1.41
Prandtl U2 (ft)	1.00	0.99	0.98	0.96	0.95	0.94	0.93	0.92
Prandtl D1 (ft)	1.63	1.61	1.58	1.57	1.55	1.35	1.37	1.32
Prandtl D2 (ft)	0.45	0.47	0.49	0.51	0.51	0.70	0.66	0.69
Pt. Gauge A (cm)	37.85	37.31	36.57	35.48	34.88	33.89	33.96	33.09
Pt. Gauge B (cm)	38.94	38.36	37.25	36.61	35.97	35.46	34.64	34.55
Pt. Gauge C (cm)	39.55	38.80	37.95	37.31	36.13	35.21	34.35	33.41
Pt. Gauge D (cm)	77.42	76.55	75.63	74.75	74.13	73.81	73.72	73.51
Pt. Gauge E (cm)	78.05	77.93	77.52	77.02	76.42	76.35	74.99	75.51
Pt. Gauge F (cm)	81.81	71.03	69.98	69.50	69.56	69.53	69.40	68.95
Tailwater Depth (in)	8.5	5.8	3.8	1.9	0.7	0		
Piezo 1 (cm)	11.1	3.6	2.7	2.3	1.8	1.4	1.3	1.1
Piezo 2 (cm)	7.8	7.3	7.2	6.9	6.6	7.3	6.9	6.2
Piezo 3 (cm)								
Piezo 4 (cm)								
Piezo 5 (cm)	18.2	17.1	15.5	14.5	13.3	12.5	11.7	10.2
Piezo 6 (cm)	9.6	9.1	8.5	7.9	7.5	7.2	6.9	6.4
Piezo 7 (cm)	10	9.3	8.4	7.6	7	6.5	6.2	5.8
Piezo 8 (cm)	10.2	9.5	8.6	7.7	6.8	6.1	5.5	5.1
Piezo 9 (cm)	10.1	9.4	8.6	7.8	7	6.2	5.5	4.7
Piezo 10 (cm)	10.1	9.4	8.6	7.8	7.1	6.5	6	5.4
Piezo 11 (in)	6.1	5.9	5.6	5.3	5	4.7	4.5	4.3
Piezo 12 (in)	6.1	6	5.8	5.6	5.1	4.9	4.7	4.4
Piezo 13 (in)	6	5.8	5.5	5.1	4.8	4.6	4.4	4.2
Piezo 14 (in)	5.8	5.5	5.2	4.8	4.6	4.3	4.2	3.9
Piezo 15 (in)	6.3	5.9	5.5	5	4.7	4.4	4.1	4
Piezo 16 (in)	8.4	7.9	7.3	6.8	6.4	5.8	5.4	4.8
Piezo 17 (in)	8.4	8.1	7.6	7.2	6.8	6.5	6.2	6
Piezo 18 (in)	9.5	9.3	8.9	8.6	8.3	8	7.8	7.5
Piezo 19 (in)	11.3	10.9	10.5	10.1	9.8	9.5	9.3	9.1
Piezo 20 (in)	13.6	13.1	12.6	11.9	11.5	11.2	10.9	10.6
Piezo 21 (in)	16.5	15.9	15.3	14.6	14	13.4	13	12.5
Piezo 22 (in)	14.8	15	15	15.1	15.1	15.1	15	15
Jump Location (in)								

Notes: TW is measured using manometer 22

Test: Weir Height 2/8D - Streamwise Position A   **Date:** 10/27/2022

Run	YC-X-1	YC-X-2	YC-X-3	YC-X-4	YC-X-5	YC-X-6	YC-X-7	YC-X-8
Time	12:07	12:31	14:56	13:11	13:38	13:57	14:18	14:40
V-notch gauge (cm)	92.02	89.80	86.90	85.06	83.00	80.61	78.41	76.48
Temp (C)	20.5	20.6	21.8	20.6	20.7	20.7	20.7	20.8
Prandtl U1 (ft)	1.14	1.15	0.94	1.17	1.19	1.20	1.21	1.20
Prandtl U2 (ft)	0.80	0.79	1.33	0.76	0.74	0.73	0.72	0.72
Prandtl D1 (ft)	0.32	0.33	0.39	0.36	0.37	0.44	0.38	0.38
Prandtl D2 (ft)	1.48	1.47	1.48	1.43	1.42	1.34	1.39	1.39
Pt. Gauge A (cm)	38.05	37.35	36.21	35.74	34.93	34.23	33.84	32.85
Pt. Gauge B (cm)	39.13	38.28	37.14	36.45	36.07	35.43	34.58	34.54
Pt. Gauge C (cm)	39.60	38.75	37.55	37.34	36.44	35.26	34.38	33.30
Pt. Gauge D (cm)	78.03	77.15	75.44	75.11	74.55	74.00	73.14	78.31
Pt. Gauge E (cm)	84.35	84.30	83.97	83.95	83.22	81.37	80.88	79.91
Pt. Gauge F (cm)	83.72	71.43	70.45	69.65	69.71	69.70	69.26	68.90
Tailwater Depth (in)	8.8	5.6	3.3	1.7	0.6			
Piezo 1 (cm)	14.5	5.9	4.3	3.9	2.6	1.7	1.3	1.2
Piezo 2 (cm)	13.1	11.5	9.8	10.4	8.4	7.5	6.3	4.8
Piezo 3 (cm)								
Piezo 4 (cm)								
Piezo 5 (cm)	22.2	19.7	18.1	16	15.4	14.6	15.5	15.3
Piezo 6 (cm)	14.6	13.8	13.1	12.6	12.1	11.6	11.2	10.8
Piezo 7 (cm)	11.7	10.6	9.5	8.7	8.1	7.8	7.9	8.5
Piezo 8 (cm)	10.5	9.6	8.5	7.7	7	6.1	5.4	5.2
Piezo 9 (cm)	10.2	9.4	8.3	7.9	7.2	6.3	5.3	4.7
Piezo 10 (cm)	10.1	9.4	8.4	7.9	7.3	6.6	6	5.4
Piezo 11 (in)	6.1	5.9	5.5	5.3	5	4.7	4.5	4.3
Piezo 12 (in)	6.2	5.9	5.6	5.4	5.1	4.9	4.6	4.4
Piezo 13 (in)	6.1	5.8	5.4	5.2	4.9	4.6	4.4	4.2
Piezo 14 (in)	5.9	5.6	5.2	4.9	4.6	4.4	4.1	3.9
Piezo 15 (in)	6.3	5.9	5.5	5.1	4.7	4.4	4.1	4
Piezo 16 (in)	8.4	7.9	7.2	6.9	6.4	5.9	5.3	4.8
Piezo 17 (in)	8.5	8	7.9	7.2	6.9	6.6	6.2	6
Piezo 18 (in)	9.6	9.2	8.8	8.6	8.3	8	7.8	7.5
Piezo 19 (in)	11.3	10.9	10.4	10.1	9.9	9.6	9.3	9.1
Piezo 20 (in)	13.7	13.1	12.2	12	11.5	11.1	10.8	10.6
Piezo 21 (in)	16.6	15.9	15.2	14.7	14.1	13.5	12.9	12.6
Piezo 22 (in)	14.8	15.1	15.1	15.1	15.1	15.1	15	15.1
Jump Location (in)								3±2

Notes: TW is measured using manometer 22

155

Test: Weir Height 3/8D - Streamwise Position A   **Date:** 10/31/2022

Run	YD-X-1	YD-X-2	YD-X-3	YD-X-4	YD-X-5	YD-X-6	YD-X-7	YD-X-8
Time	13:30	13:50	14:10	14:30	14:48	15:06	15:29	15:52
V-notch gauge (cm)	91.00	89.51	87.03	84.71	82.70	80.30	78.50	76.19
Temp (C)	20.6	20.7	20.8	20.8	20.9	20.9	21.0	21.1
Prandtl U1 (ft)	1.36	1.35	1.36	1.39	1.39	1.40	1.40	1.41
Prandtl U2 (ft)	0.98	0.99	0.98	0.95	0.95	0.93	0.93	0.92
Prandtl D1 (ft)	1.59	1.58	1.56	1.54	1.53	1.52	1.50	1.49
Prandtl D2 (ft)	0.44	0.45	0.46	0.47	0.48	0.48	0.48	0.48
Pt. Gauge A (cm)	37.53	36.86	35.68	35.40	34.89	33.96	33.69	33.05
Pt. Gauge B (cm)	38.45	37.97	37.30	36.47	35.63	35.23	34.83	34.42
Pt. Gauge C (cm)	39.04	38.64	38.11	37.08	36.30	35.26	34.28	33.27
Pt. Gauge D (cm)	87.80	86.64	85.72	85.13	84.26	83.88	83.70	82.75
Pt. Gauge E (cm)	88.05	87.33	86.83	86.16	85.77	84.95	83.66	82.36
Pt. Gauge F (cm)	72.34	71.38	70.40	69.65	70.13	69.90	69.46	69.10
Tailwater Depth (in)	7	5.1	3.3	1.6	0.3			
Piezo 1 (cm)	6.9	5.3	3.9	3.9	3.1	2.2	2.1	1.5
Piezo 2 (cm)	9.7	9.4	8.5	8.3	7.6	6	4.3	2.3
Piezo 3 (cm)								
Piezo 4 (cm)								
Piezo 5 (cm)	22.2	22	19.7	18.7	17.4	17.5	16.6	14.8
Piezo 6 (cm)	20.8	20.3	18.9	18.3	17.2	15.3	14.3	13.8
Piezo 7 (cm)	16.4	15.4	14.5	14.5	13.9	13.9	13.7	12.6
Piezo 8 (cm)	12.3	11.1	10.1	9.7	8.7	8.4	8.8	9.2
Piezo 9 (cm)	9.9	9.4	8.6	7.8	7.1	6.3	5.6	4.9
Piezo 10 (cm)	9.5	9.1	8.4	7.8	7.1	6.4	5.9	5.2
Piezo 11 (in)	6	5.8	5.5	5.3	5	4.7	4.5	4.2
Piezo 12 (in)	6.1	5.9	5.6	5.3	5.1	4.8	4.6	4.4
Piezo 13 (in)	5.9	5.8	5.4	5.2	4.8	4.6	4.4	4.2
Piezo 14 (in)	5.7	5.6	5.2	4.8	4.6	4.3	4.1	3.9
Piezo 15 (in)	6.1	5.9	5.4	5	4.7	4.4	4.1	4
Piezo 16 (in)	8.2	7.9	7.3	6.8	6.3	5.8	5.3	4.8
Piezo 17 (in)	8.2	8	7.6	7.2	6.9	6.5	6.3	6
Piezo 18 (in)	9.3	9.2	8.8	8.6	8.3	8	7.8	7.5
Piezo 19 (in)	11.1	10.8	10.4	10.1	9.8	9.5	9.3	9.1
Piezo 20 (in)	13.3	13.1	12.5	11.9	11.6	11.2	10.9	10.6
Piezo 21 (in)	16.3	16	15.3	14.6	14	13.3	13	12.5
Piezo 22 (in)	15	15.1	15.1	15.1	15.2	15.2	15.1	15
Jump Location (in)								

Notes: TW is measured using manometer 22

Test: <u>Weir Height 4/8D - Streamwise Position A</u>   **Date:** <u>11/1/2022</u>

Run	YE-X-1	YE-X-2	YE-X-3	YE-X-4	YE-X-5	YE-X-6	YE-X-7	YE-X-8
Time	11:36	12:04	12:27	12:49	13:11	13:34	14:00	14:21
V-notch gauge (cm)	91.64	89.77	87.01	84.78	82.73	80.40	78.39	76.22
Temp (C)	20.9	21.0	21.1	21.2	21.2	21.4	21.5	21.6
Prandtl U1 (ft)	1.32	1.32	1.34	1.34	1.36	1.37	1.38	1.37
Prandtl U2 (ft)	0.97	0.97	0.94	0.94	0.92	0.91	0.90	0.90
Prandtl D1 (ft)	0.44	0.46	0.48	0.48	0.49	0.49	0.49	0.50
Prandtl D2 (ft)	1.60	1.58	1.55	1.54	1.53	1.51	1.50	1.48
Pt. Gauge A (cm)	37.76	37.14	36.12	35.70	35.02	34.00	33.93	39.52
Pt. Gauge B (cm)	39.34	38.55	37.30	36.57	35.83	35.17	34.94	46.43
Pt. Gauge C (cm)	39.31	38.74	38.29	37.27	36.50	35.45	45.14	48.09
Pt. Gauge D (cm)	91.53	91.37	89.94	88.91	88.00	87.55	87.25	87.20
Pt. Gauge E (cm)	91.46	90.70	89.55	88.70	87.60	86.04	85.66	84.91
Pt. Gauge F (cm)	81.63	72.10	70.60	70.27	70.16	70.16	69.95	70.03
Tailwater Depth (in)	8	5.5	3.4	1.6	0.4			
Piezo 1 (cm)	10.1	4.8	3.6	3.1	2.7	2	1.7	2.2
Piezo 2 (cm)	11.9	10.2	7.6	5.7	4.2	2.8	2.4	2.3
Piezo 3 (cm)								
Piezo 4 (cm)								
Piezo 5 (cm)	21.2	21.1	21.1	22.1	21.6	20.9	20.6	20.6
Piezo 6 (cm)	25.8	24.9	23.3	21.7	20.9	20.1	20.3	20.3
Piezo 7 (cm)	22.3	21.6	20.7	19.9	19.3	19	19.9	20.1
Piezo 8 (cm)	17.5	16.7	16.1	16.2	16.5	16.7	19.3	20.1
Piezo 9 (cm)	13.1	12.1	11.7	12.1	12.6	14.1	17.9	20
Piezo 10 (cm)	10.5	9.7	9.1	8.7	8.7	11.8	15.1	19.8
Piezo 11 (in)	6.1	5.9	5.6	5.4	5.1	5.4	7.1	9.8
Piezo 12 (in)	6.1	5.9	5.6	5.3	5.1	5	6.5	9.4
Piezo 13 (in)	5.9	5.8	5.5	5.2	4.9	4.7	4.8	8.9
Piezo 14 (in)	5.8	5.6	5.2	4.9	4.6	4.3	4.2	8.2
Piezo 15 (in)	6.2	5.9	5.4	5.1	4.7	4.3	4.1	7.5
Piezo 16 (in)	8.8	8.3	7.8	6.8	6.4	5.8	5.3	7
Piezo 17 (in)	8.3	8.1	7.6	7.2	6.9	6.5	6.2	6.2
Piezo 18 (in)	9.4	9.2	8.8	8.6	8.3	8	7.7	7.5
Piezo 19 (in)	11.1	10.9	10.4	10.1	9.8	9.5	9.3	9.1
Piezo 20 (in)	13.5	13.2	12.6	11.9	11.5	11.2	10.8	10.5
Piezo 21 (in)	16.3	16.1	15.3	14.6	14	13.4	12.9	12.5
Piezo 22 (in)	14.9	15.1	15.1	15.2	15.2	15.2	15.1	14.9
Jump Location (in)								

Notes: TW is measured using manometer 22

Appendix J Data – Uncontrolled Outlet – Full Weirs

Eight Discharges for Each Weir Height

Test: Full Weir Height 1/8D - Streamwise Position A   **Date:** 10/6/2022

Run	ZB-X-1	ZB-X-2	ZB-X-3	ZB-X-4	ZB-X-5	ZB-X-6	ZB-X-7	ZB-X-8
Time	14:13	14:38	14:56	15:14	15:42	16:16	16:41	17:03
V-notch gauge (cm)	91.56	89.86	87.19	84.68	82.84	80.55	78.43	76.23
Temp (C)	21.4	21.5	21.6	21.6	21.7	21.8	22.0	22.1
Prandtl U1 (ft)	1.36	1.37	1.38	1.41	1.41	1.42	1.42	1.44
Prandtl U2 (ft)	1.00	1.00	0.99	0.96	0.96	0.94	0.94	0.93
Prandtl D1 (ft)	0.44	0.46	0.47	0.49	0.59	0.49	0.47	0.45
Prandtl D2 (ft)	1.61	1.59	1.57	1.54	1.49	1.49	1.49	1.47
Pt. Gauge A (cm)	37.79	37.28	36.83	35.90	35.35	34.85	34.15	33.13
Pt. Gauge B (cm)	38.81	38.38	37.16	36.65	35.77	35.07	34.67	34.60
Pt. Gauge C (cm)	39.07	38.91	38.07	37.14	36.35	35.06	34.23	33.30
Pt. Gauge D (cm)	77.45	76.62	75.33	74.54	74.12	73.96	73.96	73.94
Pt. Gauge E (cm)	77.82	77.70	77.54	77.01	76.56	75.90	74.94	74.70
Pt. Gauge F (cm)	81.04	73.22	72.53	71.32	71.14	70.66	70.40	69.71
Tailwater Depth (in)	7.8	5.7	3.4	1.7				
Piezo 1 (cm)	9.4	5.9	4.9	3.6	2.7	2.3	2.1	1.6
Piezo 2 (cm)	8.8	8.2	7.7	6.8	5.7	4.3	3.4	3.2
Piezo 3 (cm)								
Piezo 4 (cm)								
Piezo 5 (cm)	19.6	18.5	16.7	15.4	14.2	12.9	11.7	10.6
Piezo 6 (cm)	9.2	9	8.2	7.4	7.1	6.6	6.3	6.2
Piezo 7 (cm)	8.7	8.3	7.5	7	6.7	6.3	6	5.7
Piezo 8 (cm)	10	9.6	8.6	7.7	6.9	6.1	5.5	5.1
Piezo 9 (cm)	10.1	9.6	8.7	8	7.3	6.5	5.6	4.8
Piezo 10 (cm)	10	9.5	8.6	7.9	7.4	6.7	6.1	5.4
Piezo 11 (in)	6.1	5.9	5.5	5.3	5	4.8	4.5	4.2
Piezo 12 (in)	6.1	5.9	5.6	5.3	5.1	4.9	4.7	4.4
Piezo 13 (in)	6	5.8	5.4	5.1	4.9	4.6	4.4	4.3
Piezo 14 (in)	5.8	5.6	5.1	4.8	4.6	4.3	4.1	3.9
Piezo 15 (in)	6.2	6	5.5	5	4.7	4.3	4.1	4
Piezo 16 (in)	8.3	7.9	7.3	6.8	6.4	5.8	5.3	4.8
Piezo 17 (in)	8.4	8.1	7.7	7.2	6.9	6.6	6.3	6
Piezo 18 (in)	9.5	9.3	8.9	8.6	8.3	8	7.8	7.5
Piezo 19 (in)	11.1	10.9	10.4	10.1	9.8	9.6	9.3	9.1
Piezo 20 (in)	13.4	13.1	12.4	11.9	11.5	11.1	10.8	10.6
Piezo 21 (in)	16.4	16	15.3	14.6	14.1	13.4	12.9	12.5
Piezo 22 (in)	14.9	15	15.1	15.1	15.2	15.2	15.1	15
Jump Location (in)								

Notes: TW is measured using manometer 22

Test: Full Weir Height 2/8D - Streamwise Position A   **Date:** 10/7/2022

Run	ZC-X-1	ZC-X-2	ZC-X-3	ZC-X-4	ZC-X-5	ZC-X-6	ZC-X-7	ZC-X-8
Time	15:09	15:32	15:53	16:09	16:26	16:42	16:56	17:33
V-notch gauge (cm)	92.05	90.12	87.45	85.10	82.92	80.88	78.44	76.38
Temp (C)	21.5	21.5	21.4	21.4	21.4	21.4	21.4	21.5
Prandtl U1 (ft)	1.32	1.31	1.34	1.34	1.34	1.34	1.34	1.34
Prandtl U2 (ft)	0.95	0.96	0.93	0.92	0.92	0.92	0.92	0.92
Prandtl D1 (ft)	1.63	1.62	1.59	1.56	1.56	1.55	1.53	1.52
Prandtl D2 (ft)	0.46	0.48	0.50	0.52	0.51	0.52	0.52	0.50
Pt. Gauge A (cm)	37.84	37.62	36.57	35.54	35.33	34.37	33.86	33.21
Pt. Gauge B (cm)	39.24	38.25	37.34	36.57	35.91	35.44	34.81	34.48
Pt. Gauge C (cm)	39.76	38.77	38.03	37.37	36.24	35.49	34.36	33.49
Pt. Gauge D (cm)	77.97	77.11	76.00	75.06	74.56	74.15	74.14	74.17
Pt. Gauge E (cm)	83.44	83.17	82.83	82.55	82.31	81.66	80.29	79.28
Pt. Gauge F (cm)	80.66	72.08	71.30	70.72	70.18	69.77	69.73	69.34
Tailwater Depth (in)	8.9	5.9	3.7	1.8	0.5	0		
Piezo 1 (cm)	15.7	9.6	8.9	6.3	4.3	2.6	1.8	1.4
Piezo 2 (cm)	14.8	11.5	10.6	10.7	9.9	8.1	4.9	3.4
Piezo 3 (cm)								
Piezo 4 (cm)								
Piezo 5 (cm)	23.3	21.5	19.3	17.1	15.9	14.9	14.5	14.6
Piezo 6 (cm)	13.5	12.3	11.7	11.1	10.7	10.3	10.2	10
Piezo 7 (cm)	11.3	10.5	9.4	8.6	7.7	7.3	6.9	7
Piezo 8 (cm)	10.5	9.8	8.8	7.9	7	6.2	5.5	5.1
Piezo 9 (cm)	10.4	9.7	8.8	8.1	7.4	6.6	5.7	4.8
Piezo 10 (cm)	11.2	10.5	9.7	8.9	8.3	6.8	6.1	5.5
Piezo 11 (in)	6.2	5.9	5.6	5.3	5	4.8	4.5	4.3
Piezo 12 (in)	6.3	6	5.6	5.4	5.1	4.9	4.7	4.4
Piezo 13 (in)	6.2	5.8	5.5	5.2	4.9	4.7	4.4	4.2
Piezo 14 (in)	6	5.6	5.2	4.9	4.6	4.4	4.1	3.9
Piezo 15 (in)	6.4	5.9	5.5	5.1	4.7	4.4	4.1	4
Piezo 16 (in)	8.5	8	7.4	6.8	6.4	5.9	5.3	4.8
Piezo 17 (in)	8.6	8.2	7.7	7.3	6.9	6.6	6.3	6
Piezo 18 (in)	9.6	9.3	8.9	8.6	8.3	8.1	7.8	7.5
Piezo 19 (in)	11.2	10.9	10.5	10.1	9.8	9.6	9.3	9.1
Piezo 20 (in)	13.7	13.2	12.5	12	11.5	11.4	10.9	10.6
Piezo 21 (in)	16.6	16.1	15.3	14.8	14	13.5	12.9	12.5
Piezo 22 (in)	14.8	15.1	15.2	15.2	15.2	15.2	15.1	15
Jump Location (in)								

Notes: TW is measured using manometer 22

Test: Full Weir Height 3/8D - Streamwise Position A   **Date:** 10/11/2022

Run	ZD-X-1	ZD-X-2	ZD-X-3	ZD-X-4	ZD-X-5	ZD-X-6	ZD-X-7	ZD-X-8
Time	13:55	14:14	14:36	15:00	15:30	15:55	16:17	16:46
V-notch gauge (cm)	91.75	89.71	87.47	85.09	82.66	80.35	78.53	76.23
Temp (C)	21.2	21.3	21.4	21.5	21.6	21.7	21.8	22.0
Prandtl U1 (ft)	1.04	1.04	1.06	1.08	1.09	1.10	1.11	1.11
Prandtl U2 (ft)	0.69	0.69	0.67	0.65	0.63	0.62	0.62	0.61
Prandtl D1 (ft)	0.22	0.24	0.26	0.27	0.28	0.31	0.31	0.31
Prandtl D2 (ft)	1.38	1.37	1.35	1.33	1.32	1.29	1.29	1.29
Pt. Gauge A (cm)	37.98	37.01	36.56	35.93	34.76	34.36	34.06	33.00
Pt. Gauge B (cm)	39.44	38.23	37.55	36.91	36.03	35.21	34.88	34.74
Pt. Gauge C (cm)	39.12	38.47	38.13	37.29	36.00	35.05	34.69	33.34
Pt. Gauge D (cm)	78.45	77.47	76.28	75.30	80.55	80.88	81.55	81.53
Pt. Gauge E (cm)	88.23	87.84	86.61	86.36	85.50	84.71	83.66	82.20
Pt. Gauge F (cm)	82.31	72.92	71.70	70.76	70.42	70.42	70.15	69.90
Tailwater Depth (in)	8.1	5.3	3.6	1.6	0.3			
Piezo 1 (cm)	11.6	7.2	5.8	4.2	3.1	2.6	2.4	2
Piezo 2 (cm)	13.1	11.3	10.3	8.8	7.2	6.5	5.1	3.5
Piezo 3 (cm)								
Piezo 4 (cm)								
Piezo 5 (cm)	19.4	17.7	16.5	14.5	13.2	15.6	15.7	14.1
Piezo 6 (cm)	18.6	17.6	17.2	16.5	15.6	14.6	13.6	12.4
Piezo 7 (cm)	13.1	11.9	11.4	10.6	10.1	10.7	11.1	11.5
Piezo 8 (cm)	10.7	9.9	9.1	8.1	7.1	6.4	6.1	6.6
Piezo 9 (cm)	10.3	9.6	8.8	8	7.2	6.3	5.7	4.8
Piezo 10 (cm)	10.2	9.5	8.7	8	7.3	6.7	6.2	5.5
Piezo 11 (in)	6.1	5.9	5.6	5.3	5	4.7	4.5	4.3
Piezo 12 (in)	6.2	5.9	5.7	5.4	5.1	4.9	4.7	4.4
Piezo 13 (in)	6	5.8	5.5	5.2	4.9	4.6	4.4	4.2
Piezo 14 (in)	5.8	5.6	5.2	4.9	4.6	4.3	4.1	3.9
Piezo 15 (in)	6.3	6	5.5	5.1	4.7	4.4	4.1	4
Piezo 16 (in)	8.4	8	7.4	6.9	6.3	5.8	5.3	4.8
Piezo 17 (in)	8.5	8.1	7.7	7.3	6.9	6.6	6.3	6
Piezo 18 (in)	9.5	9.2	8.9	8.6	8.3	8	7.8	7.5
Piezo 19 (in)	11.2	10.8	10.5	10.1	9.8	9.5	9.3	9.1
Piezo 20 (in)	13.6	13.1	12.6	12	11.5	11.1	10.8	10.5
Piezo 21 (in)	16.4	16	15.5	14.7	14	13.4	12.9	12.5
Piezo 22 (in)	15	15.1	15.1	15.1	15.2	15.2	15	15
Jump Location (in)		2±2	2±2	3±3	4±2	5±2	6±2	6.5±2.5

Notes: TW is measured using manometer 22

Test: <u>Full Weir Height 4/8D - Streamwise Position A</u>   **Date:** <u>10/13/2022</u>

Run	ZE-X-1	ZE-X-2	ZE-X-3	ZE-X-4	ZE-X-5	ZE-X-6	ZE-X-7	ZE-X-8
Time	12:49	13:15	13:36	12:57	14:11	14:33	14:58	15:27
V-notch gauge (cm)	91.64	89.68	87.36	84.92	82.67	80.29	78.43	76.02
Temp (C)	21.3	21.3	21.3	21.2	21.2	21.2	21.2	21.2
Prandtl U1 (ft)	1.35	1.36	1.36	1.38	1.40	1.41	1.41	1.42
Prandtl U2 (ft)	0.99	0.98	0.97	0.95	0.93	0.93	0.92	0.91
Prandtl D1 (ft)	1.62	1.59	1.57	1.55	1.54	1.53	1.51	1.51
Prandtl D2 (ft)	0.45	0.47	0.49	0.50	0.50	0.51	0.52	0.50
Pt. Gauge A (cm)	37.44	37.27	36.32	35.21	34.43	34.00	33.94	33.15
Pt. Gauge B (cm)	39.05	38.48	37.60	36.52	35.67	35.22	34.83	34.51
Pt. Gauge C (cm)	39.35	38.78	38.03	37.28	36.23	35.16	34.12	33.44
Pt. Gauge D (cm)	88.23	88.25	86.68	86.41	85.91	85.57	84.91	83.90
Pt. Gauge E (cm)	91.16	90.90	90.30	89.33	88.22	86.41	84.97	83.82
Pt. Gauge F (cm)	80.94	72.91	71.80	71.37	70.95	70.64	70.30	69.94
Tailwater Depth (in)	7.9	5.4	3.5	1.6	0.5			
Piezo 1 (cm)	10.2	6.5	5.1	4.1	3.6	3.2	3	2.4
Piezo 2 (cm)	13.2	11.4	9.7	8.4	6.9	5.2	4.3	3.4
Piezo 3 (cm)								
Piezo 4 (cm)								
Piezo 5 (cm)	19.9	18.8	17.7	17.4	17.3	17.3	16.5	16.3
Piezo 6 (cm)	22.9	22.5	21.3	20.2	18.3	16.8	16.2	16.3
Piezo 7 (cm)	17.6	17.3	16.2	15.8	15.8	15.2	14.2	14
Piezo 8 (cm)	12.8	12.1	11.5	10.5	10.6	11.3	12.2	12
Piezo 9 (cm)	10.5	9.8	9.1	8.4	7.7	7	6.9	9.1
Piezo 10 (cm)	9.9	9.5	8.7	7.9	7.3	6.6	6.2	6.1
Piezo 11 (in)	6	5.9	5.6	5.3	5	4.7	4.5	4.5
Piezo 12 (in)	6.2	6	5.7	5.4	5.1	4.9	4.7	4.4
Piezo 13 (in)	6	5.8	5.5	5.2	4.9	4.6	4.4	4.2
Piezo 14 (in)	5.7	5.6	5.2	4.9	4.6	4.3	4.1	3.9
Piezo 15 (in)	6.2	5.9	5.5	5.1	4.7	4.3	4.1	4
Piezo 16 (in)	8.3	7.9	7.4	6.9	6.4	5.8	5.3	4.7
Piezo 17 (in)	8.4	8.2	7.7	7.3	6.9	6.6	6.3	6
Piezo 18 (in)	9.5	9.2	8.9	8.6	8.3	8	7.8	7.5
Piezo 19 (in)	11.2	10.9	10.5	10.1	9.8	9.6	9.3	9.1
Piezo 20 (in)	13.4	13.2	12.5	12.1	11.5	11.2	10.8	10.6
Piezo 21 (in)	16.4	16.1	15.3	14.7	14.1	13.4	12.9	12.5
Piezo 22 (in)	14.9	15.2	15.2	15.1	15.1	15.2	15.1	14.9
Jump Location (in)	10±4	9±3	9.5±3.5	10±3	10.5±3.5	11±3	12±3	20±5

Notes: TW is measured using manometer 22

Appendix K Data – Uncontrolled Outlet – No Weirs

Eight Discharges
With Prandtl Tubes at Basin Outlet

Test: <u>Weir Height N/A - Streamwise Position N/A</u>   **Date:** <u>12/20/2022</u>

Run	YYA-X-1	YYA-X-2	YYA-X-3	YYA-X-4	YYA-X-5	YYA-X-6	YYA-X-7	YYA-X-8
Time	10:44	11:10	11:22	11:59	12:18	12:33	12:52	13:13
V-notch gauge (cm)	91.61	89.83	87.23	84.88	82.59	80.43	78.40	76.36
	91.61	89.76	86.98	84.83	82.57	80.43	78.40	76.18
Temp (C)	17.5	17.5	17.5	17.5	18.0	18.0	18.0	18.0
Prandtl U1 (ft)	0.80	0.79	0.77	0.76	0.75	0.73	0.73	0.73
Prandtl U2 (ft)	1.13	1.15	1.17	1.18	1.18	1.20	1.20	1.20
Prandtl D1 (ft)	1.41	1.40	1.38	1.36	1.35	1.34	1.33	1.32
Prandtl D2 (ft)	0.24	0.26	0.27	0.30	0.31	0.32	0.32	0.32
Pt. Gauge A (cm)	37.75	37.28	36.68	35.68	34.50	33.86	33.60	33.28
Pt. Gauge B (cm)	39.11	38.43	37.31	36.50	35.97	35.33	34.94	34.52
Pt. Gauge C (cm)	39.15	38.85	37.92	37.46	36.00	35.24	34.48	33.27
Pt. Gauge D (cm)	77.48	76.51	75.03	74.50	74.05	73.83	73.47	73.48
Pt. Gauge E (cm)	74.27	73.80	73.48	73.29	73.17	72.34	71.53	70.82
Pt. Gauge F (cm)	79.82	70.32	69.87	69.64	69.24	69.02	68.82	68.73
Tailwater Depth (in)	15.4	9.9	3.8					
Piezo 1 (cm)	8	2.8	2.3	1.9	1.4	1.1	0.9	0.7
Piezo 2 (cm)	5.4	4.1	3.8	3.3	2.7	2.2	1.8	1.6
Piezo 3 (cm)								
Piezo 4 (cm)								
Piezo 5 (cm)	8.2	7.5	6.6	6.1	5.4	5	4.6	4.3
Piezo 6 (cm)	9.3	8.9	8.5	7.9	7.6	7.2	6.8	6.2
Piezo 7 (cm)	8.6	8.1	7.4	6.8	6.2	5.9	5.6	5.2
Piezo 8 (cm)	10.1	9.5	8.5	7.7	6.7	6	5.4	5
Piezo 9 (cm)	10.5	9.9	9	8.3	7.4	6.5	5.7	5
Piezo 10 (cm)	9.9	9.4	8.5	7.8	7.1	6.4	5.9	5.2
Piezo 11 (in)	6.1	5.9	5.6	5.3	5	4.7	4.5	4.3
Piezo 12 (in)	6.1	5.9	5.6	5.4	5.1	4.9	4.6	4.4
Piezo 13 (in)	6	5.8	5.5	5.2	4.9	4.6	4.4	4.2
Piezo 14 (in)	6	5.8	5.4	5.2	4.8	4.6	4.4	4.2
Piezo 15 (in)	6.2	5.9	5.5	5.1	4.7	4.3	4.1	3.9
Piezo 16 (in)	8.2	7.9	7.2	6.8	6.3	5.8	5.4	4.9
Piezo 17 (in)	8.3	8.1	7.6	7.2	6.8	6.5	6.2	6
Piezo 18 (in)	9.5	9.3	8.8	8.6	8.3	8	7.8	7.5
Piezo 19 (in)	11.2	10.9	10.4	10.1	9.8	9.5	9.3	9.1
Piezo 20 (in)	13.5	13.1	12.4	12	11.6	11.1	10.9	10.5
Piezo 21 (in)	16.4	15.9	15.2	14.6	13.9	13.3	12.9	12.5
Piezo 22 (in)	14.9	15.1	15.1	15.1	15.2	15.1	15	14.9
Jump Location (in)								

Basin Outlet Prandtl

	YYA-X-1	YYA-X-2	YYA-X-3	YYA-X-4	YYA-X-5	YYA-X-6	YYA-X-7	YYA-X-8
LDB Prandtl ΔH (cm)	29.1	34.8	38	37.4	36.05	35.35	34.25	32.85
LDB (Mx-Mn)/2 (cm)	0.05	0.1	0.1	0.1	0.05	0.05	0.05	0.05
CL Prandtl ΔH (cm)	33	32	38.9	37.6	36.15	35.5	34.7	32.85
CL (Mx-Mn)/2 (cm)	0.05	0.05	0.1	0.1	0.05	0.05	0.1	0.05
RDB Prandtl ΔH (cm)	31.5	37.1	39.5	38.3	37	36.2	34.95	33.55
RDB (Mx-Mn)/2 (cm)	0.05	0.1	0.1	0.1	0.05	0.05	0.1	0.05

Notes: Measured Velocity with three Prandtl tubes at outlet

Appendix L Data – Uncontrolled Outlet – Staggered Weirs
Eight Discharges for Each Weir Height
With Prandtl Tubes at Basin Outlet

Test: Weir Height 1/8D - Streamwise Position A   **Date:** 12/29/2022

Run	YZB-X-1	YZB-X-2	YZB-X-3	YZB-X-4	YZB-X-5	YZB-X-6	YZB-X-7	YZB-X-8
Time	13:03	13:25	13:48	14:03	14:24	14:54	15:23	15:45
V-notch gauge (cm)	91.59	89.75	87.00	84.63	82.89	80.62	78.48	76.01
	91.59	89.75	87.02	84.63	82.89	80.61	78.51	76.06
Temp (C)	18.5	18.5	18.5	18.5	18.5	18.5	19.0	19.0
Prandtl U1 (ft)	1.37	1.37	1.38	1.40	1.41	1.42	1.42	1.42
Prandtl U2 (ft)	1.02	1.02	1.00	0.98	0.98	0.97	0.96	0.96
Prandtl D1 (ft)	0.45	0.47	0.49	0.50	0.50	0.51	0.51	0.51
Prandtl D2 (ft)	1.63	1.60	1.58	1.57	1.56	1.54	1.53	1.52
Pt. Gauge A (cm)	38.07	37.28	36.65	35.70	34.97	34.56	34.05	33.25
Pt. Gauge B (cm)	38.99	38.40	37.33	36.55	36.12	35.42	34.87	34.37
Pt. Gauge C (cm)	39.32	38.84	38.24	37.21	36.23	35.15	34.08	33.34
Pt. Gauge D (cm)	77.40	76.56	75.12	74.37	74.28	73.86	73.74	73.85
Pt. Gauge E (cm)	78.00	77.61	77.36	77.13	76.52	75.83	75.21	74.75
Pt. Gauge F (cm)	82.40	72.60	71.26	71.00	70.22	69.82	69.70	69.42
Tailwater Depth (in)	14.8	8.8	2.9					
Piezo 1 (cm)	10.6	6	5	3.6	2.6	2.2	2.1	1.5
Piezo 2 (cm)	9.3	8.2	7.5	6.5	5.4	3.8	3	2.7
Piezo 3 (cm)								
Piezo 4 (cm)								
Piezo 5 (cm)	19.6	18.4	16.7	15.3	14.3	12.9	11.8	10.4
Piezo 6 (cm)	9.1	8.6	8.1	7.3	6.9	6.5	6.2	6.1
Piezo 7 (cm)	8.5	8.1	7.3	6.8	6.5	6.2	5.9	5.5
Piezo 8 (cm)	9.9	9.4	8.4	7.5	6.8	6.1	5.4	4.9
Piezo 9 (cm)	9.8	9.3	8.4	7.8	7.1	6.2	5.3	4.5
Piezo 10 (cm)	9.8	9.2	8.4	7.7	7.1	6.5	5.8	5.1
Piezo 11 (in)	6.1	5.8	5.5	5.3	5	4.8	4.5	4.2
Piezo 12 (in)	6.1	5.9	5.5	5.3	5.1	4.9	4.6	4.3
Piezo 13 (in)	6	5.8	5.4	5.1	4.9	4.7	4.4	4.2
Piezo 14 (in)	6.1	5.8	5.5	5.1	4.9	4.7	4.4	4.2
Piezo 15 (in)	6.1	5.9	5.4	5	4.7	4.4	4.1	3.9
Piezo 16 (in)	8.3	7.8	7.3	6.8	6.4	5.8	5.4	4.7
Piezo 17 (in)	8.4	8.1	7.6	7.2	6.9	6.5	6.3	6
Piezo 18 (in)	9.4	9.2	8.9	8.6	8.3	8	7.8	7.5
Piezo 19 (in)	11.2	10.9	10.5	10.1	9.8	9.6	9.3	9.1
Piezo 20 (in)	13.5	13.2	12.4	11.9	11.6	11.2	10.9	10.6
Piezo 21 (in)	16.4	16.1	15.2	14.6	14	13.4	13	12.4
Piezo 22 (in)	14.9	15.1	15.1	15.1	15.1	15.1	15.1	15
Jump Location (in)								

Basin Outlet Prandtl

	YZB-X-1	YZB-X-2	YZB-X-3	YZB-X-4	YZB-X-5	YZB-X-6	YZB-X-7	YZB-X-8
LDB Prandtl ΔH (cm)	11.4	17.4	20.35	22.4	22.85	23.05	23.1	22.54
LDB (Mx-Mn)/2 (cm)	0.1	0.1	0.05	0.05	0.05	0.1	0.1	0.1
CL Prandtl ΔH (cm)	12.1	18.05	21.5	22.3	21.4	19.15	19	22.37
CL (Mx-Mn)/2 (cm)	0.1	0.05	0.1	0.1	0.1	0.1	0.1	0.15
RDB Prandtl ΔH (cm)	13.7	18.7	20.05	21.9	21.65	22	21.8	20.12
RDB (Mx-Mn)/2 (cm)	0.1	0.1	0.05	0.1	0.1	0.1	0.1	0.14

Notes: Measured Velocity with three Prandtl tubes at outlet

Test: Weir Height 2/8D - Streamwise Position A   **Date:** 12/30/2022

Run	YZC-X-1	YZC-X-2	YZC-X-3	YZC-X-4	YZC-X-5	YZC-X-6	YZC-X-7	YZC-X-8
Time	11:26	11:52	12:08	12:26	12:42	13:01	13:23	13:41
V-notch gauge (cm)	91.82	89.83	87.16	84.93	82.80	80.61	78.48	76.05
	91.82	89.79	87.14	84.90	82.77	80.61	78.44	76.13
Temp (C)	19.5	19.0	19.0	19.5	19.5	19.5	19.5	19.5
Prandtl U1 (ft)	1.34	1.34	1.35	1.37	1.39	1.40	1.39	1.40
Prandtl U2 (ft)	1.02	1.01	0.99	0.97	0.96	0.95	0.94	0.94
Prandtl D1 (ft)	1.63	1.59	1.58	1.57	1.55	1.54	1.43	1.52
Prandtl D2 (ft)	0.46	0.49	0.49	0.50	0.51	0.51	0.62	0.52
Pt. Gauge A (cm)	38.32	37.58	36.56	35.83	34.80	34.03	33.74	33.17
Pt. Gauge B (cm)	39.32	38.46	37.16	36.53	35.77	35.34	34.64	34.51
Pt. Gauge C (cm)	39.26	38.85	37.74	37.09	36.11	35.15	34.20	33.19
Pt. Gauge D (cm)	77.90	76.98	75.64	75.17	74.14	74.11	73.72	73.42
Pt. Gauge E (cm)	83.52	82.97	82.86	82.86	82.37	81.41	79.92	79.27
Pt. Gauge F (cm)	77.50	71.92	70.65	70.16	69.74	69.47	69.35	68.89
Tailwater Depth (in)	16.2	9.1	3.1					
Piezo 1 (cm)	14.9	9.7	8.2	6.4	4.1	2.3	1.7	1.3
Piezo 2 (cm)	14.1	10.9	10.5	10.2	6.2	7.3	4.3	3
Piezo 3 (cm)								
Piezo 4 (cm)								
Piezo 5 (cm)	22.4	21.2	18.6	16.8	15.8	14.1	14.3	14.8
Piezo 6 (cm)	13.1	12.2	11.6	10.9	10.4	10.2	9.9	9.8
Piezo 7 (cm)	10.8	9.9	9	8.1	7.4	7	6.6	6.7
Piezo 8 (cm)	10.3	9.5	8.5	7.6	6.9	6.1	5.4	5
Piezo 9 (cm)	10.1	9.3	8.5	7.8	7.1	6.2	5.4	4.5
Piezo 10 (cm)	9.9	9.3	8.4	7.8	7.1	6.5	5.8	5.1
Piezo 11 (in)	6.7	6.4	6.1	5.8	5.6	5.3	5.2	5
Piezo 12 (in)	6.2	5.9	5.6	5.3	5.1	4.9	4.6	4.4
Piezo 13 (in)	6.1	5.8	5.5	5.2	4.9	4.6	4.4	4.2
Piezo 14 (in)	6.3	6	5.6	5.3	5	4.8	4.5	4.3
Piezo 15 (in)	6.3	5.9	5.5	5.1	4.7	4.4	4.1	3.9
Piezo 16 (in)	8.4	7.9	7.3	6.8	6.4	5.8	5.3	4.8
Piezo 17 (in)	8.5	8.1	7.6	7.2	6.9	6.5	6.2	6
Piezo 18 (in)	9.6	9.3	8.9	8.6	8.3	8	7.8	7.5
Piezo 19 (in)	11.2	10.9	10.5	10.1	9.8	9.6	9.3	9.1
Piezo 20 (in)	13.7	13.1	12.5	12	11.5	11.2	10.9	10.6
Piezo 21 (in)	16.5	16.1	15.3	14.6	14	13.4	12.9	12.5
Piezo 22 (in)	15	15.1	15.2	15.1	15.2	15.2	15	15
Jump Location (in)								1±1

Basin Outlet Prandtl

LDB Prandtl ΔH (cm)	3.6	16.6	21.63	22.15	22.84	22.17	20.17	16.62
LDB (Mx-Mn)/2 (cm)	0.3	0.27	0.27	0.19	0.19	0.13	0.14	0.12
CL Prandtl ΔH (cm)	5.8	19.25	25.34	27.28	27.62	23.66	19.39	15.28
CL (Mx-Mn)/2 (cm)	0.2	0.2	0.17	0.2	0.2	0.23	0.26	0.18
RDB Prandtl ΔH (cm)	5.47	18.07	21.8	20.79	20.68	20.27	18.72	15.1
RDB (Mx-Mn)/2 (cm)	0.23	0.28	0.31	0.27	0.23	0.26	0.15	0.19

Notes: Measured Velocity with three Prandtl tubes at outlet

Test: Weir Height 3/8D - Streamwise Position A   **Date:** 1/2/2023

Run	YZD-X-1	YZD-X-2	YZD-X-3	YZD-X-4	YZD-X-5	YZD-X-6	YZD-X-7	YZD-X-8
Time	12:36	13:09	13:29	13:53	14:13	14:47	15:12	15:30
V-notch gauge (cm)	91.73	89.85	87.28	84.93	82.90	80.64	78.37	76.10
	91.71	89.70	87.28	84.96	82.87	80.61	78.37	75.95
Temp (C)	19.5	19.5	19.5	20.0	20.0	20.0	20.0	20.0
Prandtl U1 (ft)	1.13	1.14	1.16	1.17	1.19	1.19	1.20	1.20
Prandtl U2 (ft)	0.83	0.81	0.80	0.78	0.76	0.75	0.74	0.74
Prandtl D1 (ft)	0.12	0.23	0.16	0.17	0.18	0.19	0.63	0.59
Prandtl D2 (ft)	1.29	1.18	1.26	1.24	1.23	1.22	0.74	0.76
Pt. Gauge A (cm)	37.97	37.43	36.78	36.04	34.72	34.43	33.96	33.07
Pt. Gauge B (cm)	38.97	38.50	37.27	36.70	35.94	35.37	34.70	34.36
Pt. Gauge C (cm)	38.95	38.66	37.93	37.28	36.31	35.34	34.34	33.19
Pt. Gauge D (cm)	83.10	82.44	82.28	81.63	81.34	81.35	82.27	82.37
Pt. Gauge E (cm)	88.93	88.02	87.61	86.67	85.63	85.22	83.53	82.41
Pt. Gauge F (cm)	82.52	72.29	71.51	70.79	70.25	70.22	69.40	69.41
Tailwater Depth (in)	15	8.5	3.1					
Piezo 1 (cm)	12.1	7.2	5.6	4.2	3.3	2.6	2.3	1.9
Piezo 2 (cm)	13	11.3	10	8.5	7.3	6.2	4.7	3.2
Piezo 3 (cm)								
Piezo 4 (cm)								
Piezo 5 (cm)	18.6	17.3	14.1	13.7	13.8	14.5	15.7	14.3
Piezo 6 (cm)	18.3	17.6	17.1	16.3	15.7	14.7	13.5	12.3
Piezo 7 (cm)	12.9	11.9	11	10.3	10.3	10.5	11.2	11.4
Piezo 8 (cm)	10.4	9.7	8.7	7.8	7	6.3	6	7
Piezo 9 (cm)	9.9	9.3	8.5	7.7	7	6.2	5.3	4.5
Piezo 10 (cm)	10.3	9.7	8.9	7.7	7.1	6.5	5.8	5
Piezo 11 (in)	6.1	5.9	5.6	5.3	5	4.8	4.5	4.2
Piezo 12 (in)	6.2	5.9	5.6	5.4	5.1	4.9	4.6	4.3
Piezo 13 (in)	6.1	5.8	5.5	5.2	4.9	4.6	4.4	4.2
Piezo 14 (in)	6.3	6	5.6	5.3	5	4.8	4.5	4.2
Piezo 15 (in)	6.2	5.9	5.5	5	4.7	4.4	4.1	3.9
Piezo 16 (in)	8.4	7.9	7.4	6.8	6.4	5.9	5.3	4.8
Piezo 17 (in)	8.4	8.1	7.6	7.2	6.9	6.5	6.2	5.9
Piezo 18 (in)	9.5	9.3	8.9	8.6	8.3	8	7.8	7.5
Piezo 19 (in)	11.2	10.9	10.5	10.1	9.8	9.5	9.3	9.1
Piezo 20 (in)	13.6	13.1	12.5	12	11.6	11.3	10.8	10.5
Piezo 21 (in)	16.6	16	15.3	14.6	14	13.5	12.9	12.5
Piezo 22 (in)	14.9	15	15	15.1	15.1	15.1	15.1	15
Jump Location (in)		2.5±2.5	2.5±2.5	4±2	5±2	5±2	6±2	7±3

Basin Outlet Prandtl

LDB Prandtl ΔH (cm)	5.04	12.61	17.22	17.74	16.12	13.91	12.44	11.47
LDB (Mx-Mn)/2 (cm)	0.14	0.23	0.21	0.21	0.17	0.12	0.1	0.11
CL Prandtl ΔH (cm)	6.14	14.68	18.27	16.44	15.12	13.83	12.27	11.65
CL (Mx-Mn)/2 (cm)	0.28	0.14	0.14	0.14	0.11	0.12	0.11	0.17
RDB Prandtl ΔH (cm)	8.1	16.17	20.37	18.86	17.75	15.37	13.2	12.3
RDB (Mx-Mn)/2 (cm)	0.37	0.2	0.24	0.22	0.15	0.09	0.12	0.06

Notes: Measured Velocity with three Prandtl tubes at outlet

Test: <u>Weir Height 4/8D - Streamwise Position A</u>   **Date:** <u>1/3/2023</u>

Run	YZC-X-1	YZC-X-2	YZC-X-3	YZC-X-4	YZC-X-5	YZC-X-6	YZC-X-7	YZC-X-8
Time	13:28	13:52	14:10	14:28	14:46	15:03	15:24	15:47
V-notch gauge (cm)	91.99	89.73	87.08	84.97	82.77	80.56	78.65	76.15
	91.92	89.63	87.05	84.94	82.75	80.58	78.60	76.11
Temp (C)	20.0	20.0	20.0	20.0	20.0	20.0	20.0	20.0
Prandtl U1 (ft)	1.32	1.34	1.34	1.36	1.38	1.39	1.39	1.39
Prandtl U2 (ft)	1.01	0.99	0.99	0.96	0.95	0.93	0.93	0.92
Prandtl D1 (ft)	0.45	0.46	0.48	0.50	0.50	0.51	0.51	0.51
Prandtl D2 (ft)	1.63	1.61	1.58	1.57	1.56	1.54	1.53	1.52
Pt. Gauge A (cm)	38.73	37.15	36.78	35.48	34.79	33.91	33.75	33.21
Pt. Gauge B (cm)	39.55	38.02	37.20	36.48	36.02	35.38	34.85	34.31
Pt. Gauge C (cm)	39.45	38.73	38.11	37.28	36.37	35.12	34.33	33.98
Pt. Gauge D (cm)	89.20	89.12	87.74	87.08	86.42	85.68	85.11	84.20
Pt. Gauge E (cm)	91.99	91.54	90.35	89.44	88.31	86.77	85.36	83.95
Pt. Gauge F (cm)	83.82	72.32	71.64	71.10	70.85	70.19	70.02	69.44
Tailwater Depth (in)	16	8	2.6					
Piezo 1 (cm)	13.3	6.4	5.1	4.1	3.6	3.1	2.8	2.3
Piezo 2 (cm)	14.3	11.4	9.4	8	6.8	5.3	4.2	3.3
Piezo 3 (cm)								
Piezo 4 (cm)								
Piezo 5 (cm)	20.4	18.2	17.9	17.5	17.5	17.1	16	16
Piezo 6 (cm)	23.1	22.9	21.2	20	18.4	16.8	16.2	16
Piezo 7 (cm)	17.8	17.1	16.2	15.5	15.7	15.2	14.5	14.2
Piezo 8 (cm)	13.3	12.3	11.2	10.3	10.3	10.5	10.7	11.8
Piezo 9 (cm)	10.3	9.7	8.8	8.1	7.4	6.7	6.7	9.3
Piezo 10 (cm)	9.8	9.3	8.4	7.8	7.1	6.5	6	6.3
Piezo 11 (in)	6.1	5.8	5.5	5.3	5	4.8	4.5	4.4
Piezo 12 (in)	6.1	5.9	5.6	5.4	5.1	4.9	4.6	4.4
Piezo 13 (in)	6	5.8	5.4	5.2	4.9	4.7	4.4	4.2
Piezo 14 (in)	6.3	6	5.6	5.3	5	4.8	4.5	4.3
Piezo 15 (in)	6.3	5.9	5.5	5.1	4.7	4.4	4.1	3.9
Piezo 16 (in)	8.4	7.9	7.3	6.9	6.4	5.9	5.4	4.8
Piezo 17 (in)	8.4	8	7.6	7.3	6.9	6.5	6.3	6
Piezo 18 (in)	9.5	9.2	8.9	8.6	8.3	8	7.8	7.5
Piezo 19 (in)	11.2	10.9	10.5	10.1	9.8	9.6	9.3	9.1
Piezo 20 (in)	13.7	13.2	12.4	12	11.5	11.2	10.8	10.5
Piezo 21 (in)	16.5	16	15.2	14.6	14	13.4	12.9	12.5
Piezo 22 (in)	14.9	15	15.1	15.1	15.2	15.1	15.1	14.9
Jump Location (in)		11±3	11±3	10±3	11±3	11.5±3.5	12±4	16±4

Basin Outlet Prandtl

LDB Prandtl ΔH (cm)	6.77	14.52	17.88	17.11	15.34	13.82	12.3	10.45
LDB (Mx-Mn)/2 (cm)	0.18	0.3	0.23	0.29	0.33	0.13	0.29	0.13
CL Prandtl ΔH (cm)	4.01	12.03	14.98	13.73	12.42	11.53	10.76	10.61
CL (Mx-Mn)/2 (cm)	0.27	0.26	0.33	0.21	0.22	0.09	0.19	0.2
RDB Prandtl ΔH (cm)	7.19	15.03	18.06	16.88	15.45	13.57	12.09	10.52
RDB (Mx-Mn)/2 (cm)	0.13	0.14	0.19	0.15	0.13	0.12	0.12	0.16

Notes: Measured Velocity with three Prandtl tubes at outlet

Appendix M Data – Uncontrolled Outlet – Full Weirs

Eight Discharges for Each Weir Height

With Prandtl Tubes at Basin Outlet

Test: Full Weir Height 1/8D - Streamwise Position A   **Date:** 1/5/2023

Run	YYB-X-1	YYB-X-2	YYB-X-3	YYB-X-4	YYB-X-5	YYB-X-6	YYB-X-7	YYB-X-8
Time	11:38	11:56	12:14	12:23	12:37	12:52	13:08	13:25
V-notch gauge (cm)	92.11	89.85	87.09	85.04	82.81	80.68	78.38	75.89
	92.17	89.75	87.03	85.01	82.80	80.69	78.34	75.62
Temp (C)	19.5	19.5	19.5	19.5	19.5	19.5	20.0	20.0
Prandtl U1 (ft)	1.02	1.04	1.04	1.08	1.07	1.07	1.08	1.09
Prandtl U2 (ft)	0.70	0.68	0.68	0.64	0.64	0.64	0.63	0.62
Prandtl D1 (ft)	1.29	1.27	1.23	1.24	1.22	1.22	1.21	1.21
Prandtl D2 (ft)	0.11	0.13	0.17	0.16	0.18	0.18	0.19	0.19
Pt. Gauge A (cm)	38.63	37.76	36.73	35.53	34.63	33.91	33.24	32.62
Pt. Gauge B (cm)	39.35	38.15	37.22	36.54	36.02	35.56	34.82	34.21
Pt. Gauge C (cm)	39.07	38.57	37.67	37.02	36.23	35.31	33.98	32.98
Pt. Gauge D (cm)	77.84	76.65	75.58	74.85	74.21	73.67	73.74	73.72
Pt. Gauge E (cm)	78.01	77.53	77.41	77.18	76.61	75.70	75.04	74.71
Pt. Gauge F (cm)	83.42	70.80	69.92	69.85	69.50	69.57	69.30	68.69
Tailwater Depth (in)	17.2	9.3	3.2					
Piezo 1 (cm)	13	3.7	2.8	2.2	1.7	1.7	1.6	0.6
Piezo 2 (cm)	11.3	6.7	6.3	5.4	4.4	3.2	2.7	2.2
Piezo 3 (cm)								
Piezo 4 (cm)								
Piezo 5 (cm)	18.6	16.8	15.4	14.3	13.1	12	10.8	9.7
Piezo 6 (cm)	9.5	9	8.3	7.8	7.4	7	6.6	6.2
Piezo 7 (cm)	9.9	9.3	8.3	7.5	6.9	6.4	6	5.6
Piezo 8 (cm)	10.3	9.4	8.4	7.6	6.8	5.9	5.4	4.8
Piezo 9 (cm)	10.1	9.2	8.4	7.8	7	6.3	5.3	4.4
Piezo 10 (cm)	10.1	9.2	8.4	7.8	7.1	6.5	5.9	4.9
Piezo 11 (in)	6.1	5.8	5.6	5.3	5	4.8	4.5	4.2
Piezo 12 (in)	6.2	5.9	5.6	5.4	5.1	4.9	4.6	4.3
Piezo 13 (in)	6	5.8	5.5	5.2	4.9	4.7	4.4	4.2
Piezo 14 (in)	6.3	6	5.6	5.3	5	4.7	4.5	4.2
Piezo 15 (in)	6.3	5.9	5.5	5.1	4.7	4.4	4.1	3.9
Piezo 16 (in)	8.5	7.9	7.3	6.9	6.4	5.8	5.3	4.6
Piezo 17 (in)	8.5	8.1	7.6	7.3	6.9	6.5	6.2	5.9
Piezo 18 (in)	9.6	9.2	8.9	8.6	8.3	8	7.7	7.4
Piezo 19 (in)	11.3	10.9	10.5	10.1	9.8	9.6	9.3	9
Piezo 20 (in)	13.7	13.3	12.4	12.1	11.5	11.2	10.8	10.5
Piezo 21 (in)	16.7	16	15.2	14.7	14	13.4	12.8	12.4
Piezo 22 (in)	14.9	15	15.1	15.1	15.2	15.1	15.1	15
Jump Location (in)								

Basin Outlet Prandtl

	YYB-X-1	YYB-X-2	YYB-X-3	YYB-X-4	YYB-X-5	YYB-X-6	YYB-X-7	YYB-X-8
LDB Prandtl ΔH (cm)	16.69	27.79	31.63	30.9	30.1	29.35	24.41	23.97
LDB (Mx-Mn)/2 (cm)	0.23	0.22	0.17	0.15	0.15	0.41	0.2	0.17
CL Prandtl ΔH (cm)	18.12	30.24	33.58	33.08	31.53	29.69	27.71	27.07
CL (Mx-Mn)/2 (cm)	0.2	0.32	0.21	0.13	0.17	0.18	0.18	0.15
RDB Prandtl ΔH (cm)	18.31	28.38	31.34	30.03	29.53	28.22	23.99	22.42
RDB (Mx-Mn)/2 (cm)	0.23	0.3	0.12	0.1	0.1	0.23	0.19	0.22

Notes: Measured Velocity with three Prandtl tubes at outlet

Test: Full Weir Height 2/8D - Streamwise Position A   **Date:** 1/10/2023

Run	YYC-X-1	YYC-X-2	YYC-X-3	YYC-X-4	YYC-X-5	YYC-X-6	YYC-X-7	YYC-X-8
Time	12:33	12:54	13:12	13:25	13:39	13:54	14:12	14:31
V-notch gauge (cm)	91.65	89.73	87.04	84.98	82.83	80.51	78.31	76.03
	91.59	89.72	87.05	84.95	82.81	80.51	78.34	75.97
Temp (C)	18.0	18.0	18.0	18.0	18.0	18.0	18.0	18.0
Prandtl U1 (ft)	1.10	1.12	1.12	1.14	1.15	1.16	1.16	1.13
Prandtl U2 (ft)	0.80	0.77	0.76	0.74	0.73	0.72	0.71	0.74
Prandtl D1 (ft)	0.14	0.15	0.17	0.18	0.20	0.19	0.20	0.20
Prandtl D2 (ft)	1.30	1.28	1.27	1.25	1.23	1.23	1.22	1.22
Pt. Gauge A (cm)	38.12	37.32	36.43	35.70	35.13	34.18	33.04	32.76
Pt. Gauge B (cm)	38.72	38.24	37.08	36.61	35.89	35.54	34.65	34.31
Pt. Gauge C (cm)	39.13	38.71	38.00	37.35	36.38	35.23	33.97	33.05
Pt. Gauge D (cm)	77.63	76.90	75.72	75.20	74.30	74.05	77.28	78.21
Pt. Gauge E (cm)	84.02	84.11	83.92	83.93	83.40	81.44	80.50	79.50
Pt. Gauge F (cm)	81.40	70.75	70.11	69.57	69.10	68.90	68.53	68.70
Tailwater Depth (in)	15.1	8.9	2.8					
Piezo 1 (cm)	12.3	5.5	4.7	3.9	2.7	1.5	1.1	1
Piezo 2 (cm)	12.3	10.6	10.5	9.8	9.2	7.8	6.1	4.1
Piezo 3 (cm)								
Piezo 4 (cm)								
Piezo 5 (cm)	21.2	19.2	17.1	16.3	15.2	14.2	15	14.9
Piezo 6 (cm)	14.2	13.7	12.9	12.4	12	11.5	11.1	10.6
Piezo 7 (cm)	11.3	10.6	9.3	8.6	7.9	7.6	7.7	8.2
Piezo 8 (cm)	10.3	9.5	8.4	7.6	6.8	5.9	5.4	5
Piezo 9 (cm)	9.9	9.2	8.3	7.8	7	6.1	5.2	4.4
Piezo 10 (cm)	9.8	9.1	8.2	7.7	7.1	6.4	5.7	5
Piezo 11 (in)	6	5.8	5.5	5.3	5	4.7	4.5	4.2
Piezo 12 (in)	6.1	5.9	5.6	5.3	5.1	4.9	4.6	4.3
Piezo 13 (in)	6	5.8	5.4	5.2	4.9	4.6	4.4	4.2
Piezo 14 (in)	6.2	6	5.6	5.3	5	4.7	4.5	4.2
Piezo 15 (in)	6.1	6	5.5	5.1	4.7	4.4	4.1	3.9
Piezo 16 (in)	8.2	8	7.3	6.8	6.4	5.8	5.3	4.8
Piezo 17 (in)	8.3	8.1	7.6	7.2	6.9	6.5	6.2	5.9
Piezo 18 (in)	9.5	9.2	8.8	8.6	8.3	8	7.7	7.5
Piezo 19 (in)	11.2	10.9	10.4	10.1	9.8	9.6	9.3	9.1
Piezo 20 (in)	13.5	13	12.5	12	11.5	11.1	10.8	10.5
Piezo 21 (in)	16.5	16	15.2	14.6	14	13.4	12.8	12.5
Piezo 22 (in)	15	15.1	15.1	15.1	15.2	15.1	15	14.9
Jump Location (in)								3±2

Basin Outlet Prandtl

LDB Prandtl ΔH (cm)	14.41	22.19	25.23	24.24	21.97	18.35	15.13	12.96
LDB (Mx-Mn)/2 (cm)	0.27	0.27	0.2	0.39	0.34	0.35	0.28	0.25
CL Prandtl ΔH (cm)	16.8	26.72	31.05	30.3	27.29	21.67	15.92	12.83
CL (Mx-Mn)/2 (cm)	0.28	0.26	0.31	0.28	0.24	0.55	0.27	0.26
RDB Prandtl ΔH (cm)	15.52	23.02	24.81	23.55	21.09	18.17	15.25	13.15
RDB (Mx-Mn)/2 (cm)	0.35	0.35	0.17	0.23	0.25	0.25	0.12	0.14

Notes: Measured Velocity with three Prandtl tubes at outlet

Test: Full Weir Height 3/8D - Streamwise Position A   **Date:** 1/12/2023

Run	YYD-X-1	YYD-X-2	YYD-X-3	YYD-X-4	YYD-X-5	YYD-X-6	YYD-X-7	YYD-X-8
Time	11:02	11:33	11:51	12:07	12:21	12:37	12:52	13:11
V-notch gauge (cm)	92.01	89.80	87.23	85.02	82.85	80.57	78.36	76.13
	92.02	89.80	87.20	84.92	82.82	80.56	78.40	76.03
Temp (C)	17.5	17.5	17.5	17.5	17.5	17.5	17.5	17.5
Prandtl U1 (ft)	1.25	1.27	1.27	1.27	1.30	1.30	1.30	1.31
Prandtl U2 (ft)	1.00	0.97	0.96	0.95	0.92	0.91	0.92	0.90
Prandtl D1 (ft)	1.60	1.56	1.55	1.53	1.52	1.50	1.50	1.49
Prandtl D2 (ft)	0.42	0.45	0.45	0.46	0.46	0.47	0.48	0.48
Pt. Gauge A (cm)	38.26	37.35	36.93	35.56	34.79	34.02	33.36	33.18
Pt. Gauge B (cm)	39.22	38.27	37.34	36.62	35.81	35.32	34.82	34.42
Pt. Gauge C (cm)	39.06	38.80	38.11	37.10	36.03	35.02	34.09	33.43
Pt. Gauge D (cm)	87.50	87.45	85.83	84.67	84.81	84.35	83.68	82.12
Pt. Gauge E (cm)	87.81	87.53	86.91	86.24	85.95	84.55	83.33	81.40
Pt. Gauge F (cm)	83.60	71.58	70.61	70.20	69.70	69.51	69.04	68.94
Tailwater Depth (in)	16.4	8.5	3.1					
Piezo 1 (cm)	13.9	5.6	4.1	4	3	2.5	1.7	1.4
Piezo 2 (cm)	13.7	10.5	8.8	8.4	7.8	5.9	3.9	2.2
Piezo 3 (cm)								
Piezo 4 (cm)								
Piezo 5 (cm)	22	20.9	19.3	18.5	17.7	17.5	16.4	14.8
Piezo 6 (cm)	21.7	20.1	18.9	18.1	16.9	15.6	14.2	13.7
Piezo 7 (cm)	16.4	16	14.4	13.9	13.8	13.9	13.4	12.6
Piezo 8 (cm)	12.2	11.6	10.1	9.3	9	8.4	9	9.8
Piezo 9 (cm)	10.2	9.5	8.6	7.9	7.1	6.3	5.5	5.1
Piezo 10 (cm)	9.9	9.1	8.4	7.7	7	6.4	5.8	5.1
Piezo 11 (in)	6.1	5.9	5.6	5.3	5	4.7	4.5	4.2
Piezo 12 (in)	6.2	5.9	5.6	5.4	5.1	4.9	4.6	4.4
Piezo 13 (in)	6.1	5.8	5.5	5.2	4.9	4.6	4.4	4.2
Piezo 14 (in)	6.4	6	5.6	5.3	5	4.8	4.5	4.3
Piezo 15 (in)	6.4	5.9	5.5	5.1	4.7	4.4	4.1	3.9
Piezo 16 (in)	8.5	7.9	7.3	6.8	6.4	5.8	5.3	4.8
Piezo 17 (in)	8.5	8.1	7.6	7.3	6.9	6.5	6.2	6
Piezo 18 (in)	9.6	9.2	8.9	8.6	8.3	8	7.7	7.5
Piezo 19 (in)	11.2	10.9	10.5	10.1	9.8	9.6	9.3	9.1
Piezo 20 (in)	13.7	13.1	12.4	11.9	11.6	11.2	10.8	10.5
Piezo 21 (in)	16.6	16	15.3	14.6	14	13.4	12.9	12.5
Piezo 22 (in)	14.9	14.9	15.1	15.1	15.1	15.1	15	15
Jump Location (in)	10±5	9±4	9±4	9±4	9±4	9±3	9±3	10±3

Basin Outlet Prandtl

LDB Prandtl ΔH (cm)	8.38	15.66	18.95	17.85	16.86	14.29	13.09	13.02
LDB (Mx-Mn)/2 (cm)	0.32	0.28	0.27	0.28	0.83	0.33	0.21	0.54
CL Prandtl ΔH (cm)	5.25	14.38	18.8	17.54	15.54	13.68	13.68	13.46
CL (Mx-Mn)/2 (cm)	0.3	0.24	0.31	0.28	0.38	0.3	0.17	0.27
RDB Prandtl ΔH (cm)	8.71	15.79	18.64	17.15	15.74	13.91	13.36	13.04
RDB (Mx-Mn)/2 (cm)	0.14	0.16	0.33	0.13	0.33	0.15	0.16	0.23

Notes: Measured Velocity with three Prandtl tubes at outlet

Test: Full Weir Height 4/8D - Streamwise Position A   **Date:** 1/12/2023

Run	YYE-X-1	YYE-X-2	YYE-X-3	YYE-X-4	YYE-X-5	YYE-X-6	YYE-X-7	YYE-X-8
Time	14:38	14:56	15:10	15:26	15:40	16:08	16:25	16:44
V-notch gauge (cm)	91.91	89.78	87.14	84.86	82.73	80.60	78.13	76.03
	91.91	89.76	87.04	84.89	82.73	80.54	78.07	75.94
Temp (C)	17.5	17.5	17.5	17.5	17.5	18.0	18.0	18.0
Prandtl U1 (ft)	1.25	1.28	1.27	1.29	1.31	1.32	1.33	1.33
Prandtl U2 (ft)	1.01	0.98	0.98	0.96	0.94	0.93	0.92	0.92
Prandtl D1 (ft)	0.43	0.45	0.47	0.48	0.51	0.49	0.50	0.52
Prandtl D2 (ft)	1.61	1.59	1.57	1.55	1.51	1.52	1.51	1.49
Pt. Gauge A (cm)	38.46	37.52	36.68	35.92	34.92	34.15	33.52	40.57
Pt. Gauge B (cm)	38.72	38.04	37.18	36.31	35.81	35.36	39.51	47.01
Pt. Gauge C (cm)	39.37	38.58	37.84	37.12	36.47	35.35	46.58	48.07
Pt. Gauge D (cm)	92.65	92.20	90.34	89.34	89.15	87.97	87.36	87.31
Pt. Gauge E (cm)	91.75	90.60	89.60	89.02	87.86	86.79	85.86	85.19
Pt. Gauge F (cm)	83.60	71.51	70.44	70.06	69.69	69.58	69.44	69.50
Tailwater Depth (in)	16.1	8.6	3.1					
Piezo 1 (cm)	13.5	4.8	3.6	2.9	2.6	2	1.6	2.2
Piezo 2 (cm)	13.6	10	7.6	6.1	4.9	2.5	1.8	1.9
Piezo 3 (cm)								
Piezo 4 (cm)								
Piezo 5 (cm)	20.7	21.3	21.1	20.7	21	20.3	20.1	20.4
Piezo 6 (cm)	26.1	24.8	23.2	21.7	20.7	19.7	20.2	20.2
Piezo 7 (cm)	22.4	21.5	20.9	19.8	19	18.1	19.9	20
Piezo 8 (cm)	18.1	17.3	17.4	15.9	15.6	15.6	19.5	19.9
Piezo 9 (cm)	13.4	13.1	12.8	11.4	12.2	12.2	18	19.8
Piezo 10 (cm)	10.3	9.8	9.3	8.3	8.5	8.5	15.7	19.6
Piezo 11 (in)	6	5.9	5.6	5.4	5.1	4.8	7.4	9.7
Piezo 12 (in)	6	5.9	5.6	5.4	5.1	4.9	6.9	9.5
Piezo 13 (in)	6	5.8	5.5	5.2	4.9	4.7	5.2	8.9
Piezo 14 (in)	6.2	6	5.6	5.3	5	4.8	4.5	8.4
Piezo 15 (in)	6.1	5.9	5.4	5	4.7	4.4	4.1	7.5
Piezo 16 (in)	8.3	7.9	7.3	6.8	6.4	5.9	5.3	6.9
Piezo 17 (in)	8.3	8.1	7.6	7.2	6.9	6.6	6.2	6.2
Piezo 18 (in)	9.4	9.2	8.8	8.6	8.3	8	7.7	7.5
Piezo 19 (in)	11.1	10.9	10.5	10.2	9.9	9.6	9.3	9.1
Piezo 20 (in)	13.5	13.2	12.4	12	11.5	11.2	10.8	10.5
Piezo 21 (in)	16.6	16.1	15.3	14.7	14	13.4	12.8	12.4
Piezo 22 (in)	14.7	15.1	15.1	15.1	15.2	15.2	15	15
Jump Location (in)		0	17±5	16±5	16±5	19±5	40±4	60.5±2.5

Basin Outlet Prandtl

LDB Prandtl ΔH (cm)	10.19	17.87	20.42	18.69	17.7	16.89	16.19	14.49
LDB (Mx-Mn)/2 (cm)	0.23	0.32	0.51	0.22	0.26	0.35	0.25	0.28
CL Prandtl ΔH (cm)	6.58	15.71	18.54	17.87	16.74	16.56	16.67	15.55
CL (Mx-Mn)/2 (cm)	0.2	0.14	0.18	0.14	0.18	0.15	0.14	0.1
RDB Prandtl ΔH (cm)	10.44	18.17	20.11	18.5	17.24	16.48	15.68	14.23
RDB (Mx-Mn)/2 (cm)	0.2	0.2	0.11	0.05	0.15	0.06	0.19	0.05

Notes: Measured Velocity with three Prandtl tubes at outlet